From structural regulation to cellular function

A multiscale view on the human TRPML2 ion channel and its role in Zika virus infection

Dissertation

zur Erlangung des Grades

DOKTOR DER NATURWISSENSCHAFTEN

im Promotionsfach Chemie

am Fachbereich Chemie, Pharmazie, Geographie und Geowissenschaften

der Johannes Gutenberg-Universität Mainz

Kerstin Karina Schwickert (geb. Viet)

geboren in Offenbach am Main

Mainz,

Juni 2023

D77 (Dissertation Universität Mainz)

Dekanin: [redacted]

1. Gutachterin: [redacted]

2. Gutachter: [redacted]

Tag der öffentlichen Prüfung:

“The whole is greater than the sum of its parts.”

- Aristotle

Summary

Zika virus (ZIKV) gained public attention during a major outbreak in the Americas in 2015/2016 when the infection was first associated with severe neurological complications, such as neonatal microcephaly. At that time, the epidemic was even declared as a public health emergency of international concern (PHEIC) by the WHO (World Health Organisation). Until now, no specific treatment or prophylactic vaccine is available. Therefore, a more in-depth knowledge about the Zika virus life cycle is required to identify host factors, which can be targeted for the development of novel drug candidates. In recent years, ion channels have emerged as important modulators of viral infections. The human cation channel TRPML2 (transient receptor potential mucolipin 2) is located in the membranes of the endolysosomal system, which plays an important role in the Zika virus life cycle.

In this thesis, the potential to address TRPML2 as an antiviral target against ZIKV was investigated. Treatment of human A549 cells with the synthetic TRPML2 agonist ML2-SA1 reduced intracellular ZIKV mRNA (messenger ribonucleic acid), protein levels and amount of released viral particles of two ZIKV strains (ZIKV French Polynesia and ZIKV Uganda) *in vitro*. Confocal laser scanning microscopy (cLSM) showed increased acidification of vesicular structures and super-resolution microscopy revealed enlarged size of multivesicular bodies (MVBs). Inhibition of lysosomal degradation did not lead to intracellular ZIKV accumulation, indicating that the antiviral effect of ML2-SA1 is not caused by increased ZIKV degradation in lysosomal compartments. Moreover, time-of-drug-addition experiments revealed that ML2-SA1 does not affect early stages of the ZIKV life cycle (such as entry), but later stages, for example viral replication. The effect on ZIKV replication was confirmed via experiments with a ZIKV *Renilla* luciferase reporter virus. A potential cause of the antiviral effect ML2-SA1 might be changes in the intracellular cholesterol distribution, which is an important factor of ZIKV replication. In fact, cLSM analyses revealed intracellular cholesterol accumulations in ML2-SA1 treated cells.

Investigations on proteins involved in complex biological processes, such as viral infections, require a profound understanding of the (structural) regulation of these proteins. TRPML channels are tetramers, one protomer consists of six transmembrane-spanning helices, the cytosolic N- and C-termini and the extracytosolic/lumenal domain (ELD), which connects the first two transmembrane helices and is the structural hallmark of the TRPML family. In this thesis, a potential function of the ELD for the structural regulation of human TRPML2 was analyzed. The ELD faces the endolysosomal lumen where, depending on whether the channel resides in early or late endosomes or lysosomes, it encounters variations in pH values and ion concentrations. Isothermal titration calorimetry (ITC) revealed that calcium interacts with an acidic amino acid motif in the central pore loop of the ELD in a pH-dependent manner. At neutral pH, calcium binds to the ELD potentially forming a block for

other cations, while at acidic pH the decreased calcium affinity might allow unhindered cation flux. This indicates that the ELD serves an important function in the endolysosomal compartment-specific regulation of TRPML2. However, interactions with Ca^{2+} did not induce significant structural changes of the isolated TRPML2 ELD as assessed via NMR (nuclear magnetic resonance) and EPR (electron paramagnetic resonance) spectroscopy.

Zusammenfassung

Das Zika-Virus (ZIKV) rückte während eines großen Ausbruchs in Nord- und Südamerika in den Jahren 2015/2016 in den Fokus der Öffentlichkeit. Zu dieser Zeit wurde die Infektion erstmals mit schweren neurologischen Komplikationen wie der neonatalen Mikrozephalie in Verbindung gebracht. Die Epidemie wurde von der WHO (*World Health Organisation*, Weltgesundheitsorganisation) sogar zu einem internationalen Gesundheitsnotfall erklärt. Bis heute gibt es weder eine spezifische Behandlung noch einen prophylaktischen Impfstoff gegen das Zika-Virus. Daher ist ein tiefergreifendes Wissen über den Lebenszyklus des Zika-Virus notwendig, um Wirtsfaktoren zu identifizieren, die für die Entwicklung neuer Arzneimittelkandidaten genutzt werden können. In den letzten Jahren haben sich Ionenkanäle als wichtige Modulatoren von Virusinfektionen erwiesen. Der menschliche Kationenkanal TRPML2 (*transient receptor potential mucolipin 2*) befindet sich in den Membranen des endolysosomalen Systems, das eine wichtige Rolle beim Zika-Virus Lebenszyklus spielt.

In dieser Arbeit wurde das Potenzial von TRPML2 untersucht, als antivirales Ziel gegen ZIKV zu dienen. Die Behandlung menschlicher A549-Zellen mit dem synthetischen TRPML2-Agonisten ML2-SA1 reduzierte *in vitro* die intrazelluläre ZIKV-mRNA (Boten-Ribonukleinsäure), die Proteinkonzentration und die Menge der freigesetzten Viruspartikel zweier ZIKV-Stämme (ZIKV Französisch-Polynesien und ZIKV Uganda). Konfokale Mikroskopie (*confocal laser scanning microscopy*, cLSM) zeigte eine verstärkte Ansäuerung von vesikulären Strukturen, sowie hochauflösende Mikroskopie eine Vergrößerung der multivesikulären Körperchen. Die Hemmung des lysosomalen Abbaus führte nicht zu einer intrazellulären ZIKV-Akkumulation, was darauf hindeutet, dass die antivirale Wirkung von ML2-SA1 nicht auf einen verstärkten ZIKV-Abbau in lysosomalen Kompartimenten zurückzuführen ist. Vielmehr ergaben Experimente zum Zeitpunkt der Wirkstoffzugabe, dass ML2-SA1 nicht die frühen Stadien des ZIKV-Lebenszyklus (wie den Eintritt), sondern spätere Stadien, z. B. die virale Replikation, beeinflusst. Die Wirkung auf die ZIKV-Replikation wurde durch Experimente mit einem ZIKV-*Renilla*-Luciferase-Reportervirus bestätigt. Eine mögliche Ursache für die antivirale Wirkung von ML2-SA1 könnten Veränderungen in der intrazellulären Cholesterolverteilung sein, die ein wichtiger Faktor der ZIKV-Replikation ist. In der Tat zeigten cLSM-Analysen intrazelluläre Cholesterolansammlungen in ML2-SA1 behandelten Zellen.

Die Untersuchung von Proteinen, die an komplexen biologischen Prozessen, wie z. B. Virusinfektionen, beteiligt sind, erfordert ein tiefes Verständnis der (strukturellen) Regulierung dieser Proteine. TRPML-Kanäle sind Tetramere, ein Protomer besteht aus sechs Transmembranhelices, den zytosolischen N- und C-Termini und der extrazytosolischen/lumenalen Domäne (ELD), die die ersten beiden Transmembranhelices verbindet und das strukturelle Markenzeichen der TRPML-Familie ist. In dieser Arbeit wurde eine mögliche Funktion der ELD von TRPML2 in Hinblick auf die Kanalregulation analysiert. Die ELD ist dem endolysosomalen Lumen

zugewandt, wo der Kanal, je nachdem, ob er sich in frühen oder späten Endosomen oder Lysosomen befindet, Schwankungen des pH-Werts und der Ionenkonzentration ausgesetzt ist. Isothermale Titrationskalorimetrie zeigte, dass Calcium mit einem sauren Aminosäuremotiv in der zentralen Porenschleife der ELD in einer pH-abhängigen Weise interagiert. Bei neutralem pH-Wert bindet Calcium an die ELD und bildet möglicherweise eine Blockade für andere Kationen, während bei saurem pH-Wert die geringere Calciumaffinität einen ungehinderten Kationenfluss ermöglichen könnte. Dies deutet darauf hin, dass die ELD eine wichtige Funktion bei der endolysosomalen Kompartiment-spezifischen Regulierung von TRPML2 erfüllt. Die Wechselwirkungen mit Ca^{2+} führten jedoch nicht zu signifikanten strukturellen Veränderungen der isolierten TRPML2 ELD, wie mittels Kernspinresonanz- und Elektronenspinresonanz-Spektroskopie festgestellt wurde.

Content

Abbreviations

A

A	adenine
AAs	amino acids
ABC	ATP binding cassette
ACE2	angiotensin-converting enzyme 2
ADAP2	arfGAP with dual pleckstrin homology (PH) domains 2
ADE	antibody-dependent enhancement
amp	ampicillin
AP2	adaptor protein complex 2
approx.	approximately
APS	ammoniumpersulfate
Arf6	ADP-ribosylation factor 6
ARNO	ARF nucleotide-binding site opener
Atg7	autophagy related 7
ATP	adenosine triphosphate

B

Bcl-2	B-cell lymphoma 2
BFA1	Bafilomycin A1
BSA	bovine serum albumin
BTFA	3-bromo-1,1,1-trifluoroacetone

C

2-CMA	2’-C-methyladenosine
2-CMC	2’-C-methylcythydine
2-CMG	2’-C-methylguanosine
2-CMU	2’-C-methyluridine
C protein	capsid protein
C	cytosine
CCL2	chemokine (C-C motif) ligand 2
CD	circular dichroism
CD4	cluster of differentiation 4
cDNA	complementary DNA
CF	cystic fibrosis
CFTR	cystic fibrosis transmembrane conductance regulator
CHRNA1	cholinergic receptor nicotinic alpha 1
cLSM	confocal laser scanning microscopy
CME	clathrin-mediated endocytosis
COPII	coat protein complex II
Cryo-EM	cryogenic electron microscopy
CW	continuous wave

D

7-deaza-2-CMA	7-deaza-2’-C-methyladenosine
Da	Dalton
DABCO	1,4-diazabicyclo[2.2.2]octane
DAPI	4’,6-diamidino-2-phenylindole
DDX3X	DEAD-box helicase 3 X-linked
DENV	Dengue virus
DEPC	diethyl pyrocarbonate
DMEM	Dulbecco’s modified eagle medium
DMSO	dimethyl sulfoxide
DNA	deoxyribonucleic acid
dNTP	deoxynucleotide triphosphate
DPP4	dipeptidyl peptidase-4
dsRNA	double-stranded RNA
DTNB	5,5'-dithio-bis-(2-nitrobenzoic acid), Ellman’s reagent
DTT	dithiotreitol

E

E protein	envelope protein
EBOV	Ebola virus
EDTA	ethylenediaminetetraacetic acid
EEA1	early endosome antigen 1
ELD	extracytosolic/lumenal domain
EPR	electron paramagnetic resonance

ER	endoplasmic reticulum
EtOH	ethanol

F

FCS	Fetal calf serum
FDA	Food and Drug Administration
FSU	Friedrich-Schiller-University, Jena

G

G	guanine
GAG	glycosaminoglycan
GAP	GTPase activating protein
Gas6	growth-arrest-specific protein 6
GPI-AP	glycosylphosphatidyl-inositol anchored protein

H

h	hour
HCV	hepatitis C virus
HEPES	4-(2-hydroxyethyl)-1-piperazineethanesulfonic acid
HEV	hepatitis E virus
HMG-CoA	3-hydroxy-3-methyl-glutaryl-coenzyme A reductase
HRV	human rhinovirus
Hsc40	heat shock cognate protein of 40 kDa
Hsc70	heat shock cognate protein of 70 kDa
HSQC	heteronuclear single quantum coherence

I

IAV	influenza A virus
IF	immunofluorescence
IFN	interferon
IMAC	immobilized metal affinity chromatography
IMPDH	inosine monophosphate dehydrogenase
IPSL	3-(2-iodoacetamido)-proxyl
IPTG	isopropyl β-D-1-thiogalactopyranoside
IRF3	interferon regulatory factor 3
ISG	IFN-stimulated genes
ITC	isothermal titration calorimetry

J

JAK	Janus kinase
JEV	Japanese Encephalitis virus

K

kDa	kilodalton

L

LAMP	lysosome-associated membrane protein
LB	lysogeny broth
LC3	microtubule-associated protein 1A/1B-light chain 3
LPS	lipopolysaccharide

M

M protein	membrane protein
MDA5	melanoma differentiation-associated protein 5
MeOH	methanol
MHC-II	major histocompatibility complex II
min	minute
mL	milliliter
ML2-SA1	mucolipin2 synthetic agonist 1
MLBs	multivesicular bodies
MLIV	Mucolipidosis type IV
ML-SA1	mucolipin synthetic agonist 1
MOI	multiplicity of infection
MRE	mean residue ellipticity
mRNA	messenger RNA

MRW	mean residue weight
MVB	multivesicular body

N

NiNTA	nickel nitrilotriacetic acid
NMR	nuclear magnetic resonance
NOD	(nucleotide-binding oligomerization domain)-like
NPC	neural progenitor cell
NPC1	intracellular cholesterol transporter Niemann-Pick C1
NS	non-structural

P

PAMP	pathogen-associated molecular pattern
PBMCs	peripheral blood mononuclear cells
PBS	phosphate buffered saline
PCR	polymerase chain reaction
PELDOR	pulsed electron electron double resonance
$PI(3,5)P_2$	phosphatidylinositol 3,5-bisphosphate
PHEIC	public health emergency of international concern
$PI(4,5)P_2$	phosphatidylinositol 4,5-bisphosphate
PIKfyve	PtdIns (3) P5-kinase
PLC	phospholipase C
PMSF	phenylmethanesulfonyl-fluoride
PolyI:C	polyinosinic:polycytidylic acid
prM protein	pre-membrane protein
ProS9	protein S
PRR	pattern-recognition-receptor

Q

qPCR	quantitative PCR

R

Rab	Ras-associated binding
RdRp	RNA-dependent RNA polymerase
rev.	reverse
RF	replication factories
RIG-1	retinoic acid-inducible gene I
RIPA	radioimmuno-precipitation assay
RLuc	Renilla luciferase
RNA	ribonucleic acid
ROS	reactive oxygen species
RT-qPCR	real-time quantitative PCR

S

s	second
SARS-CoV-2	severe acute respiratory syndrome coronavirus 2
SD	standard deviation
SDS	sodium dodecyl sulfate
SDS-PAGE	SDS polyacrylamide gel electrophoresis
SEC	size-exclusion chromatography
SP	signal peptide
SQSTM1	sequestosome 1
STAT	signal transducer and activator of transcription
STED	stimulated emission depletion
SUMO	small Ubiquitin-related modifier
SVP	subviral particle

T

T	Thymine
TAM	Tyro3, Axl, Mer
TBEV	Tick-Borne Encephalitis virus
TBS	Tris buffered saline
TBS-T	Tris buffered saline + 0.05% (v/v) Tween-20
TEMED	Tetramethylethylenediamine
TFEB	transcription factor EB
TIM	T-cell immunoglobulin and mucin domain

TLR	Toll-like receptors
TM	transmembrane
TMD	transmembrane domain
TPC	two-pore channel
TRP	transient receptor potential
TRPA	TRP ankyrin
TRPC	TRP canonical
TRPM	TRP melastatin
TRPML	TRP mucolipin
TRPN	TRP NOMPC (no mechanoreceptor potential C)
TRPP	TRP polycystin
TRPS	TRP soromelastatin
TRPV	TRP vanilloid

U

Ulp1	Ubl-specific protease 1

V

VGCC	voltage-gated Ca^{2+} channel
VSV	Vesicular Stomatitis virus
V-type ATPase	vacuolar-type ATPase

W

WB	Western blot
WNV	West Nile virus
WT	wild type

Y

YFV	Yellow Fever virus

Z

ZIKV	Zika virus

Annotation

Publications, collaborations, and supervised student projects

This thesis was carried out in the groups of [redacted] (Department of Chemistry, Johannes Gutenberg-University, Mainz; since Jan 2021: Faculty of Chemistry and Earth Sciences, Institute of Organic and Macromolecular Chemistry, Cluster of Excellence "Balance of the Microverse", Friedrich-Schiller-University, Jena) and [redacted] (Virology Department, Paul-Ehrlich-Institute, Langen) in collaboration with [redacted] (Max Planck Institute for Polymer Research, Mainz) within the Max Planck Graduate Center (MPGC).

Publications

Peer-reviewed:

Kerstin K. Viet*, Annika Wagner*, Kevin Schwickert*, Nils Hellwig, Martha Brennich, Nicole Bader, Tanja Schirmeister, Nina Morgner, Hermann Schindelin and Ute A. Hellmich, Structure of the Human TRPML2 Ion Channel Extracytosolic/Lumenal Domain. *Structure* **27**, 1246-1257.e5 (2019).[1]

*contributed equally

Manuscripts in preparation:

Kerstin K. Schwickert, Mirco Glitscher, Steffen Pfalzgraf, Daniela Bender, Robin Murra, Kevin Schwickert, Tanja Schirmeister, Ute A. Hellmich and Eberhard Hildt, The selective TRPML2 agonist ML2-SA1 impairs Zika virus infection *in vitro*. (in prep.)

Kerstin K. Schwickert, Christoph Wiedemann, Catrin Allar, Benedikt Goretzki, Olav Schiemann, Ute A. Hellmich, Structural consequences of pH-dependent cation binding to the TRPML2 ELD. (in prep.)

Collaborations

Collaborations with the following working groups are gratefully acknowledged:

- [redacted] (Institute of Pharmaceutical and Biomedical Sciences, Johannes Gutenberg-University Mainz)
  Organic synthesis
- [redacted] (Rudolf Virchow Centre for Experimental Biomedicine, Julius-Maximilians-University Würzburg)
  Crystallography
- [redacted] (Clausius-Institute of Physical and Theoretical Chemistry, Rheinische Friedrich-Wilhelms-University Bonn)
  Electron paramagnetic resonance (EPR) spectroscopy

Supervised student projects which contributed to this thesis

- [redacted], *internship* (2019)
- [redacted], *Bachelor thesis* (2019), *Die Rolle des pre-pore loops bei der Interaktion der TRPML2 Extracytosolischen/Lumenalen Domäne (ELD) mit Calcium und anderen Kationen* (The role of the pre-pore loop in the interaction of the TRPML2 extracytosolic/lumenal domain (ELD) with calcium and other cations).
- [redacted], *Bachelor thesis* (2019), *Interaktionen der Extracytosolischen/Lumenalen Domäne von humanen TRPML-Kanälen mit verschiedenen Kationen* (Interactions of the extracytosolic/lumenal domain of human TRPML channels with different cations.)
- [redacted], *Bachelor thesis* (2020), *Strukturelle Untersuchungen der regulatorischen Extracytosolischen/Lumenalen Domäne des humanen Ionenkanals TRPML2 und ihrer Wechselwirkung mit Calcium* (Structural studies of the regulatory extracytosolic/lumenal domain of the human ion channel TRPML2 and its interaction with calcium).

1 Introduction

The *Flaviviridae* family includes vector-borne RNA viruses such as Dengue (DENV), West Nile (WNV), Yellow Fever (YFV), Japanese Encephalitis (JEV), Tick-borne Encephalitis (TBEV) and Zika Virus (ZIKV).[2] Every year, these pathogens are responsible for around 400 million infections globally featuring a broad spectrum of potentially severe diseases, including vascular shock syndrome, hepatitis, encephalitis, acute flaccid paralysis, congenital abnormalities, and fetal death.[2] During the last 70 years, numerous flaviviral outbreaks have been reported, including epidemics of Dengue and West Nile virus.[2] The 2016 Zika virus epidemic in the Americas raised international concern since it can cause severe neurological complications in adults and newborns.[2]

In addition to the specific host cell membrane receptors that enable viral entry, ion channels have emerged as one of the key host cell factors for a great number of viral infections. Accordingly, human ion channels are also emerging therapeutic targets against infectious diseases.[3] Ion channels are pore-forming proteins which facilitate ion flux across lipid membranes. They enable signaling between and within cells, maintain ion homeostasis and are therefore crucial for cell survival.[4] Ion channels not only play a crucial role for the host's immune response but can also be exploited by viruses for cell infection.[5,6] For instance, T cells rely on plasma membrane calcium channels for cellular proliferation, activation, and cytotoxicity, all important processes for the adaptive immune response.[5,6] However, certain viruses can also affect the activity of calcium channels in host immune cells resulting in the downregulation of immune responses as an evasion mechanism.[7,8] Notably, viruses also require calcium mobilization for critical steps in their own "life" cycle, including host cell entry, viral replication and budding.[6] Finally, many viruses encode their own ion channels which are called "viroporins", highlighting the relevance of ion homeostasis during the infection process.[9–11] Viroporins are not only involved in viral replication and assembly, but also entry and particle release from infected cells.[9]

In this thesis, the role of the human endolysosomal ion channel TRPML2 (transient receptor potential mucolipin 2) in Zika virus infection was investigated.

1.1 Zika virus: History and pathogenesis

Zika virus is primarily transmitted by *Aedes* mosquitoes (e.g. *Aedes aegypti* and *Aedes albopictus*).[12,13] In the past decades, increased intercontinental trade and travel networks as well as climate change enabled mosquitoes to spread beyond their original range, while urbanization created new aquatic habitats.[14,15] *Aedes aegypti* is widely distributed in the subtropics and tropics, can be encountered at heights up to 1,700 m and is still present, albeit rare from heights ranging from 1,700 to 2,130 m

(Figure 1.1).[16] Unlike most other flaviviruses, ZIKV human-to-human transmission (via sexual intercourse and vertically from a mother to the unborn child) is also possible.[12]

ZIKV exhibits wide tissue tropism. For viral propagation and persistence neural, ocular, testicular and placental tissue are particularly important.[17] Furthermore, persistence of infectious particles and viral nucleic acids in several body fluids (e.g., semen, saliva, tears and urine) was reported.[18]

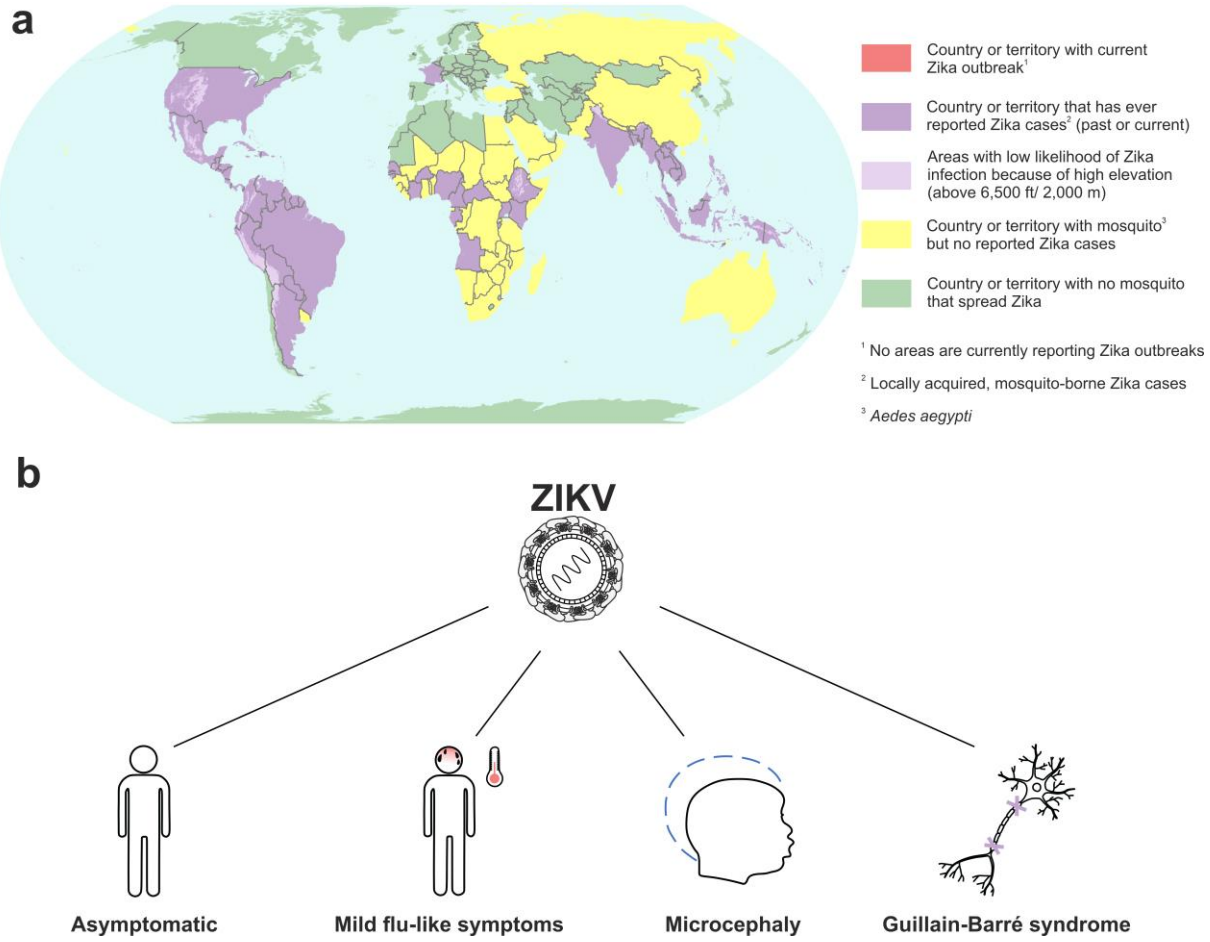

Figure 1.1: ZIKV distribution and pathogenesis. (**a**) Areas with risk of Zika. Publicly provided by the Centers for Disease Control and Prevention (CDC), current as of July 25, 2022. (**b**) Infections with Zika virus can be asymptomatic, but can also cause flu-like symptoms.[19] In addition, cases of microcephaly in newborns and Guillain-Barré syndrome have been reported after infection with the Asian ZIKV lineage.[20,21]

ZIKV was first isolated from the serum of a febrile sentinel rhesus monkey at the Zika forest in Uganda in 1947.[22] Serological data indicate that ZIKV was wide-spread throughout Africa (African lineage) and subsequently occurred in Asia (Asian lineage) without reports of severe symptoms.[23] In the approx. 20% of infected individuals where symptoms occurred, they have historically been described as mild, influenza-like illness that resolved itself within days.[19] The prototypic strain of the ZIKV Asian lineage was first isolated from mosquito pools in Bentong, Malaysia in 1966.[24,25] Based on serological studies, the first documented ZIKV outbreak in Asia may have occurred in central Java, Indonesia in 1977.[25,26] However, ZIKV infections may have been more widespread and possibly circulating asymptomatically in Southeast and South Asia.[27] The two lineages of ZIKV differ by

approx. 10% at the nucleotide level, leading to higher infectivity and changed tropism of the Asian lineage.[23] The first outbreaks gaining international attention were caused by the ZIKV Asian lineage and occurred on Yap Island, Federated States of Micronesia, in 2007[19], and in French Polynesia in 2013[28]. During the outbreak in French Polynesia, the percentage of symptomatic infections was significantly higher (50%).[29] In this thesis, one representative of the Asian lineage (ZIKV French Polynesia) and one representative of the African lineage (ZIKV Uganda) were used.

More recently, ZIKV originating from the Asian lineage was also reported in South America, specifically in Brazil in 2015, from where the virus spread rapidly across the continent.[13,30,31] The ZIKV epidemic in Brazil peaked in the early spring of 2016 and coincided with the Olympic games thus generating significant media attention. During this outbreak, ZIKV infection was first linked to neonatal microcephaly.[32,33] ZIKV was shown to infect progenitor cells of the cerebral cortex resulting in increased cell death,[34] to target microglia which can produce inflammatory cytokines[35] and to modulate the immune response of astrocytes[36,37]. Retrospective studies indicated that the French Polynesian strain also caused microcephaly. In contrast, it is hypothesized that the African lineage does not lead to such effects.[38] In addition, the Brazilian strain was shown to cause apoptosis of neural progenitor cells (NPCs) in developing brain organoid models in contrast to the African strain MR766.[39] The most commonly described symptoms during the outbreaks in French Polynesia and in the Americas were fever (72%), arthralgia and myalgia (65%), conjunctivitis (63%) and headache (46%).[40] In rare cases, also severe complications in adults have been reported including multi-organ failure, thrombocytopenia, meningitis and encephalitis.[41–43] Although ZIKV generally is not linked to fatal diseases in adults, mortality has been reported for infected cancer patients and individuals who developed Guillain-Barré syndrome.[20,41] The high ZIKV infection rates in the Americas and the association with congenital neurodevelopmental defects lead to the classification of this epidemic as an international public health emergency.[44] The number of reported cases significantly decreased in 2017, probably due to herd immunity. Seroprevalence studies indicated that 63% of the inhabitants of Salvador, Brazil, were infected during this outbreak.[45]

1.2 Zika virus structure

The positive-stranded RNA genome of ZIKV has a size of around 10.7 kb.[46] It encodes 3423 amino acids in a single open reading frame which is flanked by two untranslated regions (UTRs) containing a 5' cap structure but lack a poly-A tail (Figure 1.2a).[47,48] The viral polyprotein is cleaved by host and viral proteases into three structural proteins, the (capsid (C), pre-membrane (prM) and envelope (E) protein as well as seven non-structural (NS) proteins (NS1, NS2A, NS2B, NS3, NS4A, NS4B and NS5).[46] The non-structural proteins are responsible for viral genome replication, polyprotein processing and modulation of the host's immune response.[49] In infected cells, several of the non-structural proteins antagonize host cell signal transduction mediated by pattern-recognition-receptors (PRRs), which

typically would lead to type I interferon (IFN) induction and expression of IFN-stimulated genes (ISGs).[50]

ZIKV virions are 50 nm in size and contain the viral genome in a nucleocapsid, which is surrounded by a lipid bilayer.[51] The structural proteins E and prM/M are arranged on the surface with icosahedral symmetry (Figure 1.2b-d).[51,52] The E protein, which predominates the surface of the viral particle, consists of four domains: the stem-transmembrane domain pair and the three ectodomains I, II, and III, which can be found outside of the membrane.[53] In most ZIKV strains, the E protein is N-glycosylated at position E154 located in domain I.[54] Some of the pre-epidemic ZIKV strains from the African lineage are suggested to be less neuroinvasive since they lack this glycan .[54] The ZIKV E protein shares similarities with other flaviviruses: around 50% of the E protein sequence is conserved between various ZIKV and DENV strains, and ZIKV and the African Spondweni virus even display approx. 68% E protein amino acid identity.[49] Although the high E protein similarity could be beneficial for the patient due to production of broadly reactive protective antibodies, it also complicates virus-specific diagnostics.[55,56]

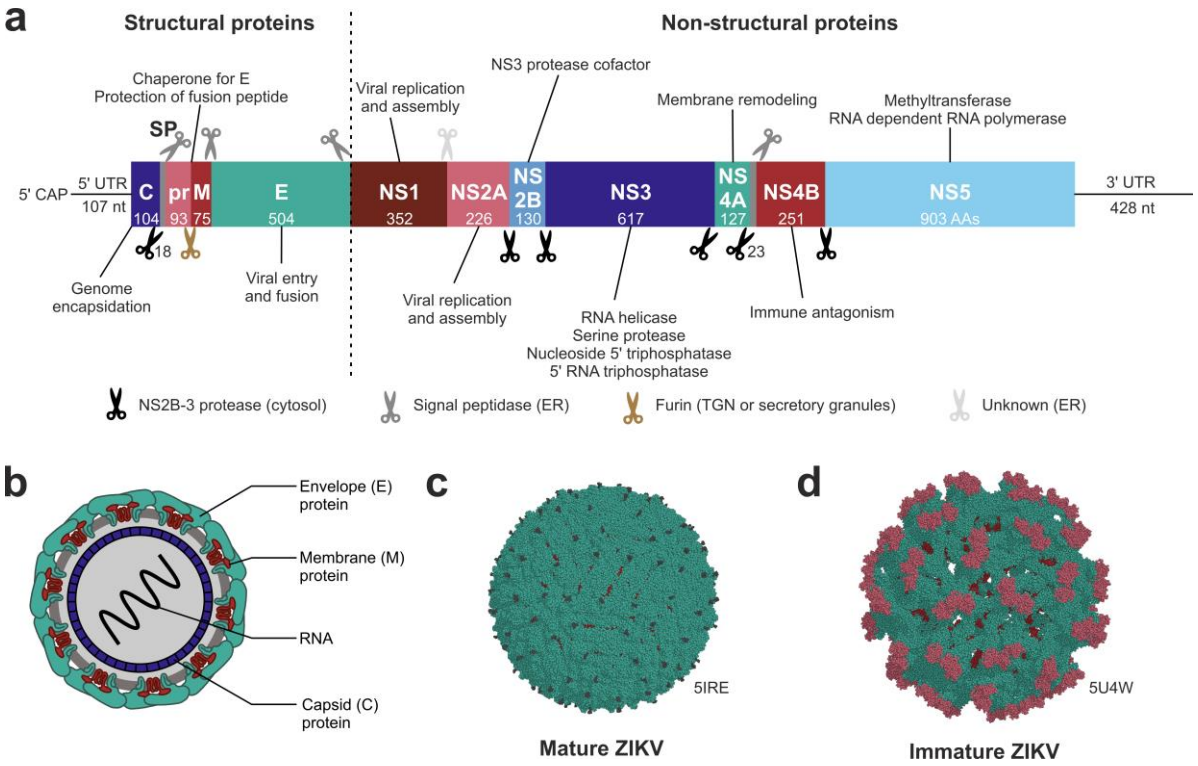

Figure 1.2: ZIKV genome organization and structure of mature and immature viral particles. (**a**) Architecture of the ZIKV genome/polyprotein. The cleavage profile of the polyprotein, the involved proteases, amino acid numbers (AAs) and functions of the individual proteins are shown (note that the figure does not provide an exhaustive list of the functions of each protein and that viral proteins interact with several host proteins, thereby expanding their respective functions in the host cell). Figure 5a is based on Sirohi *et al.*.[53] (**b**) Schematic representation of a mature ZIKV particle (same color code as in Figure 5a). (**c**-**d**) Cryo-EM (cryogenic electron microscope) structures of mature ZIKV (3.80 Å, pdb 5IRE)[51] and immature ZIKV (9.10 Å, pdb 5UAW)[57], respectively (same color code as in Figure 5a).

The M protein is a small glycoprotein that is connected to the viral membrane via its transmembrane helices. In immature virions, trimers of prM-E heterodimers are arranged in a spiked formation (Figure 1.2d).[57] Mature, infectious viral particles display a relatively smooth surface. Here, the M protein resides under the larger E protein (Figure 1.2c).[51,52] Consequently, only a few amino acids of M are solvent exposed.[53] The basic E protein organizational unit of mature ZIKV virions is a dimer, and each monomer is related to its neighbor by 2-fold symmetry.[53] Three E protein dimers lie in parallel to each other contributing to the so-called raft-configuration. In total, one virion consists of 30 rafts, thus 180 copies of each E and M proteins are embedded in the viral membrane.[53]

1.3 Zika virus life cycle

The basic stages of the flavivirus life cycle are the (I) attachment to the host cell and internalization into the host cell via clathrin-mediated endocytosis, (II) release of the viral genome into the cytosol, (III) translation of the viral proteins, (IV) replication of the genomic RNA, (V) virus assembly, (VI) maturation of the virions and (VII) the release of the viral progeny (see Figure 1.3).[58] Host ion channels are crucial for many infection stages.[3]

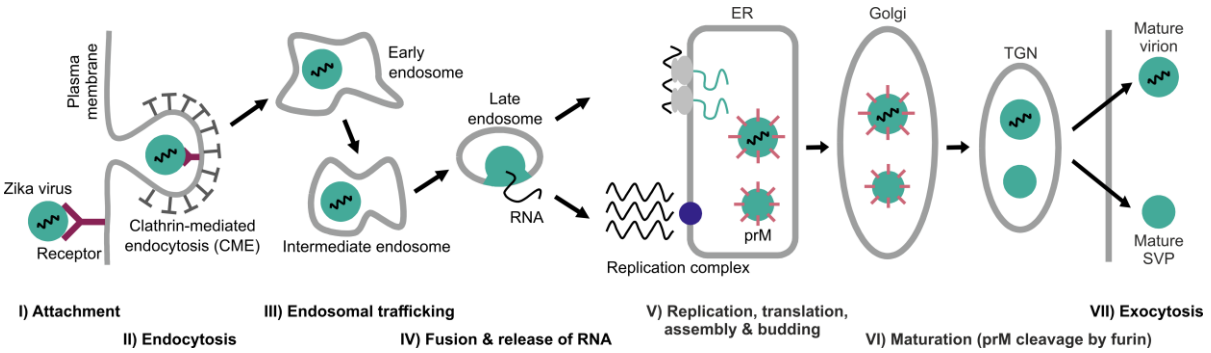

Figure 1.3: Schematic overview of the life cycle of Zika virus. For details on the individual steps, see text. ***Abbreviations:*** *CME: clathrin-mediated endocytosis, ER: endoplasmic reticulum, prM: pre-membrane protein, TGN: trans-Golgi network, SVP: subviral particle.*

I–IV: ZIKV attachment, endocytosis, endosomal trafficking, and fusion & release of RNA

Prior to infection, ZIKV particles diffuse along the cell surface.[46] Host cell attachment factors such as negatively charged glycosaminoglycans (GAGs), for example heparan sulfate and chondroitin sulfate, retain and concentrate viral particles on the cell surface and increase the probability of viral interaction with host cell entry receptors.[59] Binding to attachment factors is usually mediated by electrostatic interactions and relatively unspecific.[60] Interactions of ZIKV with entry receptors, such as C-type lectin receptors (e.g., DC-SIGN) is mostly mediated by the viral E protein.[46] ZIKV displays a relatively smooth, E-protein dominated surface (Figure 1.2).[51] Furthermore, partial ZIKV maturation (see VI–VII: Maturation and exocytosis) and dynamic E protein dimer motions (called “viral

breathing") expose otherwise buried surfaces thus facilitate interactions of viral proteins and lipids with a variety of receptors (and also attachment factors).[53,61] Phosphatidylserine receptors of the host cell TIM (T-cell immunoglobulin and mucin domain) and TAM (Tyro3, Axl, Mer) protein families can interact with ZIKV lipids.[46] The members of the TIM family bind to viral lipids directly while the members of the TAM family interact indirectly through mediators such as Gas6 (growth-arrest-specific protein 6) and protein S (ProS9).[62] Both the attachment factors and the host cell receptors contribute to the infection efficiency, thus it is often difficult to truly differentiate between their individual contributions.[60]

Host cell receptor binding of ZIKV particles is followed by clathrin-mediated endocytosis (CME).[46] This entry mechanism, which is used by ZIKV and numerous other enveloped viruses, offers many advantages over the direct release of viral genomes into the cytoplasm (performed by HIV-1 (human immunodeficiency virus 1) and herpes simplex 1, for example): the virus stays intact when attaching to the cell and no evidence remains at the cell surface (which can be detected by the host's immune system).[60] CME enables cellular uptake of viruses with a large size range from 30 nm (parvoviruses) to 400 nm (poxviruses).[60]

After ZIKV attached to one of the above-mentioned receptors, host adaptor proteins (such as AP2 (adaptor protein complex 2)) are recruited, inducing clathrin coat assembly and formation of membrane niches of ~100 nm.[63] Afterwards, the GTPase dynamin oligomerizes around the bud neck and cleaves the vesicle from the cell membrane.[64,65] The virus-containing intracellular vesicles are then transported along the cell cortex and microtubules to the endolysosomal system.[66] During trafficking, which is mediated by members of the Rab (Ras-associated binding) family of small membrane GTPases,[67] the clathrin coat is removed and the vesicles can now fuse with each other or are directed to early endosomes. These are characterized by the presence of Rab5, early endosome antigen 1 (EEA1) proteins and a lumenal pH of ca. 6.8–6.3.[68] In uninfected cells, the cargo is either sorted for degradation via multivesicular bodies (MVBs) and late endosomes (Rab7-positive, pH 6.0–6.8) to ultimately reach lysosomes (pH 4.5), or for recycling to the cell surface, exosomes, or the trans-Golgi network.[69–72] Vesicles typically reach early endosomes in less than 2 min, maturating and late endosomes in the perinuclear region after 10–12 min and lysosomes within 30–60 min.[60] During ZIKV infection, the low pH in late endosomes triggers irreversible conformational changes in the ZIKV E-protein, which concurrently transitions from a dimer to a trimer formation, thereby mediating fusion with the endosomal membrane. Ultimately, this leads to the release of the viral RNA into the cytosol.[73–77] Beyond a low pH, the fusion process is also affected by the endosomal lipid composition and viral maturity, since partial maturation exposes otherwise buried surfaces.[78–82]

Host ion channels and ion translocating membrane proteins play critical roles in all endocytosis steps. In early endosomal maturation, vacuolar-type ATPase (V-ATPase) pumps transport protons into the vesicles, leading to acidification.[83] Chloride influx through endosomal anion channels follows acidification to reduce the large positive intralumenal charge. This process is accompanied

by cation efflux by Na^+K^+/H^+ exchangers.[84–89] Generally, Calcium is involved in a variety of regulatory processes in the endolysosomal system, e.g. membrane fusion and fission, lipid trafficking and lysosomal activity.[90,91] Overexpression of the human ion TRPML2 (transient receptor potential mucolipin 2) channel, which is permeable for Ca^{2+} (and also other cations) was shown to increase the endosomal trafficking efficiency of ZIKV (please refer to section 1.7 for a detailed characterization of TRPML channels and a (putative) role of TRPMLs in infectious diseases).[92] For other viruses, for example Ebola virus (EBOV), Ca^{2+} also plays an important role during entry. EBOV enters host cells through endolysosomes positive for the intracellular cholesterol transporter Niemann-Pick C1 (NPC1) and the two-pore Ca^{2+} channel 2 (TPC2).[93] The change in Ca^{2+} and pH induces a reversible conformational transition in the EBOV glycoprotein GP2 (which is an important factor for receptor binding and viral entry). The resulting GP2 intermediate can bind to NPC1 which promotes the conformational transition into fusion-ready EBOV particles leading to release of the genome into the cytosol.[94]

V: RNA replication, translation, assembly & budding

After the release of the viral RNA from late endosomes, the translation process is initiated. The viral genome contains a 5'-cap-structure similar to cellular mRNA, which enables translation through the host-specific cap-dependent translation initiation machinery.[48,95] The N-terminus of the nascent polyprotein contains an ER (endoplasmic reticulum)-localization signal peptide (SP, see Figure 1.2). The growing viral polyprotein is co-translationally inserted into the ER.[53] NS2A, NS2B and NS4B contain several transmembrane sequences; PrM, E, NS1 and some extended stretches of NS2A, NS4A and NS4B are located in the ER lumen, while C, NS3 and NS5 are facing the cytosol. Subsequently, the polyprotein is processed by the viral protease complex NS2B-NS3 and host cell proteases which cleave bonds on the cytosolic site and in the ER lumen, respectively.[47,48]

After cleavage, ZIKV non-structural proteins form "replication factories" (RFs) on the ER membrane, building a replication-favorable microenvironment in membrane invaginations.[96,97] Both African and Asian strains induce the formation of RFs of similar architecture.[96] This segregation might enable the accumulation of metabolites required for ZIKV RNA replication and at the same time protect the viral RNA from cellular nucleases and cytosolic antiviral RNA sensors. Furthermore, it increases the speed and efficiency of the replication process.[98] Importantly, ZIKV infection not only leads to ER re-arrangements but also causes drastic re-organization of the host cell cytoskeleton.[96]

Membrane invaginations and ER-remodeling, which can be extensive, are a common feature of flavivirus infection.[96,99] In ZIKV infected cells, ER membrane curvature can be induced by NS1 dimers, which attach to the lumenal site and insert three hydrophobic regions into the membrane.[100] Via this mechanism, a negative curvature is created that evolves into spherical invaginations.[100] For DENV infection, NS4a was identified as an important factor for ER membrane alterations.[101]

Flaviviruses also rely on host factors for RF formation. DENV NS3 recruits fatty acid synthase to the replication sites to produce lipids which are integrated into the ER membrane.[102] Furthermore, flavivirus RFs are enriched with cholesterol, which improves membrane fluidity.[103]

The ER membrane invaginations allow the assembly of the ZIKV replication complex: viral RNA, the helicase NS3 and polymerase NS5 are associated with the cytosolic site of the ER membrane, the membrane proteins NS2A, NS2B, NS4A and NS4B are spanning the lipid bilayer and NS1 dimers stabilize the replication complex from the ER lumen via interactions with NS4A and NS4B.[104] The genomic (+)RNA is transcribed into a (−)RNA intermediate which serves as a template for progeny (+)RNA.[47,48] The NS5 protein contains a C-terminal RNA-dependent RNA polymerase (RdRp) domain and a N-terminal methyltransferase domain, which is responsible for transferring the mRNA cap.[105]

In studies analyzing the architecture of the flavivirus replication factories, a ca. 10 nm wide opening to the cytosol has been reported which might allow the exit of (+)RNA to be used for either polyprotein synthesis or packaging into virus particles which are budding into the ER lumen in proximity.[106] After cleavage of the ZIKV polyprotein, viral C proteins are located at the cytosolic site of the ER membrane, and the viral surface glycoproteins E and prM are associated with the lumenal site of the ER membrane.[47] After freshly transcribed viral (+)RNA has escaped the replication factories, it can interact with C proteins and together with the surface proteins E and prM, a nascent viral particle buds into the ER lumen.[47]

The ER is also the main intracellular Ca^{2+} storage organelle and ER Ca^{2+} channels have been found to be an important factor for efficient flavivirus replication.[107] In a screening of FDA (Food and Drug Administration)-approved drugs against JEV, three of the five most potent antiviral acting substances were inhibitors of voltage-gated Ca^{2+} channels (VGCCs) and affected viral replication, rather than entry.[108]

VI–VII: Maturation and exocytosis

The nascent virions accumulate in the lumen of the ER, are incorporated into COPII (coat protein complex II) vesicles and subsequently delivered to the Golgi network. Regular COPII vesicles have a diameter of ca. 60–100 nm, barely sufficient for even a single immature flavivirus particle with a size of ca. 50 nm. To increase transport efficiency, ZIKV virions associate into large paracrystalline lattices and/or clusters inside the ER and engage multiple cargo receptors for entering the secretory pathway. At least some of these formations are transported in their entirety to the plasma membrane.[96,109,110]

EM images of ZIKV infected cells suggest that the well-defined stacks of the Golgi cisternae, which are typical for non-infected cells, are no longer visible.[96,109,110] Presumably, the Golgi network is remodeled to form the membranous compartments of the ZIKV replication/assembly machinery,

thereby creating a new chimeric ER-Golgi-like structure. The low pH of the Golgi apparatus serves an important function for the glycosylation pattern of the flavivirus envelope proteins and the furin-mediated cleavage of prM. The cleavage of M leads to a rearrangement of E proteins on the virion surface.[111–114] However, prM cleavage can be inefficient, resulting in partially mature infectious virions.[53]

After viral maturation in the Golgi apparatus, virions are delivered to the extracellular space through the fusion of membranous carriers, which contain virions, with the plasma membrane.[47] EM studies identified not only small vesicles containing single virions but also large vesicles containing multiple virions close to or fusing with the plasma membrane.[109,115] None of the membranous carrier species were clathrin-coated, thus ruling out the clathrin-dependent sorting pathway from transport of infectious viral particles to the plasma membrane.[47] In addition, ZIKV was shown to hijack extracellular vesicle tetraspanin pathways for cell-to-cell transmission.[116]

1.4 Zika virus antiviral therapies

Although ZIKV infections are often asymptomatic or produce relatively mild illness with an uneventful recovery in immunocompetent individuals, the need for effective antiviral treatment is high, because ZIKV infection causes a risk for neurological complications in developing fetuses. Therefore, an anti-ZIKV drug should fulfill several requirements. Usage should be safe for both the mother and the fetus during pregnancy. In addition, the drug must be able to cross the placental and the blood-brain barrier. In addition, the spread of *Aedes* mosquitoes beyond tropical regions because of climate change increases the need for effective treatment options. Although intensive efforts have been made, no antiviral therapies or prophylactic vaccines against ZIKV are available currently.[12]

Several Zika vaccine candidates have been developed, including nucleic acid vaccines, inactivated vaccines, viral-vectored vaccines and attenuated vaccines.[117] As of 2020, 13 vaccine candidates based on various platforms have entered 17 human phase I clinical trials, with one entering phase II clinical trial.[117] However, ZIKV vaccine development faces several difficulties. The number of ZIKV infections has significantly declined in recent years, making not only testing but also funding of vaccine candidates challenging.[117] ZIKV, DENV and other flaviviruses share structural and genetic similarities, and generate poorly neutralizing cross-reactive antibodies, which can cause antibody-dependent enhancement (ADE) of infection and disease.[117–119] This means that antibodies, which may result from prior infection or vaccination, can enhance viral entry and replication during a following infection.[120] For closely related Dengue virus (DENV), few vaccines are available. The first vaccine was Dengvaxia®, which was licensed in 2015.[121] However, safety concerns arose in the third year of the phase III clinical trial, because increased hospitalizations and severe Dengue cases were observed in the youngest, non-immune vaccine recipients.[122] ADE was considered as one potential cause.[123]

Therefore, ADE is one of the major obstacles to flavivirus vaccine development. This factor also needs to be considered for future ZIKV vaccines.

Currently, treatment of ZIKV infections aims at alleviating the symptoms and includes rest and fluid intake to prevent dehydration in infected patients.[124] Acetaminophen can be used to reduce fever, headache and myalgia, while anti-histamines are used against pruritic rashes.[124,125] In contrast, acetylsalicylic acid and non-steroidal anti-inflammatory drugs are contraindicated because of an increased risk of hemorrhagic complications reported with other flaviviral infections as well as Reye's syndrome after viral infection in children and teenagers.[27]

Beyond vaccine development, different approaches can be used for discovering new potent antivirals, for example screening of compound libraries or repurposing of approved drugs with known efficiency against other diseases.[125] Additionally, natural products and antibody-based candidates have been tested.[126–128]

ZIKV antiviral compounds can be classified in direct-acting antivirals (Table 1), targeting the viral proteins, and host-directed antivirals (Table 2), which interfere with cellular process required for successful ZIKV infection.[125] Direct-acting antivirals for example target the viral RNA-dependent RNA polymerase (RdRp) and methyltransferase catalytic domain of NS5, which is responsible for transferring the mRNA cap.[125] Other compounds aim to inhibit the NS3 helicase or the NS2B-NS3 protease which is needed for processing of the viral polyprotein.[125] Certain nucleoside analogues/derivatives are safe for use in humans, as they target viral and not cellular polymerases, which can differ significantly in substrate specificity.[129]

Table 1: Examples of direct-acting ZIKV antivirals. This overview has been adapted from Baz *et al.*[125]

Direct-acting antivirals	
Name	**Mode of action**
7-deaza-2-CMA	RdRp inhibitor
2-CMA, 2-CMC, 2-CMG, 2-CMU	RdRp inhibitor
Favipiravir	RdRp inhibitor
NITD008	Pyrimidine synthesis inhibitor
Sofosbuvir	RdRp inhibitor
Galidesivir	RdRp inhibitor
Myricetin, quercetin, luteolin, isorhamnetin, apigenin, curcumin	NS2B-NS3 protease inhibitor
Niclosamide, nitazoxanide	NS2B-NS3 protease inhibitor
Temoporfin	NS2B-NS3 protease inhibitor
Novobiocin	NS2B-3 protease inhibitor
Suramin	NS2B-3 protease inhibitor

Abbreviations: *7-deaza-2-CMA (7-deaza-2'-C-methyladenosine), RdRp (RNA-dependent RNA polymerase), 2-CMA (2'-C-methyladenosine), 2-CMC (2'-C-methylcythydine), 2-CMG (2'-C-methylguanisine), 2-CMU (2'-C-methyluridine), NS (non-structural protein)*

In addition to addressing viral proteins, host-targeting antivirals also have several advantages.[125] For example, these compounds can be used to disable processes which are employed by multiple viruses. Accordingly, they have the potential to act as broad-spectrum antivirals.[125] In addition, host-targeting antivirals are less prone to incur drug resistance which can be caused by mutations in the viral genome.[130] Any molecule or pathway involved in the steps of the viral life cycle (including attachment, entry, fusion, replication, maturation and release, can be targeted.[125] For example, chloroquine was used for decades as the primary and most successful drug against malaria[131] and was repurposed to test its antiviral potential against ZIKV.[132] Chloroquine is a 4-aminoquinoline and a weak base. The unprotonated form diffuses across cell membranes to acidic vesicles and compartments such as endosomes, lysosomes, or Golgi vesicles and increases their pH.[133] This way, pH-dependent steps in the life cycle of viruses can be inhibited. Chloroquine was shown to restrict not only ZIKV,[132] but also HIV,[134] influenza A virus (IAV),[135] DENV,[136] JEV[137] and WNV[138] infections. Nonetheless, due to the lack of approved ZIKV antiviral therapies, a more detailed understanding of the ZIKV life cycle is still required.

Table 2: Examples of host-targeting ZIKV antivirals. This overview has been adapted from Baz *et al.*[125]

Host-targeting antivirals	
Name	**Mode of action**
Ribavirin	Several mechanisms, including purine synthesis inhibition
Merimepodib, mycophenolic acid	IMPDH inhibitors
Azathioprine	Purine synthesis inhibitor
6-azauridine, 5-fluorouracil	Pyrimidine synthesis inhibitor
Lovastatin	HMG-CoA reductase inhibitor
Bafilomycin A1	Inhibition of V-type ATPase
Chloroquine	Inhibition of pH-dependent steps of viral life cycle
Saliphenylhalamide	Viral entry inhibitor
Obatoclax mesylate (GX15-070)	Bcl-2 protein inhibitor
PHA-690509	Cyclin-dependent kinase inhibitor
MK-801, agamatine, ifenprodil	Neuronal cell death inhibitor
Memantine	Neuronal cell death inhibitor

Abbreviations: *IMPDH (Inosine monophosphate dehydrogenase), HMG-CoA (3-hydroxy-3-methyl-glutaryl-coenzyme A reductase), V-type ATPase (vacuolar-type adenosine triphosphatase), Bcl-2 (B-cell lymphoma 2)*

1.5 Ion channels in health and disease

Ion channels play not only an important role in viral infections, but they are also crucial for almost all cellular processes in living organisms. The immense biological significance of ion channels is highlighted by their evolutionary steadiness.[139] Ion channel-mediated signaling is one of the most ancient forms for cells to sense their environment.[139] In humans, the "channelome" accounts for up to 1% of the whole genome[140] and contains over 300 ion channels[141]. Ion channel-mediated flux of ions across membrane barriers can be used to study the channels's activity with electrical recording techniques. The patch clamp technique for high-resolution current recordings was introduced by Hamill *et al.* in 1981[142] before the first ion channel structure[143] was revealed around 20 years later. More recently, breakthroughs in high resolution imaging techniques, especially the possibility to determine the structure of large protein complexes using cryo-EM, has significantly improved the functional and structural understanding of ion channels. The incessant relevance of ion channels for the scientific community was highlighted in 2021 by the shared Nobel Prize for Physiology and Medicine awarded to David Julius and Ardem Patapoutian for their groundbreaking work on the vertebrate thermo-sensory TRPV1 (transient receptor potential vanilloid 1) and mechanosensory Piezo ion channels.[144,145]

Ion channels are crucial for essentially every physiological process and can be found in the membranes of all cell types. Around 19% of current FDA-approved drugs work by modulating ion channel activity, only drugs targeting G-protein coupled receptors are more widely used.[107,146,147] Among many others, ion channels regulate membrane potential, cell volume, organelle ion homeostasis and mitochondrial function.[107,148–150] They conduct not only Na^+, K^+, Ca^{2+} and Cl^-, but there are also ion channels permeable for metal ions such as iron (Fe^{2+}), zinc (Zn^{2+}) and magnesium (Mg^{2+}), or protons and water molecules (see Table 3 for an overview of intracellular and extracellular ion concentrations).[151] Cation channels have been intensely studied for a long time due to their essential role in regulating the membrane potential in excitable cells such as neurons and muscles as well as in non-excitable cells such as lymphocytes and endothelial cells.[152,153] On the other hand, anion channels are involved in functions such as inhibitory synaptic transmission through hyperpolarization and epithelial Cl^- flux.[154]

Table 3: Concentrations of ions intracellular and in the external environment. This table was adapted from Melkikh and Sutormina.[155]

Ion	Intracellular concentration (mM)	Extracellular concentration (mM)
Na^+	15	142
K^+	150	4
Cl^-	5	120
Ca^{2+}	10^{-4}	1
Mg^{2+}	1	0.5
$HCO3^-$	8	27
Nonpenetrating anions	155	0

A large variety of signals (e.g., mechanical stress, heat, membrane potential, extracellular transmitters, and intracellular signal molecules (Ca^{2+}, phospholipids, cyclic nucleotides or G-proteins) can initiate or inhibit cellular ion conductance.[151] The underlying mechanism can be described as “gating” and leads to changes in the structure of the ion channel pore, potentially involving multiple conformational changes of the integral membrane protein.[156–167] Some ion channels have modular domains which sense the respective stimulus and modulate changes in the pore domain via domain-domain interactions, in other cases sensor and ion channel pore are not directly linked. In addition to gating, the selectivity of a channel is important for allowing only particular ion species to cross the membrane rapidly and preventing others from passing at the same time.[151] Responsible for selectivity is a narrow filter-like structure in the center of the pore (see Figure 1.4). The interaction of the ion with amino acids in the pore constriction point leads to substitution of some or most of the water molecules surrounding the ion in solution.[143,168–172] Consequently, the strength of the ion-filter interaction is the key for selectivity.[151] In an optimal scenario, the ion sheds

its hydration waters, moves rapidly through the filter, and re-solvates on the other side of the membrane. In this way, ion channels can enable the flux of ~10^7 ions/sec along an ion gradient. In contrast, an ion that interacts too favorably with the filter will become stuck[173] and an ion that cannot make energetically favorable interactions is not able to shed its hydration waters and enter the filter.[151] Selectivity is also crucial for the direction of ion conductance.[151]

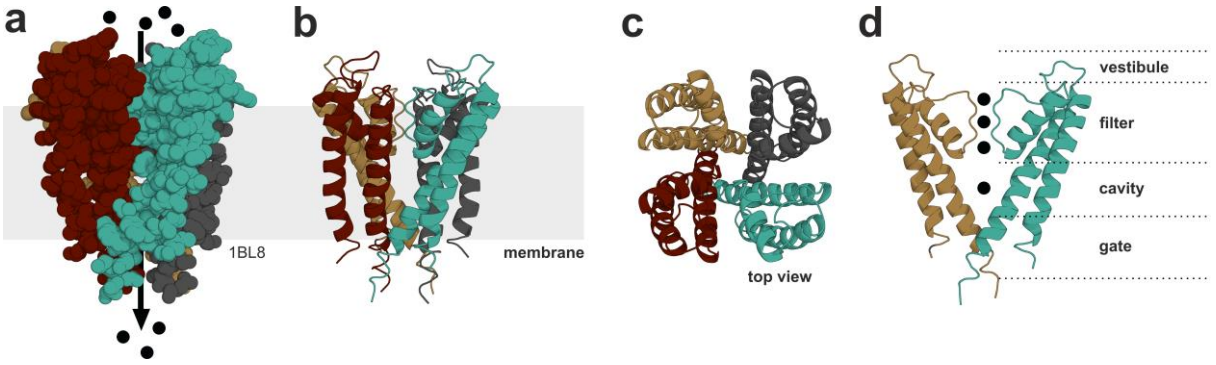

Figure 1.4: Structural determinants of ion channel selectivity and gating. Crystal structure of the KcsA potassium channel from *Streptomyces lividans* (pdb 1BL8, 3.20 Å).[143] Four monomers (shown in different colors) form a tetrameric pore structure ((**a**) and (**b**) side view, (**c**) top view). Potassium ions are indicated as black dots. Important structural features are highlighted in (**d**): the extracellular vestibule, selectivity filter, pore cavity and intracellular gate (only two monomers are shown for clarity).

Ion channels do not share a general signature sequence and may have evolved *de novo* several times in response to different physiological needs.[174] Comparative genome analysis indicated that most human ion channel families have their origins in the early metazoan.[174] The major classes of mammalian ion channels are: Kir (inward rectifier K^+) channels, voltage-gated cation channels, CLC family chloride channels, C-loop neurotransmitter receptors, P2X purinoreceptors and ASIC (acid sensing ion channel)/DEG (degenerin) family sodium channels.[174] Mammalian ion channels differ largely in their transmembrane topology and amount of subunits, ranging from 6–36 transmembrane domains 2–5 subunits.[174] Ion channels are either inward or outward rectifying. Inward rectification means that inward current flow is more easily allowed than an outward current. In contrast, outward rectification means that outward current flow is more easily allowed than outward current flow.[175]

Due to the complex structure and regulation of ion channels, already mild mutation-based changes might lead to devastating diseases, so-called “channelopathies”, which can affect the cardiovascular, musculoskeletal, nervous and immune systems.[148,150,176,177]

Disease-associated mutations can have several effects on ion channel properties. For example, they can affect the number of functional channels or the gating mechanism or lead the loss of ion channel selectivity.[151] One well-characterized example where the deletion of one single amino acid leads to a fatal inherited disease by reducing the ion channel number at the plasma membrane, is cystic fibrosis (CF). Cystic Fibrosis Transmembrane Conductance Regulator (CFTR) is an ATP-gated anion channel belonging to the ATP Binding Cassette (ABC) protein superfamily.[178–184] Here, the most

common mutation leading to CF is the deletion of phenylalanine 508 (ΔF508), which results in a failed glycosylation pattern due to an improperly folded conformation of CFTR.[185] This conformation is prevented from progressing to the Golgi where it would have been glycosylated by the ER quality control machinery.[186] The ΔF508 folding defect is so severe that the folding efficiency drops below 1%.[187] As a consequence, the number of mutant channels in the apical membrane of the pulmonary epithelial cells is reduced and the chloride transport into the airways is deficient, which is crucial for the transport of ions and water for the maintenance of mucus hydration and effective mucociliary clearance.[188]

Mutations that lead to a loss of ion selectivity have been described for the G-protein-gated inwardly rectifying potassium channel Kir3.4/GIRK4.[189] Disease mutations in this homotetrameric channel are either located directly in the selectivity filter or play a role in the stabilization of the filter's structure. This leads to a loss of potassium selectivity resulting in significant sodium currents and depolarization of the cell membrane.[189,190] In the glomerulosa cells in the adrenal cortex of the kidneys, membrane depolarization opens voltage-gated calcium channels providing Ca^{2+} influx which triggers production of the hormone aldosterone.[191] Constant aldosterone secretion can lead to hypertension that is resistant to treatment, hypokalemia and metabolic alkalosis. Severe hypertension can be a strong risk factor for cardiovascular events, for example stroke and myocardial infarction.[192]

Many channelopathies are associated with increased or decreased channel activity. For example, certain mutations in the CHRNA1 (cholinergic receptor nicotinic alpha 1) subunit of the muscle acetylcholine receptor can result in prolonged channel activation.[193] Muscle acetylcholine receptors contain of five subunits: two alpha subunits and one each of the beta, gamma and delta subunits.[194] In mammalian muscles, binding of acetylcholine to CHRNA1 leads to Na^+ influx and postsynaptic depolarization at motor endplates.[195] Therefore, mutations in CHRNA1 can lead to forms of congenital myasthenic syndromes characterized by fatigability and muscle weakness.[195,196]

Several inherited diseases are also caused by mutations of transient receptor potential (TRP) channel family members.[197] For a more detailed introduction to TRP channels, please refer to the following section. In brief, gain-of-function mutations in TRPA1 (ankyrin 1) have been linked to familial episodic pain syndrome.[198] Loss-of-function mutations in TRPML1 (mucolipin 1) lead to the lysosomal storage disorder Mucolipidosis type IV (MLIV, see section 1.7).[199,200] Mutations in TRPV4 (vanilloid 4) cause diseases which affect the skeletal and the peripheral nervous system, for example Charcot–Marie–Tooth disease type 2C.[201] Interestingly, these mutations may cause altered interactions with other proteins (e.g. the cytoskeletal remodeling GTPase RhoA) and lipids.[202–207]

1.6 Transient receptor potential (TRP) channels are an important superfamily of eukaryotic cation channels

TRP channels are a group of unspecific cation channels and particularly well-known for their function in the sensory perception of various organisms.[208] In fungi and animalia, TRP channels are found in all cellular membranes except nuclear envelope and mitochondria.[209] They have not been found in bacteria, chromista and plantae.[209]The founding member of this family is the *Drosophila* ion channel TRP.[210] Mutations in the *trp* gene led to visual impairment in *Drosophila*.[211] Mutant flies displayed a defect in light induced Ca^{2+} flux resulting in a transient rather than a continuous neuro-electrical response to persistent intense light as was the case in wild type (WT) flies.[212] Furthermore, it was observed that visual transduction in flies is dependent on phospholipase C (PLC).[213] Together this indicated that the encoded protein is a Ca^{2+} channel and resulted in the name "transient receptor potential".[214]

Structure, function, and regulation of TRP channels

TRP channels can be grouped into eight subfamilies based on sequence similarity: the six group 1 TRPs (TRPC (canonical), TRPV (vanilloid), TRPM (melastatin), TRPS (soromelastatin), TRPN (NOMPC), and TRPA (ankyrin)) and two group 2 TRPs (TRPP (polycystin) and TRPML (mucolipin)). TRPY which is expressed in yeast and only distantly related to the other TRPs, can be classified as an nineth subfamily.[208] A phylogenetic tree of the TRP superfamily is provided in Figure 1.5. The TRPC subfamily displays the greatest sequence similarity to *Drosophila* TRP.[214] In humans, six subfamilies are expressed (TRPC, TRPV, TRPM, TRPA, TRPP and TRPML). Of particular relevance for this thesis are the endolysosomal TRPML ion channels which play important roles in the immune system and viral infections and will thus be discussed in more detail below.

All members of the TRP superfamily share general structural features such as six transmembrane (TM) spanning helices (S1 through S6), cytosolic N- and C-termini and a re-entrant loop between S5 and S6 which is forming the channel pore (Figure 1.6).[215,216] Besides these general structural similarities, TRP channels strongly vary in size and the structural organization of the N- and C-termini as well as within the loops that connect the transmembrane helices (Figure 1.5). Although the progress in imaging techniques (e.g. cryo-EM) also increased the understanding about TRP structure and function, many questions remain open regarding their regulation, dynamics and domain communication.

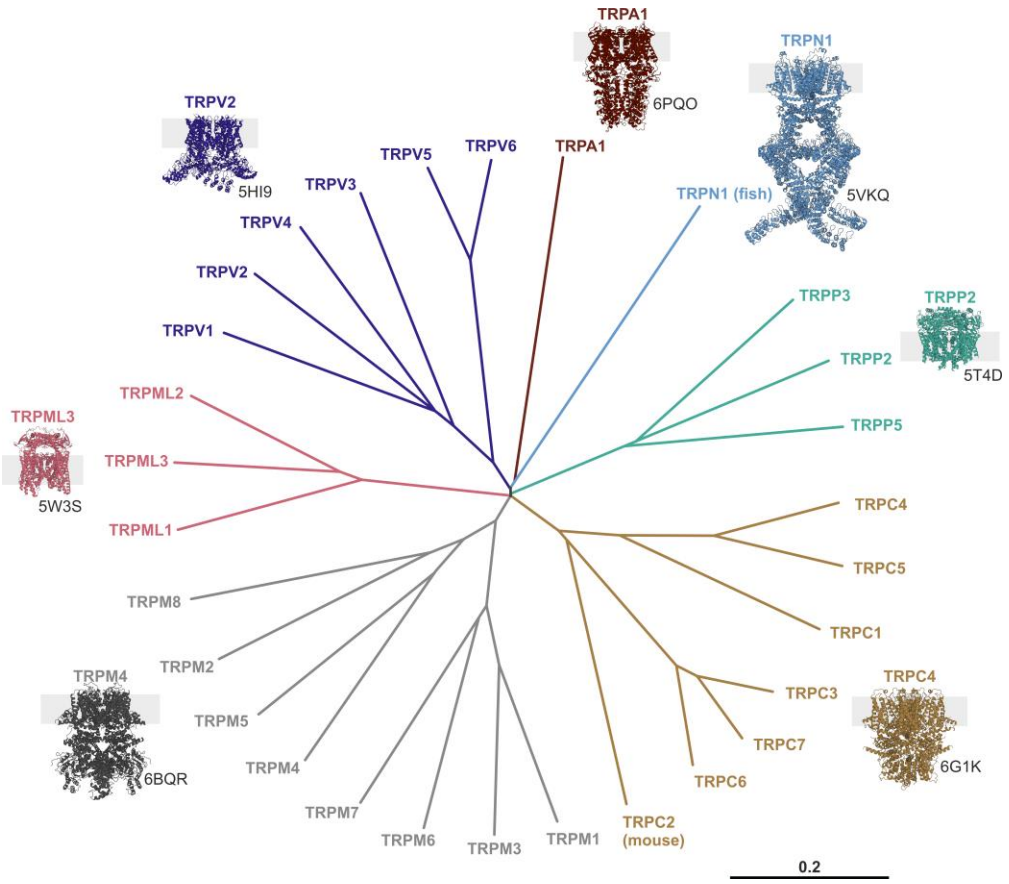

Figure 1.5: Phylogenetic tree of the TRP channel family. This figure was modified from Nilius and Owsianik.[209] The TRP subfamilies are represented by different colors. The authors aligned protein sequences using ClustalW2 at the EMBL-EBI server, PAM matrix was used for computing the phylogenetic distances (scale bar represents 0.2 substitutions) and NJplot for obtaining the unrooted tree. Structures of TRPA1 (pdb 6PQO)[217], TRPC4 (pdb 6G1K)[218], TRPM4 (pdb 6BQR)[219], NOMPC (pdb 5VKQ)[220], TRPV2 (pdb 5HI9)[221], TRPML3 (pdb 5W3S)[222] and TRPP2 (pdb 5T4D)[223] were added to point out high structural variance of N- and C-termini. In 2020, the ancient TRPS family was reported, which is not shown in this phylogenetic tree.[224] Himmel *et al.* used a phylogenetic approach to identify two eumetazoan TRPM clades and the TRPS family.[224]

TRP channels can be activated by a variety of different stimuli. For example, the TRP vanilloid 1 (TRPV1) channel is stimulated by ligands such as capsaicin (active compound from hot chili peppers), but also increased temperature.[225] In some TRP channels, even enzymatic domains can be found, i.e. TRPM6 and TRPM7 contain an atypical serine/threonine protein kinase domain, with a 3D structure resembling typical kinases despite a strong variation in amino acid sequence.[226,227]

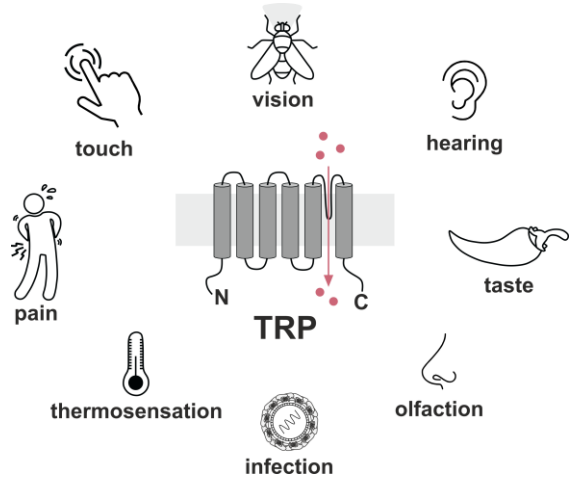

Figure 1.6: TRP channels contribute to a variety of sensory perceptions in different organisms. This includes vision in drosophila flies, hearing, touch, taste, pain, olfaction and thermosensation. The role of TRP channels in viral infections has emerged during the last years.

TRP channel-mediated modulation of intracellular Ca^{2+} homeostasis affects various processes such as apoptosis, membrane trafficking and autophagy.[215,228] These altered Ca^{2+} concentrations do not only originate from extracellular Ca^{2+} but also from intracellular storages, e.g. the ER and lysosomes.

TRP channels in viral infections

As mentioned above, altered Ca^{2+} levels also play an important role in viral entry, replication and budding. Recently, roles of TRP channels in the immune system and pathogen interactions, in particular viral infectivity depending on calcium flux, have been described. With the exception of the TRPP subfamily, members of all mammalian TRP subfamilies have been reported to be involved in viral infections.[229] For example, knockdown of TRPM2 in mouse pulmonary microvascular endothelial cells significantly reduced H9N2 influenza virus-induced ROS (reactive oxygen species)-production, DNA damage and apoptosis.[230] After human rhinovirus (HRV) infection of neuroblastoma cells, the expression of TRPA1 (which is widely expressed in several neuronal and non-neuronal cells) is upregulated at an early timepoint of 2 hpi (hours post infection) until 24 hpi.[231] TRPV4 is an important host factor during infection with Dengue (DENV), Zika (ZIKV) and hepatitis C virus (HCV), which are all members of the *Flaviviridae* family.[232] TRPV4 affects viral RNA metabolism through regulation with DDX3X (DEAD-box helicase 3 X-linked). In addition, TRPV4 colocalizes with DDX3X and mediates its nuclear localization. Application of the synthetic TRPV4 inhibitor HC067047 reduced DENV, ZIKV and HCV infectivity in Huh7 cells.[232] In addition, the TRPML family was shown to play a remarkable role in flavivirus infection.[233] This topic will be discussed in detail in section 1.7.

1.7 The role of human TRPML ion channels in viral infections and immune response

Parts of this chapter have been published in: Viet, K. K. *et al.* Structure of the Human TRPML2 Ion Channel Extracytosolic/Lumenal Domain. *Structure* **27**, 1246-1257.e5 (2019).

The majority of all TRP channels are found in the plasma membrane.[208] In contrast, the members of the human TRPML family regulate vesicular calcium release in the endolysosomal system and are involved in signal transduction, membrane trafficking and autophagy.[215,234] Since many viruses use endocytosis to enter host cells (see section 1.3), ion channels within the endolysosomal system play a potential role in the life cycle of endocytosed viruses. Indeed, TRPML channels have been linked to flavivirus infection, while TPC2 is involved in the cell entry process of Ebola virus, as mentioned in section 1.3.[92,93,235,236] Furthermore, the relevance of TRPML channels for the immune response has emerged in recent years[233], implicating these fascinating ion channels with a more general role in host/pathogen interactions.

While *Drosophila melanogaster* and *Caenorhabditis elegans* express only one TRPML protein, the mammalian TRPML family includes three members: TRPML1, TRPML2 and TRPML3.[215] The proteins share approx. 40% pairwise amino acid sequence identity levels[237] and have overlapping functional and structural properties.[234] TRPML channels are strongly inward rectifying and permeable to various cations (Na^+, K^+, Ca^{2+}, Mg^{2+}, Zn^{2+}, etc.).[238] TRPML1, TRPML2 and TRPML3 vary in their subcellular localization in the endolysosomal system (and plasma membrane, to a smaller extent) and in their tissue expression. Human TRPML1 consists of 580 amino acids and is ubiquitously expressed and located primarily in late endosomes and lysosomes.[199] It was first identified in a disease-related context: Mutations in *mcoln1*, the TRPML1 encoding gene, lead to the rare autosomal recessive disorder Mucolipidosis type IV (MLIV),[199,239] which was incidentally also the first neurological disease associated with a TRP channel. Until now, there are more than 20 MLIV causing mutations reported, most of them loss-of-function mutations.[240] Inactivation of TRPML1 results in the accumulation of heterogenous lipids and proteins in storage bodies and disruption, leading to cell death.[239,241] These effects can be observed in every tissue and every organ.[242] Patients suffering from MLIV display severe cognitive impairment and eye abnormalities.[239]

TRPML2 is the least characterized member of the TRPML family. Human TRPML2 contains 566 amino acids.[243] TRPML2 mRNA was mainly detected in lymphocytes and other cells of the immune system.[243] A potential function of TRPML2 in the innate immune response and viral infections has been suggested (see following sections). Subcellularly, TRPML2 is present in recycling endosomes, late endosomes and lysosomes, and, at low levels, in the plasma membrane.[243–245] In contrast to TRPML1 and TRPML3, TRPML2 has been identified as a mechano- and hypotonicity-sensitive channel in endolysosomal organelles.[246]

TRPML3 is mainly expressed in the kidneys, lungs, and organs of the endocrine system.[247] It is subcellularly localized in early and late endosomes, lysosomes and in the plasma membrane.[248] Human TRPML3 contains 553 amino acids. Gain-of-function mutations in *mcoln3*, the TRPML3 encoding gene, lead to the *varitint-waddler* phenotype in mice, which is characterized by hearing loss, pigmentation defects and circling behavior.[249] The physiological function of TRPML3 remains unclear, but potential roles in pain sensation,[250] sodium homeostasis[251] and non-lytic expulsion of bacteria have been suggested.[252]

Four TRPML protomers form a homo- or heterotetrameric channel.[253] Near full-length structures of all mammalian TRPML channels have been published during the last years.[222,237,254–258] Similar to other members of the TRP superfamily, one TRPML channel protomer contains six transmembrane spanning helices (S1–S6) forming the transmembrane domain (TMD). The TMD consists of the S1–S4 bundle and the ion channel pore formed by S5 and S6 (Figure 1.7).[253]

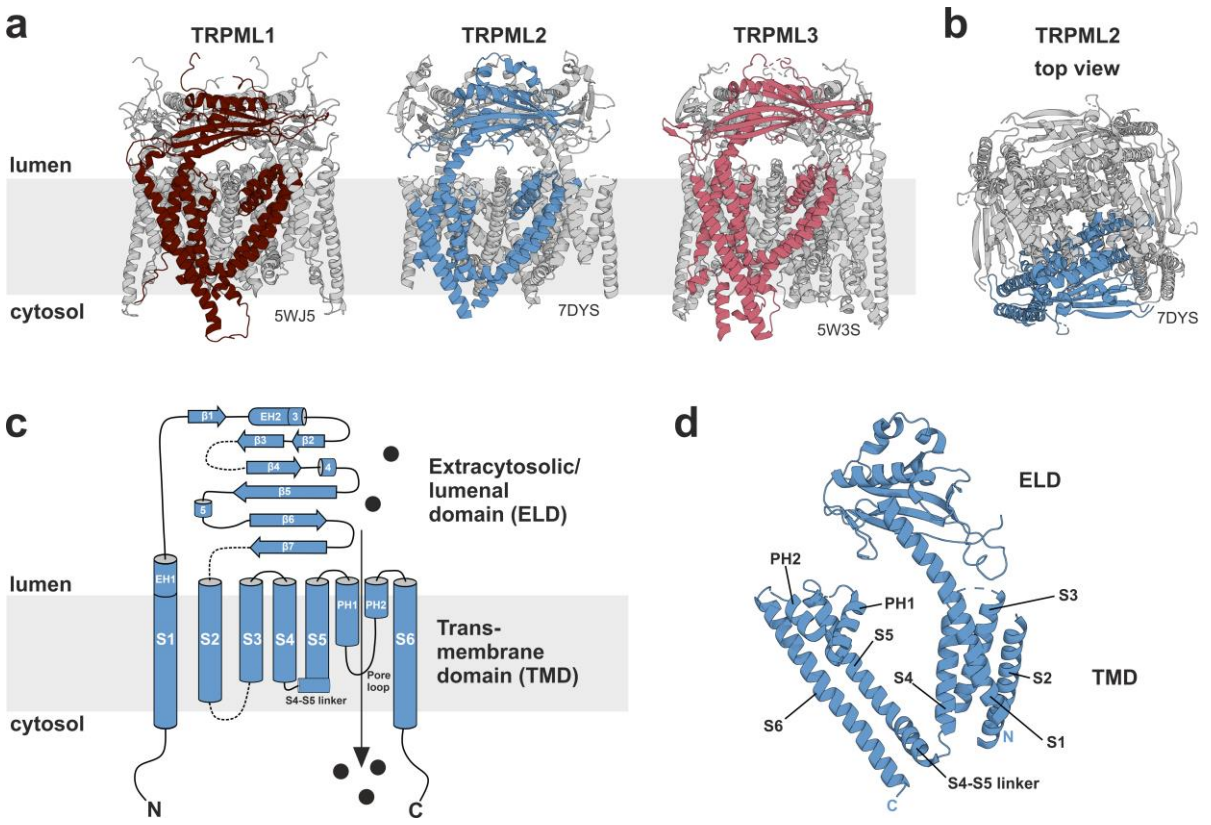

Figure 1.7: Structure of TRPML channels. (**a**) Structure of human TRPML1 at pH 7.0, 3.72 Å (pdb 5WJ5);[254] structure of mouse TRPML2 at pH 7.4, 3.14 Å (pdb 7DYS);[258] structure of human TRPML3 at pH 7.4, 4.06 Å.[237] One subunit of each tetrameric channel is highlighted in bright colors. (**b**) Tetrameric TRPML2 ion channel (pdb 7DYS), top view, central ion pore visible. (**c**) Topology model of one TRPML2 monomer, based on the structure of mmTRPML2 (pdb 7DYS) (**d**) Structure of one mmTRPML2 protomer (pdb 7DYS).

The cytosolic N- and C-termini range from 61–72 amino acids and are relatively short in comparison to other members of the TRP superfamily[259] and contain lipid and protein binding sites.[260,261] TRPML channels are activated by phosphatidylinositol 3,5-bisphosphate ($PI(3,5)P_2$), which is commonly found in endolysosomal membranes.[260] At the TRPML1 N-terminus, a polybasic patch with many positively charged amino acids (arginine and lysine) was identified as a potential binding domain for $PI(3,5)P_2$. If this polybasic domain is mutated, $PI(3,5)P_2$ regulation is lost.[260] At the plasma membrane, TRPML1 is inhibited by phosphatidylinositol 4,5-bisphosphate ($PI(4,5)P_2$), the putative binding domain is located within the same polybasic domain.[261] TRPML1 is directed to endosomes and lysosomes via two di-leucine motifs located in the N- and C-terminus.[262] In close proximity to the C-terminal di-leucine motif, TRPML1 contains three cysteine residues, which might be palmitoylated. Potentially, this could improve the association of TRPML1 with the membranes of the endolysosomal system.[262] The di-leucine targeting motifs of TRPML1 are less conserved in TRPML2 and completely absent in TRPML3. Instead, an EXXLL motif (another putative endolysosomal targeting sequence) can be found at the N-terminus of most TRPML3 species.[251]

S1 and S2 are connected through the extracytosolic/lumenal domain (ELD), which constitutes around one third of the whole channel and is a structural hallmark of the TRPML family. The ~100 kDa domain has also been termed the "I–II" linker,[263] as it is located between transmembrane helices S1 and S2 or the "polycystin–mucolipin domain".[257] The physiological role of this domain remains elusive. For TRPML1, interactions of the ELD with Hsc70 (heat shock cognate protein of 70 kDa) and with Hsc40 (heat shock cognate protein of 40 kDa) have been described.[264] Furthermore, a serine-lipase activity has been suggested for the TRPML1 ELD,[200,265] which seems highly unlikely in the light of the available structures and lipid-interaction experiments which have been carried out by [redacted] in the [redacted] group (unpublished data). The TRPML1 ELD contains four possible glycosylation sites (AAs: 159, 179, 220, 230) and linked sugars are at least partly sialylated in the Golgi.[266] Kiselyov *et al.* suggested a potential cleavage site in the ELD and that cleavage by cathepsin B might lead to inactivation of the channel.[266] The physiological relevance of this finding is currently unclear but may display an additional mode of TRPML1 regulation limiting the duration of channel activity. Unregulated TRPML1 activity may otherwise lead to a misbalanced ion homeostasis.

The TRPML ELD is exposed to different conditions (for example Ca^{2+} concentrations and pH values), as it faces either the extracellular space or the endolysosomal lumen, depending on the channel's cellular localization.[208] Typical extracellular Ca^{2+} concentrations reach up to 2 mM at pH 7.4, while reported numbers for early endosomes are 3 µM – 2 mM at pH 6.0, for late endosomes ca. 0.5 mM at pH 5.5 and for lysosomes ca. 0.5 mM at pH 4.5.[238] The structure of TRPML ELDs at different pH values have been characterized in isolation for TRPML1[263] and in the context of the full-length protein in TRPML1, TRPML2 and TRPML3 as well as in TRPP channels.[222,237,254–257,267,268] Prior to the publication of the mouse TRPML2 structure[258], we presented the first structures of the human TRPML2 ELD at

pH 4.5 and 6.5 and provided an explanation for pH-dependent Ca^{2+} interaction with this domain (see section 7.1).[1]

For TRPML1, interactions of the pre-pore loop with Ca^{2+} and H^{+} were reported by Li *et al.*.[263] The pre-pore loop is directly connected with the C-terminal residues of the extension of the S1 helix and contains a stretch of acidic residues. In the context of the full-length channel, this loop is centered of the ion channel pore which is formed by transmembrane helices S5 and S6. Based on their findings, Li *et al.* suggested a molecular model of ELD-based TRPML1 regulation: The aspartate residues in the pre-pore loop are negatively charged at pH 7.4 (which the ELD encounters in the extracellular space) thus attracting and binding extracellular Ca^{2+}, forming a block for Ca^{2+} and other cations. Lowering the pH in the endolysosomal system might lead to protonation of the aspartate residues, which weakens the Ca^{2+} block enabling cation flux. This hypothesis was supported by patch clamp experiments performed with the full-length channel: Mutation of the pre-pore loop aspartates to glutamine strongly reduced Ca^{2+} inhibition at pH 7.4.[263] The acidic motif is conserved in the TRPML family (TRPML1: ^{113}ADDT^{116}, TRPML2: ^{113}DEDD^{116}, TRPML3: ^{110}MDDT^{113}). In the context of this thesis, the Ca^{2+} affinity of the isolated wild-type TRPML2 ELD was tested using isothermal titration calorimetry (ITC) and compared with several TRPML2 ELD pre-pore loop mutants. Our results support the calcium block model for TRPML2, indicating that it could serve as a general mechanism for structural TRPML regulation (see section 7.2).

TRPML3 is inhibited by high sodium concentrations and by acidic pH, potentially due to the protonation of three histidines in the ELD.[269] Mutation of one of these histidines to alanine (H283A) leads to constitutive activity of the channel based on loss of pH regulation. In contrast, mutation of H283 to arginine leads to channel inactivation.[269]

TRPML channels in innate and adaptive immunity

Innate and adaptive immunity are essential to protect the host against harmful agents, such as viruses, bacteria, toxins, or allergens.[270] The innate immune response represents the “first line of defense” occurs immediately or within hours when the host is exposed to harmful or infectious substances or organisms.[270,271] Innate immunity is based on the genetic memory of germline-encoded receptors to sense molecular patterns of common pathogens.[272] Receptors for specific pathogen recognition include several receptor families, for example Toll-like receptors (TLRs), NOD (nucleotide-binding oligomerization domain)-like, lectin-like receptors and RIG-1 (retinoic acid-inducible gene I)-like receptors. Activation of these receptors by pathogen recognition leads to production and release of cytokines, chemokines and interferons, which in turn bind to their respective receptor, activate signaling cascades and stimulate transcription of various ISGs (interferon-stimulated genes).[273,274] Furthermore, production of chemokines and cytokines leads to the rapid recruitment of immune cells, including phagocytes (which are sub-divided into neutrophils

and macrophages), dendritic cells, mast cells, basophils, eosinophils, natural killer cells and innate lymphoid cells.[271] In contrast, adaptive immunity is defined by the ability of the host to learn to recognize a pathogen's specific antigens and to build up an antigen-specific response long-term.[272] It is therefore the basis for effective immunization against infectious diseases.[271] The cells of the adaptive immune response are antigen-specific T cells and B cells which differentiate into plasma cells to produce antibodies.[271]

The endolysosomal system has important functions in innate and adaptive immunity.[270] For example, it is involved in antigen presentation and processing, phagocytosis and release of proinflammatory mediators.[270] In recent years, direct roles for TRPML channels have emerged in various aspects of immunity.[270] In context of the innate immune response, TRPML1 was shown to be involved in the phagocytosis of large particles and in the migration of dendritic cells.[275,276] TRPML2 is expressed at low levels in a resting mouse macrophage cell line, but its expression is strongly upregulated after TLR activation, while no effect on TRPML1 and TRPML3 expression levels was observed.[245] These findings have been confirmed for bone marrow and alveolar macrophages and additionally for microglia from mice treated with several TLR activators, including PolyI:C (polyinosinic:polycytidylic acid, TLR3 ligand), LPS (lipopolysaccharides, TLR4 ligand), zymosan (TLR2 ligand), R-848 (TLR7/8 ligand) and Imiquimod (TLR7 ligand).[245] TRPML2 was also shown to play a role in chemokine and cytokine secretion of macrophages.[245,277] Absence of TRPML2 leads to intracellular accumulation and decreased secretion of CCL2 (chemokine (C-C motif) ligand 2) in bone marrow derived macrophages.[245] Furthermore, macrophage recruitment is reduced in TRPML2 deficient mice.[245] Direct activation of TRPML2 using the specific agonist ML2-SA1 (mucolipin 2 synthetic agonist 1) directly stimulated the secretion of CCL2 from bone marrow derived macrophages.[277] Presumably, the CCL2 release is mediated by the early/recycling endosomal pathway and ML2-SA1 treatment promoted endosomal trafficking.[277] The activity of TRPML2 was increasing with less acidic pH when stimulated with either $PI(3,5)P_2$ or ML2-SA1.[277] In contrast, TRPML1 shows maximal activity in highly acidic lumenal pH.[260,278] This suggests that TRPML2 is rather active in slightly acidic or neutral pH, as can be found in early endosomes and recycling endosomes than in highly acidic late endosomes and lysosomes. TRPML2 activation also led to enhanced macrophage recruitment.[277] Furthermore, TRPML2 was reported as an putative ISG; TRPML2 expression was upregulated in chimpanzee peripheral blood mononuclear cells (PBMCs) by 4-fold around 4 h post IFNα treatment.[279]

TRPMLs have been found to play multiple roles in adaptive immunity. TRPML1 co-localizes with MHC-II (major histocompatibility complex II) molecules in the endolysosomal compartment,[280] which can be transported to the cell surface upon cell stimulation, loaded with antigenic peptides and presented to antigen-specific CD4 (cluster of differentiation 4)-positive T cells[281]. TRPML2 was indicated to play an important role in the regulation of the endolysosomal system of B-lymphocytes.[282] Furthermore, TRPML2 travels along the Arf6 (ADP-ribosylation factor 6)-associated pathway and co-localizes with MHC-I, CD59, interleukin-2 receptor, β1-integrins and many

glycosylphosphatidylinositol anchored proteins (GPI-APs).[244,283–285] The Arf6-associated pathway is a clathrin-independent, plasma membrane-endosomal recycling pathway.[285] Arf6 is a small GTPase, which is also active in clathrin-mediated and clathrin-independent endocytosis and can direct transport along microtubules.[286] Viruses can take advantage of Arf6: for instance, Arf6 affects the life cycle of HIV-1, including viral entry, assembly and release.[287,288] In addition, the Arf6 GAP (GTPase activating protein) ADAP2 (ArfGAP with dual pleckstrin homology (PH) domains 2) is involved in RNA virus restriction. ADAP2 expression is upregulated by type-I interferon and ADAP2 overexpression restricts DENV and vesicular stomatitis virus (VSV) infection by interfering with viral entry and/or intracellular trafficking.[289] Arf6 is also involved in TLR signaling and interacts with the V-type ATPase, which is required for acidification of endosomes in the endoylsosomal system.[290] TRPML2 WT overexpression induces a strong activation of Arf6, while overexpression of an inactive TRPML2 pore mutant (D463D/KK) delays the recycling of internalized GPI-APs to the plasma membrane.[244] The molecular mechanism behind these findings remained elusive and need further investigation.[244]

TRPML2 overexpression enhances trafficking of certain endocytosed viruses

In 2018, it was demonstrated that stable overexpression of TRPML2 in human A549 lung adenocarcinoma cells results in increased infectivity and virus production of certain endocytosed RNA virus families, including *Flaviviridae* (e.g. ZIKV) and *Orthomyxoviridae* (e.g. influenza A virus (IAV)) which require transport to late endodomes.[92] Additionally, knockout of TRPML2 using a CRISPR/Cas9 system decreased infection with IAV in A549 and U-2 OS osteosarcoma.[92] Furthermore, channel activity is required for the enhancement of viral infection. Overexpression of an inactive TRPML2 mutant (D463D/KK) did not increase infection with IAV.[92] TRPML2 mediated enhancement of viral infection also occurred in STAT1 (signal transducer and activator of transcription 1) deficient cells, indicating that the antiviral effect is not dependent on the IFN response or linked to negative regulation of antiviral signaling.[92]

Rinkenberger and Schoggins investigated which stages of the viral life cycle are affected in TRPML2 overexpressing cells.[92] TRPML2 overexpression did not affect the attachment of IAV and YFV to the cell surface as shown by acid bypass experiments. Acridine orange staining indicated that TRPML2 overexpression did not have a significant effect on the pH of endosomes and lysosomes.[92] Experiments with biotin-tagged IAV which allow detection with streptavidin-conjugated fluorophores showed that TRPML2 overexpression does not affect the rate or the amount of endocytosed virus.[92] Interestingly, confocal microscopy showed an enhanced colocalization of IAV with late endosomes in TRPML2 overexpressing cells than in control cells. TRPML2 overexpression also promoted fusion with and escape from endosomes.[92] Furthermore, a YFV subgenomic reporter replicon containing the *Renilla* luciferase (RLuc) gene was used to uncouple viral entry from genome translation and replication by monitoring luciferase activity. TRPML2 overexpression did not affect YFV replication.[92] The authors of this study concluded that in TRPML2 overexpressing cells, the same

amount of virus is endocytosed, but more virus traffics successfully through the endolysosomal system to acidified organelles, from which they are released.[92] Since most of the experiments had been conducted with IAV, the impact of TRPML2 overexpression on flavivirus infection need to be further investigated.

In addition, a rare genetic TRPML2 variant was reported (K370Q) which fails to enhance viral infections and marks the first mutation that was reported for TRPML2 in a disease-related context.[92] Amino acid K370 is located in the loop between transmembrane helix 3 and 4 and it remains unclear if this mutation affects TRPML2's subcellular localization or activity. The frequency of this variant is rather low (approx. 3%), but is elevated (approx. 11%) in same African subpopulations and might be beneficial for the host during infection with endocytosed viruses.[92]

Although it seems surprising that TRPML2 (which is a presumed ISG) enhances viral infection, this might serve an important purpose in cells of the immune response. These cells express higher levels of basal TRPML2[245,291,292] and an TRPML2-mediated increased viral uptake might also result in increased PAMP (pathogen-associated molecular pattern) receptor activation leading to stronger immune response and improved viral clearence.[233]

Antiviral effect after treatment with TRPML agonists

Several synthetic TRPML agonists are available which serve as useful tools to study TRPML function, but also might display therapeutic potential. They belong to different substance classes, including benzensulfonamides (e.g. SN-1- or SF-21-type), thiophenesulfonamides (e.g. MK6-83), isoindolediones (e.g. ML-SA1) or isooxazolines (e.g. SN-2) among others (Figure 1.8a).[293–296] There are differences in their selectivity, potency and efficacy when they are used in different species. Activation of TRPML channels using small molecule agonists leads to Ca^{2+} flux from endosomes and lysosomes into the cytosol, which can influence vesicular fusion and fission, vesicular trafficking, lysosomal exocytosis and autophagy.[275,297,298] In addition, TRPML1 activation was shown to give rise to global Ca^{2+} signals, originating from both ER and extracellular Ca^{2+}.[299]

ML-SA1 is the best characterized TRPML agonist and was shown to restore lysosomal function and rescue Alzheimer-related alterations of the endolysosomal/autophagic system.[300] It activates TRPML1 and TRPML3 in mice and all three TRPML family members in human cells.[296] This compound induces an open conformation by interacting with a hydrophobic pocket near the pore of the channels (Figure 1.8b).[254] Based on molecular docking, this binding site was also suggested for ML2-SA1, a selective TRPML2 agonist, which stimulates CCL2 release and migration in LPS-activated macrophages.[277] In addition to agonists, several synthetic TRPML inhibitors are available. However, they are not able to discriminate between the different members of the TRPML family.[275,301]

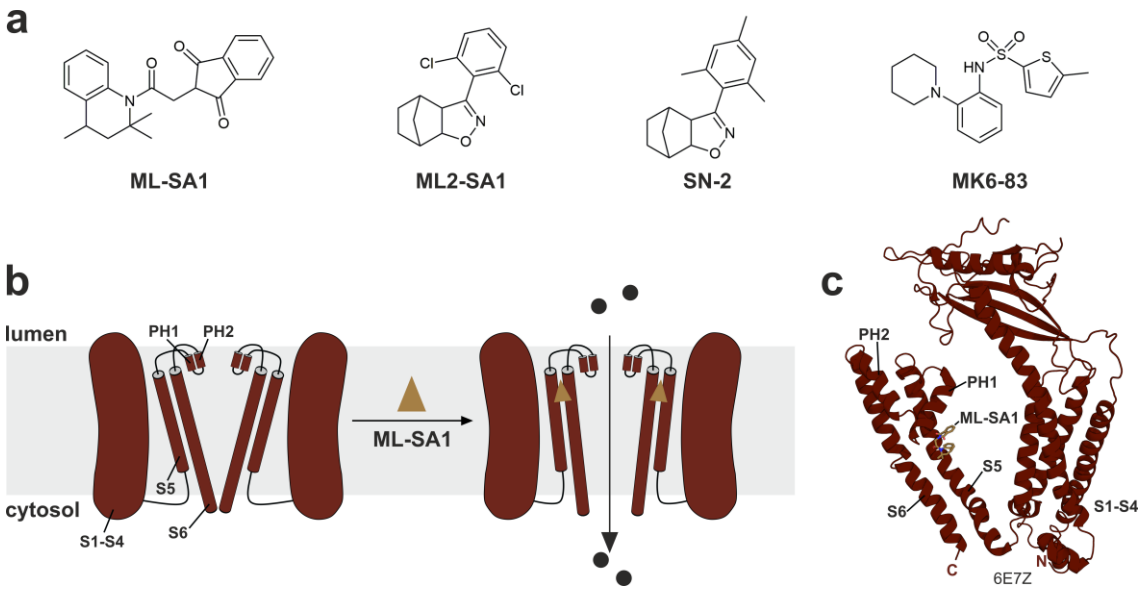

Figure 1.8: Small molecule agonists of TRPML channels. (**a**) Structures of the unspecific TRPML agonist ML-SA1, the specific TRPML2 agonist ML2-SA1, the specific TRPML3 agonist SN-2 and the specific TRPML1 and TRPML3 agonist MK6-83.[277,293,296,302] (**b**) Schematic model of agonist mediated TRPML activation. Small molecule agonists bind within a hydrophobic pocket, which is formed by transmembrane helices S5, S6 and pore helix PH1. This induces conformational changes that expand the selectivity filter and the lower gate, enabling cation flux (Figure 8b is based on Schmiege *et al.*[254]).

Due to the role of TRPML channels in viral infections, TRPML targeting compounds have emerged as potential antivirals. While overexpression of TRPML2 leads to increased infection with certain endocytosed viruses, activation of TRPML channels with ML-SA1 reduced DENV2 and ZIKV mRNA, protein and the amount of released infectious particles in a dose-dependent manner in A549 and Huh7 cells.[92,236] ML-SA1 treatment did not induce a significant upregulation of IFNβ or ISGs.[236] A time-of-drug-addition experiment indicated that viral entry, but not later stages of the DENV2 and ZIKV life cycle are affected by ML-SA1.[236] ML-SA1 did not reduce infection with Sendai virus, which directly fuses with the plasma membrane and does not require endocytosis for cell entry.[236] Moreover, the effect of ML-SA1 on autophagy was investigated in A549 and Huh7 cells. ML-SA1 induced autophagy in both cell lines.[236] Knockout of the key autophagy gene *Atg7* (autophagy related 7) and treatment with ML-SA1 still inhibited DENV2 in a dose-dependent manner, indicating that the antiviral effect of ML-SA1 is not based on the induction of autophagy.[236] Additionally, lysosomal acidification in ML-SA1 treated cells was measured. In comparison to the control, ML-SA1 promoted lysosomal acidification. Combination of ML-SA1 with leupeptin, an inhibitor of several lysosomal proteases resulted in a loss of antiviral activity.[236] It was concluded that ML-SA1 mediated TRPML activation may promote vesicle trafficking and fusion between endosomal and lysosomal membranes thereby leading to viral degradation.[236] The selective TRPML1 and TRPML3 agonist MK6-83 did not display antiviral potential, while the selective TRPML3 agonist SN-2 provoked an antiviral effect.[236] However, the antiviral potential of the selective TRPML2 agonist ML2-SA1 on flavivirus infection has not yet been analyzed. Furthermore, it was postulated that the antiviral activity of ML-SA1 or SN-2 is related to the

downregulation of TRPML2 and TRPML3 channel expression and is dependent on TRPML2 and TRPML3 channel activity.[235] The effect of specific TRPML2 activation mediated by the small molecule ML2-SA1 on ZIKV infection was investigated in the course of this thesis.

TRPML regulation has also been associated with SARS-CoV-2 (severe acute respiratory syndrome coronavirus 2) infection. For cell entry, the Corona virus Spike protein binds ACE2 (angiotensin-converting enzyme 2) or dipeptidyl peptidase-4 (DPP4).[303] Berbamine, a bis-benzylisoquinoline alkaloid, inhibits SARS-CoV-2 infection by suppressing TRPML-mediated endolysosomal trafficking of the ACE2 receptor.

Activity of TRPML channels can also be indirectly mediated by affecting the lipid composition in the endolysosomal system. PtdIns (3) P5-kinase (PIKfyve) is involved in the synthesis of $PI(3,5)P_2$, which is known to activate not only all three members of the TRPML family, but also the endolysosomal cation channels TPC1 and TPC2.[302,304–306] Apilimod, a PIKfyve inhibitor, blocks entry and infection of Ebola and Marburg virus in Huh7, Vero E6 and human primary macrophages.[307]

2 Objectives

The human cation channel TRPML2 is a remarkable player of the endolysosomal system and involved in ion homeostasis, signal transduction, autophagy and membrane trafficking.[215,234] In contrast to the other TRPML subfamily members, TRPML1 and TRPML3, the function of TRPML2 in human health and disease is far less understood. In recent years, a role for TRPML2 in innate and adaptive immunity has emerged.[270] Furthermore, TRPML2 overexpression was found to increase trafficking efficiency of endocytosed viruses.[92] In contrast, the activation of all three TRPML channels using the unspecific TRPML agonist ML-SA1 inhibited DENV2 and ZIKV infection by promoting lysosomal acidification and protease activity.[236] Until now, the potential of the TRPML2 ion channel as a putative antiviral target, e.g. through specific agonists and antagonists has not been investigated. For TRPML2, only a single highly specific agonist, ML2-SA1, has been described.[277]

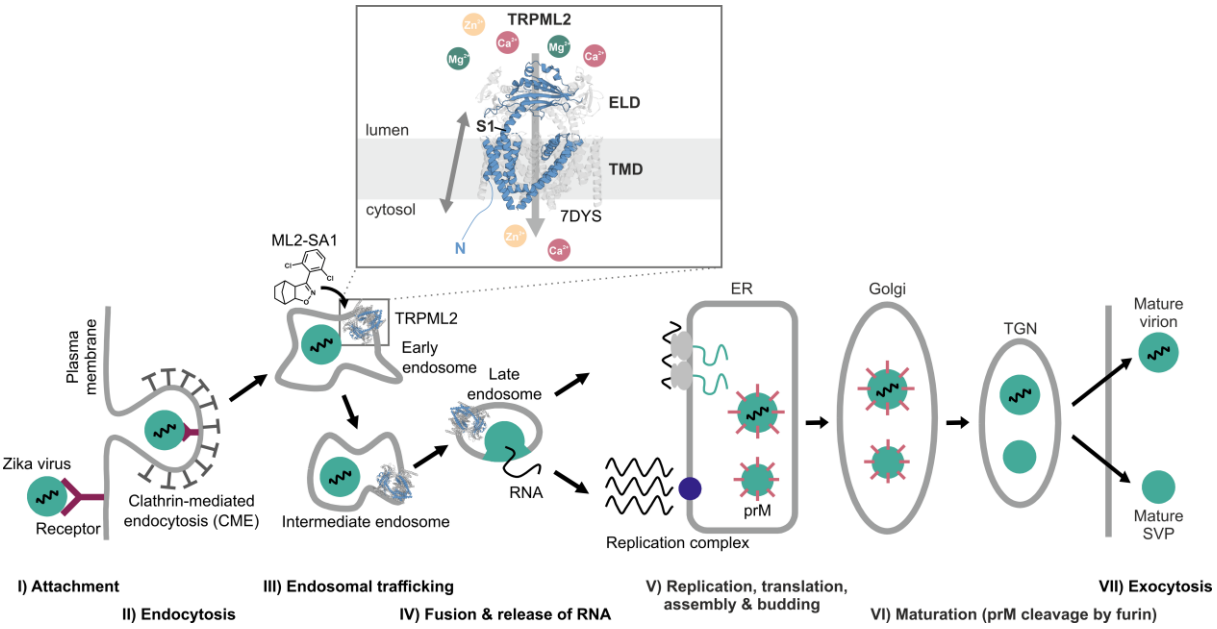

Figure 2.1: The human ion channel TRPML2 and its putative involvement in the ZIKV life cycle. ZIKV uses endocytosis to enter host cells. TRPML2 is located in the membranes of the endolysosomal system, and its activity can be modulated using the small molecule ML2-SA1. The inlet shows the structure of mouse TRPML2 at pH 7.4, 3.14 Å (pdb 7DYS). The ELD is the structural hallmark of the TRPML family and faces the endolysosomal lumen. ***Abbreviations:*** *ELD: extracytosolic/lumenal domain, TMD: transmembrane domain, CME: clathrin-mediated endocytosis, ER: endoplasmic reticulum, prM: pre-membrane protein, TGN: trans-Golgi network, SVP: subviral particle.*

ZIKV caused a major outbreak in the Americas in 2015/2016 and there is currently no specific treatment or prophylactic vaccine available. Thus, a need for new antiviral targets exists. In this thesis, the suitability of TRPML2 as an antiviral target against ZIKV was analyzed *in vitro*. The activity of TRPML2 was modulated using the specific agonist ML2-SA1. The consequences of the use of this substance allowed conclusions to be drawn about the role of TRPML2 in ZIKV infection. Experiments were performed with two ZIKV isolates, one representative of the Asian lineage (ZIKV French

Polynesia) and one representative of the African Lineage (ZIKV Uganda) to identify potential differences in the role of TRPML2 for each lineage. The impact of ML2-SA1 treatment on the morphology of the endolysosomal system was analyzed using cLSM and super-resolution microscopy.

Investigations on the role of TRPML2 in viral infections also require a detailed understanding of its structural regulation. In tetrameric TRPML channels, the ELD is a large domain of around 100 kDa (~ 200 amino acids per protomer, 4x ~ 24 kDa) and the structural hallmark of the TRPML family. However, the physiological function of this enigmatic domain remains elusive. Notably, via the first-transmembrane helix, the ELD is directly connected to the N-terminus, potentially enabling a crosstalk between the different domains. For the TRPML1 ELD, a dual-regulation by Ca^{2+} and pH was proposed by Li and coworkers.[263] Shortly, an acidic motif in the ELD's pre-pore loop is able to attract and bind Ca^{2+} at neutral pH, which the ELD encounters in the extracytosolic space, forming a block for other cations. Whereas in lysosomes, where an acidic pH is found, the acidic residues are protonated which enables cation flux. In this thesis, this model was tested for TRPML2 by determining the affinity of Ca^{2+} to the TRPML2 ELD at acidic and neutral pH using ITC. Furthermore, the binding site of Ca^{2+} was investigated and the affinity of other cations, which are conducted by TRPML2, to the ELD was analyzed. Potential effects of cation binding on the structure of the TRPML2 ELD which might be an important indicator of an inter-domain crosstalk were analyzed using high-resolution spectroscopic techniques (NMR and EPR spectroscopy).

3 Materials

3.1 Cells and viruses

Table 3.1: Bacterial strains.

Bacterial strain	Genotype	Provider
BL21-Gold (DE3) competent cells	*E. coli* B F⁻ ompT hsdS(rB⁻ mB⁻) dcm⁺ Tetr gal λ(DE3) endA I	Agilent, Santa Clara, USA
MAX Efficiency® DH5α™ competent cells	F- Φ80lacZΔM15 Δ(lacZYA-argF) U169 recA1 endA1 hsdR17 (rk-, mk+) phoA supE44 λ-thi-1 gyrA96 relA1	Invitrogen, Carlsbad, USA
Rosetta-gami™ 2(DE3) competent cells	Δ(ara-leu)7697 ΔlacX74 ΔphoA PvuII phoR araD139 ahpC galE galK rpsL (DE3) F′ [lac+ lacIq pro] gor522::Tn10 trxB pRARE2 (CamR, StrR, TetR)	Merck KGaA, Darmstadt, Germany

Table 3.2: Eukaryotic cell lines.

Cell line	Description	Provider
A549	Human epithelial lung carcinoma cells	ATCC, Manassas, USA
Vero	African green monkey kidney cells	ATCC, Manassas, USA

Table 3.3: Viruses.

Virus	Strain	Provider
ZIKV French Polynesia	H/PF/2013	European Virus Archive goes Global (EVAg), Marseille, France
ZIKV Uganda	976 Uganda	European Virus Archive goes Global (EVAg), Marseille, France
ZIKV RLuc reporter virus		Shan *et al.*[308]

3.2 Buffers and solutions

Table 3.4: Buffers and solutions for general procedures. For the composition of buffers used for specific applications, please refer to the respective methods section.

Buffer/solution	Ingredients
Anode buffer I	20% (v/v) Ethanol
	300 mM Tris base
Anode buffer II	20% (v/v) Ethanol
	25 mM Tris base
Cathode buffer	20% (v/v) Ethanol
	40 mM 6-aminohexanoic acid
Mowiol mounting medium	100 mM Tris/HCl
	10% (w/v) Mowiol
	10% (w/v) glycerol
	2.5% DABCO
	pH 8.5
PBS without Mg^{2+} and Ca^{2+}	137 mM NaCl
	2.7 mM KCl
	8.1 mM Na_2HPO4
	pH 7.4
RIPA (Radioimmunoprecipitation Assay) lysis buffer	50 mM Tris/HCl
	150 mM NaCl
	0.1% (w/v) SDS
	1% (w/v) sodium deoxycholate
	1% (v/v) Triton X-100
SDS-loading buffer (4X)	4% (w/v) SDS
	125 mM Tris/HCl
	10% (v/v) glycerol
	10% (v/v) β-mercaptoethanol
	0.02% (w/v) bromphenol blue
	pH 6.8
SDS-running buffer (10X)	250 mM Tris base pH 8.3
	2 M glycine
	1% (w/v) SDS
SDS-separating gel buffer	1.5 M Tris base
	0.4% (w/v) SDS
	pH 8.8

Table 3.4 continued.

SDS-stacking gel buffer	0.5 M Tris base 0.4% (w/v) SDS pH 6.7
TBS (1X)	20 mM Tris 150 mM NaCl pH 7.8
TBS-T (1X)	20 mM Tris 150 mM NaCl 0.05% (v/v) Tween-20 pH 7.8

3.3 Cell culture reagents

Table 3.5: Reagents for cell culture.

Reagent	**Manufacturer**
Dulbecco's Modified Eagle's Medium (DMEM) high glucose (4.5 g/L glucose)	Sigma-Aldrich, St. Louis, USA
Fetal bovine serum	Bio & Sell GmbH, Feucht, Germany
L-glutamine	Bio & Sell GmbH, Feucht, Germany
Penicillin/streptomycin	Paul-Ehrlich-Institutee (central laboratory), Langen, Germany
Trypsin/EDTA (0.05% trypsin, 0.02% EDTA in PBS)	Paul-Ehrlich-Institutee (central laboratory), Langen, Germany

3.4 Chemicals

Table 3.6: Used chemicals and reagents.

Chemical/reagent	Manufacturer
1,4-Diazabicyclo[2.2.2]octane (DABCO)	Merck Millipore, Burlington, USA
2-[4-(2-Hydroxyethyl)piperazin-1-yl]ethane-1-sulfonic acid (HEPES)	Carl Roth, Karlsruhe, Germany
2-Amino-2-(hydroxymethyl) propan-1,3-diol (Tris)	Carl Roth, Karlsruhe, Germany
3-(2-iodoacetamido)-proxyl (IPSL)	Sigma-Aldrich, St. Louis, USA
3-bromo-1,1,1-trifluoroacetone (BTFA)	Sigma-Aldrich, St. Louis, USA
4-(2-hydroxyethyl)-1-piperazineethanesulfonic acid (HEPES)	Thermo Fisher Scientific, Waltham, USA
4’,6-Diamidino-2-phenylindole (DAPI)	Sigma-Aldrich, St. Louis, USA
5,5'-Dithio-bis-(2-nitrobenzoic acid) (DTNB)	Thermo Fisher Scientific, Waltham, USA
6-Aminohexanoic acid	Carl Roth, Karlsruhe, Germany
Acetic acid	Carl Roth, Karlsruhe, Germany
Acetone	Carl Roth, Karlsruhe, Germany
Acrylamide/Bisacrylamide 37.5%	Carl Roth, Karlsruhe, Germany
Agar Agar	Carl Roth, Karlsruhe, Germany
Agarose LE	Genaxxon bioscience GmbH, Ulm, Germany
Ammoniumpersulfate (APS)	Carl Roth, Karlsruhe, Germany
Ampicillin sodium salt (Amp)	Carl Roth, Karlsruhe, Germany
Aprotinin	AppliChem GmbH, Darmstadt, Germany
β-mercaptoethanol	Carl Roth, Karlsruhe, Germany
Benzamidine hydrochloride	Sigma-Aldrich, St. Louis, USA
Bradford reagent	Sigma-Aldrich, St. Louis, USA
Bromophenol blue	Sigma-Aldrich, St. Louis, USA
BSA fraction V	Carl Roth, Karlsruhe, Germany
Calcium chloride ($CaCl_2$)	Carl Roth, Karlsruhe, Germany
Chloroform	Carl Roth, Karlsruhe, Germany
Coomassie Brilliant blue R 250	Carl Roth, Karlsruhe, Germany
Crystal violet	Sigma-Aldrich, St. Louis, USA
CutSmart buffer	New England Biolabs, Ipswich, USA
Diethyl pyrocarbonate (DEPC)	Carl Roth, Karlsruhe, Germany
Dimethylsulfoxide (DMSO)	Genaxxon bioscience GmbH, Ulm, DE
Disodium phosphate (Na_2HPO_4)	Carl Roth, Karlsruhe, Germany

Table 3.6 continued.

Dithiothreitol (DTT)	Carl Roth, Karlsruhe, Germany
dNTPs mix (10 mM each)	Thermo Fisher Scientific, Waltham, USA
Ethanol	Carl Roth, Karlsruhe, Germany
Ethidium bromide	AppliChem GmbH, Darmstadt, Germany
Filipin III	Sigma-Aldrich, St. Louis, USA
Formaldehyde (37.5%)	Carl Roth, Karlsruhe, Germany
Gel Loading Dye Purple (6x)	New England Biolabs, Ipswich, USA
Glycerol	Thermo Fisher Scientific, Waltham, USA
Glycin	Carl Roth, Karlsruhe, Germany
Hydrochloric acid	Sigma-Aldrich, St. Louis, USA
Imidazole	Carl Roth, Karlsruhe, Germany
Iron (III) chloride ($FeCl_3$)	Carl Roth, Karlsruhe, Germany
Isopropanol	Carl Roth, Karlsruhe, Germany
Isopropyl β-D-1-thiogalactopyranoside (IPTG)	Carl Roth, Karlsruhe, Germany
LB Broth (Luria/Miller)	Carl Roth, Karlsruhe, Germany
Magnesium chloride ($MgCl_2$)	Carl Roth, Karlsruhe, Germany
Methanol	Carl Roth, Karlsruhe, Germany
Monopotassium phosphate (KH_2PO_4)	Carl Roth, Karlsruhe, Germany
Monosodium phosphate (NaH_2PO_4)	Carl Roth, Karlsruhe, Germany
Mowiol	Sigma-Aldrich, St. Louis, USA
Nickel nitrilotriacetic acid (NiNTA) Agarose	QIAGEN N. V., Venlo, Netherlands
Page RulerTM Prestained Protein Ladder	Thermo Fisher Scientific, Waltham, USA
Pepstatin	AppliChem GmbH, Darmstadt, Germany
Phenylmethanesulfonyl fluoride (PMSF)	Carl Roth, Karlsruhe, Germany
Potassium chloride (KCl)	Carl Roth, Karlsruhe, Germany
Potassium ethylenediaminetetraacetic acid (K-EDTA)	Carl Roth, Karlsruhe, Germany
Potassium hydroxide (KOH)	Carl Roth, Karlsruhe, Germany
PrestoBlue™ Cell Viability Reagent	Thermo Fisher Scientific, Waltham, USA
Precision Plus Protein™ Dual Color Standards	Bio-Rad, Hercules, USA
Quick-Load® Purple 1 kb DNA Ladder	New England Biolabs, Ipswich, USA
Random hexamer primer	Thermo Fisher Scientific, Waltham, USA
RNA-Solv® Reagent	Carl Roth, Karlsruhe, Germany
Rotiphorese Gel 40 (29:1)	Carl Roth, Karlsruhe, Germany
Roti®-block (10x)	Carl Roth, Karlsruhe, Germany
SIGMA*FAST*™ Protease Inhibitor Cocktail Tablets	Sigma-Aldrich, St. Louis, USA
Sodium chloride	Carl Roth, Karlsruhe, Germany

Table 3.6 continued.

Sodium hydroxide	Sigma-Aldrich, St. Louis, USA
Sodium dodecyl sulfate (SDS)	Carl Roth, Karlsruhe, Germany
SeaPlaque™ agarose	Lonza Group AG, Basel, Switzerland
Sodium chloride (NaCl)	Carl Roth, Karlsruhe, Germany
Tetramethylethylenediamine (TEMED)	AppliChem GmbH, Darmstadt, Germany
Tris(hydroxymethyl)aminomethane (Tris)	Carl Roth, Karlsruhe, Germany
Triton X-100	Sigma-Aldrich, St. Louis, USA
Tween 20	Carl Roth, Karlsruhe, Germany
Zinc chloride ($ZnCl_2$)	Sigma-Aldrich, St. Louis, USA

3.5 Compounds for treatments

Table 3.7: Compounds used for treatment of human A549 cells with respective concentrations.

Compound	Concentration	Mode of action	Provider
Bafilomycin A1	50 nM	V-type ATPase inhibitor	Sigma-Aldrich, St. Louis, USA
Interferon α/β/γ	500 U/mL	Immune response modulators	Thermo Fisher Scientific, Waltham, USA
Leupeptin	200 µM	Thiolprotease inhibitor	AppliChem GmbH, Darmstadt, Germany
ML-SA1	100 µM	TRPML1, ML2, ML3 agonist	Merck KGaA, Darmstadt, Germany
ML2-SA1	100 µM	TRPML2 agonist	[redacted] group, Mainz, first described by Plesch *et al.*[277]
Ribavirin	100 µM	Nucleoside analogue	Selleckchem, Houston, USA

3.6 Enzymes and Kits

Table 3.8: Used enzymes.

Enzyme	Manufacturer
DNase I	AppliChem GmbH, Darmstadt, Germany
Lysozyme	Sigma-Aldrich, St. Louis, USA
RevertAid H Minus Reverse Transcriptase	Thermo Fisher Scientific, Waltham, USA
RNase	Sigma-Aldrich, St. Louis, USA
RQ1 RNase-free DNase	Promega, Madison, USA

Table 3.9: Used kits.

Kit	Manufacturer
Gaussia-GLOW juice Luciferase Assay Kit	PJK GmbH, Kleinbittersdorf, Germany
E.Z.N.A. Plasmid Mini Kit I	Omega Bio-Tek, Norcross, USA
Kapa HiFi HotStart PCR Kit	Kapa Biosystems, Inc., Wilmington, USA
Maxima™ SYBR™ Green qPCR Master Mix	Thermo Fisher Scientific, Waltham, USA

3.7 Antibodies

Table 3.10: Primary antibodies used for Western Blot (WB) and immunofluorescence stainings (IF).

Antibody	Species	Dilution (WB/IF)	Manufacturer
Anti-β-Actin A5316	Mouse	1:10,000/-	Sigma-Aldrich, St. Louis, USA
Anti-CD63	Mouse	-/1:200	Abcam, Cambridge, Great Britain
Anti-Flavivirus Group Antigen clone D1-4G2-4-15	Mouse	-/1:300	Merck Millipore, Burlington, USA
Anti-LAMP2	Goat	-/1:100	R&D Systems,Minneapolis, USA
Anti-p62	Guinea pig	1:1,000/-	ProGen Biotechnik, Heidelberg, Germany
Anti-TRPML2	Rabbit	1:500/1:100	Thermo Fisher Scientific, Waltham, USA
Anti-ZIKV E (K87)	Rabbit	1:500/1:500	Dr. Sami Akhras, Paul-Ehrlich-Institute, Langen, Germany[309]

Table 3.11: Secondary antibodies used for Western Blot (WB) and immunofluorescence stainings (IF).

Antibody	Species	Dilution (WB/IF)	Manufacturer
Anti-mouse IRDye®680RD	Donkey	1:10,000/-	LI-COR Biosciences, Lincoln, USA
Anti-mouse IRDye®800CW	Donkey	1:10,000/-	LI-COR Biosciences, Lincoln, USA
Anti-rabbit IRDye®680RD	Donkey	1:10,000/-	LI-COR Biosciences, Lincoln, USA
Anti-rabbit IRDye®800CW	Donkey	1:10,000/-	LI-COR Biosciences, Lincoln, USA
Anti-mouse IgG-Alexa 488	Donkey	-/1:1000	Invitrogen, Carlsbad, USA
Anti-mouse IgG-Alexa 546	Donkey	-/1:1000	Invitrogen, Carlsbad, USA
Anti-rabbit IgG-Alexa 488	Donkey	-/1:1000	Invitrogen, Carlsbad, USA
Anti-rabbit IgG-Alexa 546	Donkey	-/1:1000	Invitrogen, Carlsbad, USA
Anti-rabbit Cy™3	Donkey	-/1:400	Jackson ImmunoResearch, West Grove, USA
Anti-mouse STAR635P	Goat	-/1:200	Abberior, Göttingen, Germany
Anti-rabbit Atto594	Goat	-/1:200	Merck KGaA, Darmstadt, Germany

3.8 Oligonucleotides

Table 3.12: List of oligonucleotides used for site-directed mutagenesis.

Oligonucleotides	Sequence (5' – 3')
TRPML2 ELD A92-K285 D113A fwd	GGGCACGGCCGAAGACGATTAC
TRPML2 ELD A92-K285 D113A rev	CTTCGGCCGTGCCCGAGTAG
TRPML2 ELD A92-K285 E114A fwd	CACGGACGCAGACGATTACTCC
TRPML2 ELD A92-K285 E114A rev	GTCTGCGTCCGTGCCCGAG
TRPML2 ELD A92-K285 D115A fwd	GGACGAAGCCGATTACTCCTGC
TRPML2 ELD A92-K285 D115A rev	GTAATCGGCTTCGTCCGTGCCC
TRPML2 ELD A92-K285 D116A fwd	CGAAGACGCTTACTCCTGCTCAG
TRPML2 ELD A92-K285 D116A rev	GAGTAAGCGTCTTCGTCCGTGC
TRPML2 ELD A92-K285 E114A/D115A fwd	CACGGACGCAGCCGATTACTCC
TRPML2 ELD A92-K285 E114A/D115A rev	CGGCTGCGTCCGTGCCCG
TRPML2 ELD A92-K285 F105W fwd	CATTTAAACACCTGTGGCTGAAAGGCTACTC
TRPML2 ELD A92-K285 F105W rev	CTTTCAGCCACAGGTGTTTAAATGCGACCG
TRPML2 ELD A92-K285 E95C fwd	GCGTTTAAATGCGACAATACGGTCGCATTTAAACAC
TRPML2 ELD A92-K285 E95C rev	CCGTATTGTCGCATTTAAACGCACCACCAATCTG
TRPML2 ELD A92-K285 T98C fwd	GCGTTTAAAGAAGACAATTGCGTCGCATTTAAACACC
TRPML2 ELD A92-K285 T98C rev	CGACGCAATTGTCTTCTTTAAACGCACCACCAATC

Table 3.13: Sequences of oligonucleotides used for RT-qPCR.

Oligonucleotide	Sequence (5'→3')
ISG15_fwd	GAACCTCTGAGCATCCTGGTGAG
ISG15_rev	CAGAACAGGTCGTCCTGCACAC
TRPML1_fwd	GCCGTCGTCTCAAATAC
TRPML1_rev	TTGACCACTTGCAGCATC
TRPML2_fwd	ACCGTCAGAAATGCAATGG
TRPML2_rev	TCTGGCTCGGTATTTTTCAC
TRPML3_fwd	CTTTGTCATTCTGACTTGC
TRPML3_rev	AAACTCCTGCTGAAGCTGA
RPL27_fwd	AAAGCTGTCATCGTGAAGAAC
hRPL27_rev	GCTGCTACTTTGCGGGGGTAG
ZIKV_fwd	AGATCCCGGCTGAAACACTG
ZIKV_rev	TTGCAAGGTCCATCTGTCCC

3.9 Consumables

Table 3.14: Used consumables.

Consumable	Manufacturer
Cell culture flasks (T75, T175)	Greiner, Frickenhausen, Germany
Cell scrapers	Greiner, Frickenhausen, Germany
Centrifugal concentrator Vivaspin® 20 (10,000 Da cutoff)	Sartorius AG, Göttingen, Germany
Centrifugal concentrator Vivaspin® 6 (10,000 Da cutoff)	Sartorius AG, Göttingen, Germany
Dialysis membrane (12,000 Da cutoff) ZelluTrans/Roth dialysis membrane T4	Carl Roth, Karlsruhe, Germany
Falcon tubes	Greiner, Frickenhausen, Germany
Filtered pipette tips	Sartorius, Göttingen, Germany
Glass coverslips	Carl Roth, Karlsruhe, Germany
Glass slides (Objektträger)	Carl Roth, Karlsruhe, Germany
Hybond-P PVDF membrane	Merck Millipore, Burlington, USA
LightCycler Multiwell plates	Roche, Basel, Switzerland
Multiwell plates	Greiner, Frickenhausen, Germany
Page Ruler Prestained protein ladder	Thermo Fisher Scientific, Waltham, USA
RotiLabo® syringe filters (0.22 / 0.45 µm)	Carl Roth, Karlsruhe, Germany
Syrological pipettes	Greiner, Frickenhausen, Germany
Whatman filter paper	Ctyiva, Marlborough, USA

3.10 Laboratory equipment

Table 3.15: Laboratory devices used in the course of this thesis.

Device	Designation	Manufacturer
Blotter	TE77 ECL semi dry transfer unit	Ctyiva, Marlborough, USA
CD spectrometer	JASCO-815	JASCO GmbH, Pfungstadt, Germany
Centrifuge	Avanti J-26XP	Beckman Coulter, Brea, USA
Centrifuge	Centrifuge 5810 R	Eppendorf, Hamburg, Germany
Centrifuge	Heraeus Multifuge 1S-R	Heraeus, Hanau, Germany
Chromatography columns	Glass Econo-Column®	Bio-Rad, Hercules, USA
Chromatography system	NGC™ Medium-Pressure Liquid Chromatography System	Bio-Rad, Hercules, USA
Confocal laser scanning microscope system	Leica TCS SP8 System	Leica, Wetzlar, Germany
Electrophoresis chamber	Mighty small II vertical electrophoresis system SE250	Ctyiva, Marlborough, USA
EPR spectrometer	EMXnano	Bruker, Billerica, USA
EPR spectrometer	ELEXSYS E580	Bruker, Billerica, USA
Fluorimeter	FluoroMax-4	HORIBA Scientific, Kyoto, Japan
Fraction collector	Frac-920	Ctyiva, Marlborough, USA
Gel caster	Mighty small multiple gel caster SE 200	Ctyiva, Marlborough, USA
Heat block	Thermomixer compact	Eppendorf, Hamburg, Germany
High pressure cell homogenizer	HPL6	Maximator, Nordhausen, Germany
Incubation shaker	Multitron Standard	INFORS HT, Bottmingen, Switzerland
Incubator	Incubator BBD 6220	Heraeus, Hanau, Germany
Infrared imager	LI-COR Odyssey	LI-COR Biosciences, Lincoln, USA

Table 3.15 continued.

Isothermal titration calorimeter	MicroCal PEAQ-ITC Automated	Malvern Pananalytical, Malvern, Great Britain
Microcentrifuge	Centrifuge 5415 R	Eppendorf, Hamburg, Germany
Microplate reader	Infinite M1000	Tecan Group AG, Männedorf, Switzerland
NMR spectrometer	AVANCE 600 MHz	Bruker, Billerica, USA
NMR spectrometer	AVANCE 900 MHz	Bruker, Billerica, USA
pH-meter	pH electrode LE409	Mettler-Toledo, Columbus, USA
pH-meter	S20 – SevenEasy™ pH	Mettler-Toledo, Columbus, USA
Pipettes	ErgoOne® Single-Channel Pipettes	STARLAB International GmbH, Hamburg, Germany
Pipettes	Research® plus	Eppendorf, Hamburg, Germany
Plate reader	CLARIOstar Plus	BMG LABTECH, Ortenberg, Germany
Power supply for gel electrophoresis	PowerPac™ Basic power supply	Bio-Rad, Hercules, USA
Power supply for gel electrophoresis	Electrophoresis power supply EPS 301	Ctyiva, Marlborough, USA
Roller	Rocking platform WT16	Biometra, Göttingen, Germany
RT-qPCR device	LightCycler 480 Instrument II	Roche, Basel, Switzerland
Scanner	ViewPix 700	Biostep, Burkhardtsdorf, Germany
SDS-PAGE chamber and equipment	Mini-PROTEAN Tetra cell	Bio-Rad, Hercules, USA
SEC column	HiLoad 16/600 Superdex 200 pg	Ctyiva, Marlborough, USA
SEC column	Superdex 200 10/300 GL	Ctyiva, Marlborough, USA
Anion exchange column	RESOURCE Q	Ctyiva, Marlborough, USA
SEC column	ENrich™ SEC 650 10 x 300	Bio-Rad, Hercules, USA
Sonicator	SonoPuls MS73	BanGermanylin, Berlin, Germany
Sonifier	Branson Sonifier 250	Branson, Dietzenbach, Germany

Table 3.15 continued.

Super-resolution microscope system	Leica Stellaris 8 System	Leica, Wetzlar, Germany
Table centrifuge	neoLab Mini Star D-6020	neoLab Migge GmbH, Heidelberg, Germany
Temperature controlled vortexer	Multi-Therm	Benchmark Scientific, Sayreville, USA
UV-Vis spectrophotometer	NanoDrop 2000c	Thermo Fisher Scientific, Waltham, USA
Vortexer	RS-VA 10	Phoenix Instrument GmbH, Garbsen, Germany
	Vortex®Genie 2	Scientific Industries, Bohemia, USA
Water bath	Water bath1228-2F	VWR, Darmstadt, Germany
Weighing scale	Satorius balance LP 6000 200S	Sartorius, Göttingen, Germany
Weighing scale	Precision balance PLJ 600-2GM	KERN & SOHN GmbH, Balingen, Germany
Weighing scale	PS 4500.R2 Precision Balance	Radwag Balances and Scales, Radom, Poland

3.11 Software

Table 3.16: Software used for data acquisition and processing as well as thesis writing and illustration.

Software	Supplier
ChemBioDraw® Ultra 13.0	PerkinElmer Inc., Waltham, USA
Clustal Omega	EMBL-EBI, Hinxton, Great Britain https://www.ebi.ac.uk/Tools/msa/clustalo/
CorelDRAW Graphics Suite 2019	Corel Corporation, Ottawa, Canada
ExPASy Swiss Bioinformatics Resource Portal[310]	SIB Swiss Institute of Bioinformatics, Lausanne, Switzerland https://www.expasy.org/
FIJI	https://fiji.sc/
GraphPad Prism 8	GraphPad Software, San Diego, USA
Image Studio™ Lite Quantification Software	LI-COR Biosciences, Lincoln, USA
LAS X Control Software	Leica Microsystems, Wetzlar, Germany
LightCycler 480 SW1.5.1	Roche, Basel, Switzerland
Mendeley	Elsevier, Amsterdam, Netherlands
Microsoft 365	Microsoft, Redmond, USA
Origin 8	OriginLab, Northampton, USA
PyMOL	Schrödinger Inc., New York, USA
TECAN iControl	Tecan Group AG, Männedorf, Switzerland
TopSpin® 4.0.6	Bruker, Billerica, USA

4 Methods

4.1 Cells culture and Zika virus infections

Human epithelial lung carcinoma cells (A549) and African green monkey kidney cells (Vero) cells were maintained in Dulbecco's modified Eagle medium (DMEM) containing 4.5 g/L D-glucose supplemented with 10% fetal bovine serum, 100 U/mL penicillin and 100 µg/mL in 5% CO_2 and 95% relative humidity at 37 °C. Passaging of cells was performed every three to four days using a trypsin-EDTA solution (0.05% trypsin, 0.02% EDTA in PBS). The following cell densities were seeded for experiments in multi-well plates:

Table 4.1: Used cell densities for seeding in multi-well plates.

Multiwell plate	Cell density
6-well plate	3x 10^5 cells/well
12-well plate	1.5x 10^5 cells/well
96-well plate	1x 10^4 cells/well

For ZIKV infection experiments, cells were infected with either the ZIKV French Polynesia H/PF/2013 isolate or the 976 Uganda isolate with a multiplicity of infection (MOI) of 1. The inoculum was removed 16 h post infection and cells were washed once with PBS. At the desired time points, supernatants were collected and stored at −80 °C (where applicable) and cells were washed with PBS and harvested for subsequent experiments. Treatment with compounds was started two hours before infection and substances were refreshed during infection and 16 h and 24 h post infection to guarantee constant levels of compounds in cells, if not stated otherwise. DMSO was used as a vehicle control.

4.2 Cell viability assay

Cell viability assays were performed using PrestoBlue® Cell viability reagent according to the manufacturer's protocol. PrestoBlue® is a cell-permeable resazurin-based solution. When added to cells, the PrestoBlue® reagent is modified by the reducing environment of viable cells, thus a color change from blue to red that can be detected using fluorescence or absorbance measurements allows to quantify cell viability.A549 cells were seeded in a flat-bottom 96-well plate and treated with ML2-SA1 and ML-SA1 with concentrations ranging from 12.5 µM to 200 µM for 24 h and 48 h, respectively. After an incubation period of 1 h at 37 °C with PrestoBlue® Cell viability reagent, the fluorescence of the reagent was measured in a microplate reader Infinite M1000.

4.3 Time-of-addition experiment

A549 cells were seeded in 6-well plates and infected with the ZIKV French Polynesia or Uganda isolate (MOI=1) for one hour. Treatment with 50 nM Bafilomycin A1, 100 µM ML-SA1, 100 µM ML2-SA1 and 100 µM Ribavirin (dissolved in DMSO, stock concentrations 5 µM (Bafilomycin A1) and 10 mM (ML-SA1, ML2-SA1, Ribavirin)) was started at the respective timepoint (2 h before infection, during infection, 1 h, 6 h, 16 h and 22 h post infection). Complete media changes were performed during infection and 1 h post infection. At 24 h post infection, cells were washed once with PBS and lysed with RIPA buffer for subsequent Western blot analyses.

4.4 SDS polyacrylamide gel electrophoresis (SDS-PAGE) and Western blotting

For cell harvesting, A549 cells were washed with PBS, lysed with 100 µL RIPA buffer per well (including suitable amount of protease inhibitors) and scraped from plates. Afterwards, lysates were sonified (10 s, 20% intensity) and the protein concentration was determined using Bradford Reagent. Samples containing 75 µg protein in SDS loading buffer were heated for 10 min at 95 °C and loaded on an SDS-PAGE (10% SDS) and separated using a voltage of 100 V. Afterwards, protein was transferred to a nitro-cellulose membrane by semi-dry western blotting. The membranes were blocked with 1X Roti-block for 1 h and incubated overnight with the respective primary antibodies (Table 3.10) which have been diluted in blocking solution. The following day, membranes were washed with TBS buffer containing 0.05% Tween (TBS-T) and then incubated with the respective fluorophore-conjugated secondary antibodies (Table 3.11) diluted in blocking solution. After another washing step with TBS-T, fluorescence detection was performed using a LI-COR Odyssey system. Signal intensity was quantified using the Image Studio™ Lite software and normalized to the signal intensity of the respective loading control.

Additionally, SDS PAGE was used to verify the success of the purification of the TRPML2 ELD construct from *E. coli* (see section 4.11). After proteins were separated according to their respective molecular mass, the gels with the resulting protein bands were stained with Coomassie staining solution and destained to control protein purity.

4.5 RNA isolation, reverse transcription and real-time quantitative PCR (RT-qPCR)

For cell harvesting, A549 cells were washed with PBS and lysed with RNA-Solv® Reagent. Total intracellular RNA was isolated following the method described by Chomczynski and Sacchi.[311] Afterwards, DNA was digested using the RQ1 RNAse-free DNase and total RNA was transcribed into cDNA with random hexamer primer and RevertAid H Minus Reverse Transcriptase following the manufacturer's protocol. mRNA levels were quantified using the Maxima™ SYBR™ Green qPCR

Master Mix Kit for real-time quantitative PCR (RT-qPCR). RT-qPCR was performed using a LightCycler®480 System according to the following protocol:

Figure 4.1: RT-qPCR protocol

Program	Temperature (°C)	Hold (s)	Ramp Rate (°C/s)	Cycles
Initial denaturation	95	600	4.4	1
Denaturation	95	15	4.4	
Annealing	56	30	2.2	45
Elongation	72	30	4.4	
Melting	95	60	4.4	
	56	30	2.2	1
	97	–	0.1	
Cooling	37	30	2.2	–

Primers used for determination of intracellular mRNA levels are listed in Table 3.13. The n-fold expression was calculated using the $2^{-\Delta\Delta Ct}$ method.[312] The housekeeping gene human ribosomal protein L27 (hRPL27) was used for normalization.

4.6 Plaque assay

After the respective treatment of A549 cells with 100 µM ML2-SA1 and infection with ZIKV French Polynesia and ZIKV Uganda, supernatants were collected at the respective harvesting timepoint and stored at −80 °C. For plaque assays, Vero cells were seeded on a six-well plate (3x 10^5 cells per well) and infected with serial dilutions of sample supernatant which beforehand was centrifugated at 5 min at 5000 rpm to remove cell debris. The inoculum was removed two hours post infection and the cells were covered with 0.4% SeaPlaque™ agarose in medium. After 20 min at RT for solidification of the agarose/medium mixture, cells were incubated in 5% CO_2 and 95% relative humidity at 37 °C for five days. Then, the cells were fixed with 4% formaldehyde in PBS for 20 min and stained with 0.1% crystal violet in 20% ethanol. The cells were washed with water and plaques in the cell layer were counted. Virus titers are described as plaque forming units per mL (PFU/mL) and are presented in relation to the respective DMSO control.

4.7 Confocal laser scanning microscopy and super-resolution microscopy

Cells were seeded on glass coverslips in a 12-well plate and at the desired time-point fixed with either ice-cold ethanol:acetone (1:1) for 10 min or with 4% para-formaldehyde in PBS for 20 min at RT. Blocking and permeabilization were performed by the addition of 5% BSA in TBS-T for 15 min at RT. Samples were incubated with the respective primary antibodies (Table 3.10) for 1 h at RT followed by a washing step with TBS-T and incubation with the respective secondary antibodies (Table 3.11) for 1 h at RT and DAPI (250 ng/mL) for cell nuclei visualization. After a final washing step with TBS-T, coverslips were mounted with mowiol mounting medium on microscope slides and analyzed using a confocal Leica SP8 microscope.

For staining of intracellular cholesterol and oxysterols, cells were fixed with 4% paraformaldehyde in PBS for 20 min at RT. Blocking was performed with 5% BSA in TBS supplemented with 0.1 mg/mL filipin III for 30 min at RT. Samples were incubated with the respective primary antibodies (Table 3.10) for 1 h at RT followed by a washing step with TBS and incubation with the respective secondary antibodies (Table 3.11) and 0.1 mg/mL filipin III for 1 h at RT. After a final washing step with TBS, coverslips were mounted with mowiol mounting medium on microscope slides and analyzed using a confocal Leica SP8 microscope.

Super-resolution microscopy was performed with [redacted] ([redacted] group, Paul-Ehrlich-Institute, Langen). Beforehand, samples were incubated with secondary antibodies (STAR635P and Atto594, see Table 3.11), which are suitable for STED (stimulated emission depletion). DAPI was not used for cell nuclei visualization, because it can cause high background signal. For image acquisition, a Leica Stellaris 8 microscope system was used, which was equipped with a white light laser for fluorescence excitation and three STED lasers for fluorescence inhibition. For dual-color STED, a single STED line (775 nm) was used. Immunofluorescence images were deconvoluted using the LasX Lightning tool.

Acquisition and analysis of all images were performed using the LAS X software or FIJI.

4.8 ZIKV luciferase reporter assay

ZIKV luciferase reporter assays were performed by [redacted] and [redacted] ([redacted] group, Paul-Ehrlich-Institute, Langen). A549 cells were seeded with a density of 2x 10^5 cells/well in a 12-well plate. The following day, cells were infected with 10 genome equivalents (GEs) of ZIKV luciferase reporter virus for 4 h in the presence of 100 µM ML2-SA1/ML-SA1. At 4 h and 24 h post infection, compounds were refreshed to ensure constant level during the experiment. At 48 hpi, cells were washed, lysed and the luciferase activity was determined using the Gaussia GLOW-Juice Kit according to the manufacturer's protocol.

4.9 Statistical analysis of cell culture experiments

Results are depicted as mean of at least three independent experiments ± standard deviation (SD), unless stated otherwise. All data were analyzed using the software GraphPad Prism and student t test was used to analyze statistical relevance. The level of statistical relevance shown in the graphs are expressed with asterisks (*) that correspond to the following *p*-values: *$p < 0.05$, **$p < 0.01$, ***$p < 0.001$, ****$p < 0.0001$.

4.10 Cloning of TRPML2 ELD constructs

A plasmid containing the sequence of TRPML2 ELD A92-K285 cloned into a pET11a vector was provided by [redacted] ([redacted] group, Friedrich-Schiller-University, Jena). Point mutations were introduced by site-directed mutagenesis using the Kapa HiFi HotStart PCR Kit. Oligonucleotides were purchased from Sigma Aldrich (Table 3.12). For plasmid multiplication, *E. coli* DH5α competent cells were transformed with the respective plasmid via heat shock transformation. After growth in LB medium, plasmids were isolated with the E.Z.N.A. Plasmid Mini Kit I and then sequenced to ensure *mcoln2* gene sequence identity with databases (Uniprot accession nr Q8IZK6, human TRPML2). Sequencing was performed by StarSEQ GmbH (Mainz, Germany) and Eurofins Scientific (Luxemburg).

4.11 Expression and purification of TRPML2 ELD constructs

TRPML2 ELD construct purification follows the protocol published by Li and coworkers.[263] His_6SUMO-tagged ELD containing plasmids were transformed into *E. coli* Rosetta-gami™ (DE3) competent cells via heat shock transformation. Cells were grown at 37 °C in LB medium containing 100 µg/mL ampicillin to an OD_{600} of 1.0. After cooling the cell suspension to 22 °C, protein expression was induced with 100 µM isopropyl β-D-1-thiogalactopyranoside (IPTG) and cells were grown for another 15 h before being harvested by centrifugation (6200 g, 10 min, 4 °C). Cells pellets were resuspended in lysis buffer (50 mM NaP_i (pH 8.0), 300 mM NaCl, 2.5% glycerol, 5 mM imidazole) before adding lysozyme, RNase, DNase, 1 mM phenylmethanesulfonylfluoride (PMSF), 1 mM benzamidine and one SIGMAFAST™ protease inhibitor cocktail tablet. Cells were lysed by sonification or a Maximator high pressure homogenizer and the lysate cleared by centrifugation (1 h, 48,384 g, 4 °C). All following purification steps were carried out at 4 °C. The supernatant was loaded onto a NiNTA-column and the flow through was discarded. The column was extensively washed with lysis buffer and afterwards eluted with a buffer containing 50 mM NaP_i (pH 8.0), 300 mM NaCl, 2.5% glycerol, 500 mM imidazole). Ulp1 protease was added to the eluted protein in a 1:15 molar ratio to remove the His_6SUMO-tag. The mixture was dialyzed overnight against a buffer including 50 mM NaPi (pH 8.0), 150 mM NaCl and 2.5% glycerol. After dialysis, reverse IMAC (immobilized metal affinity chromatography) was used to separate His-tagged Ulp1, cleaved His_6SUMO-tag and uncleaved

TRPML ELD from cleaved ELD. ELD containing fractions were identified using a 15% SDS-PAGE, concentrated using centrifugal concentrators and purified on a Superdex 200 column (10 mM HEPES pH 7.5, 150 mM NaCl). Peak fractions containing ELD were collected, concentrated, frozen in liquid nitrogen and stored at −20 °C until further use (**procedure A**).

Alternatively, Ulp1 digest and dialysis were carried out in 25 mM NaP_i pH 8.0, 30 mM NaCl, 2.5% glycerol. Size exclusion chromatography on a Superdex 200 column (buffer containing 25 mM NaP_i (pH 8.0), 30 mM NaCl, 2.5% glycerol) was performed directly after dialysis. Peak fractions were collected and analyzed using 15% SDS-PAGE. ELD fractions were subjected to a RESOURCE Q anion exchange chromatography column to remove further impurities. The column was washed with 25 mM NaP_i (pH 8.0), 30 mM NaCl, 2.5% glycerol and protein was eluted via a salt gradient using a buffer containing 25 mM NaP_i (pH 8.0), 1 M NaCl, 2.5% glycerol. Peak fractions containing ELD were collected, concentrated, frozen in liquid nitrogen and stored at −20 °C until further use (**procedure B**).

Physicochemical properties of TRPML2 ELD constructs were determined using the ProtParam tool by ExPasy (https://web.expasy.org/protparam/). TRPML2 ELD construct characteristics before Ulp1 cleavage can be found in the appendix (Table 10.1).

Table 4.2: TRPML2 ELD construct characteristics after Ulp1 cleavage. pI and $\varepsilon_{280\,nm}$ were calculated with the ExPASy ProtParam tool.

#	ELD construct	AAs	MW / Da	pI	$\varepsilon_{280\,nm}$
p329	TRPML2 ELD A92-K285 WT	194	22,543.27	5.02	20,650
p582	TRPML2 ELD A92-K285 D113A	194	22,499.26	5.12	20,650
p583	TRPML2 ELD A92-K285 E114A	194	22,485.23	5.11	20,650
p584	TRPML2 ELD A92-K285 D115A	194	22,499.26	5.12	20,650
p585	TRPML2 ELD A92-K285 D116A	194	22,499.26	5.12	20,650
p587	TRPML2 ELD A92-K285 E114A/D115A	194	22,441.22	5.22	20,650
p687	TRPML2 ELD A92-K285 F105W	194	22,582.30	5.02	26,150
p646	TRPML2 ELD A92-K285 E95C	194	22,517.29	5.11	20,775
p647	TRPML2 ELD A92-K285 T98C	194	22,545.30	5.02	20,775

#: Internal [redacted] group plasmid (p) numbers

4.12 Ulp1 expression and purification

The pET28 plasmid containing the Ulp1 encoding sequence was kindly provided by Prof. Dr. Jens Wöhnert (Goethe-University of Frankfurt, Germany). It was transformed into *E. coli* BL21-Gold(DE3) competent cells. Cells were grown in LB medium containing 0.1 mg/mL kanamycin at 37 °C to an OD_{600} of 0.8 – 0.9. Protein expression was induced by addition of 1 mM IPTG and cells were grown for further 4 h at 37 °C before being harvested by centrifugation (6200 g, 10 min, 4 °C). Cell pellets were resuspended in lysis buffer (20 mM Tris pH 8.0, 20 mM imidazole, 300 mM NaCl, 0.1% (v/v) Triton X-100, 1 mM DTT) and DNase, RNase and lysozyme were added. Lysis was performed by sonification and the lysates cleared via centrifugation (1 h, 48,384 g, 4 °C). The subsequent purification steps were all performed at 4 °C. The supernatant was loaded onto a NiNTA-column and the flow through was discarded. After washing with a buffer including (20 mM Tris pH 8.0, 20 mM imidazole, 300 mM NaCl), the protein was eluted stepwise using 100, 150, 200 and 250 mM imidazole. Fractions containing Ulp1 were identified using a 15% SDS-PAGE and pooled fractions were dialyzed overnight against 75 mM Tris pH 8.0, 50% glycerol, 0.5 mM DTT, 1 mM EDTA. The following day, the samples were aliquoted, frozen in liquid nitrogen and stored at −80 °C until further use.

4.13 Circular dichroism (CD) spectroscopy

CD measurements were performed on a JASCO-815 CD spectrometer with a 1 mm quartz cuvette. Purified protein was dialyzed overnight into a buffer containing 10 mM NaP_i, 15 mM NaCl set to the desired pH value. Protein concentrations were adjusted to 5 µM in 200 µL. Spectra were recorded at 20 °C in a spectral range between 190 – 260 nm with 1 nm scanning intervals, 5 nm bandwidth and 50 nm/min scanning speed. All spectra were obtained from the automatic averaging of ten measurements with automatic baseline correction. The measured ellipticity θ in degrees (deg) was converted to the mean residue ellipticity (MRE):

$$MRE_\lambda = \frac{MRW \cdot \theta_\lambda}{10 \cdot d \cdot c} \quad (1)$$

Here, MRE_λ is the mean residue ellipticity and θ_λ is the measured ellipticity at wavelength λ. d describes the pathlength and c is the protein concentration in g/mL. MRW is the mean residue weight:

$$MRW = \frac{M_W}{N-1} \quad (2)$$

M_W is the molecular weight of the protein in Da and N is the number of residues.

4.14 Analytical size exclusion chromatography (SEC)

Analytical size exclusion was performed with an Enrich SEC 650 10 x300 or a Superdex 200 10/300 GL column, respectively. Purified protein was dialyzed overnight into a buffer containing 10 mM NaP_i, 15 mM NaCl set to the desired pH value. Protein concentrations were adjusted to 12.5 µM in 200 µL.

4.15 Isothermal titration calorimetry (ITC)

ITC measurements were carried out at 25 °C using a MicroCal PEAG-ITC Automated instrument. For each measurement, purified protein was dialyzed overnight into a buffer (10 mM HEPES, 15 mM NaCl) set to the desired pH value (pH 7.4, 6.5 and 4.5). Protein concentrations were adjusted to 400 µM (unless stated otherwise). After an initial delay of 60 s, 19 serial injections of 2 µL (from a 15 mM stock solution) every 150 s were carried out (first injection: 0.4 µL). The reference power was set to 10 µcal/s and stirring speed to 750 rpm. For each condition, two independent experiments were performed. As control experiments, the stock solution was titrated into the respective buffer solution. The thermograms were processed using the MicroCal PEAQ-ITC Analysis Software assuming a "one set of sites" models. For fitting of experimental data, the heat released from the i^{th} injection ($\Delta Q(i)$) was calculated using the following function:

$$\Delta Q(i) = Q(i) + \frac{dV_i}{V_0}\left[\frac{Q(i)+Q(i-1}{2}\right] - Q(i-1) \quad (3)$$

Here, V_0 is the active cell volume and dV_i is the i^{th} injection volume. Errors for affinity constants present standard deviations based on two independent measurements.

4.16 Tryptophan fluorescence spectroscopy

Tryptophan fluorescence spectroscopy measurements were carried on a FluoroMax-4 fluorimeter with an excitation wavelength of 300 nm and a detection range between 310 – 400 nm. Purified protein was dialyzed overnight into a buffer containing 10 mM NaP_i, 15 mM NaCl set to the desired pH value and protein concentrations were adjusted to 5 µM in 200 µL.

4.17 Ellman's test

Ellman's test was performed to verify the efficiency of the labeling procedure in which the TRPML2 ELD E95C mutant was incubated with BTFA (3-bromo-1,1,1-trifluoroacetone) for subsequent ^{19}F-NMR and IPSL (3-(2-iodoacetamido)-proxyl) for EPR (electron paramagnetic resonance) measurements, respectively. Experiments were carried out in a 96 well-plate. In one well, 2 mM/20 nmol Ellman's reagent (5,5'-dithio-bis-(2-nitrobenzoic acid), DTNB) in 100 mM Tris pH 8.0 were filled up to a total volume of 200 µL per well. The protein was titrated to the solution in 2 nmol steps and the solution

was mixed carefully and allowed to equilibrate for two minutes. Afterwards, the absorbance was measured at 412 nm at RT with a CLARIOstar Plus plate reader.

4.18 ^{1}H-^{15}N HSQC NMR measurements

E. coli Rosetta-gami™ (DE3) competent cells were transformed with the plasmid encoding the WT TRPML2 ELD A92-K285 and grown in commercially available ^{2}H-^{15}N labeled Silantes medium. Protein expression and purification was performed as described in section 4.11, procedure A.

Spectra were recorded by [redacted] and [redacted] at 298 K in 10 mM HEPES pH 7.5, 150 mM NaCl, supplemented with 10% D_2O on a Bruker AVANCE 900 MHz spectrometer at the Centre for Biomolecular Magnetic Resonance, Goethe University, Frankfurt. $CaCl_2$ titrations were performed with a 1 M $CaCl_2$ stock yielding final concentrations of 2.5 mM and 10 mM $CaCl_2$ in solution. Measurements were performed using standard pulse sequences and processed using the TopSpin 4.0.6 software.

4.19 ^{19}F-NMR measurements

The TRPML2 ELD E95C construct was expressed and purified as described in 4.11, procedure B. During purification, the protein-bound NiNTA-beads were transferred to a falcon and incubated overnight under gentle rotation with a 15-fold excess of BTFA at pH 6 and 4 °C. The following day, the purification was continued as described above (section 4.11).

^{19}F-NMR spectra of TFA-labeled TRPML2 ELD E95C were recorded together with [redacted] ([redacted] group, Friedrich-Schiller-University, Jena) on a Bruker AvanceIII HD 600 MHz spectrometer system equipped with a helium cooled QCI 600S3 H&F/P/C-N-D-05 Z XT probe at 298 K using a protein concentration of 50 µM. Buffers contained 10 mM HEPES, 15 mM NaCl and supplemented with 10% D_2O and titrations were performed with 40 mM stock solutions of $CaCl_2$, $MgCl_2$, $FeCl_3$, and $ZnCl_2$. For ^{19}F-NMR spectra, a standard 90° pulse sequence without ^{1}H decoupling was used. The length of the ^{19}F 90° pulse was the standard 11 µs determined for this probe at an incident power of 4.18 W. Spectra were acquired with 8192 complex data points and a spectral width of 50.3 ppm at a transmitter frequency offset of −80 ppm. This corresponds to an acquisition time of 0.144 s and with a dwell time of 17.6 µs, the resolution of the FID was 6.9 Hz. The number of scans for each experiment was 128 with an interscan delay of 1 s. This time was sufficient for a complete return of the ^{19}F magnetization to thermal equilibrium, so that there was no saturation of the ^{19}F signal due to an insufficient interscan delay. For direct referencing, the ^{1}H signal of an external sample containing 0.1 mM DSS (sodium trimethylsilylpropanesulfonate) in aqueous buffer at 25 °C was set to 0 ppm and the ^{19}F signals were indirectly referenced using the magnetogyric ratio.[313]

4.20 Electron paramagnetic resonance (EPR) spectroscopy

The TRPML2 ELD E95C construct was expressed and purified as described in 4.11, procedure B. During purification, the protein-bound NiNTA-beads were transferred to a falcon and incubated overnight under gentle rotation with a 15-fold excess of IPSL at pH 8 and 4 °C. The following day, the purification was continued as described above (section 4.11).

EPR measurements were performed together with [redacted] in the group of [redacted], Rheinische Friedrich-Wilhelms-University, Bonn). Continuous-wave (CW) EPR measurements of free IPSL (100 µM) and TRPML2 ELD E95C-PSL were carried out in 10 mM HEPES, 15 mM NaCl (deuterated buffer) on a EMXnano (Bruker) using the following settings: microwave power 0,631 mW; resolution 900; video gain 64 dB; modulation amplitude 1.0 G; time constant 20.48 ms, conversion time 50.14 ms; 64 scans for IPSL and sample and 100 scans for the TRPML2 ELD E95C sample.

PELDOR (pulsed electron double resonance) measurements were performed on an ELEXSYS E580 (Bruker) spectrometer using a FlexLine probe with a Q-band resonator ER5106QT-2 (Bruker). Microwave pulses were amplified via a 150 W TWT amplifier (model 187Ka). To guarantee a working temperature of 50 K, a continuous flow helium cryostat CF935 (Oxford Instruments) and a temperature control system iTC 503S (Oxford Instruments) were used. PELDOR measurements with the TRPML2 ELD E95C-PSL (100 µM in 10 mM HEPES, 15 mM NaCl, with and without 400 µM $CaCl_2$, pH 7.4/6.5 (deuterated buffer)) were carried out with the standard four-pulse sequence π/2(νdet)-τ1-π(νdet)-(τ1 + t)-π(νpump)-(τ2 – t)-π(νdet)-τ2-echo. Pump pulse frequency and magnetic field were adjusted to be on resonance with the maximum of the nitroxide spectrum. The frequency of the detection pulse was set 100 MHz lower than the pump pulse frequency. The pump pulse had a duration of 20 ns. Pulse lengths of 12 and 24 ns were applied for the detection π/2- and π-pulses, respectively. To eliminate receiver offsets, the detection π/2-pulse was phase-cycled. The τ1 interval was set to 260 ns and was incremented during each experiment eight times with a step of 16 ns. The τ2 interval was set to 10 µs. The position of the pump pulse relative to the primary echo was increased in steps of 16 ns. All PELDOR measurements were performed at 50 K with a shot repetition time of 2 ms. The signal was averaged over 50 – 200 runs to obtain a good signal to noise ratio.

Part I: The Role of the human TRPML2 ion channel in Zika virus infection

The human TRPML2 protein is an unselective cation channel involved in ion homeostasis, signal transduction and membrane trafficking in the endolysosomal system.[234] Endocytosis is a common mechanism for multiple viruses (including flaviviruses) to enter host cells. Recent studies indicated a role for TRPML2 in infection with endocytosed viruses.[92,236] Overexpression of TRPML2 increased infectious virus production of several viruses (for example YFV and ZIKV) and promoted endosomal trafficking of influenza A virus (IAV).[92] In contrast, when all three TRPML subfamily members were unspecifically activated with chemical agonists, ZIKV and DENV entry into host cells was inhibited due to an increase in lysosomal acidification and acidic protease activity.[236] Thus, the individual role of TRPML2 in the infection process of endocytosed viruses remains elusive.

In this thesis, the role of TRPML2 in ZIKV infection has been investigated. In the last few years, ZIKV outbreaks affected millions of people and presented a serious threat for public health.[44] Until now, there is no specific treatment or prophylactic vaccine against ZIKV available. Nevertheless, the probability of a new outbreak is high and the habitat of ZIKV vectors, i.e. mosquitoes of the Aedes species is expanding due to climate change.

Herein, the responsiveness of TRPML2 to interferons, important modulators of innate immunity, was tested in uninfected cells before quantifying the impact of ZIKV infection on TRPML2 expression levels. The potential of TRPML2 as an antiviral target was elucidated through use of the TRPML2-specific agonist ML2-SA1[277]. The consequences of ML2-SA1 treatment for different phases of the ZIKV life cycle were analyzed and a reduction of viral infectivity could be observed. Since the ZIKV life cycle shares similarities with that of other flaviviruses, TRPML2 might serve as a new drug target and the small molecule ML2-SA1 as a starting point for a new class of (pan-)antivirals.

5 Results

5.1 Interferon treatment does not induce TRPML2 overexpression in A549 cells

Interferons have a central role in the innate immune response. Pathogens including viruses, are recognized by host cells through pathogen-specific recognition receptors (PRRs). Activation of PRRs leads to production and release of interferons, which bind to their respective receptor, activate signaling cascades and stimulate transcription of ISGs.[273,274] In a macrophage cell line, TRPML2 expression was shown to be upregulated after TLR activation, while no effect on TRPML1 and TRPML3 expression was observed.[245] In addition, TRPML2 mRNA levels were elevated 4-fold in chimpanzee peripheral blood mononuclear cells following IFNα exposure at 4h post-treatment.[279]

To investigate if IFN treatment provokes an increase of TRPML2 mRNA and protein levels in uninfected cells, the lung adenocarcinoma cell line A549 was chosen for this study. A549 cells express TRPML2 at moderate levels and are highly susceptible for various ZIKV strains, an important criterion for subsequent ZIKV infection experiments.[314,315]

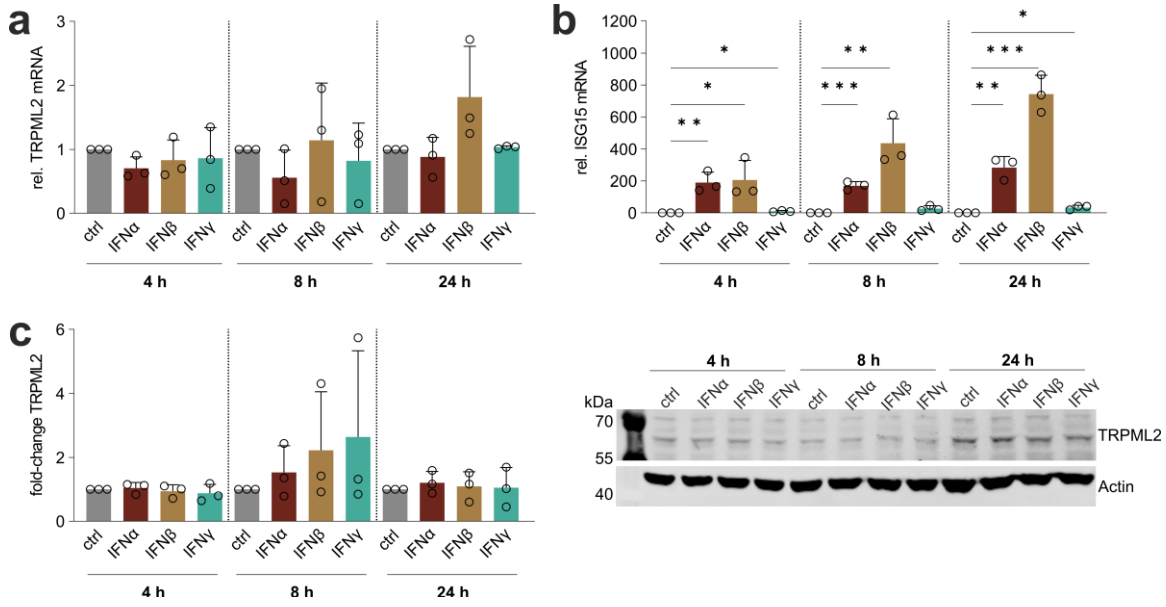

Figure 5.1: Interferon treatment did not induce TRPML2 overexpression in A549 cells. A549 cells were treated with 500 U/mL interferon (IFN) α, β and γ and harvested after 4 h, 8 h and 24 h post treatment. (**a**, **b**) Relative fold-change in intracellular TRPML2 and ISG15 (interferon-stimulated gene 15) mRNA levels assessed via RT-qPCR. (**c**) Relative fold-change in TRPML2 protein as assessed via Western Blot analyses. One representative Western Blot is shown on the right. Data are normalized to the respective control (ctrl) and expressed as mean ± SD from $n = 3$ biological replicates. Statistical significance was determined by using an unpaired *t*-test. *$p < 0.05$, **$p < 0.01$, ***$p < 0.001$, ****$p < 0.0001$.

Uninfected A549 cells were treated with interferon α, β and γ for 4 h, 8 h and 24 h. As seen in Figure 5.1a and c, treatment of A549 cells with interferons does neither lead to a significant increase nor decrease of TRPML2 mRNA and protein levels at the chosen timepoints as compared to the control.

ISG15 (as a representative ISG) mRNA levels were tested for each timepoint and confirmed the effectiveness of the IFN treatment (Figure 5.1b).

5.2 Zika virus infection reduces both TRPML2 mRNA and protein levels

While TRPML2 overexpression was shown to enhance ZIKV infection,[92] the effect of ZIKV infection on endogenous TRPML2 remained elusive. Therefore, A549 cells were infected with two ZIKV isolates, one member of the more ancient African lineage (ZIKV Uganda) and one member of the Asian lineage (ZIKV French Polynesia). TRPML2 mRNA and protein levels were monitored using RT-qPCR and Western Blot analyses (Figure 5.2).

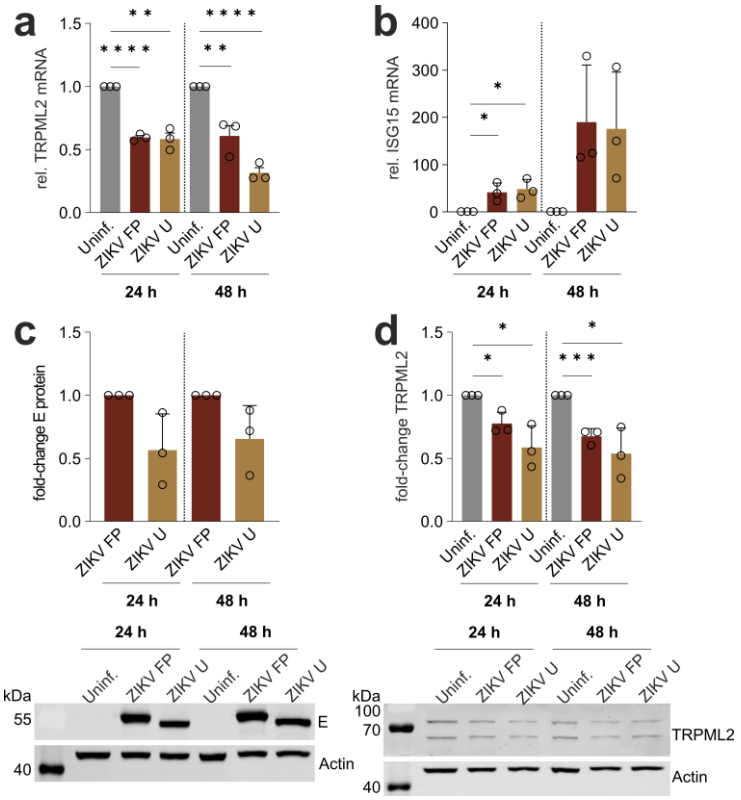

Figure 5.2: Effect of ZIKV infection on TRPML2 mRNA and protein levels. A549 cells were infected (MOI = 1) with ZIKV French Polynesia (H/PF/2013) or Uganda (976 Uganda) and harvested after 24 h and 48 h. (**a**, **b**) Relative fold-change in intracellular TRPML2 and ISG15 mRNA levels as assessed via RT-qPCR. (**c**, **d**) Relative fold-change of ZIKV E protein (**c**) and TRPML2 (**d**) expression as assessed via Western Blotting. One representative Western Blot is shown below. Data are normalized to the respective uninfected (uninf.) control (**a**, **b**, **d**) or to the ZIKV French Polynesia infected sample (**c**) for each timepoint and are expressed as mean ± SD from $n = 3$ biological replicates. Statistical significance was determined by using an unpaired t-test. *$p < 0.05$, **$p < 0.01$, ***$p < 0.001$, ****$p < 0.0001$.

The infection with either ZIKV strain reduced TRPML2 mRNA and protein levels significantly after 24 h and 48 h in A549 cells (Figure 5.2a and c). The increase in ISG15, which can serve as a monitor for ISG induction, is less pronounced in ZIKV infected cells (Figure 5.2b) compared to uninfected

cells upon IFN treatment (Figure 5.1b). In the previous section, it was already demonstrated that high IFN concentrations do not increase TRPML2 expression in A549 cells (Figure 5.1).

In addition to TRPML2 and ISG15, the effect of ZIKV infection on the mRNA levels of the other two TRPML members, TRPML1 and TRPML3, was investigated (Figure 5.3).

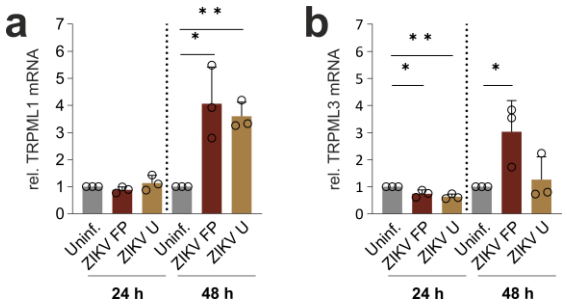

Figure 5.3: Effect of ZIKV infection on TRPML1 and TRPML3 mRNA levels. A549 cells were infected (MOI = 1) with ZIKV French Polynesia (H/PF/2013) and Uganda (976 Uganda) and harvested after 24 h and 48 h. (**a**, **b**) Relative fold-change in intracellular TRPML1 and TRPML3 mRNA levels as assessed via RT-qPCR. Data are normalized to the respective uninfected (uninf.) control for each timepoint and are expressed as mean ± SD from n = 3 biological replicates. Statistical significance was determined by using an unpaired t-test. *p < 0.05, **p < 0.01, ***p < 0.001, ****p < 0.0001.

In ZIKV infected A549 cells, no clear trend can be observed for TRPML1 and TRPML3 mRNA levels. ZIKV infection caused an increase of TRPML1 mRNA not after 24 h but after 48 h. For TRPML3 mRNA levels in ZIKV infected cells, a decrease was detected after 24 h but an increase after 48 h.

5.3 Treatment with the TRPML2 agonist ML2-SA1 leads to increased acidification of the endolysosomal system

To investigate the role of TRPML2 in viral infection, the TRPML2 specific agonist ML2-SA1 was used to modulate TRPML2 activity. For this study, ML2-SA1 was synthesized by [redacted] in a two-step synthesis, see appendix Figure 10.1.[316] The compound was first reported by Plesch *et al.* in 2018 and is the only currently available specific TRPML2 agonist.[277] Before investigating the putative antiviral effect of ML2-SA1, its cell toxicity was tested in uninfected A549 cells (Figure 5.4). A549 cells were incubated with micromolar concentrations of ML2-SA1 (12.5 µM, 25 µM, 50 µM, 100 µM and 200 µM) for 24 h and 48 h. Of note, low micromolar concentrations of ML2-SA1 were also used by Plesch *et al.* to stimulate CCL2 release.[277] Afterwards, a PrestoBlue® assay was performed.

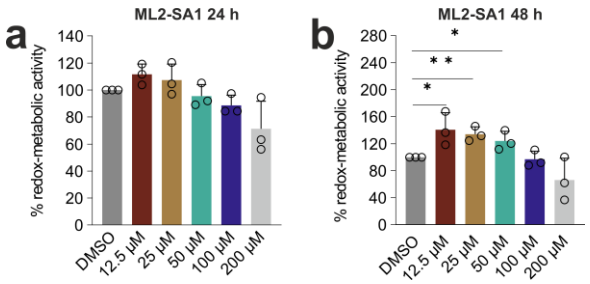

Figure 5.4: ML2-SA1 is non-toxic to A549 cells. Cell viability of A549 cells upon 24 h (**a**) and 48 h (**b**) treatment with 12.5 µM to 200 µM ML2-SA1 as assessed via PrestoBlue® assay. Values are expressed as % of intact cells referred to the experimental control. Data are expressed as mean ± SD from $n = 3$ biological replicates. Statistical significance was determined by using an unpaired *t*-test. *$p < 0.05$, **$p < 0.01$, ***$p < 0.001$, ****$p < 0.0001$.

No significant cell toxicity was observed after 24 h upon treatment of A549 cells in a concentration range from 12.5 µM to 100 µM ML2-S1 (Figure 5.4a). For 200 µM ML2-SA1, a mild but not significant decrease in the percentage of redox metabolic activity was observed after 24 and 48 h (Figure 5.4). After 48 h, an increase in the percentage of redox metabolic activity was detected for 12.5, 25 and 50 µM ML2-SA1 (Figure 5.4b). For the following experiments, a concentration of 100 µM ML2-SA1 was used. DMSO served as a vehicle control.

To investigate the effect of ML2-SA1 treatment and TRPML2 activation on the acidification of endolysosomal vesicles, uninfected A549 cells were co-treated with ML2-SA1 and the V-type ATPase inhibitor Bafilomycin A1 (BFA1), which prevents endolysosomal acidification. To label acidic organelles in living cells, e.g. lysosomes and late endosomes, the (fixable) fluorescent dye lysotracker was added. Subsequently, immunostaining was performed with an antibody against the lysosomal marker LAMP2 to assess changes in the size and distribution of LAMP2-positive vesicles.

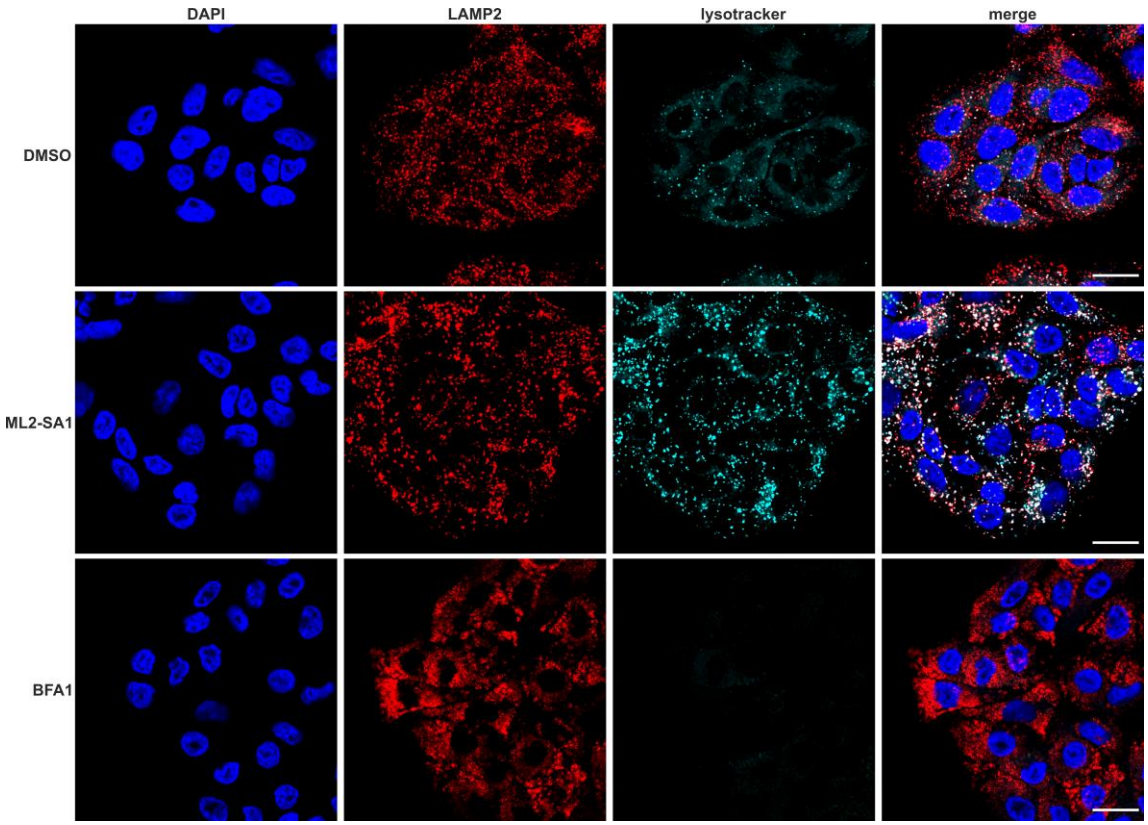

Figure 5.5: Treatment of A549 cells with the TRPM2 agonist ML2-SA1 leads to increased acidification of the endolysosomal system. Representative confocal laser scanning microscopy (cLSM) images of uninfected A549 cells treated with 100 µM ML2-SA1 and 50 nM BFA1, a V-type ATPase inhibitor. Cells were fixed 24 h post treatment and lysotracker (cyan) was added one hour before fixation to stain acidic organelles. Nuclei were stained with DAPI in blue and the lysosomal marker protein LAMP2 (red) was visualized using a LAMP2-specific antibody. Scale bar: 20 µM.

In comparison to the DMSO-treated control, ML2-SA1-treated cells display more and enlarged lysotracker-positive vesicles (Figure 5.5). In addition, enlarged LAMP2-positive vesicles are also observed. In BFA1-treated cells, almost no lysotracker positive vesicles can be found as expected. Furthermore, a drastic increase in LAMP2-positive vesicles is observed. BFA1 causes accumulation of cellular waste which cannot be degraded by lysosomal proteases when the endolysosomal pH is too high.[317,318]

5.4 ML2-SA1 treatment reduces titers of two ZIKV isolates

In recent years, there has been increasing attention on the role of endolysosomal ion channels in infectious diseases and many of these channels are now considered potential targets for novel antiviral drugs.[107] Xia *et al.* tested the antiviral potential of TRPML agonists.[236] They showed that the unspecific TRPML channel agonist ML-SA1 inhibited DENV2 (TSV01 isolate) and ZIKV (Puerto Rico PRVABC59 isolate) infection in A549 cells in a dose-dependent manner. Likewise, the selective TRPML3 agonist SN-2 showed a similar antiviral effect against DENV2 and ZIKV, while this was not the case for the TRPML1 and TRPML3 agonist MK6-83.[236] Until now, the antiviral potential of selective TRPML2 activation has not been evaluated. Therefore, different concentrations of the specific TRPML2 agonist ML2-SA1 ranging from 25 µM to 200 µM were tested for their antiviral potential against two ZIKV isolates (ZIKV French Polynesia and ZIKV Uganda). ML2-SA1 was added to A549 cells two hours before infection and afterwards the compound was refreshed during every medium change to assure its constant presence.

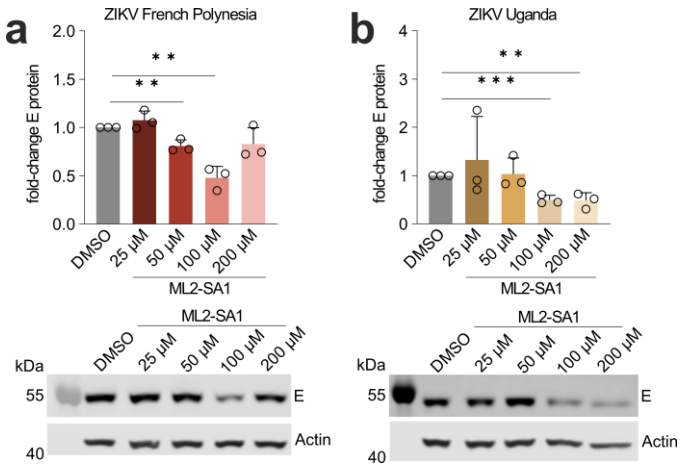

Figure 5.6: ML2-SA1 reduces ZIKV E protein levels in a dose-dependent manner. A549 cells were treated with varying concentrations of ML2-SA1 ranging from 25 µM to 200 µM for 2 h before infection. Subsequently, cells were infected (MOI = 1) with ZIKV French Polynesia (H/PF/2013) or ZIKV Uganda (976 Uganda). Cells were harvested 24 hpi. Western blotting was used to detect the relative fold-change of E protein ((**a**) ZIKV French Polynesia, (**b**) ZIKV Uganda). Respective representative Western Blots are shown below. Data are normalized to the respective DMSO control and are expressed as mean ± SD from n = 3 biological replicates. Statistical significance was determined by using an unpaired t-test. *$p < 0.05$, **$p < 0.01$, ***$p < 0.001$, ****$p < 0.0001$.

ML2-SA1 reduced infection of A549 cells with both ZIKV isolates in a dose-dependent manner (Figure 5.6). For ZIKV Uganda infected cells, ML2-SA1 concentrations of 100 µM and 200 µM significantly reduced the intracellular ZIKV E protein amount (Figure 5.6b). For ZIKV French Polynesia infected cells, ML2-SA1 concentrations of 50 µM and 100 µM led to a significant effect, while treatment with 200 µM did not lead to a significant reduction of intracellular ZIKV E protein in comparison to the DMSO control (Figure 5.6a).

The results depicted in Figure 5.6 are the first results indicating an antiviral potential of the selective TRPML2 agonist ML2-SA1. To further characterize the impact of ML2-SA1 treatment on the ZIKV infection process, intracellular ZIKV mRNA, E protein levels and the amount of released viral particles were monitored. A549 cells were treated with 100 µM ML2-SA1, infected with ZIKV French Polynesia and Uganda and harvested 24 hpi and 48 hpi, respectively (Figure 5.7).

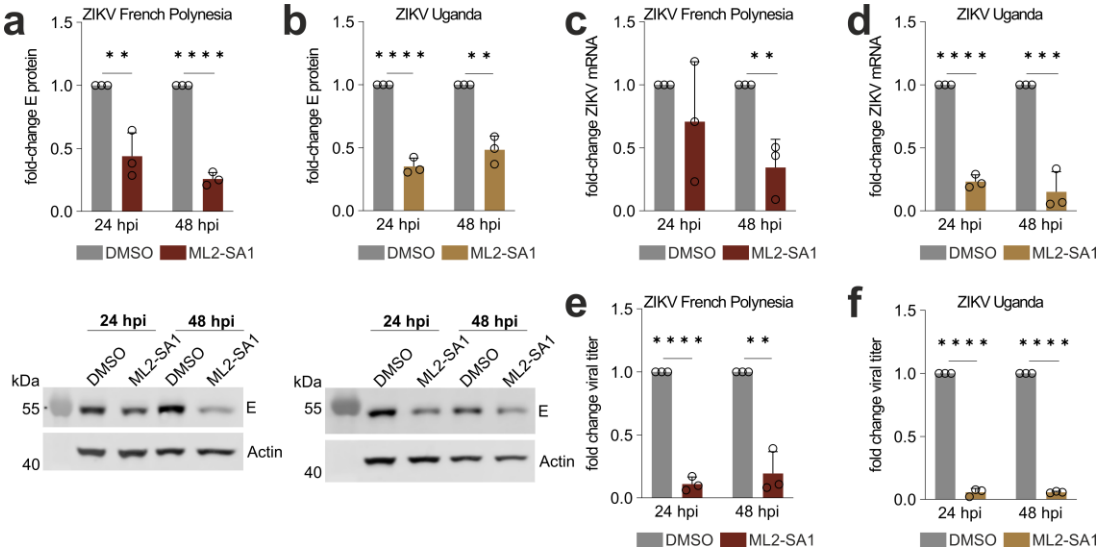

Figure 5.7: ML2-SA1 reduces intracellular ZIKV E protein and mRNA levels as well as the amount of released viral particles. A549 cells were treated with 100 µM ML2-SA1 for 2 h before infection. Cells were infected (MOI = 1) with the ZIKV French Polynesia (H/PF/2013) or ZIKV Uganda (976 Uganda) isolate and harvested 24 hpi and 48 hpi. (**a**, **b**) Relative fold-change of viral E protein as assessed via Western Blotting. One representative Western Blot is shown below. (**c**, **d**) Relative fold-change in intracellular ZIKV mRNA as assessed via RT-qPCR. (**e**, **f**) Amount of released infectious ZIKV particles assessed via a plaque assay. Data are normalized to the respective DMSO control for each timepoint and are expressed as mean ± SD from $n = 3$ biological replicates. Statistical significance was determined by using an unpaired *t*-test. *$p < 0.05$, **$p< 0.01$, ***$p < 0.001$, ****$p < 0.0001$.

ML2-SA1 did not only reduce the amount of intracellular ZIKV E protein of both isolates (Figure 5.7a, b), it also significantly decreased intracellular ZIKV mRNA levels as assessed by RT-qPCR (Figure 5.7c, d). Furthermore, the amount of released viral particles, as assessed by plaque assays, was significantly diminished (Figure 5.7e, f).

To test if ML2-SA1 interferes with early infection stages (e.g. causes increased lysosomal degradation of ZIKV and thereby decreases the amount of released viral RNA into the cytosol) or later infection stages (impairment of viral replication), further experiments were performed.

5.5 ML2-SA1 treatment causes accumulation of ZIKV E protein in CD63-positive vesicles

It was shown by Plesch *et al.* that treatment with the small molecule ML2-SA1 leads to activation of TRPML2 and release of Ca^{2+} and other cations from the endolysosomal lumen into the cytosol.[277] The local increase of the important second messenger Ca^{2+} might trigger the activation of various signaling cascades and might have a direct impact on the endolysosomal system, for example differences in intracellular vesicle size and distribution. To investigate the effect of ML2-SA1 on the morphology of the endolysosomal system in infected cells, super-resolution microscopy was performed (Figure 5.8**)**. In such an experiment, any accumulation of ZIKV particles in the endolysosomal system should also be visible, which might support the hypothesis that ML2-SA1 leads to increased lysosomal ZIKV degradation.

For super-resolution microscopy, A549 cells were treated with ML2-SA1 and infected with ZIKV Uganda. After fixation, immunostaining was performed with antibodies against the ZIKV E protein and human CD63, a marker for multivesicular bodies (MVBs). MVBs are specialized endosomes that contain membrane-bound intralumenal vesicles, which are formed by invagination and budding into the MVB lumen. The content of MVBs can either be degraded (via fusion with lysosomes) or released from the cell (via fusion with the plasma membrane).[319] Moreover, MVBs are the origin of exosomes.[320]

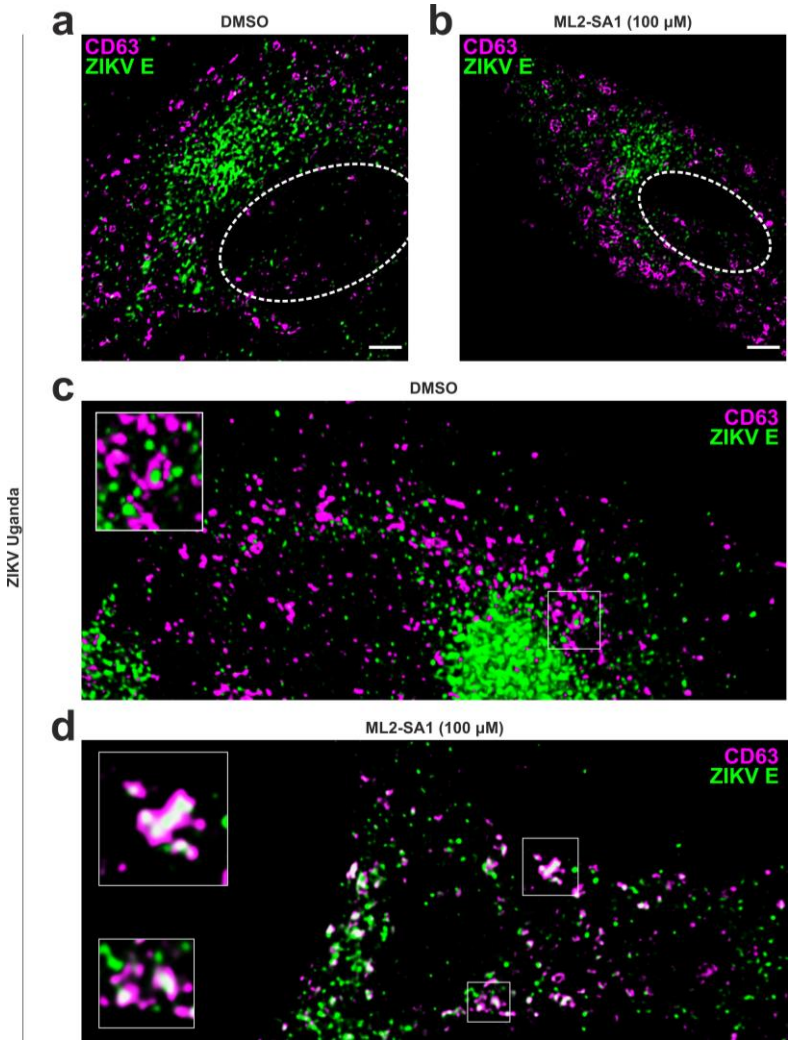

Figure 5.8: ML2-SA1 treatment leads to accumulation of ZIKV E protein in the endolysosomal system of infected A549 cells. (**a**, **b**) Representative super resolution microscopy images of A549 cells treated with 100 µM ML2-SA1 and infected with ZIKV Uganda (976 Uganda) and the corresponding DMSO control. Cells were fixed 24 hpi. Immunostaining was performed using antibodies against ZIKV E protein (shown in green) and CD63 (magenta). The position of the cell nucleus is indicated by a dotted circle. Scale bar: 2 µM. (**c**, **d**) 3D reconstructions.

ML2-SA1 treatment increased the size of CD63-positive MVBs in comparison to the DMSO control (Figure 5.8). In untreated cells, ZIKV E protein signal was concentrated around the nucleus. In ML2-SA1 treated cells, the ZIKV E protein signal was more distributed. Furthermore, 3D reconstructions revealed an accumulation of ZIKV E protein in CD63-positive vesicles of ML2-SA1 treated cells. In untreated cells, ZIKV E was located in close proximity to CD63-positive vesicles, but E protein was not found to accumulate inside of them.

5.6 Inhibition of lysosomal degradation does not lead to an increase of intracellular ZIKV E protein in ML2-SA1 treated cells

The results presented above suggest that ZIKV may face increased lyososomal degradation in ML2-SA1-treated cells. This is in agreement with a study by Xia *et al.* who reported an increased lysosomal degradation of DENV2 and ZIKV when cells had been treated with the unspecific TRPML-agonist ML-SA1.[236]

To confirm this hypothesis for ML2-SA1-treatment, A549 cells were treated with both Leupeptin and ML2-SA1. The tripeptide Leupeptin is a membrane-permeable thiolprotease inhibitor that inhibits the lysosomal proteases Cathepsin B, H and L.[321,322] Thus, inhibition of lysosomal proteases should lead to an increase of intracellular E protein detectable by Western Blot if ML2-SA1 treatment increases lysosomal accumulation of ZIKV (see Figure 5.9a). As a control for the effectiveness of Leupeptin treatment, changes in p62 protein levels were detected using a p62-specific antibody.

p62, also called sequestosome 1 (SQSTM1), is a common autophagy marker.[323] Autophagy is a conserved catabolic process, responsible for the delivery of cytoplasmic components and nonfunctional organelles to lysosomes for degradation and recycling.[324] p62 identifies and binds ubiquitinated proteins and transports them via membrane bound LC3 (microtubule-associated protein 1A/1B-light chain 3) to the phagophore for degradation. Afterwards, p62 itself is degraded by autolysosomes. Therefore, p62 can be used as a marker for autophagic flux.[325] Decreased p62 levels can be observed, when autophagy is induced, in contrast, p62 accumulates when autophagy is inhibited.[326] Leupeptin-mediated inhibition of lysosomal degradation led to the intracellular accumulation of p62 in mouse *in vivo* experiments.[327]

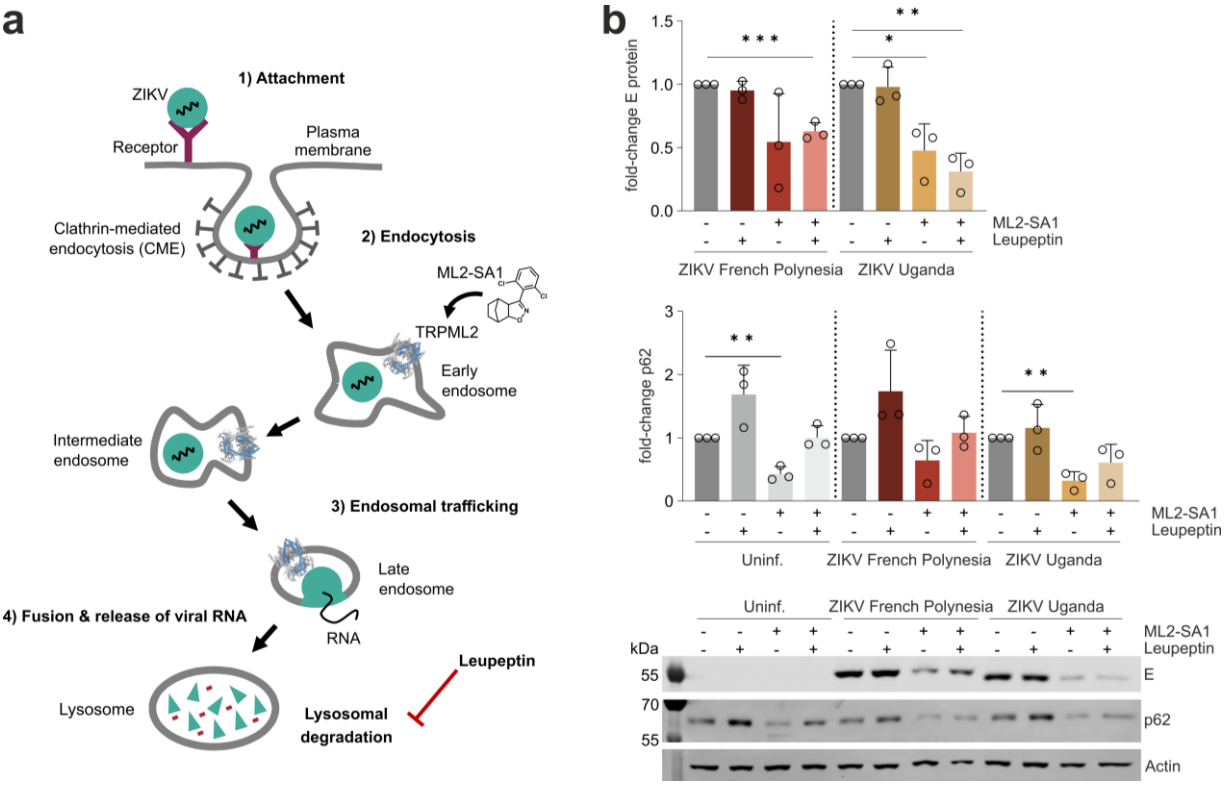

Figure 5.9: Inhibition of lysosomal degradation with Leupeptin in ML2-SA1 treated cells does not increase the amount of intracellular ZIKV E protein. A549 cells were treated with 100 µM ML2-SA1 and/or 0.1 mg/mL Leupeptin for 2 h before infection. Cells were infected (MOI = 1) with the ZIKV French Polynesia (H/PF/2013) and ZIKV Uganda (976 Uganda) isolate and harvested 24 hpi and 48 hpi. (**a**) Schematic overview of ZIKV entry. ML2-SA1 activates the human cation channel TRPML2 in the endolysosomal system. Leupeptin inhibits lysosomal proteases leading to accumulation of intracellular waste. (**b**) Relative fold-change of E protein and p62 as assessed via Western Blotting. One representative Western Blot is shown below. Data are normalized to the respective DMSO control and are expressed as mean ± SD from $n = 3$ biological replicates. Statistical significance was determined by using an unpaired *t*-test. *$p < 0.05$, **$p < 0.01$, ***$p < 0.001$, ****$p < 0.0001$.

In uninfected and ZIKV infected A549 cells, only Leupeptin treatment but not combination of Leupeptin with ML2-SA1 increased p62 levels (Figure 5.9b). However, these changes are not statistically significant due to high standard deviations. Interestingly, only ML2-SA1 treatment decreased p62 levels which is an indicator for enhanced autophagy.

In ZIKV infected A549 cells, only Leupeptin treatment did not alter ZIKV E protein levels (Figure 5.9b). When trafficking through the endolysosomal system, ZIKV fuses with the membranes of late endosomes, so the amount of intracellular E protein is presumably not changed when lysosomal degradation is inhibited, as ZIKV already escaped the endolysosomal system at higher pH values. However, somewhat surprisingly, an increase of intracellular ZIKV E protein was not observed in cells that have been treated with both ML2-SA1 and Leupeptin. If the antiviral effect of ML2-SA1 is not due to an increase of lysosomal degradation of ZIKV, it may instead affect later stages of the viral life cycle. Thus, in the following, the effects of ML2-SA1 treatment on early and late viral life cycle stages has been tested.

5.7 ML2-SA1 does not affect the early ZIKV life cycle stages

To investigate which stages of the ZIKV life cycle are affected by ML2-SA1 treatment, time-of-addition experiments were performed. Time-of-addition experiments can be used to elucidate the mechanism or target of a given compound in cell culture.[328] Since the life cycle of most viruses follows defined stages, time-of-addition experiments can be applied to any virus/drug combination. The standard protocol of time-of-addition experiments begins by infecting cells for a defined period of time (for example one hour), then unbound virus is removed to synchronize the infection process (also see Figure 5.10a).[328] Test compounds are subsequently added to the cells at defined time points.[328] This way, a time-of-intervention profile is generated, which can be compared with other, well characterized antivirals.[328] Basic prerequisites for this experiment are a highly susceptible cell line, well-established reference compounds and a fixed harvest time.[328] For ZIKV, time-of-addition experiments have been performed by other groups using a duration of 24 h for one replicative cycle, in which compounds have been added at timepoints during early and late stages resembling entry and post-inoculation phase.[236,329]

It has to be considered, that in previous experiments in this thesis, cells were pre-treated with ML2-SA1 for two hours before infection. At later timepoints, ML2-SA1 was replenished during the media exchange to ensure the constant exposure of the cells to the compound during the duration of the entire experiment.

In this time-of-addition experiment set-up, A549 cells were infected with the ZIKV Uganda isolate and ML2-SA1 was added at defined timepoints, starting from −2 h before infection until 22 h after infection resembling the entry and post-inoculation phase of the ZIKV life cycle. For reference, cells were also treated with ML-SA1, Bafilomycin A1, which restricts ZIKV entry by inhibiting the V-type ATPase and Ribavirin, a nucleoside analogue, which inhibits ZIKV replication. Before time-of-addition experiments were performed, cell toxicity of ML-SA1 in A549 cells was determined using a PrestoBlue® assay (see appendix Figure 10.2). No significant decrease in the percentage of redox metabolic activity was observed upon treatment with 100 µM ML-SA1 after 24 and 48 h. A decrease in the percentage of redox metabolic activity was detected for 200 µM ML-SA1 after 24 and 48 h. After 48 h, an increase in the percentage of redox metabolic activity was detected for 12.5, 25 and 50 µM ML-SA1 indicating a proliferative effect of ML-SA1. For subsequent time-of-addition experiments, a concentration of 100 µM ML-SA1 was used.

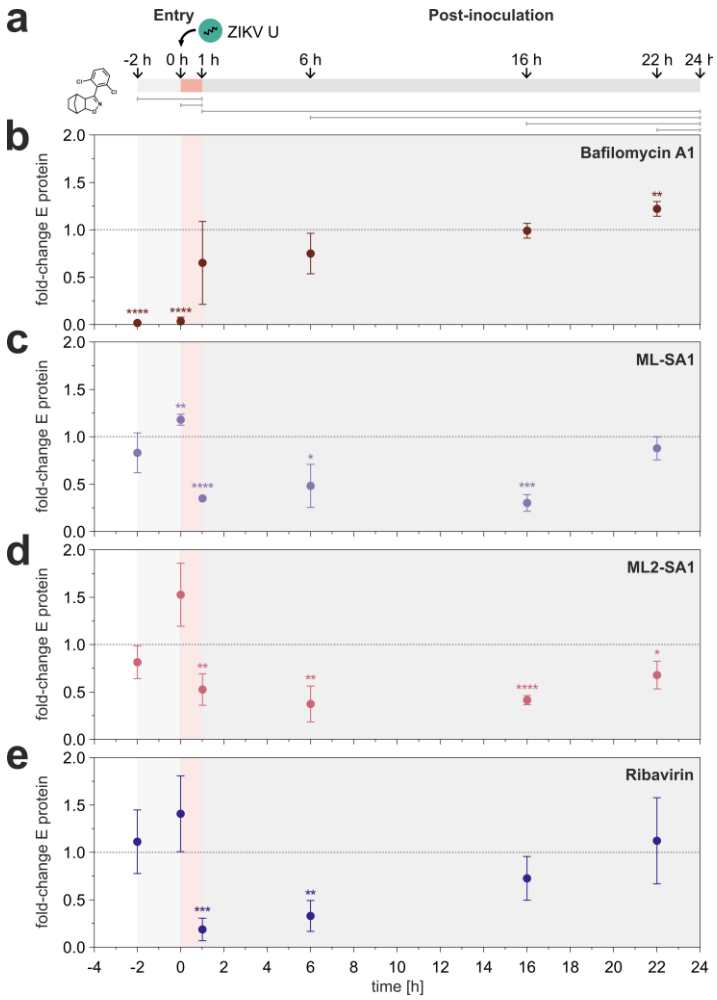

Figure 5.10: Time of addition experiment. (**a**) A549 cells were infected with ZIKV Uganda (976 Uganda) isolate for one hour (MOI = 1), then unbound virus was removed. Treatment with 50 nM Bafilomycin A1, 100 µM ML-SA1, 100 µM ML2-SA1 and 100 µM Ribavirin was started at −2h before infection, during infection, as well as 1 h, 6 h, 16 h and 22 h after infection. Gray lines below the time scale indicate the respective incubation period, in which the compounds were present, after the treatment was started. (**b**–**e**) Relative fold-change of ZIKV E protein in samples treated with 50 nM Bafilomycin A1 (**b**), 100 µM ML-SA1 (**c**), 100 µM ML2-SA1 (**d**) and 100 µM Ribavirin (**e**) was assessed via Western Blotting. Representative Western Blots are shown in appendix Figure 10.5. Results are normalized to the respective DMSO control of each timepoint and are expressed as mean ± SD from $n = 3$ biological replicates. Statistical significance was determined by using an unpaired *t*-test. *$p < 0.05$, **$p < 0.01$, ***$p < 0.001$, ****$p < 0.0001$.

As expected, when present during early infection stages, BFA1 strongly suppressed viral entry (Figure 5.10b), while Ribavirin affected the later stages of the viral life cycle (Figure 5.10e), such as replication. Surprisingly, ML2-SA1 does not lead to an antiviral effect when added during the entry process, but at later stages (Figure 5.10d), similar to the replication inhibitor Ribavirin (Figure 5.10e). ML-SA1 behaved similarly to ML2-SA1 indicating a role in later ZIKV life cycle stages (Figure 5.10c).

In addition to the experiments shown here for the ZIKV Uganda isolate, time-of-addition experiments were performed with ZIKV French-Polynesia-infected cells (appendix Figure 10.3) and led to similar

results. Based on these time-of-addition experiments, both unspecific TRPML agonist ML-SA1 and specific TRPML2 agonist ML2-SA1 inhibited ZIKV infection during later stages of the viral life cycle.

As shown before in this thesis (Figure 5.7e, f), ML2-SA1 does not increase the amount of released viral particles. It thus seems feasible that the main mode of action of the tested TRPML channel agonists and their cause of antiviral activity is due to an interference with ZIKV replication.

5.8 ML2-SA1 affects Zika virus replication

Key stages of ZIKV replication (including translation and cleavage of the viral polyprotein, replication of viral RNA and formation of progeny ZIKV particles) take place in replication factories (RFs) in the ER of the host cell (see section 1.3). To verify whether ML2-SA1 indeed affects viral replication, as suggested by the time of addition experiments (Figure 5.10 and appendix Figure 10.3), a ZIKV *Renilla* luciferase (RLuc) reporter assay was performed. This assay provides a versatile tool for antiviral testing through the introduction of the RLuc gene at the viral capsid coding sequence as first described by Shan *et al.* in 2016.[308]

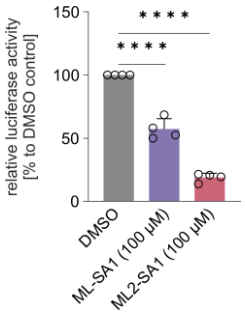

Figure 5.11: ML-SA1 and ML2-SA1 inhibit ZIKV replication. A549 were treated with 100 µM ML-SA1 and 100 µM ML2-SA1 and simultaneously infected with ZIKV RLuc reporter virus for for 4 h. Compounds were refreshed during each media change. 48 h post infection, luciferase activity was determined. Results are normalized to the DMSO control and are expressed as mean ± SD from n = 4 biological replicates. Statistical significance was determined by using an unpaired t-test. *$p < 0.05$, **$p < 0.01$, ***$p < 0.001$, ****$p < 0.0001$.

After treatment of A549 cells with the unspecific TRPML agonist ML-SA1 or the specific TRPML2 agonist ML2-SA1, a significant decrease of luciferase activity for both compounds was observed. This effect was more pronounced for ML2-SA1 compared to ML-SA1.

Additionally, confocal laser scanning microscopy revealed a significant decrease of dsRNA in ZIKV Uganda isolate infected A549 cells upon ML2-SA1 treatment (Figure 5.12).

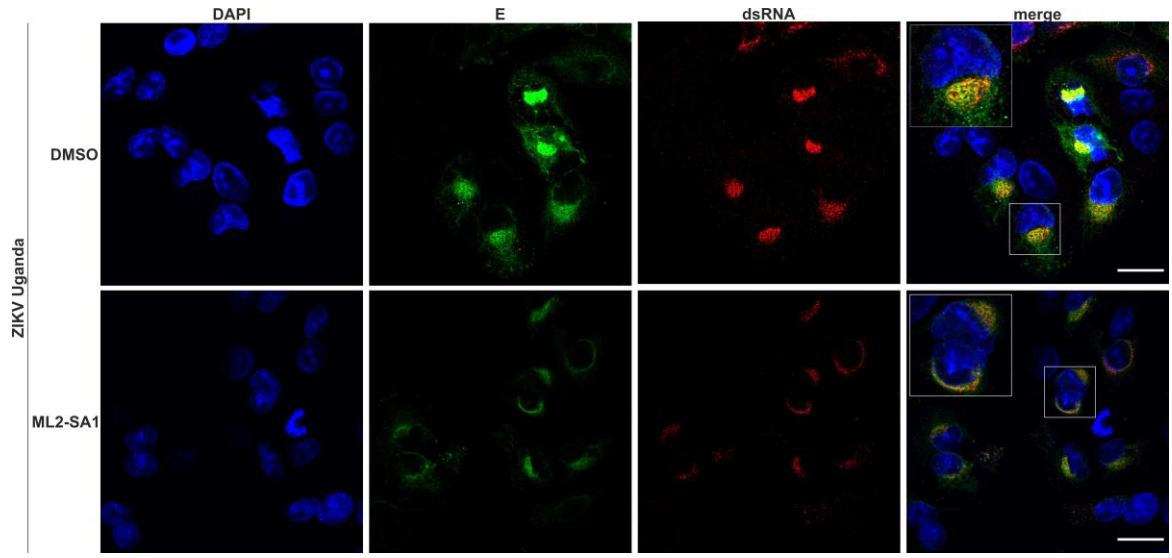

Figure 5.12: ML2-SA1 reduces the size of ZIKV replication factories. Representative confocal laser scanning microscopy (cLSM) images of A549 cells which have been treated with 100 µM ML2-SA1 for 2 h before infection. Cells were infected (MOI = 1) with the ZIKV Uganda (976 Uganda) isolate and fixed 24 hpi. Nuclei were stained with DAPI in blue and ZIKV E protein (green) and ZIKV dsRNA (red) were visualized using specific antibodies. Scale bar: 20 µM.

dsRNA intermediates are formed during RNA replication in ZIKV replication factories. ZIKV replication leads to a massive remodeling of the ER and the cytoskeleton.[96] Furthermore, the nuclear morphology is altered to form a characteristic, bean-like shape, with dense ER accumulating in the perinuclear region.[96] Addition of ML2-SA1 prevented the formation of pronounced ZIKV replication sites.

5.9 ML2-SA1 treatment leads to intracellular cholesterol accumulation

Effective ZIKV replication requires several host cell factors including cholesterol. This sterol lipid plays an important role in the formation or maintenance of flaviviral replication factories by affecting membrane rigidity and inducing negative membrane curvature.[330,331] In addition, cholesterol is involved in flavivirus entry, assembly, release, and control of the type I Interferon response.[332,333] Cholesterol transport has also been linked to TRPML channels: TRPML1 was shown to regulate lysosomal lipid and cholesterol trafficking.[296]

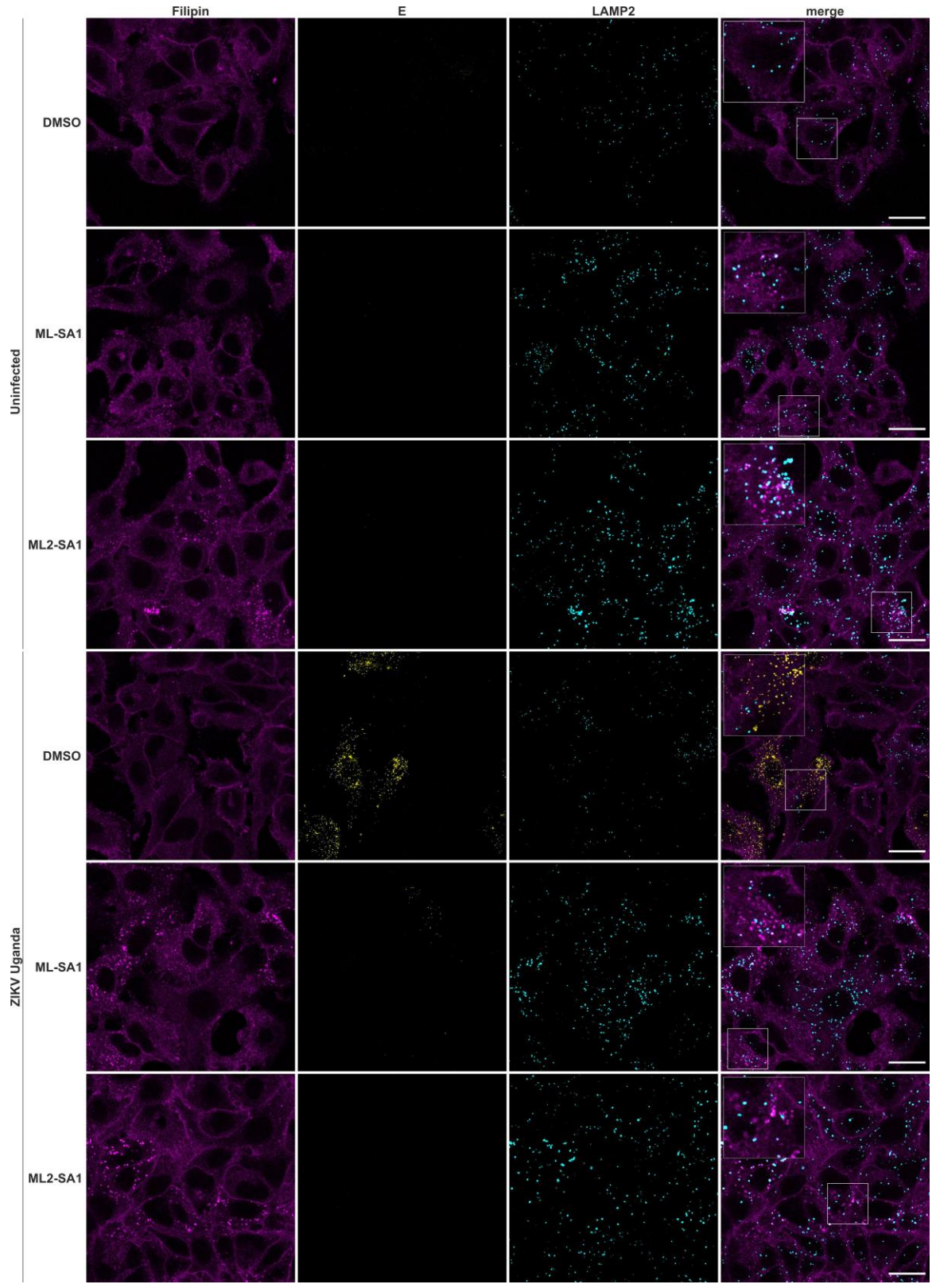

Figure 5.13: Treatment with ML-SA1 or ML2-SA1 leads to cholesterol accumulation in uninfected and ZIKV Uganda infected cells. Representative confocal laser scanning microscopy (cLSM) images of A549 cells which have been treated with 100 µM ML2-SA1 for 2 h before infection. Cells were infected (MOI = 1) with the ZIKV Uganda (976 Uganda) isolate and fixed 24 hpi. Intracellular cholesterol was stained using filipin (magenta) and ZIKV E protein (green) and the lysosomal marker LAMP2 (cyan) were visualized using specific antibodies. Scale bar: 20 µM.

Using immunofluorescence, the consequences of addition of the unspecific TRPML agonist ML-SA1 or the specific TRPML2 agonist ML2-SA1 on intracellular cholesterol levels was assessed (Figure 5.13). Interestingly, pronounced cholesterol accumulation can be observed in dot-like structures in cells which have been treated with ML-SA1 and ML2-SA1, regardless of whether they were infected with ZIKV or not. When comparing the effect of different ML2-SA1 incubation periods (8 h vs. 16 h) in uninfected cells, an increase in the size of cholesterol accumulations over time can be found (appendix Figure 10.6). Consistent with previous findings, ML2-SA1-treatment enlarges the size of LAMP2-positive structures (Figure 5.5). Notably, treatment with ML-SA1 had a similar effect (Figure 5.13).

All in all, inhibition of ZIKV infection by the TRPML2 specific agonist ML2-SA1 seems to be a complex interplay of several factors. ML2-SA1 significantly reduced intracellular ZIKV E protein levels, mRNA and the amount of released viral particles (Figure 5.7). Although increased lysosomal acidification of the endolysosomal system was observed upon ML2-SA1 treatment (Figure 5.5), no intracellular accumulation of ZIKV could be detected when lysosomal degradation was inhibited by the protease inhibitor leupeptin (Figure 5.9). Time-of-addition experiments indicated that ML-SA1 and ML2-SA1 could even induce a mild proviral effect when the compounds were present only during the early stages of the infection process (Figure 5.10). At later timepoints, treatment with both compounds led to a pronounced antiviral effect (Figure 5.10). RLuc assays confirmed the inhibition of ZIKV replication (Figure 5.11). Furthermore, the size of replication factories was reduced in ML2-SA1 treated cells (Figure 5.12). Treatment with ML-SA1 and ML2-SA1 led to intracellular cholesterol accumulation which might be a hint on impaired cholesterol trafficking (Figure 5.13).

6 Discussion

6.1 TRPML2 is not interferon-inducible in A549 cells and is down-regulated after ZIKV infection

In this thesis, the role of the human endolysosomal cation channel TRPML2 in the life cycle of ZIKV was investigated. In the past, TRPML2 overexpression was shown to enhance infectious virus production of several endocytosed viruses (for example IAV, YFV and ZIKV).[92] Furthermore, a role for the human endolysosomal cation channel TRPML2 in innate immunity was suggested in recent years.[245,270] TRPML2 was shown to be expressed at low levels in a resting mouse macrophage cell line, but was strongly up-regulated after TLR activation, in contrast to the other TRPML family members TRPML1 and TRPML3.[245] TRPML2 was also involved in chemokine and cytokine secretion of macrophages.[245,277] In addition, TRPML2 was reported as an putative ISG as its expression was upregulated in chimpanzee PBMCs by 4-fold around 4 h post IFNα treatment. IFNs are an important factor of innate immunity and are produced and released by host cells after being exposed to pathogens, including viruses.[273,274]

Before the consequences of ZIKV infection on TRPML2 expression levels were tested in this thesis, it was examined if TRPML2 expression is induced in uninfected human A549 cells upon interferon-treatment (Figure 5.1). Neither TRPML2 mRNA nor protein levels were significantly increased upon IFN-treatment at the chosen timepoints (4 h, 8 h and 24 h post-treatment), although a significant increase in ISG15 mRNA levels confirmed the effectiveness of the treatment. The interferons used in this study (IFNα, β and γ) can be divided into different categories. IFNα and β are type I interferons.[334] All type I IFNs bind to a common cell-surface receptor, called type I IFN receptor.[335–337] IFN γ, the only type II IFN, is a markedly different cytokine in comparison to the type I IFNs and binds to a different cell-surface receptor (type II IFN receptor).[336,338–340] Both type I and II IFNs activate JAK (Janus kinase)-STAT (signal transducer and activator of transcription) signaling pathways as well as several other signaling cascades.[341–345] As shown here, neither type I nor type II IFNs induced TRPML2 overexpression in uninfected A549 cells (Figure 5.1). However, responsiveness to IFNs is cell-type specific.[346] It might be possible that TRPML2 levels are elevated in other cell lines upon IFN treatment. Lanford *et al.* reported increased amounts of TRPML2 mRNA only for PBMCs of IFNα treated chimpanzees but not for liver tissue, which was also analyzed. All in all, the effect of IFNs on TRPML2 expression seems negligible in A549 cells.

In the next step, the consequences of ZIKV infection on TRPML2 expression levels was investigated. Although the consequences of TRPML2 overexpression on infection with endocytosed viruses was investigated before,[92] the effect of infection on endogenous TRPML2 remained elusive. Both ZIKV isolates that were used in this study (ZIKV Uganda, a representative of the African lineage and ZIKV French Polynesia, a representative of the Asian lineage) reduced TRPML2 mRNA and protein levels

after 24 h and 48 h (Figure 5.2). For TRPML1 and TRPML3 mRNA levels, no clear trend was observed (Figure 5.3).

In ZIKV-infected A549 cells, the induction of the interferon-stimulated gene ISG15 was diminished (Figure 5.2) in comparison to the induction of ISG15 in IFN-treated uninfected A549 cells (Figure 5.1). Several viruses including ZIKV have developed strategies to suppress innate immunity.[347] ZIKV non-structural proteins antagonize the host's interferon production and downstream signaling.[347] For example, viral proteins NS3 and NS4A prevent sensing of viral RNA in the cytosol by interfering with the intracellular PRRs RIG-I (retinoic acid inducible gene I) and MDA5 (melanoma differentiation-associated protein 5).[50] In addition, ZIKV interferes with IFN signaling pathways by inhibiting JAK1 and STAT activity: NS5 targets human STAT2 for proteasomal degradation[347,348] and prevents the activating phosphorylation of STAT1 and STAT2[349]. NS1, NS2A, NS2B and NS4B reduce the phosphorylation and activation of TBK1 (TANK-binding kinase 1) leading to an inhibition of IFNβ induction. Furthermore, NS1, NS2A, NS2B, NS4A, NS4B and NS5 inhibit IRF3 (interferon regulatory factor 3) phosphorylation, which reduces downstream IFN transcription.[50]

In contrast to TRPML2, TRPML1 and TRPML3 expression was reported not to be upregulated in a macrophage cell line after TLR activation, indicating a higher significance of TRPML2 in innate immunity.[245]As mentioned before, the effect of IFNs on TRPML2 expression was negligible in uninfected A549 cells (Figure 5.1) and the suppression of innate immunity during ZIKV infection may explain why TRPML2 levels have not been elevated in ZIKV-infected cells (Figure 5.2). However, the underlying mechanism behind the reduction of endogenous TRPML2 in infected cells remains unclear and needs further evaluation. As mentioned before, other groups have shown that TRPML2 levels were elevated in macrophage cell lines after type I IFN treatment and therefore TRPML2 was labeled as an ISG.[92] At the same time, TRPML2 was shown to increase infection with certain endocytosed viruses.[92] Therefore, TRPML2 would be one of the very few ISGs that actually enhance viral infection.[350] Rinkenberger and Schoggins presented a model how this might be beneficial for the host.[92] In non-immune cells, endogenous TRPML2 expression may lead to increased viral uptake which benefits the virus. However, in immune cells, which express higher levels of endogenous TRPML2, increased viral infection might lead to increased PAMP (pathogen-associated molecular pattern) recognition, stronger immune response, and an improved viral clearance. Following this hypothesis, ZIKV may suppress TRPML2 expression to escape the innate immune response.

6.2 The TRPML2-specific agonist ML2-SA1 has an antiviral effect against ZIKV

In this thesis, the TRPML2 specific agonist ML2-SA1 was used to modulate TRPML2 activity and to assess the role of this ion channel in the ZIKV infection process. First reported by Plesch *et al.*, ML2-SA1 is the only TRPML2-specific agonist currently available.[277] Similar to the unspecific TRPML agonist ML-SA1, ML2-SA1 is thought to bind in the transmembrane region based on molecular

docking studies.[277] Agonist binding induces channel opening.[277] Furthermore, dependent on the presence of TRPML2 in the cell, ML2-SA1 directly stimulates the release of the chemokine CCL2 from macrophages by promoting trafficking through early and recycling endosomes.[277]

Besides TPC channels, TRPML channels are the most important Ca^{2+} channels in the endolysosomal system. TRPML activation leads to Ca^{2+} flux from endosomes and lysosomes into the cytosol, which can influence vesicular fusion and fission, vesicular trafficking, autophagy, and lysosomal exocytosis.[275,297,298] Lysotracker staining of uninfected ML2-SA1-treated A549 cells indicated that ML2-SA1 treatment led to increased acidification of the endolysosomal system and potentially also increased vesicle fusion which resulted in the larger size of LAMP2-positive structures (Figure 5.5). In work reported by other groups, TRPML2 overexpression did not lead to increased acidification when acridine orange was used as a pH sensor.[92] For the unspecific TRPML agonist ML-SA1, increased lysosomal acidification was described after flow cytometry analysis.[236] It thus remains unclear whether the observed increased acidification upon ML2-SA1 treatment occurs directly due to TRPML2-dependent stimulation of a cation flux from endolysosomes into the cytosol[277] or an indirect, hitherto unexplored, effect.

In the following, the antiviral potential of ML2-SA1 was tested in A549 cells. In ZIKV French Polynesia and ZIKV Uganda infected cells, ML2-SA1 reduced intracellular ZIKV-E protein in a dose-dependent manner (Figure 5.6). For ZIKV French Polynesia infected cells, ML2-SA1 concentrations of 50 µM and 100 µM lead to a significant antiviral effect, while treatment with 200 µM ML2-SA1 did not lead to a significant reduction of intracellular ZIKV E protein in comparison to the DMSO control. A potential reason might be the mild (but not significant) cell toxicity of 200 µM ML2-SA1 in a 24 h treatment (Figure 5.4) which might counteract the antiviral effect. Of note, the ML2-SA1 concentrations found to lead to a reduction of intracellular ZIKV E protein are in a similar range as the effective ML-SA1 concentrations against ZIKV and DENV2 in A549 cells, reported by Xia *et al.*.[236]

Afterwards, the consequences of ML2-SA1 treatment on the ZIKV infection process was analyzed in more detail. ML2-SA1 significantly reduced ZIKV intracellular E protein and mRNA level as well as the amount of released viral particles when cells were harvested 24 h and 48 h post infection (Figure 5.7). These findings open different possibilities for the interpretation of the antiviral effect of TRPML2 activation mediated by ML2-SA1 treatment. First, the simultaneous reduction of ZIKV mRNA, E protein, and amount of released infectious particles could indicate that ZIKV is degraded in the endolysosomal system directly following cell entry. Degradation of ZIKV in lysosomes would prevent or reduce the release of ZIKV mRNA into the cytosol and therefore interrupt the ZIKV life cycle at an early stage. This hypothesis would be in accordance with the results from the lysotracker staining, which indicated an increased acidification, hence increased proteolytic activity, of the endolysosomal system (Figure 5.5). Another possibility might be that ML2-SA1 interferes with effective ZIKV replication.

6.3 The antiviral effect of ML2-SA1 is not caused by enhanced lysosomal degradation of ZIKV

Super-resolution microscopy was performed to detect the potential accumulation of ZIKV particles in the host cell endolysosomal system upon ML2-SA1 treatment. The method was also applied to analyze possibly resulting changes in size and distribution of multivesicular bodies (MVBs, Figure 5.8). Indeed, ML2-SA1 treatment increased the size of CD63-positive vesicles in comparison to the DMSO control. As mentioned before, activation of TRPMLs by small molecule agonists leads to Ca^{2+} flux from endosomes and lysosomes into the cytosol which was reported to influence vesicular fusion and fission, vesicular trafficking, lysosomal exocytosis and autophagy.[275,297,298] Furthermore, Plesch *et al.* reported the stimulation of CCL2 secretion in ML2-SA1-treated macrophages based on enhanced endosomal trafficking.[277] The increased size of MVBs that can be observed in super-resolution images of ML2-SA1-treated A549 cells (Figure 5.8) might also be an indicator of increased vesicle trafficking and membrane fusion.

It is perceivable that ML2-SA1-mediated TRPML2 activation might affect the interaction of TRPML2 with other proteins. In comparison to TRPML1 and TRPML3, only a very limited number of TRPML2 protein interaction partners have been described.[351] It was reported by Karacsonyi *et al.* that TRPML2 travels along the Arf6 associated pathway.[244] Moreover, heterologous overexpression of TRPML2 increases activity of the small GTPase Arf6 by seven-fold and leads to enhanced vesicle fusion and formation of large vesicles in HeLa cells.[244] It remains unclear if TRPML2 directly interacts with Arf6 or if it modulates the activity of specific Arf6 GEFs or GAPs (GTPase-activating proteins). Nonetheless, TRPML2 activation by ML2-SA1 in our A549 cells could potentially lead to a similar effect as was observed in HeLa cells,[244] thereby resulting in the abnormal CD36-positive vesicle structures observed here. Possibly, an increase in trafficking causes the accumulations of ZIKV in CD63-positive vesicles, which were revealed by 3D reconstructions (Figure 5.8).

To confirm the hypothesis that ZIKV may face increased lysosomal degradation in ML2-SA1-treated cells, A549 cells were treated with the protease inhibitor leupeptin and ML2-SA1. Unexpectedly, inhibition of lysosomal proteases did not lead to an increase intracellular E protein. This argued against the hypothesis that ML2-SA1 promotes lysosomal degradation of ZIKV. Furthermore, a decrease of p62 suggested enhanced autophagy, caused by ML2-SA1 treatment. Several roles for TRPML channels in autophagy have been suggested. For instance, TRPML1-mediated Ca^{2+} release induces the dephosphorylation of TFEB (transcription factor EB) by the phosphatase calcineurin, leading to TFEB nuclear translocation and transcriptional activation of autophagic and lysosomal genes.[298,352,353] Cellular samples from MLIV patients showed defects in macroautophagy, which were characterized by the accumulation of autophagic markers such as LC3 and p62.[354–356] Overexpression of TRPML3 was shown to impair autophagosome maturation.[248,357] However, the role of TRPML2 in autophagy has not been characterized in detail. Recently, TRPML2 was shown to also activate TFEB, leading to the expression of B7 costimulatory molecules on dendritic cells.[358] Our results display a

first tentative hint for a link between ML2-SA1-mediated specific TRPML2 activation and induction of autophagy. However, further experiments, for example testing of other autophagy markers such as LC3, must be performed to validate this connection.

Xia *et al.* reported induction of autophagy in ML-SA1 treated A549 and Huh7 cells. However, ML-SA1 treatment still reduced DENV2 infection in a dose-dependent manner when autophagy was blocked. Therefore, the antiviral activity of ML-SA1 seems to be independent of autophagy.[236] The authors presented acidification of lysosomes, increased protease activity and viral lysosomal degradation as the main mechanisms of the antiviral effect of ML-SA1. Based on the results of the combined ML2-SA1/Leupeptin treatment, this does not appear to be the case with ML2-SA1, although ZIKV E accumulations were observed in CD63-positive vesicles (Figure 5.8).

6.4 ML2-SA1 impairs ZIKV replication, presumably by altering cholesterol trafficking

To narrow down the role of TRPML2 in the ZIKV life cycle and to test whether early or late stages of the viral life cycle are affected by ML2-SA1-mediated TRPML2 activation, time-of-addition experiments were performed with ML2-SA1 as well as ML-SA1, Bafilomycin A1 (BFA1) and Ribavirin as reference compounds (Figure 5.10). As expected, the V-type ATPase inhibitor BFA1 strongly suppressed viral entry, while the nucleoside analogue Ribavirin affected later stages of the ZIKV life cycle (such as replication). Both ML2-SA1 and ML-SA1 also affected later stages of the viral life cycle, similar to the replication inhibitor Ribavirin.

For ML-SA1, this is different from what was postulated by Xia *et al.* who suggested that ML-SA1 affects viral entry. However, it should be noted that in their publication, Xia *et al.* did not provide data for reference compounds in the context of their time-of-addition experiments. Furthermore, according to their materials and methods section, they did not remove unbound virus after infection which is important for synchronizing the infection process.[236] For both ML-SA1 and ML2-SA1 addition at early infection stages, slightly proviral effects could be observed. As discussed before, activation of TRPMLs (leading to Ca^{2+} flux into the cytosol) might lead to increased endolysosomal trafficking and therefore promote infection during the early stages of the ZIKV life cycle.

The impact of ML2-SA1 and ML-SA1 on ZIKV replication was confirmed using a ZIKV RLuc reporter assay. Notably, the effect was more pronounced for ML2-SA1 in comparison to ML-SA1 (Figure 5.11). Furthermore, cLSM revealed a strong decrease of dsRNA in ZIKV Uganda infected A549 cells upon ML2-SA1 treatment (Figure 5.12). ML2-SA1 prevented the formation of pronounced ZIKV replication sites in the ER, which are a common feature of flaviviral infection.[96,99] There, key stages of viral replication take place, which include translation and cleavage of the viral polyprotein, viral RNA replication and formation of progeny ZIKV particles.[99] For effective flavivirus replication, several

host cell factors are required, for example DENV NS3 recruits fatty acid synthase to the replication sites to produce lipids which are then integrated into the ER membrane.[102] Moreover, flavivirus replication factories are enriched with cholesterol, which improves membrane fluidity.[103] Staining of intracellular cholesterol with filipin revealed pronounced cholesterol accumulation in dot-like structures in uninfected and ZIKV-infected cells, which have been treated with ML2-SA1 (Figure 5.13).

A published lipidomics study showed that ZIKV significantly alters the host cell lipid composition, with most pronounced changes observed within subclasses of sphingolipids.[359] Of note, TRPML1 was shown to be inhibited by the sphingolipid sphingomyelin.[296] In addition, cholesterol esters were enriched in ZIKV-infected cells.[359] As mentioned before, cholesterol serves important functions in the formation if ZIKV replication factories.[332] In uninfected cells, only around 1% of unesterified cholesterol is found in the ER.[360,361] Ca^{2+} channel modulators have previously been shown to reduce ZIKV replication by interfering with intracellular cholesterol trafficking. For instance, Lacidipine inhibits L-type calcium channels (LTCCs) which are located in the plasma membrane of vascular smooth muscle cells.[362,363] This drug also inhibits ZIKV replication, presumably by altering intracellular trafficking of cholesterol and other lipids. However, the molecular mechanisms behind these findings remained unclear.[364]

Here, for the first time, ML2-SA1-mediated TRPML2 activity was linked to changes in intracellular cholesterol distribution. This may also relate to published studies showing that ML-SA1-mediated unspecific TRPML activation as well as TRPML1 overexpression can rescue trafficking defects in NPC1 (Niemann-Pick disease, type C intracellular cholesterol transporter 1) deficient cells.[296] The dot-like cholesterol accumulations which were observed in ML-SA1- and ML2-SA1-treated uninfected and infected cells in this thesis could be an indicator for alterations in cholesterol trafficking which might lead to low abundance of cholesterol in the ER. As a consequence, impaired formation or maintenance of ZIKV replication factories may ensue. Alterations in cellular cholesterol distribution may thus represent the molecular basis for the observed antiviral effect of ML2-SA1.

While host-cholesterol is also an important factor during viral entry,[332] our time-of-addition experiment indicated that ML-SA1 and ML2-SA1 affect later stages of the ZIKV life cycle, specifically viral replication. Further investigations are thus needed to analyze the effects of ML2-SA1 (and ML-SA1) treatment on cholesterol trafficking in more detail. Finally, potential off-target effects of ML-SA1/ML2-SA1 treatment cannot be excluded. To rule out this possibility, TRPML knockdown experiments need to be performed.

Part II: Structural regulation of the human TRPML2 Extractosolic/Lumenal Domain (ELD)

Understanding complex processes such as viral infections requires analyzing of the function and regulation of the individual factors involved. As shown in the last chapter, TRPML2 plays a remarkable role in ZIKV infection. However, a lot of questions regarding the structural regulation of TRPML2 in the endolysosomal system (for example by Ca^{2+} and pH) remain open. Therefore, the structure of the human TRPML2 extracytosolic/lumenal domain (ELD), the structural hallmark of the TRPML family, was determined. Although this domain constitutes around one third of the whole channel, its physiological function remains enigmatic. Here, a potential role of the ELD in pH-dependent regulation of the whole channel was suggested.

Parts of this chapter have been published in: **Kerstin K. Viet***, Annika Wagner*, Kevin Schwickert*, Nils Hellwig, Martha Brennich, Nicole Bader, Tanja Schirmeister, Nina Morgner, Hermann Schindelin and Ute A. Hellmich, Structure of the Human TRPML2 Ion Channel Extracytosolic/Lumenal Domain. *Structure* **27**, 1246-1257.e5 (2019).[1]

*contributed equally

7 Results

7.1 Structure of the human TRPML2 ELD

TRPML2 is the least described member of the TRPML family with regard to both its cellular function and its structural characterization. Several full-length structures of TRPML1 and TRPML3 and structures of the isolated ELD of TRPML1 have been published in recent years.[222,237,254–258,263] For TRPML2, one full-length structure of mouse TRPML2 in lipid nanodiscs is available.[258] To investigate the structure and dynamics of the isolated human TRPML2 ELD, the protein was heterologously expressed from *E. coli* and purified. Details about the expression and purification protocol can be found in the methods section 4.11 and in the appendix (section 10.7). At pH 6.5, a 2.0 Å structure (pdb 6HRR, construct: A92–K285) and at pH 4.5, a 2.95 Å structure (pdb 6HRS, construct: G84–K285) of the human TRPML2 ELD was determined.[1] With these crystal structures of the human TRPML2 ELD at different pH values, we provided the first structural information available for the human TRPML2.

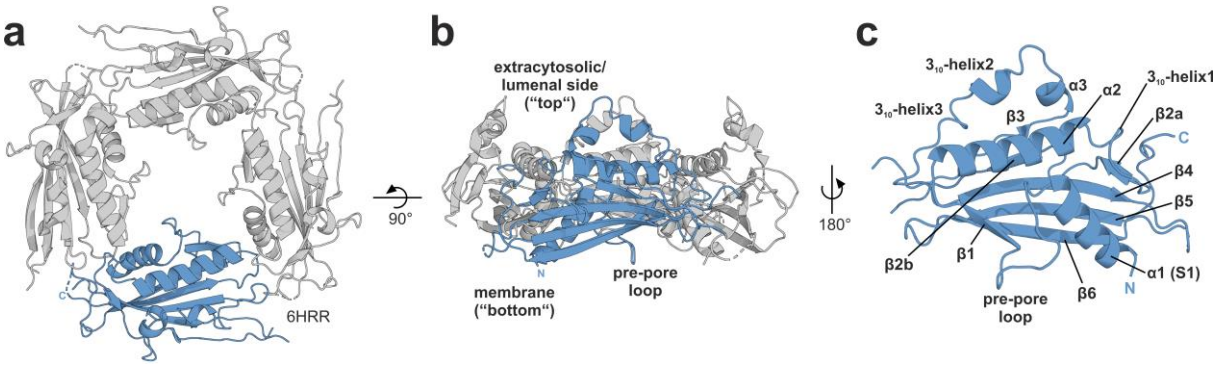

Figure 7.1: Crystal structure of the human TRPML2 Extracytosolic/Lumenal Domain (ELD). (**a**) Structure of the human TRPML2 ELD (pdb 6HRR) at 2.0 Å resolution and pH 6.5 (top view, one monomer shown in blue). The ELD forms a tetramer even in the absence of the rest of the channel. The pre-pore loops of all four subunits are extended into the central pore. (**b**) Side view of the TRPML2 ELD tetramer. (**c**) TRPML2 ELD monomer, individual helices and β strands are indicated.

The overall tetramer dimensions are ~85 x 85 Å parallel to the membrane plane and ~35 Å perpendicular to it. Similar to the TRPML1 and TRPML3 ELDs,[237,263] the TRPML2 ELD displays a tetrameric assembly that exhibits C_4 rotational symmetry (Figure 7.1a,b).

In line with Li *et al.* who determined the structures of the TRPML1 ELD at pH 4.5, 6.5 and 7.5 and observed no significant differences between their structures,[263] no significant alterations between the TRPML2 ELD pH 6.5 and 4.5 structure could be found.[1] In our crystal structures, the N-terminus is fully resolved and the first amino acid residues, which extend the transmembrane helix S1 in the full-length protein, also adopt an α-helical conformation in the isolated TRPML2 ELD (Figure 7.1c). In contrast, the C-terminus is disordered and/or unresolved. The last visible residue with clearly observable electron density is found between AAs 281 and 284 in different monomers. In the full-length channel, the disordered C-terminal residues would also adopt an α-helical conformation

corresponding to transmembrane helix S2, but in the absence of the transmembrane domain and the lipid environment, this helix seems to be not stable. Beyond the first long α helix S1/α1, each TRPML2 ELD monomer is folded into an additional long α helix (α2), one short α helix (α3), as well as three 3_{10} helices and six β strands (β1 – β6), which form a single antiparallel β sheet (Figure 7.1).[1]

Our crystal structures of the human TRPML2 ELD can be compared to the cryo-EM structure of the mouse TRPML2 ELD which was solved in the context of the whole channel (Figure 7.2).[258] The cryo-EM structure of full-length mouse TRPML2 in lipid nanodiscs at 3.14 Å resolution (pdb 7DYS) was presented by Song *et al.* in 2022.[258] The structure in the apo state revealed an inactive conformation at pH 7.4. N-terminus (AAs 1 - 65) and C-terminus (AAs 518 - 566) as well as several loops connecting the transmembrane helices could not be modeled due to poor density.[258] Within the boundaries of AAs A92–K/R285, which comprises our domain construct, human and mouse TRPML2 display 75.8% identity. A sequence alignment of the human and mouse TRPML2 ELDs can be found in the appendix (Figure 10.9).

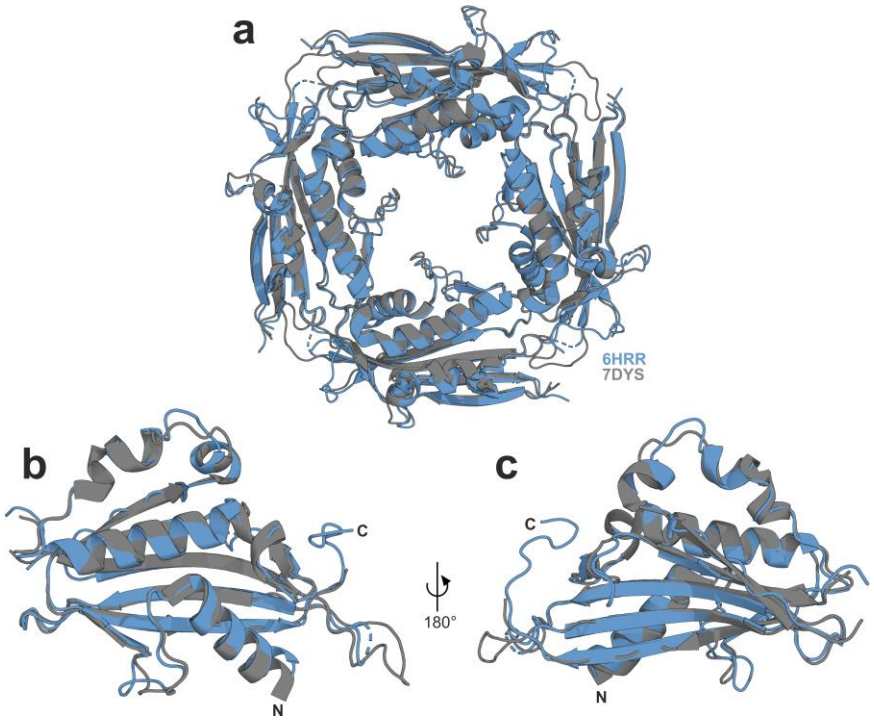

Figure 7.2: Comparison of the human TRPML2 ELD at pH 6.5 and mouse TRPML2 ELD at pH 7.4. (**a**) Structure alignment of tetrameric hsTRPML2 (pdb 6HRR), pH 6.5[1] at 2.0 Å resolution (shown in blue) and tetrameric mmTRPML2 (pdb 7DYS), pH 7.4[258] at 3.14 Å resolution, (shown in grey). (**b**, **c**) Structure alignments of hsTRPML2 (6HRR) and mmTRPML2 (7DYS) monomers.

Notably, the main secondary structure elements (the two long α helices and the six-stranded antiparallel β sheet) and the C_4 symmetrical architecture are conserved not only in the structures of human and mouse TRPML2 at different pH values, but also in the crystal structures of the TRPML1 ELD[263] and the cryo-EM structures of the full-length TRPML1, TRPML2 and TRPML3 channels.[1,222,237,254–258] The cryo-EM structure of mmTRPML2 at pH 7.4 and our crystal structures of the

isolated hsTRPML2 ELD at pH 6.5 (pdb 6HRR) and pH 4.5 (pdb 6HRS) enable the comparison of TRPML2 ELDs at three physiological relevant pH values. The pre-pore diameters at the narrowest points are in a similar range (12.5 Å at V112 at pH 7.4 vs. 12.0 Å at S110 at pH 6.5 and 13 Å at S110 pH 4.5).[1,258] This mild variance could be due to structural changes caused by the different pH environment. However, the lack of the TMD may have affected the size of our hsTRPML2 ELD structures.

7.2 Ca^{2+} interacts with the acidic TRPML2 ELD pre-pore loop residues in a pH-dependent manner

In the human TRPML2 ELD, the C-terminal residues of the N-terminal α1/S1 helix directly lead into a loop consisting of 12 residues (K107-S118). Since this loop is centered on top of the ion channel pore formed by transmembrane helix S5 and S6 in the full-length channel, this loop will be referred to as pre-pore loop. It contains a stretch of four acidic residues (^{113}DEDD^{116}). N-terminal from the DEDD motif, the TRPML2 ELD pre-pore loop contains a glycine- and serine/threonine-rich sequence (^{108}GYSGT^{112}) indicating a relatively high flexibility of this region. However, the pre-pore loop is well resolved in the TRPML2 ELD structures (also see Figure 7.3a).[1,258]

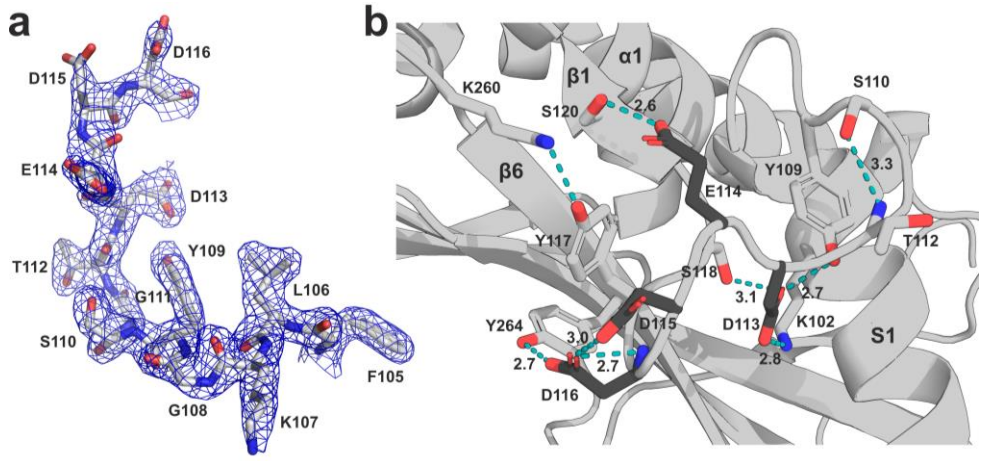

Figure 7.3: Electron density map and hydrogen bonding network of the TRPML2 ELD pre-pore loop. (**a**) SIGMAA-weighted $2F_o - F_c$ electron density for the TRPML2 pre-pore loop at pH 6.5 (pdb 6HRR). (**b**) Structure of one human TRPML2 ELD monomer (pdb 6HRR) at 2.0 Å resolution and pH 6.5. With the exceptions of the backbone amides of T112 and D116, only side-chain interactions are shown. The respective hydrogen bond distances are indicated in Å. The four acidic residues of the pre-pore loop are shown in dark gray.

The pre-pore loop is stabilized by a complex set of hydrogen bonds (Figure 7.3b) which connects it both to the S1 helix and the C-terminal region of the ELD:

(1) A hydrogen bond is formed between the side chain of S110, which marks the constriction site of the TRPML2 ELD pore, and the main chain atoms of T112.
(2) One of the side chain oxygens of D113 forms a bifurcated H-bond with the side chains of Y109 located in the pre-pore loop and S118 in β1, while the other is H-bonded to Nε of K102 in S1. Importantly, mutation of D113 to alanine or asparagine led to insoluble misfolded protein (data not shown), highlighting the importance of this residue for the structural integrity of the ELD.
(3) A weak interaction can be found between the side chain of E114A and the backbone amide and a more favorable bond with the side chain of S120 in β1. Additionally, the backbone amide of E114A forms a bifurcated hydrogen bond with the backbone carbonyls of Y117 and S118.
(4) The side chain of D116 forms a hydrogen bond with the side chain of Y264 in β6.

In addition, the carboxylate groups of D115 and D116 are in close proximity (2.9 – 3.0 Å). This distance could be an indicator for a hydrogen bond between a protonated, neutral carboxy group and a non-protonated carboxylate group. Alternatively, a distance of 3.0 Å between two Asp/Glu carboxylates could indicate a metal binding site.[365] The acidic patch in the pre-pore loop is conserved among the members of the TRPML family. In TRPML1 (^{111}DGADDT^{116}) and TRPML3 (^{108}DRMDDT^{113}), similar acidic motifs can be found.[1] For TRPML1, a model for the dual regulation of this cation channel by Ca^{2+} and pH has been suggested by Li and coworkers.[263] The acidic amino acid residues of the ELD's pre-pore loop are negatively charged at a neutral pH of 7.4 and are therefore able to attract and bind Ca^{2+} to form a "block" for other cations. This renders the channel inactive. Lower pH values which can be found for example in late endosomes and lysosomes lead to protonation of the acidic residues and weaken the Ca^{2+} block thereby enabling cation flux.

In the tetrameric TRPML2 full-length channel at pH 7.4, a cation would encounter a ring of 16 acidic residues (four from each subunit) before it could pass through the ion channel pore. To investigate whether the calcium block model could also apply for TRPML2, the interaction of the TRPML2 ELD with Ca^{2+} at different pH values was measured using isothermal titration calorimetry (ITC, Figure 7.4). ITC measurements allow to determine binding constants and thermodynamic parameters of reactions in a broad concentration range without requiring elaborated labeling schemes. However, for determining K_D values of weak binding events (e.g. protein-protein-interactions or protein-ion-interactions) high concentrations of protein (and ligand) are required.

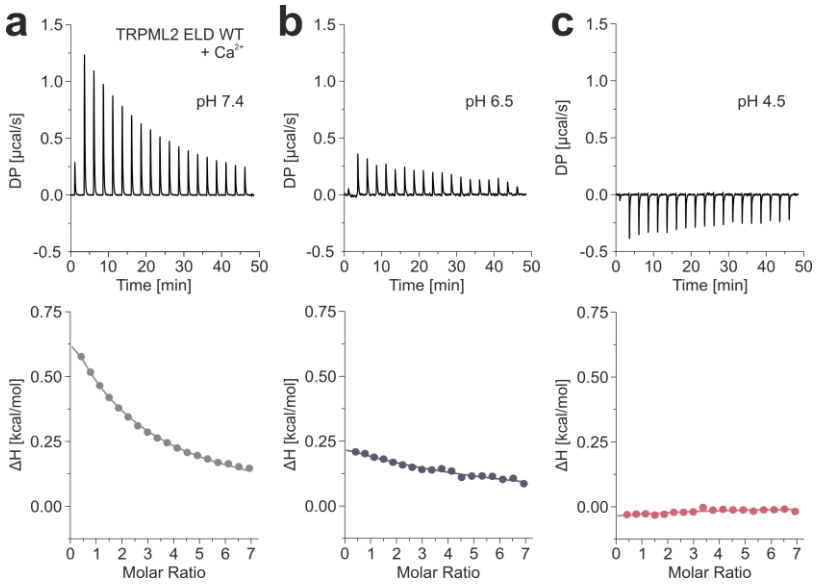

Figure 7.4: The wild-type (WT) human TRPML2 ELD binds Ca^{2+} in a physiologically relevant concentration range at near neutral pH, but not at lower pH values. ITC thermograms (top) and integrated heat signatures with fitted curves (bottom) of the titrations of $CaCl_2$ (15 mM stock solution) to the WT TRPML2 ELD (400 µM) at pH 7.4 (**a**), pH 6.5 (**b**) and pH 4.5 (**c**).

At pH 7.4, the TRPML2 ELD interacted with Ca^{2+} with a K_D of 2.97 ± 0.11 mM (Figure 7.4a). The binding reaction was endothermic and entropy driven, possibly due to the release of water molecules from the hydration shell of the pre-pore loop residues. At pH 6.5, the Ca^{2+} affinity was reduced by more than four-fold (Figure 7.4b). Due to the very low binding affinity no reliable K_D value could be determined. At pH 4.5, no interaction between Ca^{2+} and the TRPML2 ELD could be observed (Figure 7.4c). Representative ITC thermograms of control titrations ($CaCl_2$ into buffer) can be found in the appendix (Figure 10.11).

To confirm the acidic pre-pore loop patch as the Ca^{2+} binding site, the four residues of the ^{113}DEDD^{116} motif were mutated. As mentioned before, mutagenesis of D113 to alanine to asparagine resulted in insoluble, misfolded protein, suggesting that the main function of this residue is the stabilization and folding of the pre-pore loop structure. In contrast, mutagenesis of E114, D115, and D116 to alanine led to soluble, tetrameric, and structurally intact protein as confirmed by CD spectroscopy and analytical SEC (Figure 7.5)

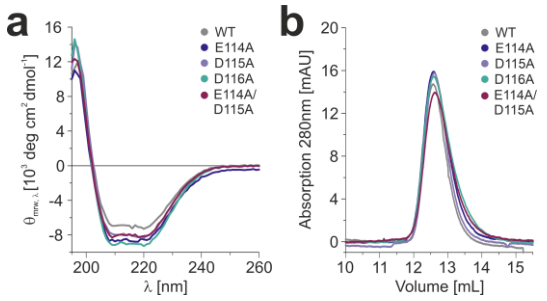

Figure 7.5: Mutation of pre-pore loop amino acid residues to alanine does not affect secondary structure and tetrameric integrity of the TRPML2 ELD. Circular dichroism (CD) spectroscopy (**a**) and analytical SEC (**b**) of WT TRPML2 ELD and pre-pore loop mutants (TRPML2 ELD E114A, D115A, D116A, E114A/D115A).

ITC measurements with the TRPML2 ELD E114A and D115A mutants showed a significant decrease but not the complete loss in Ca^{2+} affinity at pH 7.4 (Figure 7.6). For the TRPML2 ELD D116A mutant a reduction of Ca^{2+} affinity was also observed, although not to the degree of the E114A and D115A mutants. Therefore, the TRPML2 ELD E114A/D115A double mutant was also generated. This mutant further decreased Ca^{2+} affinity, thus confirming a pH dependent Ca^{2+} binding site in the center of the TRPML2 ELD pre-pore loop.

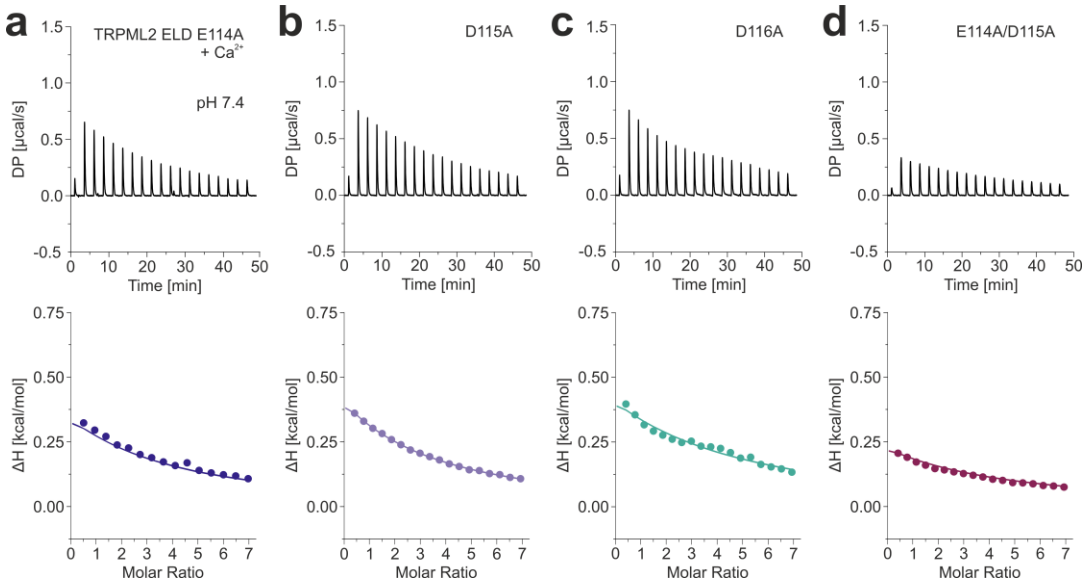

Figure 7.6: Mutation of pre-pore loop amino acid residues to alanine impairs Ca^{2+} binding ability of the TRPML2 ELD. ITC thermograms (top) and integrated heat signatures with fitted curves (bottom) of the titrations of $CaCl_2$ (15 mM stock solution) to the TRPML2 ELD pre-pore loop mutants (TRPML2 ELD E114A (**a**, 330 µM due to low protein yields), D115A (**b**, 400 µM), D116A (**c**, 400 µM) and E114A/D115A (**d**, 400 µM)) at pH 7.4.

These results strongly support the Ca^{2+} block model which was proposed by Li *et al.* for TRPML1.[263] Therefore, it may represent a general regulatory mechanism for TRPML channels which may be dependent on the pH value of different cellular compartments and potentially the structural orientation of the pre-pore loop acidic residues (see section 7.4).

7.3 The wild-type TRPML2 ELD binds to a variety of cations with different affinities

TRPML channels play an outstanding role in the lysosomal cation homeostasis, not only for Ca^{2+} but also other mono- and divalent cations.[215,234] Notably, the TRPML1 related disease Mucolipidosis type IV is linked with accumulation of chelatable Zn^{2+} in lysosomes.[366] To further investigate the binding process of cations other than Ca^{2+} to the ELD, ITC measurements with Mg^{2+} and Zn^{2+} were performed at neutral pH and compared to the data with Ca^{2+} (Figure 7.7a, b, c).

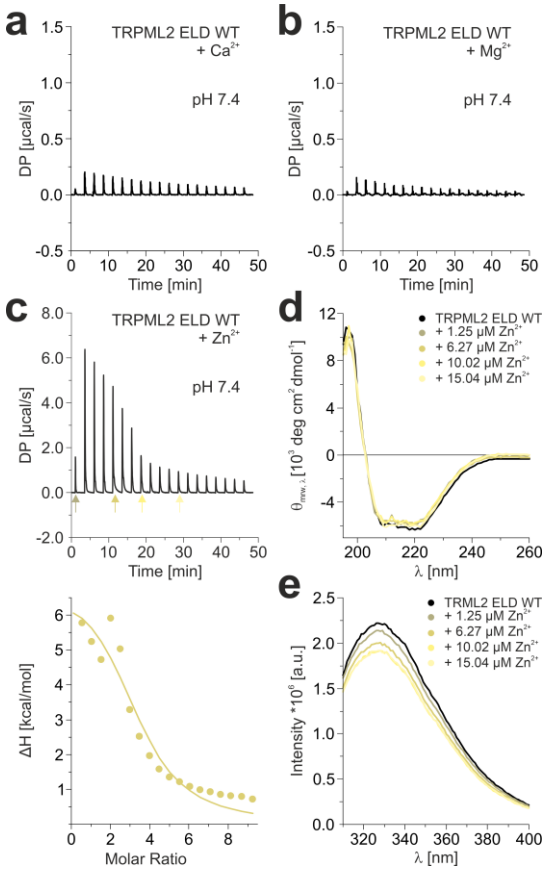

Figure 7.7: Investigations on the binding affinities of Mg^{2+} and Zn^{2+} to the WT TRPML2 ELD in comparison to Ca^{2+}. (**a**, **b**) ITC thermograms of the titrations of $CaCl_2$ (**a**, 5 mM stock solution) and $MgCl_2$ (**b**, 5 mM stock solution) to the WT TRPML2 ELD (100 µM) at pH 7.4. Because of the low binding affinities, integrated heat signatures are not shown. (**c**) ITC thermograms (top) and integrated heat signatures with fitted curves (bottom) of the titration of $ZnCl_2$ (5 mM stock solution) to the WT TRPML2 ELD (100 µM) at pH 7.4. (**d**) CD spectroscopy of the TRPML2 ELD WT in presence of different Zn^{2+} concentrations (ELD to Zn^{2+} ratio corresponding to characteristic peaks in the corresponding ITC thermogram (**c**, highlighted by colored arrows). (**e**) Tryptophan fluorescence measurements of the TRPML2 ELD WT in presence of different Zn^{2+} concentrations (ELD to Zn^{2+} ratio corresponding to characteristic peaks in the corresponding ITC thermogram (**c**, highlighted by colored arrows).

Titration of $ZnCl_2$ to the WT TRPML2 ELD using the above-mentioned concentrations for Ca^{2+} (titration of 15 mM $CaCl_2$ to 400 µM protein) led to a very strong signals and precipitation of the protein. Therefore, titrations with lower protein and $ZnCl_2$ concentrations were carried out (data not shown). Figure 7.7c shows the titration of 5 mM $ZnCl_2$ to 100 µM TRPML2 ELD WT. Similar to Ca^{2+}, Zn^{2+} bound to TRPML2 ELD WT in an endothermic reaction. Nevertheless, protein precipitation could be observed after the experiment was completed (further lowering of protein and $ZnCl_2$ concentrations led to significant decrease of a detectable signal). The broadening of the peaks corresponding to the fifth and sixth $ZnCl_2$ injection and the following signal decrease also indicated two reactions (presumably binding of Zn^{2+} to the ELD followed by protein aggregation). Notably, the titration of $ZnCl_2$ to buffer only also caused a considerable endothermic signal. Representative ITC thermograms of the titrations of $CaCl_2$, $MgCl_2$ and $ZnCl_2$ can be found in the appendix (Figure 10.12).

In contrast to Zn^{2+}, Mg^{2+} bound with a very low affinity to the TRPML2 ELD (Figure 7.7b: titration of 5 mM $MgCl_2$ to 100 µM WT TRPML2 ELD). The affinity of Mg^{2+} to the TRPML2 ELD was also lower than the affinity to Ca^{2+} using the same concentrations (Figure 7.7a: titration of 5 mM $CaCl_2$ to 100 µM WT TRPML2 ELD). To investigate whether aggregation of the TRPML2 ELD during $ZnCl_2$ titration occurs due to the high protein and ligand concentrations, circular dichroism (CD) spectroscopy measurements were performed Figure 7.7d). Defined amounts of $ZnCl_2$ corresponding to characteristic peaks in the respective ITC thermogram (Figure 7.7c) were added to WT TRPML2 ELD samples. As seen in Figure 7.7d, the presence of $ZnCl_2$ did not affect the secondary structure of the TRPML2 ELD at low concentrations (5 µM of protein).

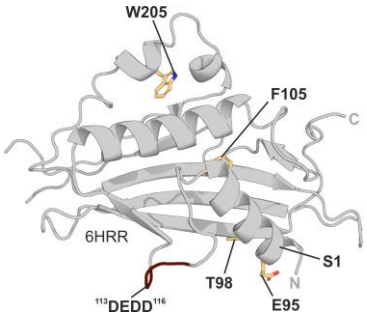

Figure 7.8: Human TRPML2 ELD amino acid residues relevant for this thesis. Structure of one human TRPML2 ELD monomer (pdb 6HRR) at 2.0 Å resolution and pH 6.5.[1] Highlighted are amino acid residues E95, T98, F105 and W205 in lightorange and the acidic ^{113}DEDD^{116} motif in red.

As an alternative to study conformational dynamics, which requires only small protein amounts, tryptophan fluorescence measurements were carried out with the same protein/ligand ratio as in the CD measurements. The only native tryptophan of the TRPML2 ELD is located in the 3_{10}-helix2 (Figure 7.8). Besides small quenching effects observed at higher Zn^{2+} concentrations, no shifting of fluorescence maxima could be observed (Figure 7.7e). However, the distance between the native tryptophan (W205) and the putative ion binding site in the pre-pore loop with the highly acidic ^{113}DEDD^{116} motif is relatively large. Therefore, a mutation was introduced into the extension of S1

near the pre-pore loop (F105W) in the hopes to use a W residue closer to the cation binding site as a reporter (Figure 7.8). However, purification of TRPML2 ELD F105W was not successful and led to insoluble protein. Lowering the temperature during the expression in *E. coli* from 22 °C to 16 °C did not lead to an improvement. This indicated that F105 which is facing a set of β sheets (Figure 7.8), plays a role in the ELD structural integrity.

7.4 Interaction with cations does not induce structural changes in the TRPML2 ELD

As mentioned above, the WT TRPML2 ELD did not only bind Ca^{2+} but also Mg^{2+} and Zn^{2+} with different affinities. However, it remains unclear, if the binding of cations to the acidic pre-pore loop motif leads to structural changes of the ELD. The highly acidic pre-pore loop is directly connected to transmembrane helix S1. Binding of cations might lead to a structural re-orientation of the pre-pore loop, which might be directed to the trans-membrane domain and ultimately to the channel pore. The effect of neutral and acidic pH values (pH 7.4, 6.5, 4.5) and presence and absence of $CaCl_2$ on the overall structure of the WT TRPML2 ELD was analyzed using CD spectroscopy and analytical SEC.[1] These different conditions did not affect ELD secondary structure. Variation of pH or addition of Ca^{2+} only slightly changed the elution volume of the ELD in analytical SEC, presumably due to a change in protein surface charges and thus altered interactions with the SEC column in the presence of divalent cations in the running buffer.[1]

However, it must be considered that CD and SEC are low-resolution methods and are potentially not suitable to detect changes on a molecular level. To further elucidate the structural impact of Ca^{2+} on the TRPML2 ELD in solution, NMR measurements were performed. NMR spectroscopy uses the magnetic spin properties of atomic nuclei.[367] During the measurements, molecules are placed in a magnetic field, so that the magnetic moments of individual nuclei can align with the field.[367] When the sample is irradiated with pulses of radio frequency electromagnetic radiation, NMR-active nuclei (containing a magnetic spin, such as ^{1}H, ^{13}C, ^{15}N or ^{31}P) will resonate at certain frequencies.[367] These different frequencies are obtained as NMR peaks in relation to a reference signal and are called chemical shifts. The chemical shift depends on the molecular environment of the nucleus and is different for each atom, unless two atoms are magnetically equivalent.[367] In larger molecules, peaks often overlap due to limited resolving power. Therefore, NMR can be expanded to two or more dimensions enabling correlation plots between nuclei.[367] ^{1}H-^{15}N HSQC (heteronuclear single quantum coherence) spectra correlate the amide nitrogen and proton chemical shifts in two dimensions, leading to observable signals for each amino acid of a peptide chain or protein, with the exception of proline, which lacks a ^{1}H-^{15}N pair.[367,368] The Trp side chain Nε-Hε groups and Asn/Gln side chain Nδ-Hδ2/ Nε-Hε2 are also visible. Each ^{1}H, ^{15}N-HSQC spectrum is then a unique fingerprint of the protein

and yields information on folding, or putative impurities.[369].[368] ^{1}H-^{15}N HSQC spectra of the ^{2}H-^{15}N-labeled WT TRPML2 ELD were recorded at pH 7.4 in the presence and absence of Ca^{2+} (Figure 7.9).

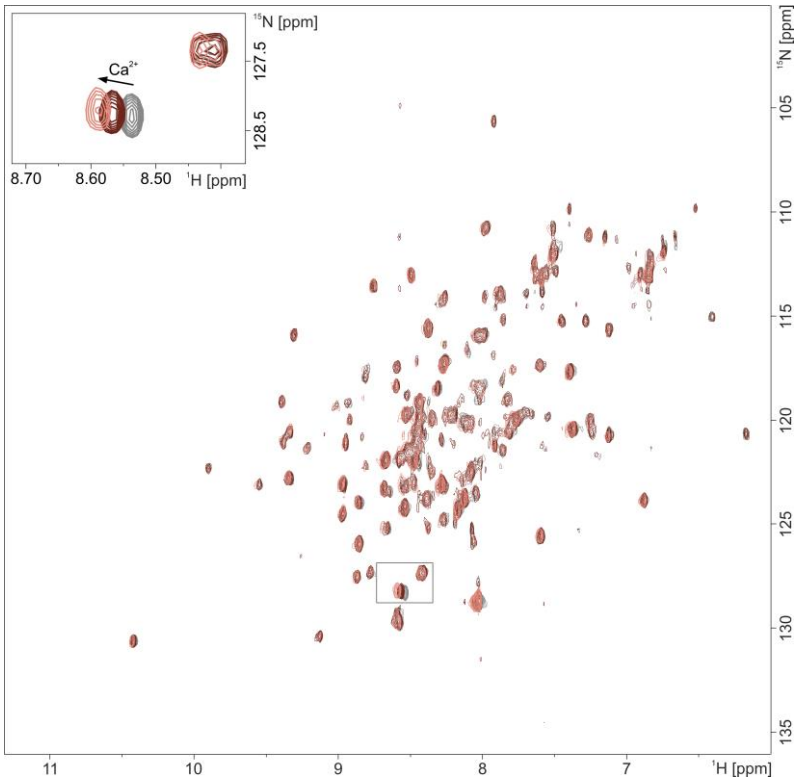

Figure 7.9: The human WT TRPML2 ELD is highly symmetric. ^{1}H-^{15}N-HSQC spectra of the human WT TRPML2 ELD (120 µM) at pH 7.4 in the absence (grey) and presence of Ca^{2+} (red: 2.5 mM $CaCl_2$, pink: 10 mM $CaCl_2$). Spectra were recorded at 298 K in 10 mM HEPES pH 7.5, 150 mM NaCl.

As mentioned above, the TRPML2 ELD forms stable tetramers even in the absence of the rest of the channel. The relatively low number of peaks indicated a high symmetry of the tetrameric, ~100 kDa TRPML2 ELD, which was also observed in the crystal structures. Furthermore, the peak dispersion confirmed proper folding of the TRPML2 ELD. With one notable exception (inlet), the addition of Ca^{2+} did not lead to significant chemical shift changes, indicating that potential structural changes are very subtle and/or that Ca^{2+} binding is not sensed by many TRPML2 ELD residues.

To further elucidate the question if cation binding leads to a structural re-arrangement of the TRPML2 ELD pre-pore loop, a post-translational approach was followed to introduce a “reporter” in close proximity to the pre-pore loop. The amino acid E95 at the extension of transmembrane helix S1 was mutated to cysteine, yielding TRPML2 ELD E95C. Cysteines can covalently react with labels (for example BTFA (3-bromo-1,1,1-trifluoroacetone) for ^{19}F-NMR and IPSL (3-(2-iodoacetamido)-proxyl) for EPR (electron paramagnetic resonance) spectroscopic measurements (Figure 7.10a, b). Originally, the TRPML2 ELD constructs which are used in this study contain five native cysteines, four of them form disulfide bridges. The fifth cysteine is located in the pre-pore loop and was found to be inaccessible for labelling attempts both with BTFA and IPSL (data not shown).

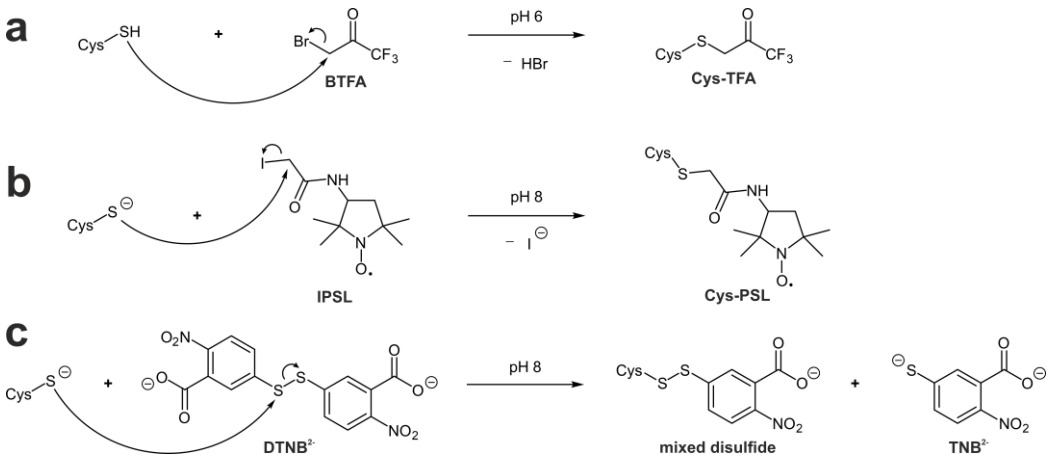

Figure 7.10: Cysteine labeling reactions. Covalent reactions of cysteine with (**a**) BTFA (3-bromo-1,1,1-trifluoroacetone) for ^{19}F-NMR (**b**) IPSL (3-(2-iodoacetamido)-proxyl) for EPR (**c**) Ellman's reagent ($DTNB^{2-}$, 5,5'-dithio-bis-(2-nitrobenzoic acid) for determination of labeling efficiency.

TRPML2 ELD E95C was heterologously expressed and purified successfully. CD spectroscopy and analytical size exclusion chromatography confirmed the structural and tetrameric integrity of the mutant in comparison to the wild type (Figure 7.11b, c). Furthermore, ITC showed that this construct still interacts with Ca^{2+} binding at pH 7.4. Based on the titration of 15 mM $CaCl_2$ to 400 µM TRPML2 ELD E95C a K_D of 2.83 ± 0.24 mM was determined (see Figure 7.11a, please compare Figure 7.4a (TRPML2 ELD WT: K_D = 2.97 ± 0.11 mM)). Therefore, TRPML2 ELD E95C can be used to investigate the structural consequences of pH-dependent ion binding via ^{19}F-NMR and EPR spectroscopy.

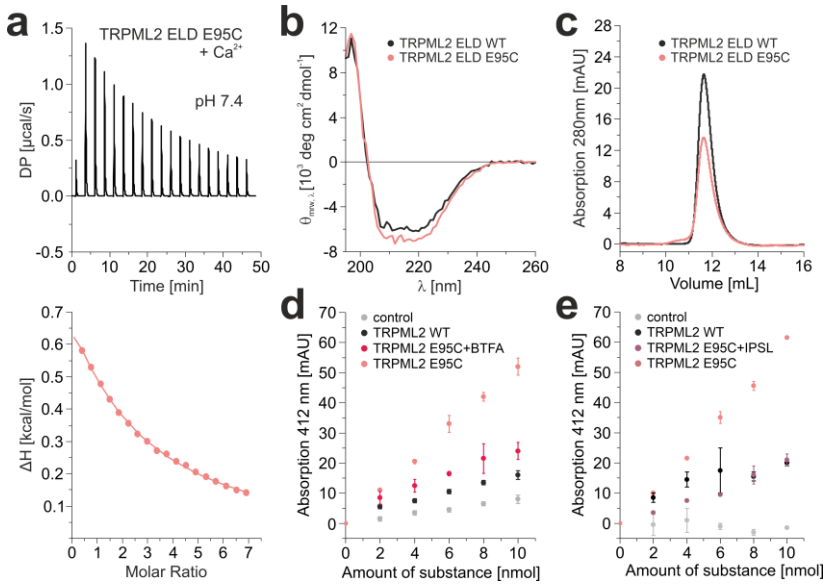

Figure 7.11: TRPML2 ELD E95C shows similar structural properties and affinity to Ca^{2+} as the wild-type protein and can be labeled for ^{19}F-NMR and EPR measurements. (**a**) ITC thermograms (top) and integrated heat signatures with fitted curves (bottom) of the titrations of $CaCl_2$ (15 mM stock solution) to TRPML2 ELD E95C (400 µM) at pH 7.4. (**b**) CD spectroscopy of the WT TRPML2 ELD and E95C mutant. (**c**) Analytical SEC of the WT TRPML2 ELD and E95C mutant. (**d**, **e**) Ellman's test with WT TRPML2 ELD, unlabeled E95C mutant and E95C mutant which was labeled with BTFA (**d**) for ^{19}F-NMR measurements or IPSL (**e**) for EPR measurements. TRPML2 ELD constructs were titrated in 0.4 nmol steps (2 µL of a 200 µM sample) to 20 nmol Ellman's reagent (control: buffer (10 mM HEPES, 15 mM NaCl)).

To determine the labeling efficiency, the so-called Ellman's test[370] was performed for the TRPML2 ELD. To assess the labeling efficiency, an Ellman's assay was carried out using DNTB (5,5-dithio-bis-2-nitrobenzoic acid, Ellman's reagent). Ellman's reagent reacts with free sulfhydryl groups at neutral or alkaline pH forming 5-thio-2-nitrobenzoic acid (TNB^{2-}) which has a yellow color (Figure 7.10c). The absorption at 412 nm can then be measured. To assess the quality of the setup and elucidate which protein concentration will be required, tests with β-mercaptoethanol in different concentrations were carried out (see appendix, Figure 10.10). The higher the concentration of added β-mercaptoethanol, the higher was the amount of TNB^{2-} that was formed and the higher the absorption at 412 nm. The first labeling attempts using purified TRPML2 ELD E95C with BTFA remained unsuccessful (data not shown). However, protein which was labeled with BTFA and IPSL during the purification procedure, bound to the NiNTA beads (see methods sections 4.19 and 4.20 for details) showed much lower absorption values in comparison to the unlabeled control, similar to the wild type (Figure 7.11d, e), indicating a high labeling efficiency.

For further experiments, a second ELD mutant (T98C) was cloned. Residue T98 is located closer to the putative cation binding site and in a "more buried" position (Figure 7.8). While expression and purification of TRPML2 ELD T98C was successful and led to soluble protein, labeling of this residue with BTFA and IPSL was not possible as assessed by Ellman's test (data not shown), potentially due to its more buried position.

Next, ^{19}F-NMR measurements were performed with BTFA treated TRPML2 ELD E95C to investigate whether addition of ligands to the pre-pore loop of the ELD leads to conformational changes within the S1 helix. This would be a first indication that transmembrane communication via binding of metal ions is a possibility in TRPML channels. ^{19}F is not a natural component of biomolecules in contrast to ^{1}H, ^{13}C, ^{15}N and ^{31}P. Therefore, it can be used as a site-specific reporter allowing to draw conclusions regarding structure, dynamics and ligand-interactions of high biological systems.[371] In addition, fluorine does not cause steric hinderance as its atomic radius is very close to that of a proton.[371] Fluorine labels can be incorporated directly into proteins during expressions or as a post-purification tag.[371] as done here for the TRPML2 ELD.

^{19}F-NMR measurements of TFA-labeled TRPML2 ELD E95C showed that the protein could indeed be efficiently fluorinated (Figure 7.12). The ^{19}F-NMR spectra showed a single peak. Free BTFA was also tested in buffer, importantly its ^{19}F resonance showed a different chemical shift indicative of a different chemical environment, once the TFA group was attached to the protein and the Br^- leaving group has been discarded.

Furthermore, ^{19}F-NMR spectra were recorded for both free BTFA and TRPML2 ELD E95C-TFA at pH 6.5 and 4.5. For free BTFA, no chemical shift change could be observed at pH 6.5 in comparison to pH 7.4. At pH 4.5, the peak intensity was strongly decreased and a small second peak at higher ppm is detected. For TRPML2 ELD E95C-TFA, a slight shift to lower ppm could already be observed at pH 6.5, compared to pH 7.4. At pH 4.5, the signal further shifted to higher ppm (in comparison to pH 7.4) and became very broad and barely detectable. As a shift to higher ppm values in comparison to neutral pH could be observed for both free BTFA and TRPML2 ELD E95C-TFA at lower pH, the effect was not indicative of structural changes of the TRPML2 ELD at different pH values. Notably, when the pH 4.5 samples of free BTFA and TRPML2 ELD E95C-TFA were re-set to pH ~7 – 8 (via addition of NaOH solution), the peaks shifted back to lower ppm in both cases.

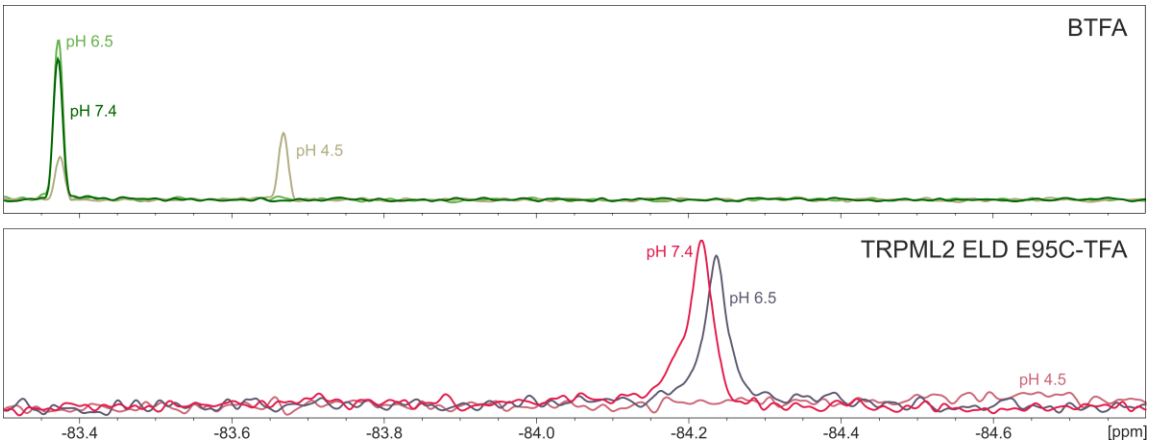

Figure 7.12: The human TRPML2 ELD E95C mutant was successfully labeled with BTFA for ^{19}F-NMR measurements. ^{19}F-NMR spectra of free BTFA in buffer at three pH values relevant for TRPML2 physiology (50 µM, top panel, dark green, pH7.4; light green, pH 6.5; grey, pH 4.5) and TRPML2 ELD E95C-TFA (50 µM, bottom panel). Spectra were recorded at 298 K in 10 mM HEPES, 15 mM NaCl at pH 7.4, pH 6.5 and pH 4.5 (red, violet, pink. respectively).

For the ^{19}F-labeled ELD, titrations with calcium chloride were carried out at pH 7.4 and pH 6.5. Titrations with magnesium chloride, zinc chloride and iron(III) chloride were performed at pH 7.4 (Figure 7.13).

With increasing cation concentrations, a decrease of signal intensity could be observed for all titrations. Line broadening could be an indicator of protein-ligand interactions, depending on the exchange rate, transverse relaxation rate and the fraction of the ligand in free and bound state.[372] However, protein aggregation was visually noticed after the measurements and confirmed via analytical SEC (data not shown). To test if protein aggregation is reversible, millimolar amounts of EDTA were added at the end point of the titration. Notably, the signal could be "rescued" in the presence of $ZnCl_2$ only and not in the presence of $CaCl_2$, $MgCl_2$ and $FeCl_3$. This indicated that the line broadening and decrease in signal intensity was caused by protein aggregation. As mentioned before, protein aggregation was also observed when $ZnCl_2$ was titrated to the TRPML2 ELD during ITC measurements, but not when low protein amounts were used to verify structural integrity using CD spectroscopy. This indicated that protein aggregation is dependent on the used protein concentration.

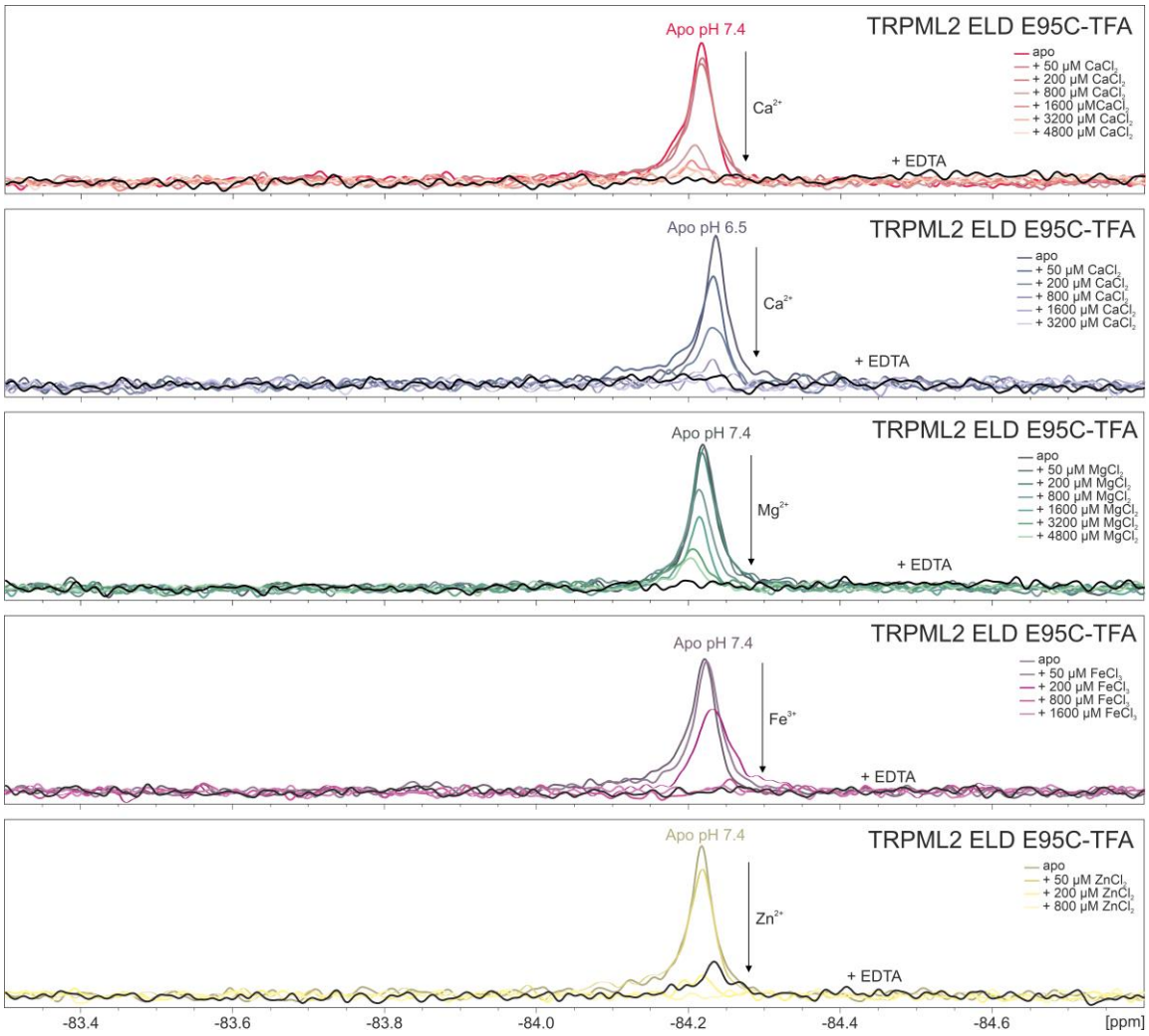

Figure 7.13: Titration of cations to the fluorine-labeled TRPML2 ELD E95C mutant induced decreased signal intensity and line broadening in ^{19}F-NMR measurements. ^{19}F-NMR spectra of TRPML2 ELD E95C-TFA (50 µM, top panel) titrated with $CaCl_2$ (at pH 7.4: concentrations: 50 µM to 4.8 mM, at pH 6.5: concentrations: 50 µM to 3.2 mM), $MgCl_2$ (50 µM to 4.8 mM), $FeCl_3$ (50 µM to 1.6 mM) and $ZnCl_2$ (50 µM to 800 µM). Spectra were recorded at 298 K in 10 mM HEPES, 15 mM NaCl at pH 7.4 and pH 6.5 At the respective titration endpoints, EDTA (10 mM) was added (shown in black).

As a complementary approach to ^{19}F-NMR spectroscopy, EPR spectroscopy was used to characterize the structural consequences of cation binding to the TRPML2 ELD. EPR spectroscopy is a powerful tool for investigating paramagnetic species, including organic and inorganic radicals, and paramagnetic triplet states.[373] EPR and NMR have similar working principles. NMR focuses on the interaction of an external magnetic field with isotopic nuclei while EPR measures the absorption of microwave radiation by an unpaired electron spin in the presence of an external magnetic field.[373] Thus, EPR experiments require the introduction of unpaired electrons into proteins and other biomolecules. The site-specific introduction (typically via attachment to cysteine side chains) is commonly referred to as site-directed spin labeling (SDSL).[374,375] Most widely used spin labels are based on nitroxide radicals.[376] Nitroxides are heterocyclic free radicals which carry an unpaired electron (S = 1/2) in a N–O· bond.[376] The nitrogen atom has a 99.6% natural abundance of the isotope

^{14}N, which contains a nuclear spin I = 1. Bulky substituents such as methyl groups in close proximity to the nitrogen sterically shield the radical and provide stability *in vitro*.[376] For EPR measurements of the TRPML2 ELD, the TRPML2 ELD E95C mutant was labeled with the spin label IPSL during purification of the protein. Generally, the purification was performed under non-reducing conditions as nitroxides are not stable under reducing conditions.[376] Successful labeling was confirmed via Ellman's test (Figure 7.9e).

Initially, continuous-wave (CW) EPR measurements with the IPSL-labeled TRPML2 ELD E95C mutant at pH 7.4 were performed to elucidate the labeling efficiency. During CW-EPR experiments, spectra are collected by placing a sample into a microwave field of constant frequency ν, and varying the external magnetic field, B_0.[373] CW-EPR spectra of nitroxide spin labels contain three lines due to the hyperfine interaction with the ^{14}N nucleus.[377] The spectral line shape demonstrates the mobility of the spin-label side chain. The mobility is dependent on neighboring amino acid side chains and secondary structure components in its close environment.[373]

As seen in Figure 7.14, the spectrum of sole IPSL contains sharper spectral line shapes in comparison to the labeled protein indicating efficient labeling and absence of free IPSL. The broader spectral line shapes obtained for the labeled protein were caused by the decreased rotational correlation time of the label due to attachment to the protein. A spin count (i.e. protein labeling efficiency) of 80.37% was determined.

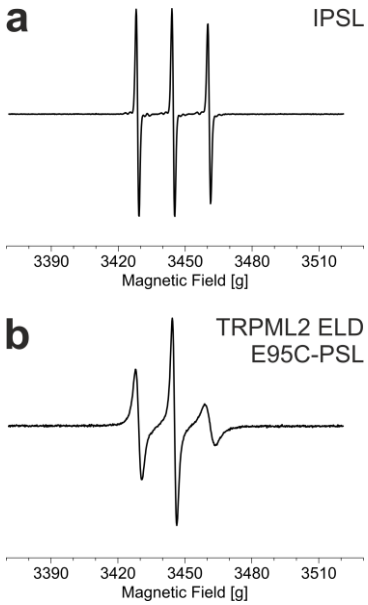

Figure 7.14: The TRPML2 ELD E95C mutant was successfully labeled with the nitroxide spin label IPSL. CW-EPR spectra of IPSL (100 µM) and TRPML2 ELD E95C-PSL (100 µM protein concentration) were recorded at 298 K in 10 mM HEPES, 15 mM NaCl at pH 7.4.

Next, PELDOR (pulsed electron double resonance, also called double electron electron resonance (DEER)) experiments were conducted with the IPSL-labeled TRPML2 ELD E95C mutant at pH 7.4 and 6.5 (Figure 7.15). Due to precipitation of the labeled protein at pH 4.5, measurements at this pH value were not possible. In pulsed EPR experiments, the magnetic field is fixed, and the spectra are recorded by exciting a large frequency range simultaneously with a single high-power microwave pulse at a given frequency ν.[373] Because the relaxation times are too short for most of the biological molecules at RT, pulsed EPR measurements are generally performed at cryogenic temperatures.[373]

In PELDOR spectroscopy, a dipolar coupling between two spins is measured by monitoring one set of spins while exciting another set of spins with a second microwave frequency.[373] This allows measurement of the distance between them, if they are in relatively close proximity, since the magnetic dipolar coupling frequency between two spin labels is inversely proportional to the cube of the distance (r^3).[378–381] Other techniques which are used for distance estimations within and between proteins, such as FRET (Förster energy resonance transfer), require two different relatively large chromophores. In contrast, EPR distance measurements can be performed with two identical, much smaller spin labels.[382–384]

PELDOR can be used for measuring distances between 10 and 80 Å.[377] Based on the crystal structure of the WT TRPML2 ELD at pH 6.5 (pdb 6HRR),[1] the distance between amino acids E95 is approx. 36 Å in two neighbored monomers and approx. 52 Å in the diagonal (Figure 7.15a).

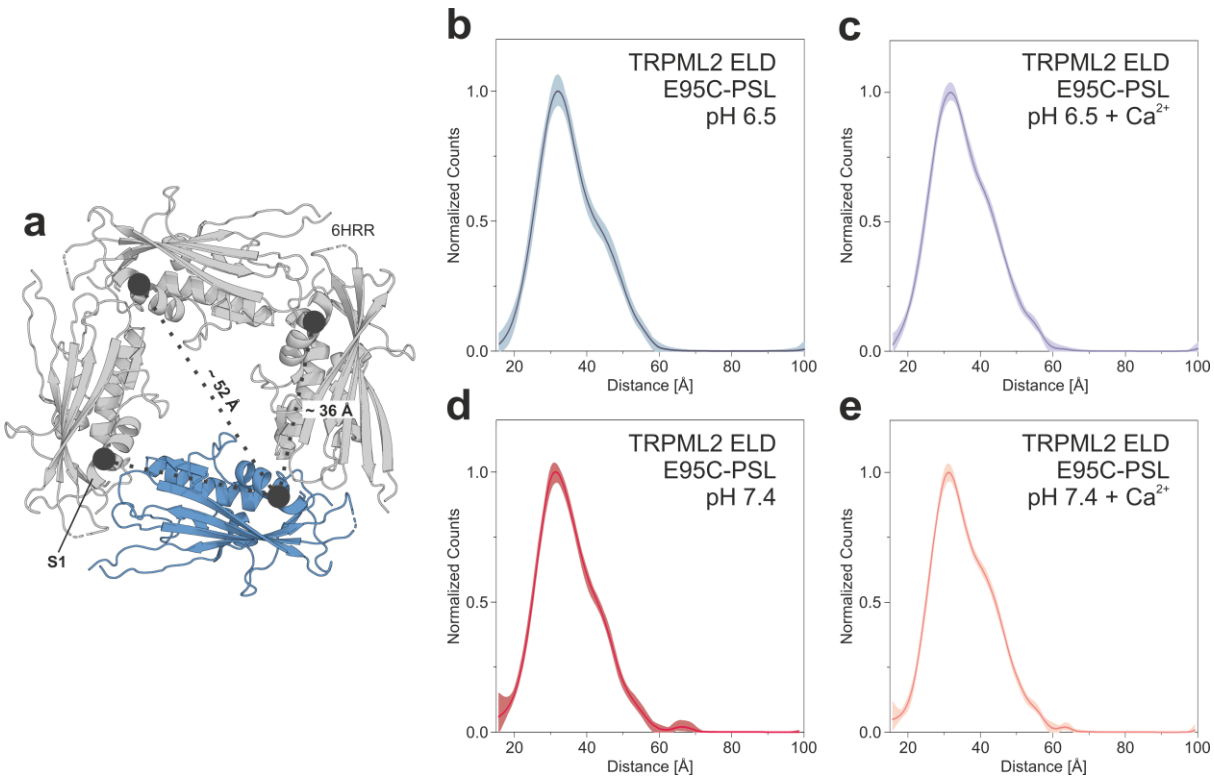

Figure 7.15: Ca^{2+} and pH do not affect the distances between nitroxide spin labels attached to the N-terminus of the TRPML2 ELD E95C mutant. (**a**) Structure of the human WT TRPML2 ELD (pdb 6HRR) at 2.0 Å resolution[1] viewed from the membrane plane. Position of amino acid E95 is indicated in each monomer by a grey sphere. Distances between these amino acids in the tetrameric ELD have been determined using PyMOL. For EPR measurements, E95 was mutated to cysteine to allow labeling with the nitroxide spin label IPSL. (**b**–**e**) PELDOR-based inter-nitroxide distance distributions, error estimates are shown as shades. PELDOR measurements on the IPSL-labeled TRPML2 E95C mutant (100 µM) were performed at 50 K in deuterated buffer containing 10 mM HEPES, 15 mM NaCl, 30% glycerol at pH 6.5 (**b**), 6.5 + 400 µM $CaCl_2$ (**c**), pH 7.4 (**d**), 7.4 + 400 µM $CaCl_2$ (**e**). Respective time traces can be found in appendix Figure 10.14.

As seen in Figure 7.15b–e, similar PELDOR-derived inter-nitroxide distance distributions could be observed at pH 6.5 and pH 7.4 in the presence and absence of Ca^{2+}. The distance distributions displayed a bell-like shape which contained one major peak at approx. 30 Å and a smaller peak at approx. 45 Å. These results were in the same range as the distances obtained from the crystal structure, indicating that PELDOR was successfully performed on the labeled TRPML2 ELD E95C mutant. In this set-up, distances between four spin labels (one in each subunit) were measured. Because of the high symmetry of the protein, only two distances in a 2:1 ratio could be observed corresponding to the major peak approx. 30 Å and smaller peak at approx. 45 Å. However, different pH values and the presence of Ca^{2+} did not have a significant impact on the distance distributions, only the larger distance seemed to become a little bit more prominent (the molecular mechanism behind these observations remains elusive). Thus, pH and Ca^{2+} are presumably not able to alter the relative position of the TRPML2 ELD S1 helix and pre-pore loop.

8 Discussion

8.1 The pH-dependent Ca^{2+} affinity of the TRPML2 ELD indicates a role of the ELD in the regulation of the whole channel

The extracytosolic/lumenal domain (ELD) is an important structural hallmark of TRPML and TRPP channels. The ~ 100 kDa domain constitutes around one third of the whole channel and has also been termed "I-II" linker as it is located between transmembrane helices S1 and "polycystin-mucolipin domain" (or "TOP domain" (tetragonal opening for polycystins) for TRPP channels).[257,263,267] While the TRPML ELD is formed on top of the transmembrane domain, the TRPP TOP domain directly contacts the pore turret of the adjacent chain and the VSLD (voltage-sensor-like domain) of its own chain, which provides opportunities for the TOP domain to influence the opening of the pore filter and to control channel activity.[267] In contrast, the impact of the TRPML ELD on the regulation of the full-length channel remained elusive.

The TRPML ELD and is exposed to different conditions (e.g. Ca^{2+} concentrations and pH values) as it faces either the endolysosomal space or the extracellular lumen, depending on the channel's cellular localization.[208] Our crystal structures of the human TRPML2 ELD at pH 6.5 (pdb 6HRR, 2.0 Å, see Figure 7.1) and pH 4.5 (pdb 6HRS, 2.95 Å) marked the first structural information available for human TRPML2 and allowed the comparison with the ELDs of other TRPML channels at different pH values (see Viet *et al.*[1]). Comparing the ELDs of TRPML1, TRPML2 and TRPML3, the overall architecture is highly similar (two long α helices and a six-stranded antiparallel β-sheet).[1,222,237,254–257,263] Differences were described with regard to the ELD pre-pore loop architecture. The pre-pore loop is directly connected with the extension of the S1 helix and contains a stretch of acidic amino acid residues. In the full-length channel, the pre-pore loop is centered of the ion channel pore, which is formed by S5 and S6. At acidic pH, the human TRPML3 ELD pre-pore was closed, while the TRPML1 and TRPML2 displayed wider conformations. These findings may present a rational explanation for observed differences in organelle-specific channel activation. While TRPML1 was described to be activated at low pH in the lysosome, TRPML3 is inhibited under the same conditions.[237,260,269] For TRPML2, it was suggested that the channel is inhibited at low pH, while others described it to be activated at acidic pH, similar to TRPML1.[208,234,385] Presentation of the full-length cryo-EM structure of mouse TRPML2 at pH 7.4 by Song *et al.*[258] allowed the comparison of TRPML2 ELDs at three physiological relevant pH values. Notably, all three structures display similar pre-pore diameters.[1,258] Alignment of our high-resolution hsTRPML2 ELD structure at pH 6.5 and mmTRPML2 at pH 7.4 showed a high structural similarity (Figure 7.2).

For TRPML1, Li *et al.* reported interactions of the pre-pore loop with Ca^{2+} and H^+ and suggested a molecular model of ELD-based TRPML1 regulation ("Ca^{2+} block model").[263] The aspartate residues in the pre-pore loop are negatively charged at pH 7.4 (which the ELD encounters in the extracellular

space) thus attracting and binding extracellular Ca^{2+}, forming a block for Ca^{2+} and other cations. Lower pH values in the endolysosomal system might lead to protonation of the aspartate residues, which weakens the Ca^{2+} block enabling cation flux.[263]

In this thesis, it was shown that the TRPML2 ELD interacts with Ca^{2+} in a pH-dependent manner (Figure 7.4). At pH 7.4, a K_D of 2.97 ± 0.11 mM was determined. Therefore, the affinity to Ca^{2+} is in a physiological relevant concentration range and would be sufficient to block the channel in the presence of millimolar Ca^{2+} concentrations. Additionally, a fast reversal of the cation block would be possible if the pH value drops. The Ca^{2+} binding site in the acidic pre-pore loop motif was verified by mutating the acidic pre-pore loop residues to alanine, which resulted in decreased Ca^{2+} affinity (Figure 7.6), confirming the Ca^{2+} block model for TRPML2.[1] As acidic motifs in the pre-pore loop can be found in all TRPML channels, this suggests that it is a general regulatory mechanism of the TRPML family. The Ca^{2+} block model was tested by Li *et al.* in the context of the TRPML1 full-length channel using patch clamp experiments. All 12 aspartate residues in the pre-pore loop region (D111, D114 and D115 in each subunit) were simultaneously mutated to glutamine. These mutations strongly impaired Ca^{2+} inhibition at pH 7.4, while a decrease in pH to 4.6 attenuated Ca^{2+} inhibition of the mutant channel. All in all, this indicates that the pH dependent Ca^{2+} affinity of the ELD may play an important role in the organelle-specific, structural regulation of TRPML channels.

8.2 Cation binding does not lead to structural changes of the TRPML2 ELD that could potentially be propagated to the transmembrane domain

The spatial proximity of the pre-pore loop (harboring the Ca^{2+} binding site) to the extension of S1 suggests that potential structural rearrangements of the TRPML2 ELD may be propagated to the transmembrane region. This may directly affect the activity of the channel. In addition to Ca^{2+}, the affinity of the TRPML2 ELD to other cations, for which TRPML2 is permeable, was investigated. In comparison to Ca^{2+}, the TRPML2 ELD showed a higher affinity to Zn^{2+} and a slightly lower affinity to Mg^{2+}. However, titration of $ZnCl_2$ to the TRPML2 ELD led to protein aggregation which might have negatively affected the quality of the ITC measurement which was used to determine the binding affinity. In contrast to the cytosol, which exhibits very low Zn^{2+} concentrations (approx. 0.1 nM), intracellular vesicles such as lysosomes contain micromolar to millimolar Zn^{2+} concentrations and function as Zn^{2+} stores.[386–388]

Using various high-resolution spectroscopic approaches ($^{1}H^{15}N$-HSQC (Figure 7.9), ^{19}F-NMR (Figure 7.13), PELDOR (Figure 7.15)) no significant changes in the TRPML2 ELD structure upon cation binding and at different pH values were observed. Potentially, structural changes are very small and cannot be resolved with the applied methods. In our crystal structures at pH 6.5 and 4.5, also no significant structural differences can be observed regarding the architecture of the pre-pore loop which is well-resolved in both crystal structures indicating low flexibility. In the cryo-EM full-length

structure of mmTRPML2, the pre-pore loop is also well-resolved, and a similar pre-pore diameter compared to our crystal structures at pH 4.5 and 6.5. Furthermore, a complex set of hydrogen bonds was identified in the human TRPML2 ELD which might stabilize the pre-pore loops position.[1] In the TRPML1 ELD structures obtained at different pH values presented by Li et al., also no significant structural changes can be observed.

The confirmation of the Ca^{2+} block model for TRPML2 suggests that the TRPML2 ELD plays indeed an important role in the regulation of the whole channel although it might not be linked to pronounced structural changes which could be potentially transmitted to the transmembrane domain via the S1 helix. However, these results do not exclude a potential structural crosstalk between the TRPML2 domains. Potentially, protein and lipid interactions at the N-terminus induce structural changes which are transmitted to the ELD via S1. To pursue this approach, studies with the full-length channel are required.

9 Conclusion & outlook

TRPML2 is a member of the TRPML subfamily of TRP ion channels. The three human TRPML family members are tetrameric, unspecific cation channels located in the membranes of the endolysosomal system (and in the plasma membrane, to a lesser extent).[234,238] TRPML channels are involved in several processes crucial for normal cell functioning, e.g. ion homeostasis, signal transduction and autophagy.[234,238] In comparison to TRPML1 and TRPML3, the physiological role and structural characteristics of TRPML2 are far less understood. In recent years, a potential role for TRPML2 in innate and adaptive immunity as well as in viral infections has emerged.[92,236,270] TRPML2 overexpression was shown to increase endosomal trafficking efficiency of certain RNA viruses, for example influenza A virus (IAV) and Zika virus (ZIKV).[92] In addition, treatment with the unspecific TRPML agonist ML-SA1 inhibited Dengue (DENV) and ZIKV infection by promoting lysosomal acidification and protease activity.[236]

In terms of the structure of TRPML2, only the full-length structure of mouse TRPML2 and our crystal structures of the human isolated extracytosolic/lumenal domain (ELD) are available.[1,258] In contrast, several full-length and structures of TRPML1 and TRPML3 as well as structures of the isolated TRPML1 ELD have been determined.[222,237,254–257,263] Beyond the structures, the functional regulation of TRPMLs needs further investigation. Until now, the question whether there is (stimulus-dependent) structural crosstalk between the individual TRPML domains (ELD, transmembrane domain (TMD), N- and C-termini) remains unanswered. In this thesis, a multiscale view on the TRPML2 ion channel was applied on the one hand to elucidate the role of TRPML2 in ZIKV infection. On the other hand, the pH-dependent Ca^{2+} interaction of the TRPML2 ELD which may play an important role in a putative interdomain crosstalk and the endolysosomal compartment-specific regulation of the full-length channel, was investigated.

9.1 TRPML2 activation inhibits ZIKV replication *in vitro*

In the first part of this thesis, the selective TRPML2 agonist ML2-SA1, which was described by Plesch *et al.,*[277] was used *in vitro* to analyze the implications for the ZIKV life cycle (see Figure 9.1). ML2-SA1 induced a pronounced antiviral effect against two ZIKV isolates, one representative of the African lineage (ZIKV Uganda) and one representative of the Asian lineage (French Polynesia). cLSM and super-resolution microscopy revealed increased acidification of the endolysosomal system upon ML2-SA1-treatment and accumulation of ZIKV in CD63-positive vesicles. When lysosomal degradation was inhibited, no intracellular ZIKV accumulation was observed, indicating that the antiviral effect of ML2-SA1 against ZIKV is not based on increased lysosomal ZIKV degradation. In contrast, Xia *et al.* suggested that the antiviral effect of the unspecific agonist ML-SA1, which activates all three human TRPML channels, is caused by increased acidification and protease activity.[236] Xia *et*

al. hypothesized that ML-SA1 affects early stages of the flavivirus life cycle based on a time-of-addition experiment that was carried out. However, it needs to be considered that they did not include reference compounds and did not synchronize the infection process, which is an important prerequisite for this type of experiment.[236] Our time-of-addition experiments, which included ML2-SA1, ML-SA1 as well as the entry inhibitor Bafilomycin A1 and the replication inhibitor Ribavirin for reference, indicated that ML2-SA1 and ML-SA1 induced a mild proviral effect when the compounds were present during the early stages of the infection process, presumably due to increased endosomal trafficking and enhanced acidification, which may promote ZIKV fusion in late endosomes. Of note, activation of TRPMLs by small-molecules leads to Ca^{2+} flux from endosomes and lysosomes into the cytosol which was reported to influence vesicular trafficking, vesicular fusion and fission, lysosomal exocytosis and autophagy.[275,297,298]

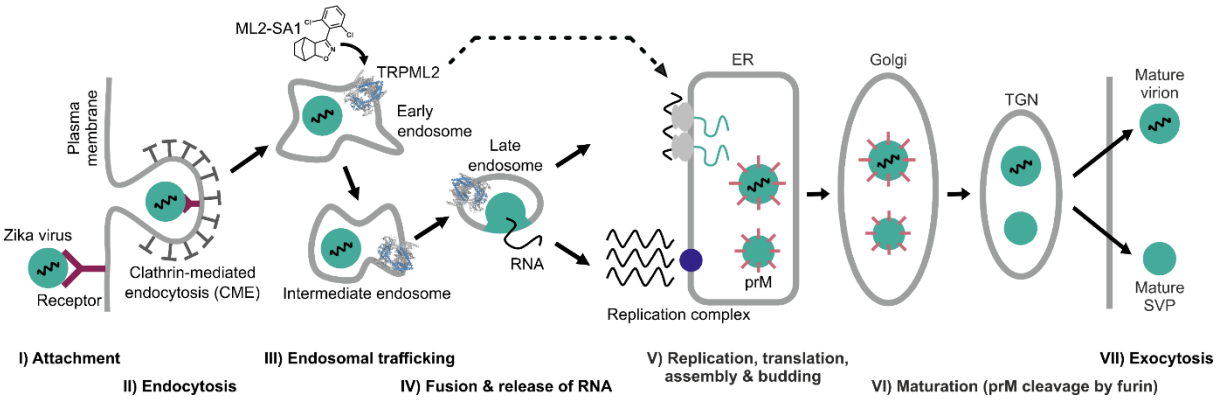

Figure 9.1: ML2-SA1 treatment inhibits ZIKV replication. TRPML2 is an endolysosomal cation channel which can be activated using the small-molecule ML2-SA1. The endolysosomal system plays a remarkable role for ZIKV infection. A combination of various techniques was used in this thesis to investigate the consequences of ML2-SA1 treatment on the individual stages of the ZIKV life cycle (see text). Surprisingly, ML2-SA1 treatment inhibits ZIKV replication, presumably by interfering with cholesterol trafficking. Cholesterol is required in the ER membranes for effective formation of ZIKV replication factories. ***Abbreviations:*** *CME: clathrin-mediated endocytosis, ER: endoplasmic reticulum, prM: pre-membrane protein, TGN: trans-Golgi network, SVP: subviral particle.*

When ML2-SA1 treatment was started at later timepoints of the viral life cycle, it resulted in a pronounced antiviral effect against ZIKV. Experiments with a ZIKV *Renilla* luciferase reporter virus confirmed the inhibition of viral replication. Furthermore, the size of replication factories was reduced upon ML2-SA1 treatment and intracellular cholesterol accumulations were observed in uninfected and ZIKV-infected cells, which might be indicative for impaired cholesterol trafficking. Cholesterol is an important host cell factor and required in the membranes of the ER for the formation of ZIKV replication factories. In the next steps, the effect of ML2-SA1 treatment on the cholesterol metabolism should be investigated in more detail, for example by additional treatment with cholesterol modulators.

From the combination of my results, I conclude that ML2-SA1 affects later stages of the ZIKV life cycle and diminishes ZIKV replication but may also display a mild pro viral effect when present

during the early stages of the life cycle (see Figure 9.1). To rule out potential off-target effects, TRPML2 knockdown experiments could be performed. Furthermore, the ML2-SA1-mediated Ca^{2+} flux from the endolysosomal into the cytosol could be confirmed in A549 cells for example by using dextran coupled Ca^{2+} sensors. Investigations on the autophagy marker p62 in ML2-SA1-treated cells have indicated an induction of autophagy, which could be further analyzed by using other autophagy markers, for example LC3. Recently, TRPML2 was shown to activate TFEB, leading to TFEB nuclear translocation and transcriptional activation of autophagic and lysosomal genes as well as expression of B7 costimulatory molecules on dendritic cells.[358]

9.2 The selective TRPML2 agonist shows pan-antiviral potential

Due to the high similarity of the life cycle of flaviviruses, it seems likely that ML2-SA1 also shows antiviral potential against other flaviviruses such as DENV, West Nile virus (WNV) and yellow fever virus (YFW). As mentioned before, Xia *et al.* showed that the unspecific TRPML agonist ML-SA1 inhibits DENV and ZIKV infection.[236] The time-of-addition experiments and ZIKV RLuc assays presented in this thesis indicated that both ML2-SA1 and ML-SA1 affect ZIKV replication. Therefore, it seems reasonable to assume that ML2-SA1 has pan-flaviviral potential and ML2-SA1 should be tested concerning anti-viral effects against other flaviviruses, for example DENV.

As shown in this thesis, ML2-SA1 increased acidification of the endolysosomal system. Many viruses, for example hepatitis E virus (HEV) depend on endocytosis for their life cycle.[389] In his Bachelor thesis, [redacted] demonstrated with the help of [redacted] (both [redacted] group, Paul-Ehrlich-Institute, Langen) that ML2-SA1-treatment of A549 cells persistently infected with HEV decreased the release of HEV virions and increased the colocalisation of viral proteins with the lysosomal marker Lamp2, as confirmed via confocal laser scanning microscopy.[390] All in all, ML2-SA1 could serve as a new lead structure for the development of novel pan-antiviral drug candidates, although the cause of the antiviral effect of ML2-SA1 might be different for different virus families.

9.3 The ELD potentially regulates TRPML2 by interacting with Ca^{2+} in a pH-dependent manner

In the second part of this thesis, the structural consequences of changes of Ca^{2+} and pH in a physiological relevant range on the TRPML2 ELD was analyzed. The ELD is the structural hallmark of the TRPML family. Until now, the impact of the TRPML ELD on the regulation of the full-length channel remained largely unclear. In contrast, the TOP domain of TRPP channels, which displays similar structural features as the TRPML ELD, was shown to be able to influence the opening of the pore filter and to control channel activity by its direct contacts with the pore turrets of the adjacent chain and the voltage-sensor-like domain of its own chain.[267] The TRPML ELD is exposed to various

pH values and ion concentrations when the channel is trafficking through the endolysosomal system. The organelle-specific pH was shown to play a role in the activity of TRPML channels: TRPML1 was described to be activated at low pH in the lysosome, in contrast, TRPML3 is inhibited under the same conditions.[237,260,269] For TRPML2, it was suggested that the channel is inhibited at low pH, while others described it to be activated at acidic pH, similar to TRPML1.[208,234,385]

Using ITC and mutagenesis, it was demonstrated in this thesis that the TRPML2 ELD interacts with Ca^{2+} in a pH-dependent manner thereby confirming the Ca^{2+} block model proposed for TRPML1.[263] While not yet shown for TRPML3 or TRPML channels from other species, this indicates that the Ca^{2+} block model may be a general mode of regulation for the TRPML subfamily of ion channels. Furthermore, it was found that other cations bind to the TRPML2 ELD with different affinities. However, high-resolution spectroscopic approaches ($^{1}H^{15}N$-HSQC, ^{19}F-NMR, PELDOR) did not reveal significant structural changes at varying pH values and in the presence of cations. In combination with the before-mentioned pH-dependent Ca^{2+} binding in the ELD's central pore, this indicates that the TRPML2 ELD could play a putative "passive" role in the structural regulation of the full-length channel. This regulation does not seem to be linked to significant structural changes which might have been transmitted to the TMD and N-terminus via the first transmembrane helix (S1). However, this does not exclude an interdomain communication between ELD, TMD and N-terminus. Potentially, signals are transmitted from the N-terminus (for example caused by lipid or protein interaction) to the TMD and ELD but not the other way round.

All in all, the results of this thesis contributed to a better understanding of the function of the TRPML2 ELD. In the next steps, the position of the label which was used for ^{19}F-NMR and PELDOR experiments could be varied within the S1 helix and the pre-pore loop to detect potential minor structural differences upon changes in pH and cation concentrations. In addition, ^{19}F-tryptophan could be incorporated as a reporter in the WT TRPML2 ELD and pre-pore loop mutants. Of note, the TRPML2 ELD contains only one native tryptophan W205, which is located in the 3_{10}-helix2 (see Figure 7.8). To test the Ca^{2+} block model for full-length TRPML2, a functioning TRPML2 overexpression system is required. In the full-length channel, mutation of the acidic pre-pore loop motif to alanine may decrease the affinity to Ca^{2+} at neutral pH and a block for other cations may not be formed as a consequence. Thus, cation flux might be increased at neutral pH.

9.4 A TRPML2 overexpression system could be used to investigate the consequences of TRPML2 mutations on ZIKV infection

Cells stably expressing TRPML2 pre-pore loop mutants could be infected with ZIKV. As reported by Rinkenberger and Schoggins, TRPML2 overexpression enhances endosomal trafficking of endocytosed viruses[92] and it would be interesting to investigate if similar effects would be observed for the pre-pore loop mutants. Furthermore, the TRPML2 overexpression system could be used to

study the functional consequences of the naturally occurring TRPML2 mutation K370Q. In addition, pre-pore loop mutations and K370Q could also be combined in one construct.

The rare genetic TRPML2 variant K370Q was the first mutation that was reported for TRPML2 in a disease-related context.[92] This natural variant is overrepresented in certain African subpopulations.[92] It was hypothesized that this mutation which fails to enhance viral infections, might be beneficial for the carrier against viral diseases.[92] While it was confirmed that TRPML2 K370 is expressed in a similar level in comparison to the wild type, it remains completely unclear, whether this mutation affects the activity or subcellular localization of this ion channel.[92] As channel activity was shown to be important for the proviral effect of TRPML2 overexpression, it seems likely that the activity of the K370Q mutant is decreased. In cells overexpressing TRPML2 K370Q, the activity of the channel could be studied using lysosomal patch clamp experiments and the subcellular localization via immunofluorescence.

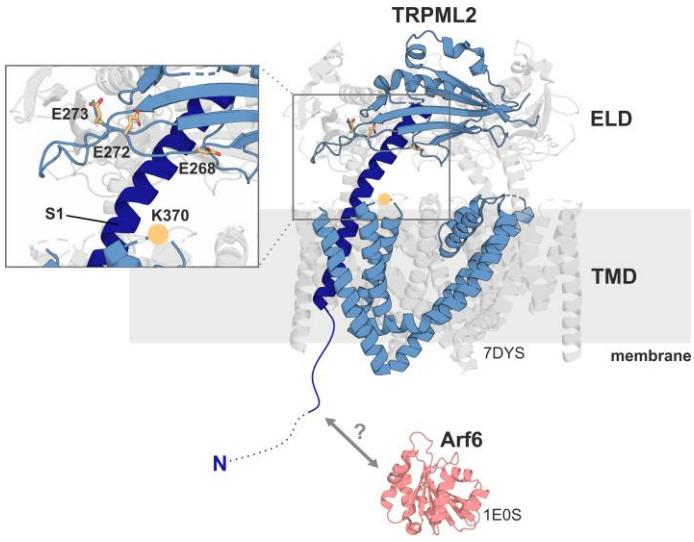

Figure 9.2: Potential structural interaction between amino acid residues K370 in the transmembrane domain (TMD) and E268, E272 and E272 in the extracytosolic/lumenal domain (ELD) of TRPML2. K370 is located in the loop between transmembrane helix 3 and 4, this loop is not resolved in the structure of mouse TRPML2 at pH 7.4, 3.14 Å (pdb 7DYS). The approximate position of K370Q is highlighted by a yellow sphere. In addition, amino acid residues E268, E272 and E273 in the TRPML2 ELD are highlighted (see inlet). Via the first transmembrane helix S1 (highlighted in dark blue), the ELD is directly connected with the N-terminus, which is potentially involved in the interaction with other proteins (see section 9.5). The small GTPase Arf6 (2.28 Å, pdb 1E0S) is a potential interaction partner of TRPML2. TRPML2 isoform 2 misses the first 28 amino acids (indicated by a dotted line), in comparison to isoform 1.

Furthermore, the structural basis of the K370Q mutant could be investigated. The amino acid K370 is located between S3 and S4 and might be in a suitable position for interactions with the ELD (for example a salt bridge between K370 and residues E268, E272 or E273, see Figure 9.2). Although the distance between the putative position of K370Q is approx. 20 Å in the structure of mouse TRPML2, it needs to be considered that the loop between S3 and S4 is not resolved in this structure and that the

distance between TMD and ELD could be shorter when the channel is in its native environment. For the formation of salt bridges, the distance required is around 4 Å.[391]

Potentially, mutagenesis of E268, E272 or E273 (for example to the apolar amino acid alanine) should have the same effects as the K370Q mutant regarding channel activity (which could be assessed by lysosomal patch clamp, see above) and subcellular localization (immunofluorescence). This would indicate an unknown interaction of the TRPML2 transmembrane core and the ELD.

9.5 Is the TRPML2 N-terminus involved in the enhancement of viral infectivity?

A well-functioning TRPML2 overexpression system could also be used for investigations on the TRPML2 N-terminus. In mice, there are two TRPML2 isoforms, isoform 1 is the canonical full-length wild type and isoform 2 misses the first 28 N-terminal amino acids.[392] Preliminary results of experiments with cells which have been transiently transfected with a human TRPML2 construct missing the first 28 N-terminal amino acids indicated that the shortened construct is not able to enhance infection to the same extent compared to the wild type. Confirmed differences in the enhancement of ZIKV infection could suggest a crucial role of the N-terminus. Potential differences might be based on a yet unknown interaction of the TRPML2 N-terminus with other proteins. Another possibility could be altered interactions with membranes. The [redacted] group (Friedrich-Schiller-University, Jena) was able to show for TRPML1 that the first ~ 30 amino acids play an outstanding role in the regulation of this channel by lipids (C. Guhl *et al.*, unpublished).

Karacsonyi et al. reported in 2007 that TRPML2 is trafficked via the Arf6-associated pathway.[244] Arf6 is a small GTPase involved in clathrin-mediated and clathrin-independent endocytosis.[286] Heterologous over-expression of TRPML2 increases Arf6 activity by seven-fold.[244] This leads to enhanced vesicle fusion and formation of large vesicles in HeLa cells. However, it remains unclear if TRPML2 directly interacts with Arf6 or if it modulates the activity of specific Arf6 GEFs or GAPs. As a second aspect, Arf6 plays a crucial role in TLR signaling (TRPML2 mRNA levels are also upregulated in macrophages after TLR activation).[245,286] Arf6 and its GEF ARNO (ARF nucleotide-binding site opener) are interacting with the multimeric V-type ATPase, which controls the acidification of endosomes and lysosomes.[393] To investigate whether enhancement of ZIKV infectivity in TRPML2 overexpressing cells is dependent on the Arf6 pathway, co-immunoprecipitation with the cell lysate and Arf6/ARNO antibodies could be performed. Furthermore, colocalization of TRPML2 and Arf6/ARNO could be checked via immunostaining. In this context, it could be very interesting if differences between the long and the short TRPML2 constructs could be observed.

10 Appendix

10.1 ML2-SA1 synthesis

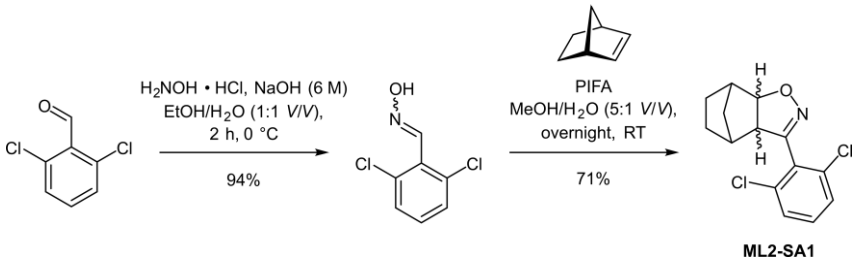

Figure 10.1: Synthesis of the specific TRPML2 agonist ML2-SA1. ML2-SA1 was synthesized by [redacted] ([redacted] group, Johannes Gutenberg-University Mainz) according to a two-step procedure from McIntosh *et al.*[394] and Plesch *et al.*[277] Starting from 2,6-dichlorobenzyldehyde, the respective benzaldoxime was prepared by treatment with hydroxylamine hydrochloride. In the second step, the benzaldoxime was brought to reaction with norbornene in the presence of (bis(trifluoroacetoxy)iodo)benzene (PIFA) to yield ML2-SA1 as a mixture of two enantiomers.[316]

10.2 Cell viability ML-SA1 treatment

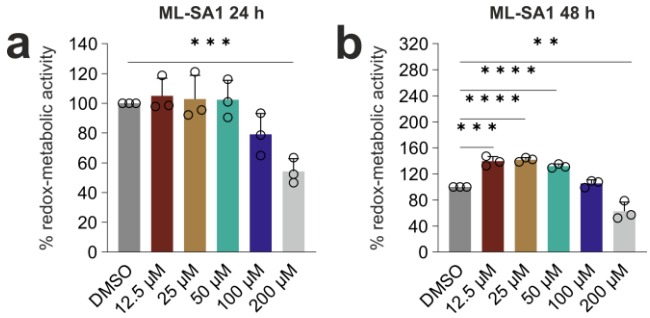

Figure 10.2: ML-SA1 is only toxic to A549 cells at high concentrations. Cell viability of A549 cells upon 24 h (**a**) and 48 h (**b**) treatment with increasing concentrations (12.5 µM to 200 µM) of ML-SA1 as assessed via the PrestoBlue® assay. Values are expressed as % of intact cells referred to the experimental control. Data are expressed as mean ± SD from $n = 3$ biological replicates. Statistical significance was determined by using unpaired *t*-test. *$p < 0.05$, **$p < 0.01$, ***$p < 0.001$, ****$p < 0.0001$.

10.3 ML2-SA1 affects later stages of the viral life cycle in A549 cells infected with the ZIKV French Polynesia strain

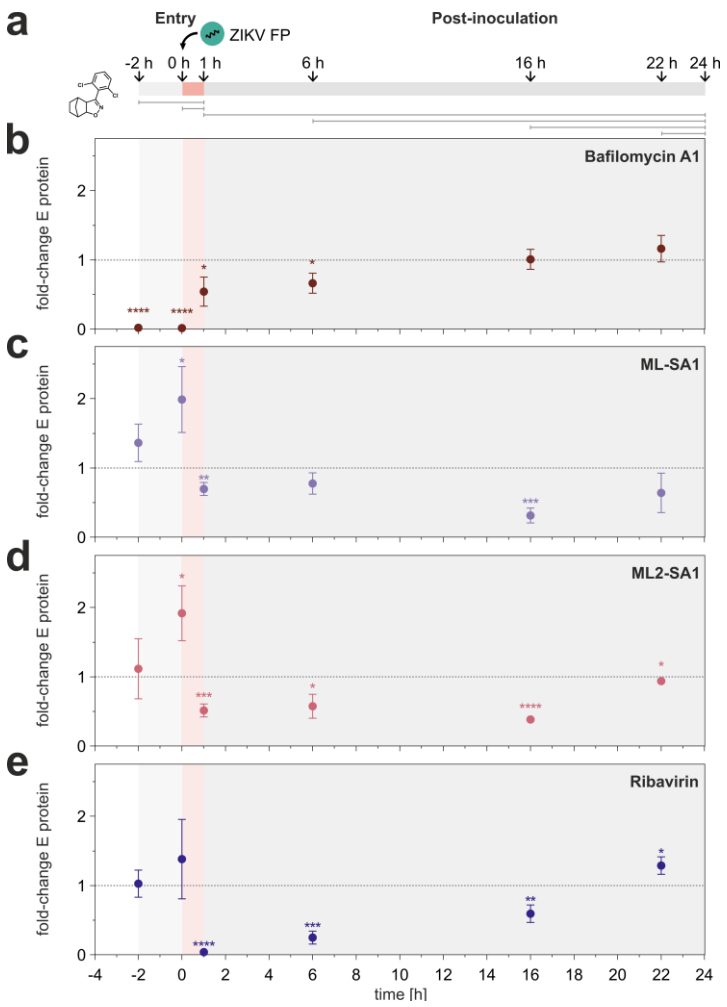

Figure 10.3: Time-of-addition experiments of ZIKV French Polynesia-infected A549 cells treated with Bafilomycin A1, ML-SA1 or ML2-SA1. a) A549 cells were infected with ZIKV French Polynesia (H/PF/2013) isolate for one hour (MOI = 1), then unbound virus was removed. Treatment with 50 nM Bafilomycin A1, 100 µM ML-SA1, 100 µM ML2-SA1 and 100 µM Ribavirin was started at −2h before infection, during infection, 1 h, 6 h, 16 h and 22 h after infection. Gray lines below the time scale indicate the respective incubation period, in which the compounds were present, after the treatment was started. (**b**–**e**) Relative fold-change of ZIKV E protein in samples treated with 50 nM Bafilomycin A1 (**b**), 100 µM ML-SA1 (**c**), 100 µM ML2-SA1 (**d**) and 100 µM Ribavirin (**e**) was assessed via Western Blotting. Representative Western Blots are shown in Figure 10.4. Results are normalized to the respective DMSO control of each timepoint and are expressed as mean ± SD from n = 3 biological replicates. Statistical significance was determined by using unpaired t-test. *$p < 0.05$, **$p < 0.01$, ***$p < 0.001$, ****$p < 0.0001$.

10.4 Time-of-addition experiments: representative Western Blots

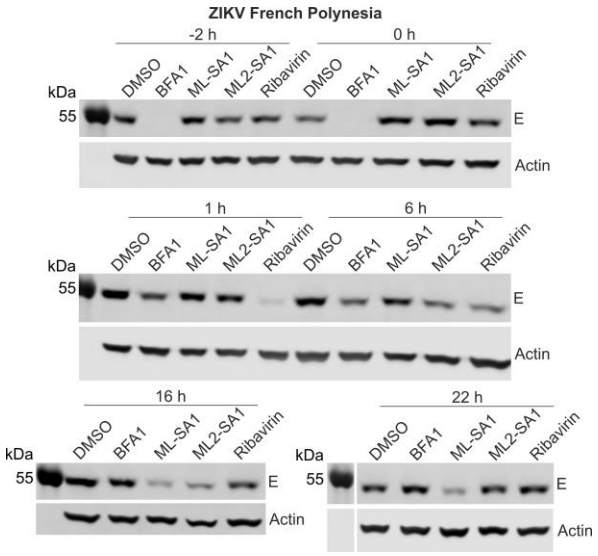

Figure 10.4: Representative Western blots from time-of-addition experiments with ZIKV French Polynesia. A549 cells were infected with ZIKV French Polynesia (H/PF/2013) isolate for one hour (MOI = 1), then unbound virus was removed. Treatment with 50 nM Bafilomycin A1, 100 µM ML-SA1, 100 µM ML2-SA1 and 100 µM Ribavirin was started at the respective timepoint.

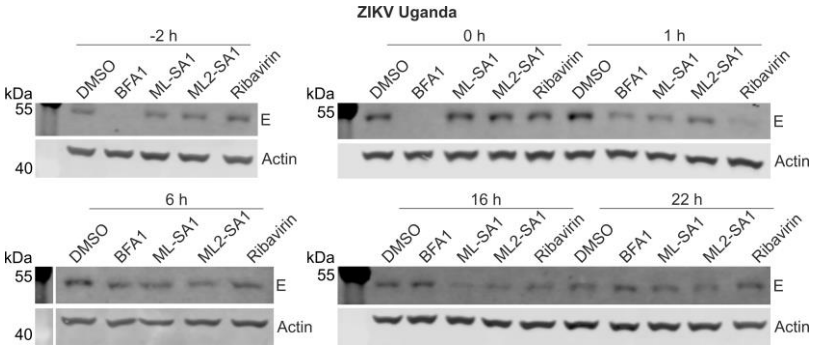

Figure 10.5: Representative Western blots from time-of-addition experiments with ZIKV Uganda A549 cells were infected with ZIKV Uganda (976 Uganda) isolate for one hour (MOI = 1), then unbound virus was removed. Treatment with 50 nM Bafilomycin A1, 100 µM ML-SA1, 100 µM ML2-SA1 and 100 µM Ribavirin was started at the respective timepoint.

10.5 Time-dependent accumulation of cholesterol in ML2-SA1-treated A549 cells

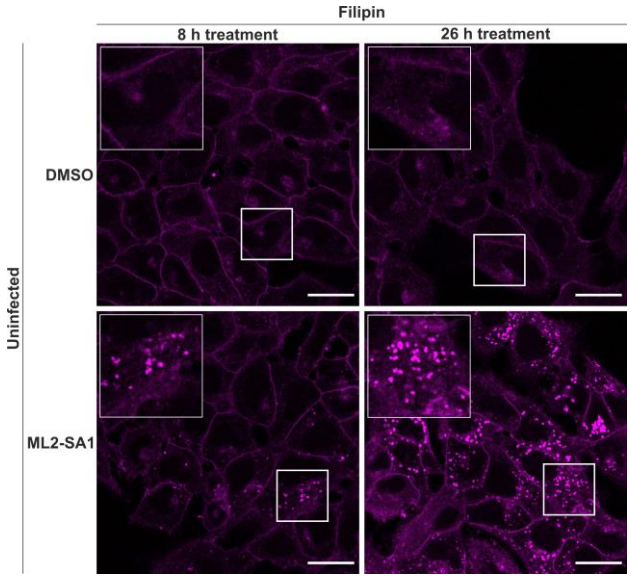

Figure 10.6: Time-dependent formation of cholesterol accumulations in ML2-SA1 treated A549 cells. Representative confocal laser scanning microscopy (CLSM) images of A549 cells which have been treated with 100 µM ML2-SA1 for 8 h and for 26 h. Intracellular cholesterol was stained using Filipin (magenta). Scale bar: 20 µM.

10.6 Sequences and biophysical properties of heterologously expressed human TRPML2 ELD constructs

Listed below are the sequneces of heterologously expressed human TRPML2 ELD constructs used in this thesis. A His_6SUMO tag (shown in grey), which was introduced to enhance solubility of the respective TRPML2 ELD construct (black), was removed during purification. Point mutations are shown in green. DNA (respective top row) and protein (bottom row) sequences are depicted for each construct.

His_6SUMO -TRPML2 ELD A92-K285

```
atggctagcggtcatcaccatcatcatcacgggtccgaggtcaagccagaagtcaagcct
 M  A  S  G  H  H  H  H  H  H  G  S  E  V  K  P  E  V  K  P
gagactcacatcaatttaaaggtgtccgatggatcttcagagatcttcttcaagatcaag
 E  T  H  I  N  L  K  V  S  D  G  S  S  E  I  F  F  K  I  K
aaaaccaccccactgcgtcggctgatggaagcgttcgctaaacgtcagggtaaagagatg
 K  T  T  P  L  R  R  L  M  E  A  F  A  K  R  Q  G  K  E  M
gacagcctgcgctttctgtatgatggcattcgcattcaggcggatcagaccccggaagac
 D  S  L  R  F  L  Y  D  G  I  R  I  Q  A  D  Q  T  P  E  D
ctggacatggaagataacgatatcattgaggcccatcgtgaacagattggtggtgcgttt
 L  D  M  E  D  N  D  I  I  E  A  H  R  E  Q  I  G  G  A  F
aaagaagacaatacggtcgcatttaaacacctgttcctgaaaggctactcgggcacggac
 K  E  D  N  T  V  A  F  K  H  L  F  L  K  G  Y  S  G  T  D
gaagacgattactcctgctcagtttatacccaggaagatgcgtacgaaagtattttcttt
 E  D  D  Y  S  C  S  V  Y  T  Q  E  D  A  Y  E  S  I  F  F
gccatcaaccagtatcatcaactgaaagacattaccctgggcacgctgggctacggtgaa
 A  I  N  Q  Y  H  Q  L  K  D  I  T  L  G  T  L  G  Y  G  E
aacgaagataatcgtatcggcctgaaagtttgcaaacaacactataagaaaggcaccatg
 N  E  D  N  R  I  G  L  K  V  C  K  Q  H  Y  K  K  G  T  M
ttcccgtccaacgaaacgctgaacattgataatgacgtggaactggactgtgttcagctg
 F  P  S  N  E  T  L  N  I  D  N  D  V  E  L  D  C  V  Q  L
gatctgcaagacctgagcaaaaaaccgccggattggaaaaatagcagcttttccgtctg
 D  L  Q  D  L  S  K  K  P  P  D  W  K  N  S  S  F  F  R  L
gaattttaccgcctgctgcaggtcgaaatctcattccatctgaaaggcattgatctgcaa
 E  F  Y  R  L  L  Q  V  E  I  S  F  H  L  K  G  I  D  L  Q
accatccactcgcgcgaactgccggactgctatgtgttccagaacacgatcatcttcgat
 T  I  H  S  R  E  L  P  D  C  Y  V  F  Q  N  T  I  I  F  D
aacaaagcacatagtggtaaaatcaaaatctacttcgattccgacgctaaaatcgaagaa
 N  K  A  H  S  G  K  I  K  I  Y  F  D  S  D  A  K  I  E  E
tgtaaagatctgaacatcttcggcagcacgcagaaataa
 C  K  D  L  N  I  F  G  S  T  Q  K  -
```

His_6SUMO -TRPML2 ELD A92-K285 D113A

```
atggctagcggtcatcaccatcatcatcacgggtccgaggtcaagccagaagtcaagcct
 M  A  S  G  H  H  H  H  H  H  G  S  E  V  K  P  E  V  K  P
gagactcacatcaatttaaaggtgtccgatggatcttcagagatcttcttcaagatcaag
 E  T  H  I  N  L  K  V  S  D  G  S  S  E  I  F  F  K  I  K
aaaaccaccccactgcgtcggctgatggaagcgttcgctaaacgtcagggtaaagagatg
 K  T  T  P  L  R  R  L  M  E  A  F  A  K  R  Q  G  K  E  M
gacagcctgcgctttctgtatgatggcattcgcattcaggcggatcagaccccggaagac
 D  S  L  R  F  L  Y  D  G  I  R  I  Q  A  D  Q  T  P  E  D
```

```
ctggacatggaagataacgatatcattgaggcccatcgtgaacagattggtggtgcgttt
 L  D  M  E  D  N  D  I  I  E  A  H  R  E  Q  I  G  G  A  F
aaagaagacaatacggtcgcatttaaacacctgttcctgaaaggctactcgggcacggcc
 K  E  D  N  T  V  A  F  K  H  L  F  L  K  G  Y  S  G  T  A
gaagacgattactcctgctcagtttatacccaggaagatgcgtacgaaagtattttcttt
 E  D  D  Y  S  C  S  V  Y  T  Q  E  D  A  Y  E  S  I  F  F
gccatcaaccagtatcatcaactgaaagacattaccctgggcacgctgggctacggtgaa
 A  I  N  Q  Y  H  Q  L  K  D  I  T  L  G  T  L  G  Y  G  E
aacgaagataatcgtatcggcctgaaagtttgcaaacaacactataagaaaggcaccatg
 N  E  D  N  R  I  G  L  K  V  C  K  Q  H  Y  K  K  G  T  M
ttcccgtccaacgaaacgctgaacattgataatgacgtggaactggactgtgttcagctg
 F  P  S  N  E  T  L  N  I  D  N  D  V  E  L  D  C  V  Q  L
gatctgcaagacctgagcaaaaaaccgccggattggaaaaatagcagcttttccgtctg
 D  L  Q  D  L  S  K  K  P  P  D  W  K  N  S  S  F  F  R  L
gaattttaccgcctgctgcaggtcgaaatctcattccatctgaaaggcattgatctgcaa
 E  F  Y  R  L  L  Q  V  E  I  S  F  H  L  K  G  I  D  L  Q
accatccactcgcgcgaactgccggactgctatgtgttccagaacacgatcatcttcgat
 T  I  H  S  R  E  L  P  D  C  Y  V  F  Q  N  T  I  I  F  D
aacaaagcacatagtggtaaaatcaaaatctacttcgattccgacgctaaaatcgaagaa
 N  K  A  H  S  G  K  I  K  I  Y  F  D  S  D  A  K  I  E  E
tgtaaagatctgaacatcttcggcagcacgcagaaataa
 C  K  D  L  N  I  F  G  S  T  Q  K  -
```

His_6SUMO -TRPML2 ELD A92-K285 E114A

```
atggctagcggtcatcaccatcatcatcacgggtccgaggtcaagccagaagtcaagcct
 M  A  S  G  H  H  H  H  H  H  G  S  E  V  K  P  E  V  K  P
gagactcacatcaatttaaaggtgtccgatggatcttcagagatcttcttcaagatcaag
 E  T  H  I  N  L  K  V  S  D  G  S  S  E  I  F  F  K  I  K
aaaaccaccccactgcgtcggctgatggaagcgttcgctaaacgtcagggtaaagagatg
 K  T  T  P  L  R  R  L  M  E  A  F  A  K  R  Q  G  K  E  M
gacagcctgcgctttctgtatgatggcattcgcattcaggcggatcagaccccggaagac
 D  S  L  R  F  L  Y  D  G  I  R  I  Q  A  D  Q  T  P  E  D
ctggacatggaagataacgatatcattgaggcccatcgtgaacagattggtggtgcgttt
 L  D  M  E  D  N  D  I  I  E  A  H  R  E  Q  I  G  G  A  F
aaagaagacaatacggtcgcatttaaacacctgttcctgaaaggctactcgggcacggac
 K  E  D  N  T  V  A  F  K  H  L  F  L  K  G  Y  S  G  T  D
gcagacgattactcctgctcagtttatacccaggaagatgcgtacgaaagtattttcttt
 A  D  D  Y  S  C  S  V  Y  T  Q  E  D  A  Y  E  S  I  F  F
gccatcaaccagtatcatcaactgaaagacattaccctgggcacgctgggctacggtgaa
 A  I  N  Q  Y  H  Q  L  K  D  I  T  L  G  T  L  G  Y  G  E
aacgaagataatcgtatcggcctgaaagtttgcaaacaacactataagaaaggcaccatg
 N  E  D  N  R  I  G  L  K  V  C  K  Q  H  Y  K  K  G  T  M
ttcccgtccaacgaaacgctgaacattgataatgacgtggaactggactgtgttcagctg
 F  P  S  N  E  T  L  N  I  D  N  D  V  E  L  D  C  V  Q  L
gatctgcaagacctgagcaaaaaaccgccggattggaaaaatagcagcttttccgtctg
 D  L  Q  D  L  S  K  K  P  P  D  W  K  N  S  S  F  F  R  L
gaattttaccgcctgctgcaggtcgaaatctcattccatctgaaaggcattgatctgcaa
 E  F  Y  R  L  L  Q  V  E  I  S  F  H  L  K  G  I  D  L  Q
accatccactcgcgcgaactgccggactgctatgtgttccagaacacgatcatcttcgat
 T  I  H  S  R  E  L  P  D  C  Y  V  F  Q  N  T  I  I  F  D
aacaaagcacatagtggtaaaatcaaaatctacttcgattccgacgctaaaatcgaagaa
 N  K  A  H  S  G  K  I  K  I  Y  F  D  S  D  A  K  I  E  E
```

```
tgtaaagatctgaacatcttcggcagcacgcagaaataa
 C  K  D  L  N  I  F  G  S  T  Q  K  -
```

His_6SUMO -TRPML2 ELD A92-K285 D115A

```
atggctagcggtcatcaccatcatcatcacgggtccgaggtcaagccagaagtcaagcct
 M  A  S  G  H  H  H  H  H  H  G  S  E  V  K  P  E  V  K  P
gagactcacatcaatttaaaggtgtccgatggatcttcagagatcttcttcaagatcaag
 E  T  H  I  N  L  K  V  S  D  G  S  S  E  I  F  F  K  I  K
aaaaccaccccactgcgtcggctgatggaagcgttcgctaaacgtcagggtaaagagatg
 K  T  T  P  L  R  R  L  M  E  A  F  A  K  R  Q  G  K  E  M
gacagcctgcgctttctgtatgatggcattcgcattcaggcggatcagaccccggaagac
 D  S  L  R  F  L  Y  D  G  I  R  I  Q  A  D  Q  T  P  E  D
ctggacatggaagataacgatatcattgaggcccatcgtgaacagattggtggtgcgttt
 L  D  M  E  D  N  D  I  I  E  A  H  R  E  Q  I  G  G  A  F
aaagaagacaatacggtcgcatttaaacacctgttcctgaaaggctactcgggcacggac
 K  E  D  N  T  V  A  F  K  H  L  F  L  K  G  Y  S  G  T  D
gaagccgattactcctgctcagtttatacccaggaagatgcgtacgaaagtattttcttt
 E  A  D  Y  S  C  S  V  Y  T  Q  E  D  A  Y  E  S  I  F  F
gccatcaaccagtatcatcaactgaaagacattaccctgggcacgctgggctacggtgaa
 A  I  N  Q  Y  H  Q  L  K  D  I  T  L  G  T  L  G  Y  G  E
aacgaagataatcgtatcggcctgaaagtttgcaaacaacactataagaaaggcaccatg
 N  E  D  N  R  I  G  L  K  V  C  K  Q  H  Y  K  K  G  T  M
ttcccgtccaacgaaacgctgaacattgataatgacgtggaactggactgtgttcagctg
 F  P  S  N  E  T  L  N  I  D  N  D  V  E  L  D  C  V  Q  L
gatctgcaagacctgagcaaaaaaccgccggattggaaaaatagcagcttttccgtctg
 D  L  Q  D  L  S  K  K  P  P  D  W  K  N  S  S  F  F  R  L
gaattttaccgcctgctgcaggtcgaaatctcattccatctgaaaggcattgatctgcaa
 E  F  Y  R  L  L  Q  V  E  I  S  F  H  L  K  G  I  D  L  Q
accatccactcgcgcgaactgccggactgctatgtgttccagaacacgatcatcttcgat
 T  I  H  S  R  E  L  P  D  C  Y  V  F  Q  N  T  I  I  F  D
aacaaagcacatagtggtaaaatcaaaatctacttcgattccgacgctaaaatcgaagaa
 N  K  A  H  S  G  K  I  K  I  Y  F  D  S  D  A  K  I  E  E
tgtaaagatctgaacatcttcggcagcacgcagaaataa
 C  K  D  L  N  I  F  G  S  T  Q  K  -
```

His_6SUMO -TRPML2 ELD A92-K285 D116A

```
atggctagcggtcatcaccatcatcatcacgggtccgaggtcaagccagaagtcaagcct
 M  A  S  G  H  H  H  H  H  H  G  S  E  V  K  P  E  V  K  P
gagactcacatcaatttaaaggtgtccgatggatcttcagagatcttcttcaagatcaag
 E  T  H  I  N  L  K  V  S  D  G  S  S  E  I  F  F  K  I  K
aaaaccaccccactgcgtcggctgatggaagcgttcgctaaacgtcagggtaaagagatg
 K  T  T  P  L  R  R  L  M  E  A  F  A  K  R  Q  G  K  E  M
gacagcctgcgctttctgtatgatggcattcgcattcaggcggatcagaccccggaagac
 D  S  L  R  F  L  Y  D  G  I  R  I  Q  A  D  Q  T  P  E  D
ctggacatggaagataacgatatcattgaggcccatcgtgaacagattggtggtgcgttt
 L  D  M  E  D  N  D  I  I  E  A  H  R  E  Q  I  G  G  A  F
aaagaagacaatacggtcgcatttaaacacctgttcctgaaaggctactcgggcacggac
 K  E  D  N  T  V  A  F  K  H  L  F  L  K  G  Y  S  G  T  D
gaagacgcttactcctgctcagtttatacccaggaagatgcgtacgaaagtattttcttt
 E  D  A  Y  S  C  S  V  Y  T  Q  E  D  A  Y  E  S  I  F  F
gccatcaaccagtatcatcaactgaaagacattaccctgggcacgctgggctacggtgaa
 A  I  N  Q  Y  H  Q  L  K  D  I  T  L  G  T  L  G  Y  G  E
```

```
aacgaagataatcgtatcggcctgaaagtttgcaaacaacactataagaaaggcaccatg
 N  E  D  N  R  I  G  L  K  V  C  K  Q  H  Y  K  K  G  T  M
ttcccgtccaacgaaacgctgaacattgataatgacgtggaactggactgtgttcagctg
 F  P  S  N  E  T  L  N  I  D  N  D  V  E  L  D  C  V  Q  L
gatctgcaagacctgagcaaaaaaccgccggattggaaaaatagcagctttttccgtctg
 D  L  Q  D  L  S  K  K  P  P  D  W  K  N  S  S  F  F  R  L
gaattttaccgcctgctgcaggtcgaaatctcattccatctgaaaggcattgatctgcaa
 E  F  Y  R  L  L  Q  V  E  I  S  F  H  L  K  G  I  D  L  Q
accatccactcgcgcgaactgccggactgctatgtgttccagaacacgatcatcttcgat
 T  I  H  S  R  E  L  P  D  C  Y  V  F  Q  N  T  I  I  F  D
aacaaagcacatagtggtaaaatcaaaatctacttcgattccgacgctaaaatcgaagaa
 N  K  A  H  S  G  K  I  K  I  Y  F  D  S  D  A  K  I  E  E
tgtaaagatctgaacatcttcggcagcacgcagaaataa
 C  K  D  L  N  I  F  G  S  T  Q  K  -
```

His_6SUMO -TRPML2 ELD A92-K285 E114A/D115A

```
atggctagcggtcatcaccatcatcatcacgggtccgaggtcaagccagaagtcaagcct
 M  A  S  G  H  H  H  H  H  H  G  S  E  V  K  P  E  V  K  P
gagactcacatcaatttaaaggtgtccgatggatcttcagagatcttcttcaagatcaag
 E  T  H  I  N  L  K  V  S  D  G  S  S  E  I  F  F  K  I  K
aaaaccaccccactgcgtcggctgatggaagcgttcgctaaacgtcagggtaaagagatg
 K  T  T  P  L  R  R  L  M  E  A  F  A  K  R  Q  G  K  E  M
gacagcctgcgctttctgtatgatggcattcgcattcaggcggatcagaccccggaagac
 D  S  L  R  F  L  Y  D  G  I  R  I  Q  A  D  Q  T  P  E  D
ctggacatggaagataacgatatcattgaggcccatcgtgaacagattggtggtgcgttt
 L  D  M  E  D  N  D  I  I  E  A  H  R  E  Q  I  G  G  A  F
aaagaagacaatacggtcgcatttaaacacctgttcctgaaaggctactcgggcacggac
 K  E  D  N  T  V  A  F  K  H  L  F  L  K  G  Y  S  G  T  D
gcagccgattactcctgctcagtttatacccaggaagatgcgtacgaaagtattttcttt
 A  A  D  Y  S  C  S  V  Y  T  Q  E  D  A  Y  E  S  I  F  F
gccatcaaccagtatcatcaactgaaagacattaccctgggcacgctgggctacggtgaa
 A  I  N  Q  Y  H  Q  L  K  D  I  T  L  G  T  L  G  Y  G  E
aacgaagataatcgtatcggcctgaaagtttgcaaacaacactataagaaaggcaccatg
 N  E  D  N  R  I  G  L  K  V  C  K  Q  H  Y  K  K  G  T  M
ttcccgtccaacgaaacgctgaacattgataatgacgtggaactggactgtgttcagctg
 F  P  S  N  E  T  L  N  I  D  N  D  V  E  L  D  C  V  Q  L
gatctgcaagacctgagcaaaaaaccgccggattggaaaaatagcagctttttccgtctg
 D  L  Q  D  L  S  K  K  P  P  D  W  K  N  S  S  F  F  R  L
gaattttaccgcctgctgcaggtcgaaatctcattccatctgaaaggcattgatctgcaa
 E  F  Y  R  L  L  Q  V  E  I  S  F  H  L  K  G  I  D  L  Q
accatccactcgcgcgaactgccggactgctatgtgttccagaacacgatcatcttcgat
 T  I  H  S  R  E  L  P  D  C  Y  V  F  Q  N  T  I  I  F  D
aacaaagcacatagtggtaaaatcaaaatctacttcgattccgacgctaaaatcgaagaa
 N  K  A  H  S  G  K  I  K  I  Y  F  D  S  D  A  K  I  E  E
tgtaaagatctgaacatcttcggcagcacgcagaaataa
 C  K  D  L  N  I  F  G  S  T  Q  K  -
```

His_6SUMO -TRPML2 ELD A92-K285 F105W

```
atggctagcggtcatcaccatcatcatcacgggtccgaggtcaagccagaagtcaagcct
 M  A  S  G  H  H  H  H  H  H  G  S  E  V  K  P  E  V  K  P
gagactcacatcaatttaaaggtgtccgatggatcttcagagatcttcttcaagatcaag
```

```
 E  T  H  I  N  L  K  V  S  D  G  S  S  E  I  F  F  K  I  K
aaaaccaccccactgcgtcggctgatggaagcgttcgctaaacgtcagggtaaagagatg
 K  T  T  P  L  R  R  L  M  E  A  F  A  K  R  Q  G  K  E  M
gacagcctgcgctttctgtatgatggcattcgcattcaggcggatcagaccccggaagac
 D  S  L  R  F  L  Y  D  G  I  R  I  Q  A  D  Q  T  P  E  D
ctggacatggaagataacgatatcattgaggcccatcgtgaacagattggtggtgcgttt
 L  D  M  E  D  N  D  I  I  E  A  H  R  E  Q  I  G  G  A  F
aaagaagacaatacggtcgcatttaaacacctgtggctgaaaggctactcgggcacggac
 K  E  D  N  T  V  A  F  K  H  L  W  L  K  G  Y  S  G  T  D
gaagacgattactcctgctcagtttatacccaggaagatgcgtacgaaagtattttcttt
 E  D  D  Y  S  C  S  V  Y  T  Q  E  D  A  Y  E  S  I  F  F
gccatcaaccagtatcatcaactgaaagacattaccctgggcacgctgggctacggtgaa
 A  I  N  Q  Y  H  Q  L  K  D  I  T  L  G  T  L  G  Y  G  E
aacgaagataatcgtatcggcctgaaagtttgcaaacaacactataagaaaggcaccatg
 N  E  D  N  R  I  G  L  K  V  C  K  Q  H  Y  K  K  G  T  M
ttcccgtccaacgaaacgctgaacattgataatgacgtggaactggactgtgttcagctg
 F  P  S  N  E  T  L  N  I  D  N  D  V  E  L  D  C  V  Q  L
gatctgcaagacctgagcaaaaaaccgccggattggaaaaatagcagcttttccgtctg
 D  L  Q  D  L  S  K  K  P  P  D  W  K  N  S  S  F  F  R  L
gaattttaccgcctgctgcaggtcgaaatctcattccatctgaaaggcattgatctgcaa
 E  F  Y  R  L  L  Q  V  E  I  S  F  H  L  K  G  I  D  L  Q
accatccactcgcgcgaactgccggactgctatgtgttccagaacacgatcatcttcgat
 T  I  H  S  R  E  L  P  D  C  Y  V  F  Q  N  T  I  I  F  D
aacaaagcacatagtggtaaaatcaaaatctacttcgattccgacgctaaaatcgaagaa
 N  K  A  H  S  G  K  I  K  I  Y  F  D  S  D  A  K  I  E  E
tgtaaagatctgaacatcttcggcagcacgcagaaataa
 C  K  D  L  N  I  F  G  S  T  Q  K  -
```

His_6SUMO -TRPML2 ELD A92-K285 E95C

```
atggctagcggtcatcaccatcatcatcacgggtccgaggtcaagccagaagtcaagcct
 M  A  S  G  H  H  H  H  H  H  G  S  E  V  K  P  E  V  K  P
gagactcacatcaatttaaaggtgtccgatggatcttcagagatcttcttcaagatcaag
 E  T  H  I  N  L  K  V  S  D  G  S  S  E  I  F  F  K  I  K
aaaaccaccccactgcgtcggctgatggaagcgttcgctaaacgtcagggtaaagagatg
 K  T  T  P  L  R  R  L  M  E  A  F  A  K  R  Q  G  K  E  M
gacagcctgcgctttctgtatgatggcattcgcattcaggcggatcagaccccggaagac
 D  S  L  R  F  L  Y  D  G  I  R  I  Q  A  D  Q  T  P  E  D
ctggacatggaagataacgatatcattgaggcccatcgtgaacagattggtggtgcgttt
 L  D  M  E  D  N  D  I  I  E  A  H  R  E  Q  I  G  G  A  F
aaatgcgacaatacggtcgcatttaaacacctgttcctgaaaggctactcgggcacggac
 K  C  D  N  T  V  A  F  K  H  L  F  L  K  G  Y  S  G  T  D
gaagacgattactcctgctcagtttatacccaggaagatgcgtacgaaagtattttcttt
 E  D  D  Y  S  C  S  V  Y  T  Q  E  D  A  Y  E  S  I  F  F
gccatcaaccagtatcatcaactgaaagacattaccctgggcacgctgggctacggtgaa
 A  I  N  Q  Y  H  Q  L  K  D  I  T  L  G  T  L  G  Y  G  E
aacgaagataatcgtatcggcctgaaagtttgcaaacaacactataagaaaggcaccatg
 N  E  D  N  R  I  G  L  K  V  C  K  Q  H  Y  K  K  G  T  M
ttcccgtccaacgaaacgctgaacattgataatgacgtggaactggactgtgttcagctg
 F  P  S  N  E  T  L  N  I  D  N  D  V  E  L  D  C  V  Q  L
gatctgcaagacctgagcaaaaaaccgccggattggaaaaatagcagcttttccgtctg
 D  L  Q  D  L  S  K  K  P  P  D  W  K  N  S  S  F  F  R  L
gaattttaccgcctgctgcaggtcgaaatctcattccatctgaaaggcattgatctgcaa
 E  F  Y  R  L  L  Q  V  E  I  S  F  H  L  K  G  I  D  L  Q
```

```
accatccactcgcgcgaactgccggactgctatgtgttccagaacacgatcatcttcgat
 T  I  H  S  R  E  L  P  D  C  Y  V  F  Q  N  T  I  I  F  D
aacaaagcacatagtggtaaaatcaaaatctacttcgattccgacgctaaaatcgaagaa
 N  K  A  H  S  G  K  I  K  I  Y  F  D  S  D  A  K  I  E  E
tgtaaagatctgaacatcttcggcagcacgcagaaataa
 C  K  D  L  N  I  F  G  S  T  Q  K  -
```

His_6SUMO -TRPML2 ELD A92-K285 T98C

```
atggctagcggtcatcaccatcatcatcacgggtccgaggtcaagccagaagtcaagcct
 M  A  S  G  H  H  H  H  H  H  G  S  E  V  K  P  E  V  K  P
gagactcacatcaatttaaaggtgtccgatggatcttcagagatcttcttcaagatcaag
 E  T  H  I  N  L  K  V  S  D  G  S  S  E  I  F  F  K  I  K
aaaaccaccccactgcgtcggctgatggaagcgttcgctaaacgtcagggtaaagagatg
 K  T  T  P  L  R  R  L  M  E  A  F  A  K  R  Q  G  K  E  M
gacagcctgcgctttctgtatgatggcattcgcattcaggcggatcagaccccggaagac
 D  S  L  R  F  L  Y  D  G  I  R  I  Q  A  D  Q  T  P  E  D
ctggacatggaagataacgatatcattgaggcccatcgtgaacagattggtggtgcgttt
 L  D  M  E  D  N  D  I  I  E  A  H  R  E  Q  I  G  G  A  F
aaagaagacaattcgcgtcgcatttaaacacctgttcctgaaaggctactcgggcacggac
 K  E  D  N  C  V  A  F  K  H  L  F  L  K  G  Y  S  G  T  D
gaagacgattactcctgctcagtttatacccaggaagatgcgtacgaaagtattttcttt
 E  D  D  Y  S  C  S  V  Y  T  Q  E  D  A  Y  E  S  I  F  F
gccatcaaccagtatcatcaactgaaagacattaccctgggcacgctgggctacggtgaa
 A  I  N  Q  Y  H  Q  L  K  D  I  T  L  G  T  L  G  Y  G  E
aacgaagataatcgtatcggcctgaaagtttgcaaacaacactataagaaaggcaccatg
 N  E  D  N  R  I  G  L  K  V  C  K  Q  H  Y  K  K  G  T  M
ttcccgtccaacgaaacgctgaacattgataatgacgtggaactggactgtgttcagctg
 F  P  S  N  E  T  L  N  I  D  N  D  V  E  L  D  C  V  Q  L
gatctgcaagacctgagcaaaaaaccgccggattggaaaaatagcagcttttccgtctg
 D  L  Q  D  L  S  K  K  P  P  D  W  K  N  S  S  F  F  R  L
gaattttaccgcctgctgcaggtcgaaatctcattccatctgaaaggcattgatctgcaa
 E  F  Y  R  L  L  Q  V  E  I  S  F  H  L  K  G  I  D  L  Q
accatccactcgcgcgaactgccggactgctatgtgttccagaacacgatcatcttcgat
 T  I  H  S  R  E  L  P  D  C  Y  V  F  Q  N  T  I  I  F  D
aacaaagcacatagtggtaaaatcaaaatctacttcgattccgacgctaaaatcgaagaa
 N  K  A  H  S  G  K  I  K  I  Y  F  D  S  D  A  K  I  E  E
tgtaaagatctgaacatcttcggcagcacgcagaaataa
 C  K  D  L  N  I  F  G  S  T  Q  K  -
```

Table 10.1: TRPML2 ELD construct characteristics before Ulp1 cleavage. pI and $\varepsilon_{280\,nm}$ were calculated with the ExPASy ProtParam tool.

#	ELD construct	AAs	MW / Da	pI	$\varepsilon_{280\,nm}$
p329	His_6SUMO-TRPML2 ELD A92-K285 WT	292	33,783.90	5.44	22,140
p582	His_6SUMO-TRPML2 ELD A92-K285 D113A	292	33,739.89	5.52	22,140
p583	His_6SUMO-TRPML2 ELD A92-K285 E114A	292	33,725.87	5.52	22,140
p584	His_6SUMO-TRPML2 ELD A92-K285 D115A	292	33,739.89	5.52	22,140
p585	His_6SUMO-TRPML2 ELD A92-K285 D116A	292	33,739.89	5.52	22,140
p587	His_6SUMO-TRPML2 ELD A92-K285 E114A/D115A	292	33,681.86	5.60	22,140
p687	His_6SUMO-TRPML2 ELD F105W	292	33,822.94	5.44	27,640
p646	His_6SUMO-TRPML2 ELD A92-K285 E95C	292	33,757.93	5.52	22,265
p647	His_6SUMO-TRPML2 ELD A92-K285 T98C	292	33,785.94	5.44	22,265

#: Internal [redacted] group plasmid (p) numbers.

10.7 Purification of heterologously expressed TRPML ELD constructs

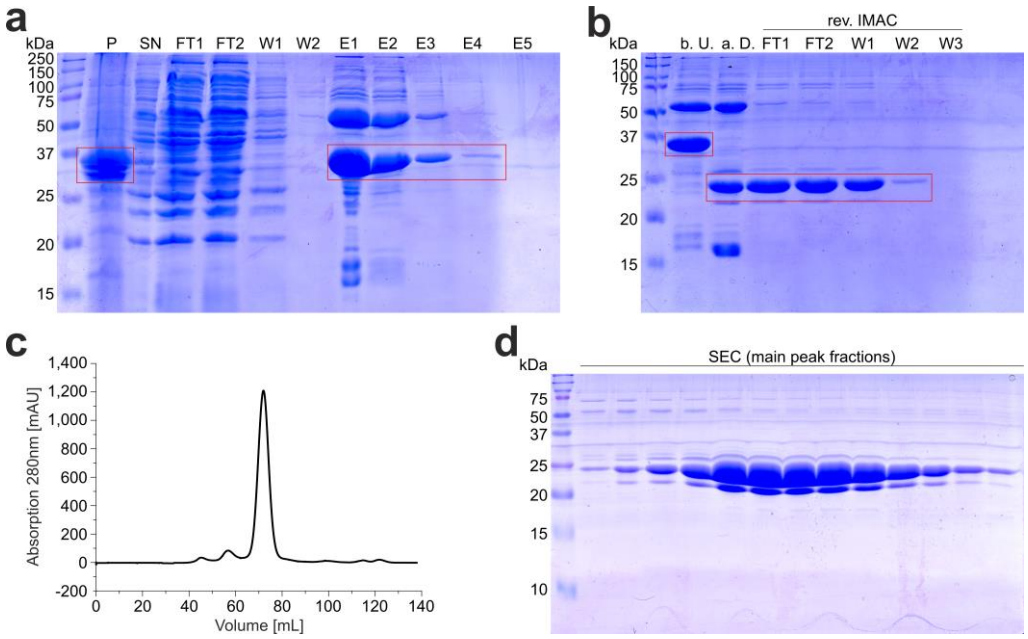

Figure 10.7: Purification of the human TRPML2 ELD A92-K285 according to purification procedure A (see section 4.11). (**a**) Purification of TRPML2 ELD via IMAC (NiNTA). 15% SDS-PAGE was used to visualize individual steps. (Coomassie stained, P: pellet, SN: supernatant, FT: flow-through, W: wash steps, E: elution steps, TRPML2 ELD protein bands are highlighted by red boxes). (**b**) After incubation with the protease Ulp1 to remove the SUMO-tag and subsequent dialysis, a reverse IMAC was carried out to remove Ulp1, cleaved HisSUMO-tag and uncleaved protein (15% SDS-PAGE, Coomassie stained, b. U.: before Ulp1, a. D.: after dialysis, FT: flow-through, W: wash steps, TRPML2 ELD protein bands are highlighted by red boxes). (**c**) After rev. IMAC, SEC was performed. (**d**) Coomassie-stained 15% SDS-PAGE of the SEC run shown in (**c**).

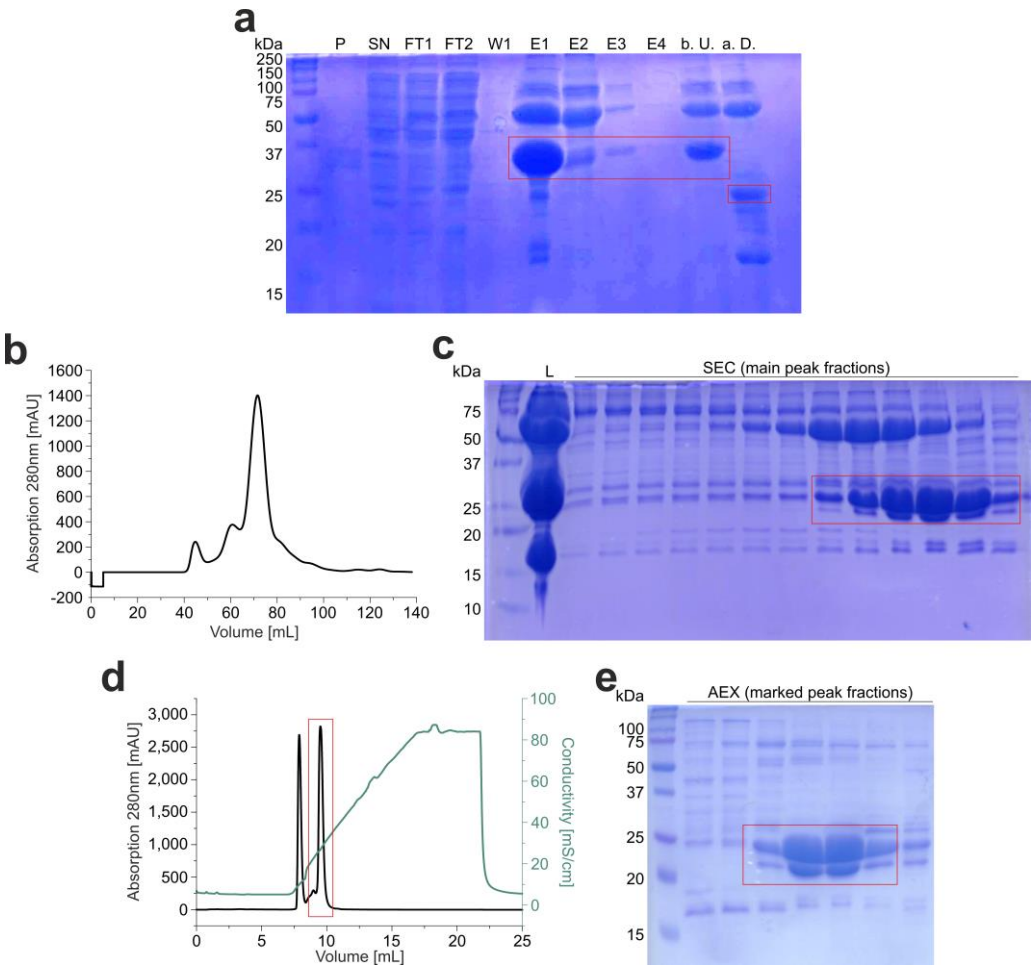

Figure 10.8: Purification of the human TRPML2 ELD A92-K285 according to purification procedure B (see section 4.11). (**a**) Purification of TRPML2 ELD via IMAC (NiNTA). After incubation with the protease Ulp1 to remove the SUMO-tag, dialysis was performed. 15% SDS-PAGE was used to visualize individual steps. (Coomassie stained, P: pellet, SN: supernatant, FT: flow-through, W: wash steps, E: elution steps, b. U.: before Ulp1, a. D.: after dialysis, TRPML2 ELD protein bands are highlighted by red boxes). (**b**) SEC was performed. (**c**) Coomassie-stained 15% SDS-PAGE of the SEC run shown in (**b**). (**d**) Anion exchange chromatography was performed. (**e**) Coomassie-stained 15% SDS-PAGE of the SEC run shown in (**d**), TRPML2 ELD protein bands are highlighted by red boxes.

10.8 Sequence alignment of human and mouse TRPML2 ELD

```
hsTRPML2_A92-K285       AFKEDNTVAFKHLFLKGYSGTDEDDYSCSVYTQEDAYESIFFAINQYHQLKDITLGTLGY     60
mmTRPML2_A92-R285       AFKEDNTVAFKHLFLKGFSGVDEDDYSCSIYTQENTYESIFFAIKQYRHLKNISLATLGY     60
                        ******************:**.********:****::********:**::**:*:*.****

hsTRPML2_A92-K285       GENEDNRIGLKVCKQHYKKGTMFPSNETLNIDNDVELDCVQLDLQDLSKKPPDWKNSSFF     120
mmTRPML2_A92-R285       GESEDNRTGLKVCKQHYKTGAMFSSNETLNIDSDIETDCIHLDLQVLTTEPEDWAQTSFF     120
                        **.**** **********.*:** ********.*:* **::**** *:.:* ** ::***

hsTRPML2_A92-K285       RLEFYRLLQVEISFHLKGIDLQTIHSRELPDCYVFQNTIIFDNKAHSGKIKIYFDSDAKI     180
mmTRPML2_A92-R285       RLDFYRLVQVDISFALKGIDLQAVHSREIPDCYLFQNTITFDNTAHSGKIKIYLNSEANI     180
                        **:****:**:*** *******::****:****:***** ***.*********::*:*:*

hsTRPML2_A92-K285       EECKDLNIFGSTQK   194
mmTRPML2_A92-R285       EECKNMNISGSTQR   194
                        ****::** ****:
```

Figure 10.9: Sequence alignment of hsTRPML2 ELD and mmTRPML2 ELD. Sequence alignment was performed with Clustal Omega (UniprotKBs: Q8IZK6, Q8K595). The acidic residues in the pre-pore loop (^{113}DEDD^{116}) are highlighted in pink, the cysteine residues forming disulfide bonds (C164/C190 and C243/C274) are highlighted in yellow.

10.9 Optimization of Ellman’s test

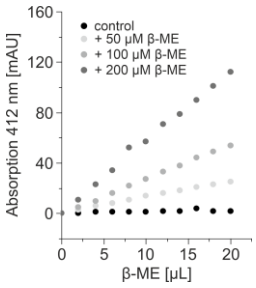

Figure 10.10: Optimization of Ellman's test using β-mercaptoethanol (β-ME) solutions. Solutions with different concentrations of β-ME (50, 100 and 200 µM β-ME, control: water) were titrated in 2 µL-steps to 20 nmol Ellman’s reagent to assess the amount of TRPML ELD needed to properly perform the assay (see Figure 7.11d, e). The absorption at 412 nm was measured.

10.10 Controls for isothermal titration calorimetry (ITC)

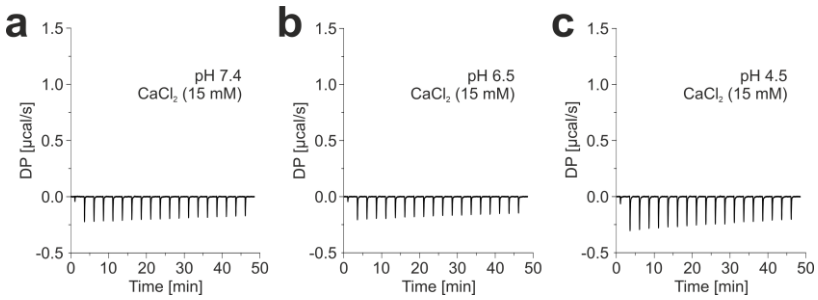

Figure 10.11: Controls for Isothermal Titration Calorimetry (ITC) on TRPML2 ELD: Titrations of $CaCl_2$ into buffers at varying pH values. Heat signatures of $CaCl_2$ (15 mM stock solution) titrations into buffers (10 mM HEPES, 15 mM NaCl) at pH 7.4 (**a**), 6.5 (**b**) and pH 4.5 (**c**).

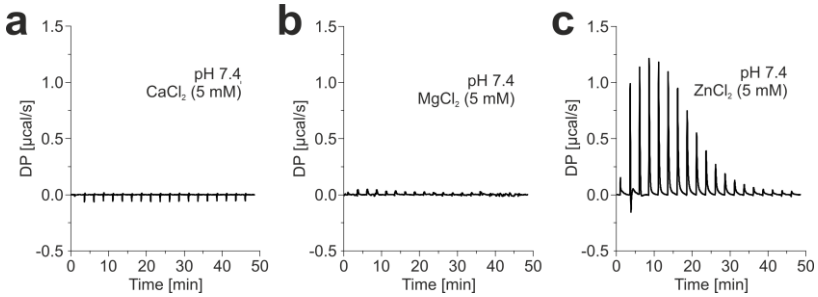

Figure 10.12: Controls for Isothermal Titration Calorimetry (ITC) on TRPML2 ELD: Titrations of $CaCl_2$, $MgCl_2$ and $ZnCl_2$ into buffers at pH 7.4. Heat signatures of $CaCl_2$ (**a**, 5 mM stock solution), $MgCl_2$ (**b**, 5 mM stock solution) and $ZnCl_2$ (**c**, 5 mM stock solution) titrations into buffers (10 mM HEPES, 15 mM NaCl) at pH 7.4.

10.11 pH-dependency of ^{19}F chemical shift of free BTFA and TRPML2 ELD E95C-TFA

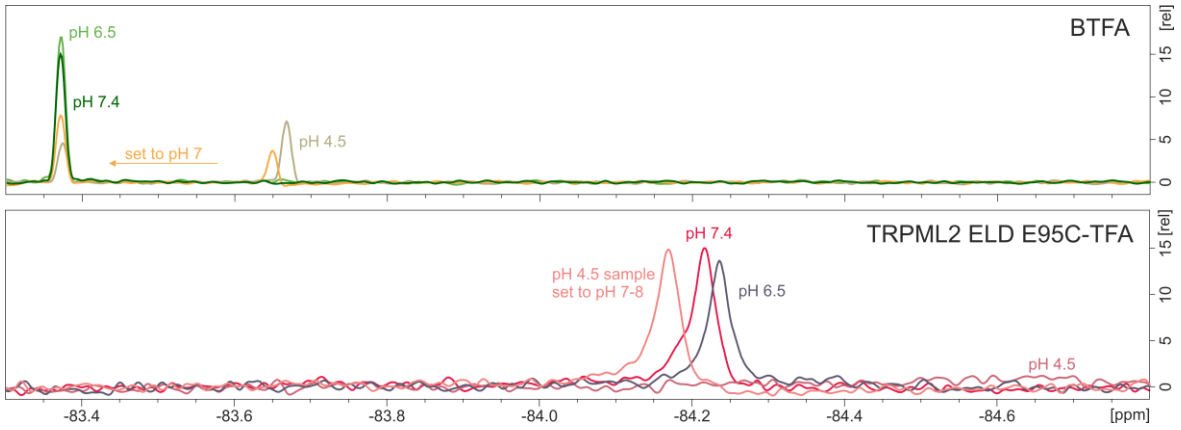

Figure 10.13: The chemical shift of both free BTFA and TRPML2 ELD E95C-TFA in ^{19}F-NMR spectra is pH-dependent. ^{19}F-NMR spectra of free BTFA (50 µM, top panel) and TRPML2 ELD E95C-TFA (50 µM, bottom panel). Spectra were recorded at 298 K in 10 mM HEPES, 15 mM NaCl at pH 7.4, pH 6.5 and pH 4.5. pH 4.5 samples were set back to pH ~7–8 by addition of NaOH solution.

10.12 PELDOR time traces

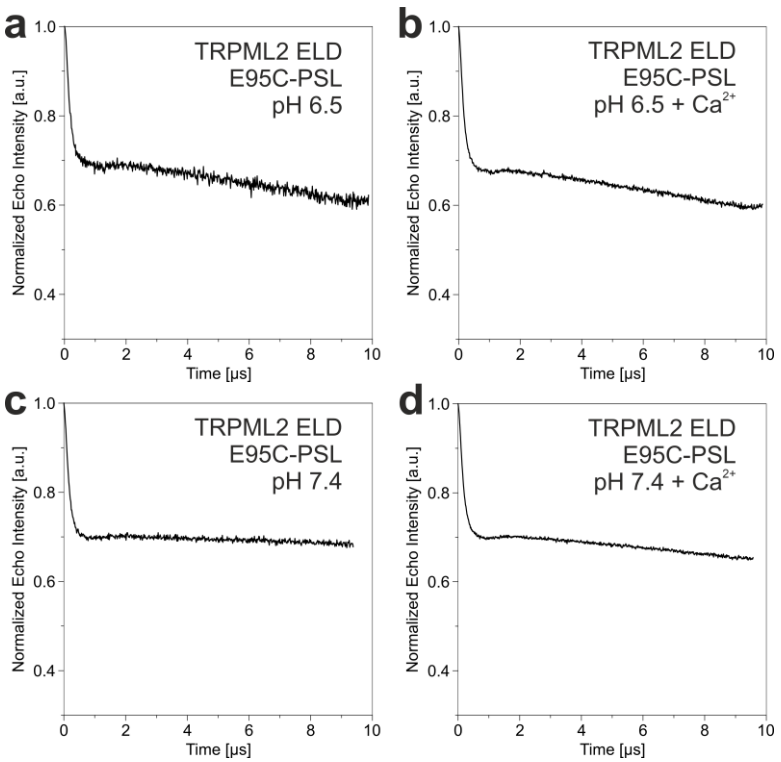

Figure 10.14: Time traces of PELDOR measurements performed with the IPSL-labeled TRPML2 E95C mutant. PELDOR measurements on the IPSL-labeled TRPML2 E95C mutant (100 µM) were performed at 50 K in deuterated buffer containing 10 mM HEPES, 15 mM NaCl, 30% glycerol at (**a**) pH 6.5, (**b**) 6.5 + 400 µM $CaCl_2$, (**c**) pH 7.4, (**d**) 7.4 + 400 µM $CaCl_2$.

List of figures

List of tables

References

1. Viet, K. K. *et al.* Structure of the Human TRPML2 Ion Channel Extracytosolic/Lumenal Domain. *Structure* **27**, 1246-1257.e5 (2019).

2. Pierson, T. C. & Diamond, M. S. The continued threat of emerging flaviviruses. *Nat. Microbiol.* **5**, 796–812 (2020).

3. Hover, S., Foster, B., Barr, J. N. & Mankouri, J. Viral dependence on cellular ion channels - an emerging anti-viral target? *J. Gen. Virol.* **98**, 345–351 (2017).

4. Dolphin, A. C., Insel, P. A., Blaschke, T. F. & Meyer, U. A. Introduction to the Theme "Ion Channels and Neuropharmacology: From the Past to the Future". *Annu. Rev. Pharmacol. Toxicol.* **60**, 1–6 (2020).

5. Bohmwald, K. *et al.* Modulation of Adaptive Immunity and Viral Infections by Ion Channels. *Front. Physiol.* **12**, 736681 (2021).

6. Zhou, Y., Frey, T. K. & Yang, J. J. Viral calciomics: interplays between Ca2+ and virus. *Cell Calcium* **46**, 1–17 (2009).

7. Fenard, D. *et al.* Nef is physically recruited into the immunological synapse and potentiates T cell activation early after TCR engagement. *J. Immunol.* **175**, 6050–6057 (2005).

8. Sloan, D. D. *et al.* Inhibition of TCR signaling by herpes simplex virus. *J. Immunol.* **176**, 1825–1833 (2006).

9. Nieva, J. L., Madan, V. & Carrasco, L. Viroporins: structure and biological functions. *Nat. Rev. Microbiol.* **10**, 563–574 (2012).

10. Luis Nieva, J. & Carrasco, L. Viroporins: Structures and Functions beyond Cell Membrane Permeabilization. *Viruses* vol. 7 5169–5171 (2015).

11. Royle, J., Dobson, S. J., Müller, M. & Macdonald, A. Emerging Roles of Viroporins Encoded by DNA Viruses: Novel Targets for Antivirals? *Viruses* **7**, 5375–5387 (2015).

12. Pierson, T. C. & Graham, B. S. Zika Virus: Immunity and Vaccine Development. *Cell* **167**, 625–631 (2016).

13. Pielnaa, P. *et al.* Zika virus-spread, epidemiology, genome, transmission cycle, clinical manifestation, associated challenges, vaccine and antiviral drug development. *Virology* **543**, 34–42 (2020).

14. Egid, B. R. *et al.* Review of the ecology and behaviour of Aedes aegypti and Aedes albopictus in Western Africa and implications for vector control. *Curr. Res. Parasitol. Vector-Borne Dis.* **2**, 100074 (2022).

15. Braack, L., Gouveia de Almeida, A. P., Cornel, A. J., Swanepoel, R. & de Jager, C. Mosquito-borne arboviruses of African origin: review of key viruses and vectors. *Parasit. Vectors* **11**, 29 (2018).

16. Lozano-Fuentes, S. *et al.* The dengue virus mosquito vector Aedes aegypti at high elevation in Mexico. *Am. J. Trop. Med. Hyg.* **87**, 902–909 (2012).

17. Shaily, S. & Upadhya, A. Zika virus: Molecular responses and tissue tropism in the mammalian host. *Rev. Med. Virol.* **29**, e2050 (2019).

18. Miner, J. J. & Diamond, M. S. Zika Virus Pathogenesis and Tissue Tropism. *Cell Host Microbe* **21**, 134–142 (2017).

19. Duffy, M. R. *et al.* Zika virus outbreak on Yap Island, Federated States of Micronesia. *N. Engl.*

J. Med. **360**, 2536–2543 (2009).

20. Dirlikov, E. *et al.* Postmortem Findings in Patient with Guillain-Barré Syndrome and Zika Virus Infection. *Emerg. Infect. Dis.* **24**, 114–117 (2018).

21. Delaney, A. *et al.* Population-Based Surveillance of Birth Defects Potentially Related to Zika Virus Infection - 15 States and U.S. Territories, 2016. *MMWR. Morb. Mortal. Wkly. Rep.* **67**, 91–96 (2018).

22. DICK, G. W. A., KITCHEN, S. F. & HADDOW, A. J. Zika virus. I. Isolations and serological specificity. *Trans. R. Soc. Trop. Med. Hyg.* **46**, 509–520 (1952).

23. Weaver, S. C. *et al.* Zika virus: History, emergence, biology, and prospects for control. *Antiviral Res.* **130**, 69–80 (2016).

24. Marchette, N. J., Garcia, R. & Rudnick, A. Isolation of Zika virus from Aedes aegypti mosquitoes in Malaysia. *Am. J. Trop. Med. Hyg.* **18**, 411–415 (1969).

25. Hu, T., Li, J., Carr, M. J., Duchêne, S. & Shi, W. The Asian Lineage of Zika Virus: Transmission and Evolution in Asia and the Americas. *Virol. Sin.* **34**, 1–8 (2019).

26. Olson, J. G., Ksiazek, T. G., Suhandiman & Triwibowo. Zika virus, a cause of fever in Central Java, Indonesia. *Trans. R. Soc. Trop. Med. Hyg.* **75**, 389–393 (1981).

27. Musso, D. & Gubler, D. J. Zika Virus. *Clin. Microbiol. Rev.* **29**, 487–524 (2016).

28. Cao-Lormeau, V.-M. Zika Virus, French Polynesia, South Pacific, 2013. *Emerg. Infect. Dis. J.* **20**, 1960 (2014).

29. Aubry, M. *et al.* Zika Virus Seroprevalence, French Polynesia, 2014-2015. *Emerg. Infect. Dis.* **23**, 669–672 (2017).

30. Adebayo, G., Neumark, Y., Gesser-Edelsburg, A., Ahmad, W. A. & Levine, H. Zika pandemic online trends, incidence and health risk communication: a time trend study. *BMJ Glob. Heal.* **2**, e000296 (2017).

31. Tognarelli, J. *et al.* A report on the outbreak of Zika virus on Easter Island, South Pacific, 2014. *Arch. Virol.* **161**, 665–668 (2016).

32. ECDC, E. C. Rapid risk assessment: Zika virus epidemic in the Americas: potential association with microcephaly and Guillain-Barré syndrome. *Eur. Cent. Dis. Prev. Control S* (2015).

33. Schuler-Faccini, L. *et al.* Possible Association Between Zika Virus Infection and Microcephaly - Brazil, 2015. *MMWR. Morb. Mortal. Wkly. Rep.* **65**, 59–62 (2016).

34. Tang, H. *et al.* Zika Virus Infects Human Cortical Neural Progenitors and Attenuates Their Growth. *Cell Stem Cell* **18**, 587–590 (2016).

35. Lum, F.-M. *et al.* Zika Virus Infects Human Fetal Brain Microglia and Induces Inflammation. *Clin. Infect. Dis. an Off. Publ. Infect. Dis. Soc. Am.* **64**, 914–920 (2017).

36. Meertens, L. *et al.* Axl Mediates ZIKA Virus Entry in Human Glial Cells and Modulates Innate Immune Responses. *Cell Rep.* **18**, 324–333 (2017).

37. Retallack, H. *et al.* Zika virus cell tropism in the developing human brain and inhibition by azithromycin. *Proc. Natl. Acad. Sci. U. S. A.* **113**, 14408–14413 (2016).

38. Cauchemez, S. *et al.* Association between Zika virus and microcephaly in French Polynesia, 2013-15: a retrospective study. *Lancet (London, England)* **387**, 2125–2132 (2016).

39. Cugola, F. R. *et al.* The Brazilian Zika virus strain causes birth defects in experimental models. *Nature* **534**, 267–271 (2016).

40. Musso, D. *et al.* Zika virus in French Polynesia 2013-14: anatomy of a completed outbreak.

Lancet. Infect. Dis. **18**, e172–e182 (2018).

41. Swaminathan, S., Schlaberg, R., Lewis, J., Hanson, K. E. & Couturier, M. R. Fatal Zika Virus Infection with Secondary Nonsexual Transmission. *The New England journal of medicine* vol. 375 1907–1909 (2016).

42. Karimi, O. *et al.* Thrombocytopenia and subcutaneous bleedings in a patient with Zika virus infection. *Lancet (London, England)* vol. 387 939–940 (2016).

43. Carteaux, G. *et al.* Zika Virus Associated with Meningoencephalitis. *The New England journal of medicine* vol. 374 1595–1596 (2016).

44. Who. WHO Director-General summarizes the outcome of the Emergency Committee regarding clusters of microcephaly and Guillain-Barré syndrome. *World Heal. Organ.* (2016).

45. Netto, E. M. *et al.* High Zika Virus Seroprevalence in Salvador, Northeastern Brazil Limits the Potential for Further Outbreaks. *MBio* **8**, (2017).

46. Agrelli, A., de Moura, R. R., Crovella, S. & Brandão, L. A. C. ZIKA virus entry mechanisms in human cells. *Infect. Genet. Evol.* **69**, 22–29 (2019).

47. Sager, G., Gabaglio, S., Sztul, E. & Belov, G. A. Role of Host Cell Secretory Machinery in Zika Virus Life Cycle. *Viruses* vol. 10 (2018).

48. Garcia-Blanco, M. A., Vasudevan, S. G., Bradrick, S. S. & Nicchitta, C. Flavivirus RNA transactions from viral entry to genome replication. *Antiviral Res.* **134**, 244–249 (2016).

49. Pierson, T. C. & Diamond, M. S. The emergence of Zika virus and its new clinical syndromes. *Nature* **560**, 573–581 (2018).

50. Serman, T. M. & Gack, M. U. Evasion of Innate and Intrinsic Antiviral Pathways by the Zika Virus. *Viruses* **11**, (2019).

51. Sirohi, D. *et al.* The 3.8 Å resolution cryo-EM structure of Zika virus. *Science* **352**, 467–470 (2016).

52. Kostyuchenko, V. A. *et al.* Structure of the thermally stable Zika virus. *Nature* **533**, 425–428 (2016).

53. Sirohi, D. & Kuhn, R. J. Zika Virus Structure, Maturation, and Receptors. *J. Infect. Dis.* **216**, S935–S944 (2017).

54. Annamalai, A. S. *et al.* Zika Virus Encoding Nonglycosylated Envelope Protein Is Attenuated and Defective in Neuroinvasion. *J. Virol.* **91**, (2017).

55. Barba-Spaeth, G. *et al.* Structural basis of potent Zika-dengue virus antibody cross-neutralization. *Nature* **536**, 48–53 (2016).

56. Fernandez, E. *et al.* Human antibodies to the dengue virus E-dimer epitope have therapeutic activity against Zika virus infection. *Nat. Immunol.* **18**, 1261–1269 (2017).

57. Prasad, V. M. *et al.* Structure of the immature Zika virus at 9 Å resolution. *Nat. Struct. Mol. Biol.* **24**, 184–186 (2017).

58. Kaufmann, B. & Rossmann, M. G. Molecular mechanisms involved in the early steps of flavivirus cell entry. *Microbes Infect.* **13**, 1–9 (2011).

59. Kim, S. Y., Li, B. & Linhardt, R. J. Pathogenesis and Inhibition of Flaviviruses from a Carbohydrate Perspective. *Pharmaceuticals (Basel).* **10**, (2017).

60. Mercer, J., Schelhaas, M. & Helenius, A. Virus Entry by Endocytosis. *Annu. Rev. Biochem.* **79**, 803–833 (2010).

61. Kuhn, R. J., Dowd, K. A., Beth Post, C. & Pierson, T. C. Shake, rattle, and roll: Impact of the

dynamics of flavivirus particles on their interactions with the host. *Virology* **479–480**, 508–517 (2015).

62. Amara, A. & Mercer, J. Viral apoptotic mimicry. *Nat. Rev. Microbiol.* **13**, 461–469 (2015).

63. Traub, L. M. Regarding the amazing choreography of clathrin coats. *PLoS Biol.* **9**, e1001037 (2011).

64. Cocucci, E., Gaudin, R. & Kirchhausen, T. Dynamin recruitment and membrane scission at the neck of a clathrin-coated pit. *Mol. Biol. Cell* **25**, 3595–3609 (2014).

65. Boulant, S., Kural, C., Zeeh, J.-C., Ubelmann, F. & Kirchhausen, T. Actin dynamics counteract membrane tension during clathrin-mediated endocytosis. *Nat. Cell Biol.* **13**, 1124–1131 (2011).

66. Aschenbrenner, L., Lee, T. & Hasson, T. Myo6 facilitates the translocation of endocytic vesicles from cell peripheries. *Mol. Biol. Cell* **14**, 2728–2743 (2003).

67. Novick, P. & Brennwald, P. Friends and family: the role of the Rab GTPases in vesicular traffic. *Cell* **75**, 597–601 (1993).

68. Jovic, M., Sharma, M., Rahajeng, J. & Caplan, S. The early endosome: a busy sorting station for proteins at the crossroads. *Histol. Histopathol.* **25**, 99–112 (2010).

69. Huotari, J. & Helenius, A. Endosome maturation. *EMBO J.* **30**, 3481–3500 (2011).

70. Maxfield, F. R. & McGraw, T. E. Endocytic recycling. *Nat. Rev. Mol. Cell Biol.* **5**, 121–132 (2004).

71. Maxfield, F. R. & Yamashiro, D. J. Endosome acidification and the pathways of receptor-mediated endocytosis. *Adv. Exp. Med. Biol.* **225**, 189–198 (1987).

72. Owczarek, K. *et al.* Zika virus: mapping and reprogramming the entry. *Cell Commun. Signal.* **17**, 41 (2019).

73. Nour, A. M., Li, Y., Wolenski, J. & Modis, Y. Viral membrane fusion and nucleocapsid delivery into the cytoplasm are distinct events in some flaviviruses. *PLoS Pathog.* **9**, e1003585 (2013).

74. Espósito, D. L. A., Nguyen, J. B., DeWitt, D. C., Rhoades, E. & Modis, Y. Physico-chemical requirements and kinetics of membrane fusion of flavivirus-like particles. *J. Gen. Virol.* **96**, 1702–1711 (2015).

75. Gollins, S. W. & Porterfield, J. S. pH-dependent fusion between the flavivirus West Nile and liposomal model membranes. *J. Gen. Virol.* **67 (Pt 1)**, 157–166 (1986).

76. Modis, Y., Ogata, S., Clements, D. & Harrison, S. C. Structure of the dengue virus envelope protein after membrane fusion. *Nature* **427**, 313–319 (2004).

77. Dai, L. *et al.* Structures of the Zika Virus Envelope Protein and Its Complex with a Flavivirus Broadly Protective Antibody. *Cell Host Microbe* **19**, 696–704 (2016).

78. Mukherjee, S. *et al.* Enhancing dengue virus maturation using a stable furin over-expressing cell line. *Virology* **497**, 33–40 (2016).

79. Kostyuchenko, V. A., Zhang, Q., Tan, J. L., Ng, T.-S. & Lok, S.-M. Immature and mature dengue serotype 1 virus structures provide insight into the maturation process. *J. Virol.* **87**, 7700–7707 (2013).

80. Dowd, K. A., Mukherjee, S., Kuhn, R. J. & Pierson, T. C. Combined effects of the structural heterogeneity and dynamics of flaviviruses on antibody recognition. *J. Virol.* **88**, 11726–11737 (2014).

81. Zaitseva, E., Yang, S.-T., Melikov, K., Pourmal, S. & Chernomordik, L. V. Dengue virus ensures its fusion in late endosomes using compartment-specific lipids. *PLoS Pathog.* **6**, e1001131 (2010).

82. Rawle, R. J., Webster, E. R., Jelen, M., Kasson, P. M. & Boxer, S. G. pH Dependence of Zika Membrane Fusion Kinetics Reveals an Off-Pathway State. *ACS Cent. Sci.* **4**, 1503–1510 (2018).

83. Pamarthy, S., Kulshrestha, A., Katara, G. K. & Beaman, K. D. The curious case of vacuolar ATPase: regulation of signaling pathways. *Mol. Cancer* **17**, 41 (2018).

84. Stauber, T. & Jentsch, T. J. Sorting motifs of the endosomal/lysosomal CLC chloride transporters. *J. Biol. Chem.* **285**, 34537–34548 (2010).

85. Scheel, O., Zdebik, A. A., Lourdel, S. & Jentsch, T. J. Voltage-dependent electrogenic chloride/proton exchange by endosomal CLC proteins. *Nature* **436**, 424–427 (2005).

86. Steinberg, B. E. *et al.* A cation counterflux supports lysosomal acidification. *J. Cell Biol.* **189**, 1171–1186 (2010).

87. Brett, C. L., Tukaye, D. N., Mukherjee, S. & Rao, R. The yeast endosomal Na+K+/H+ exchanger Nhx1 regulates cellular pH to control vesicle trafficking. *Mol. Biol. Cell* **16**, 1396–1405 (2005).

88. Huynh, K. K. & Grinstein, S. Regulation of vacuolar pH and its modulation by some microbial species. *Microbiol. Mol. Biol. Rev.* **71**, 452–462 (2007).

89. Van Dyke, R. W. Na+/H+ exchange modulates acidification of early rat liver endocytic vesicles. *Am. J. Physiol.* **269**, C943-54 (1995).

90. Luzio, J. P., Bright, N. A. & Pryor, P. R. The role of calcium and other ions in sorting and delivery in the late endocytic pathway. *Biochem. Soc. Trans.* **35**, 1088–1091 (2007).

91. Gerasimenko, J. V, Tepikin, A. V, Petersen, O. H. & Gerasimenko, O. V. Calcium uptake via endocytosis with rapid release from acidifying endosomes. *Curr. Biol.* **8**, 1335–1338 (1998).

92. Rinkenberger, N. & Schoggins, J. W. Mucolipin-2 Cation Channel Increases Trafficking Efficiency of Endocytosed Viruses. *MBio* **9**, (2018).

93. Simmons, J. A. *et al.* Ebolavirus Glycoprotein Directs Fusion through NPC1+ Endolysosomes. *J. Virol.* **90**, 605–610 (2016).

94. Das, D. K. *et al.* Conformational changes in the Ebola virus membrane fusion machine induced by pH, Ca2+, and receptor binding. *PLoS Biol.* **18**, e3000626 (2020).

95. Mazeaud, C., Freppel, W. & Chatel-Chaix, L. The Multiples Fates of the Flavivirus RNA Genome During Pathogenesis . *Frontiers in Genetics* vol. 9 (2018).

96. Cortese, M. *et al.* Ultrastructural Characterization of Zika Virus Replication Factories. *Cell Rep.* **18**, 2113–2123 (2017).

97. Rossignol, E. D., Peters, K. N., Connor, J. H. & Bullitt, E. Zika virus induced cellular remodelling. *Cell. Microbiol.* **19**, (2017).

98. Paul, D. & Bartenschlager, R. Architecture and biogenesis of plus-strand RNA virus replication factories. *World J. Virol.* **2**, 32–48 (2013).

99. van den Elsen, K., Quek, J. P. & Luo, D. Molecular Insights into the Flavivirus Replication Complex. *Viruses* **13**, (2021).

100. Ci, Y. *et al.* Zika NS1-induced ER remodeling is essential for viral replication. *J. Cell Biol.* **219**, (2020).

101. Miller, S., Kastner, S., Krijnse-Locker, J., Bühler, S. & Bartenschlager, R. The non-structural protein 4A of dengue virus is an integral membrane protein inducing membrane alterations in a 2K-regulated manner. *J. Biol. Chem.* **282**, 8873–8882 (2007).

102. Heaton, N. S. *et al.* Dengue virus nonstructural protein 3 redistributes fatty acid synthase to sites of viral replication and increases cellular fatty acid synthesis. *Proc. Natl. Acad. Sci. U. S. A.* **107**, 17345–17350 (2010).

103. Mackenzie, J. M., Khromykh, A. A. & Parton, R. G. Cholesterol manipulation by West Nile virus perturbs the cellular immune response. *Cell Host Microbe* **2**, 229–239 (2007).

104. Apte-Sengupta, S., Sirohi, D. & Kuhn, R. J. Coupling of replication and assembly in flaviviruses. *Curr. Opin. Virol.* **9**, 134–142 (2014).

105. Westaway, E. G. *et al.* Flaviviridae. *Intervirology* **24**, 183–192 (1985).

106. Welsch, S. *et al.* Composition and three-dimensional architecture of the dengue virus replication and assembly sites. *Cell Host Microbe* **5**, 365–375 (2009).

107. Charlton, F. W. *et al.* Ion Channels as Therapeutic Targets for Viral Infections: Further Discoveries and Future Perspectives. *Viruses* **12**, (2020).

108. Wang, S. *et al.* Screening of FDA-Approved Drugs for Inhibitors of Japanese Encephalitis Virus Infection. *J. Virol.* **91**, (2017).

109. Liu, J. *et al.* A novel sheet-like virus particle array is a hallmark of Zika virus infection. *Emerg. Microbes Infect.* **7**, 69 (2018).

110. Barreto-Vieira, D. F. *et al.* Structural investigation of C6/36 and Vero cell cultures infected with a Brazilian Zika virus. *PLoS One* **12**, e0184397 (2017).

111. Ward, A. M. *et al.* The Golgi associated ERI3 is a Flavivirus host factor. *Sci. Rep.* **6**, 34379 (2016).

112. Hoffmann, H.-H. *et al.* Diverse Viruses Require the Calcium Transporter SPCA1 for Maturation and Spread. *Cell Host Microbe* **22**, 460-470.e5 (2017).

113. Li, L. *et al.* The flavivirus precursor membrane-envelope protein complex: structure and maturation. *Science* **319**, 1830–1834 (2008).

114. Yu, I.-M. *et al.* Structure of the immature dengue virus at low pH primes proteolytic maturation. *Science* **319**, 1834–1837 (2008).

115. Burlaud-Gaillard, J. *et al.* Correlative scanning-transmission electron microscopy reveals that a chimeric flavivirus is released as individual particles in secretory vesicles. *PLoS One* **9**, e93573 (2014).

116. York, S. B. *et al.* Zika Virus Hijacks Extracellular Vesicle Tetraspanin Pathways for Cell-to-Cell Transmission. *mSphere* **6**, e0019221 (2021).

117. Pattnaik, A., Sahoo, B. R. & Pattnaik, A. K. Current Status of Zika Virus Vaccines: Successes and Challenges. *Vaccines* **8**, (2020).

118. Crill, W. D. & Chang, G.-J. J. Localization and characterization of flavivirus envelope glycoprotein cross-reactive epitopes. *J. Virol.* **78**, 13975–13986 (2004).

119. Stiasny, K., Kiermayr, S., Holzmann, H. & Heinz, F. X. Cryptic properties of a cluster of dominant flavivirus cross-reactive antigenic sites. *J. Virol.* **80**, 9557–9568 (2006).

120. Xu, L., Ma, Z., Li, Y., Pang, Z. & Xiao, S. Antibody dependent enhancement: Unavoidable problems in vaccine development. *Adv. Immunol.* **151**, 99–133 (2021).

121. Thomas, S. J. Is new dengue vaccine efficacy data a relief or cause for concern? *npj Vaccines* **8**, 55 (2023).

122. Hadinegoro, S. R. *et al.* Efficacy and Long-Term Safety of a Dengue Vaccine in Regions of Endemic Disease. *N. Engl. J. Med.* **373**, 1195–1206 (2015).

123. Halstead, S. B. Licensed Dengue Vaccine: Public Health Conundrum and Scientific Challenge. *Am. J. Trop. Med. Hyg.* **95**, 741–745 (2016).

124. da Silva, S., Oliveira Silva Martins, D. & Jardim, A. C. G. A Review of the Ongoing Research on Zika Virus Treatment. *Viruses* **10**, (2018).

125. Baz, M. & Boivin, G. Antiviral Agents in Development for Zika Virus Infections. *Pharmaceuticals (Basel).* **12**, (2019).

126. Batista, M. N. *et al.* Natural Products Isolated from Oriental Medicinal Herbs Inactivate Zika Virus. *Viruses* **11**, (2019).

127. Haddad, J. G. *et al.* Doratoxylon apetalum, an Indigenous Medicinal Plant from Mascarene Islands, Is a Potent Inhibitor of Zika and Dengue Virus Infection in Human Cells. *Int. J. Mol. Sci.* **20**, (2019).

128. Niu, X. *et al.* Convalescent patient-derived monoclonal antibodies targeting different epitopes of E protein confer protection against Zika virus in a neonatal mouse model. *Emerg. Microbes Infect.* **8**, 749–759 (2019).

129. De Clercq, E. & Neyts, J. Antiviral agents acting as DNA or RNA chain terminators. *Handb. Exp. Pharmacol.* 53–84 (2009) doi:10.1007/978-3-540-79086-0_3.

130. Bekerman, E. & Einav, S. Infectious disease. Combating emerging viral threats. *Science* **348**, 282–283 (2015).

131. Al-Bari, M. A. A. Targeting endosomal acidification by chloroquine analogs as a promising strategy for the treatment of emerging viral diseases. *Pharmacol. Res. Perspect.* **5**, e00293 (2017).

132. Delvecchio, R. *et al.* Chloroquine, an Endocytosis Blocking Agent, Inhibits Zika Virus Infection in Different Cell Models. *Viruses* vol. 8 (2016).

133. Browning, D. J. Pharmacology of Chloroquine and Hydroxychloroquine. *Hydroxychloroquine and Chloroquine Retinopathy* 35–63 (2014) doi:10.1007/978-1-4939-0597-3_2.

134. Tsai, W. P., Nara, P. L., Kung, H. F. & Oroszlan, S. Inhibition of human immunodeficiency virus infectivity by chloroquine. *AIDS Res. Hum. Retroviruses* **6**, 481–489 (1990).

135. Ooi, E. E., Chew, J. S. W., Loh, J. P. & Chua, R. C. S. In vitro inhibition of human influenza A virus replication by chloroquine. *Virol. J.* **3**, 39 (2006).

136. Farias, K. J. S., Machado, P. R. L. & da Fonseca, B. A. L. Chloroquine inhibits dengue virus type 2 replication in Vero cells but not in C6/36 cells. *ScientificWorldJournal.* **2013**, 282734 (2013).

137. Zhu, Y.-Z. *et al.* Japanese encephalitis virus enters rat neuroblastoma cells via a pH-dependent, dynamin and caveola-mediated endocytosis pathway. *J. Virol.* **86**, 13407–13422 (2012).

138. Boonyasuppayakorn, S., Reichert, E. D., Manzano, M., Nagarajan, K. & Padmanabhan, R. Amodiaquine, an antimalarial drug, inhibits dengue virus type 2 replication and infectivity. *Antiviral Res.* **106**, 125–134 (2014).

139. Herrington, J. & Arey, B. J. Chapter 6 - Conformational Mechanisms of Signaling Bias of Ion Channels. in (ed. Arey Pharmacology and Therapeutics, B. J. B. T.-B. S. in P.) 173–207 (Academic Press, 2014). doi:https://doi.org/10.1016/B978-0-12-411460-9.00006-9.

140. Venter, J. C. *et al.* The sequence of the human genome. *Science* **291**, 1304–1351 (2001).

141. Yu, F. H., Yarov-Yarovoy, V., Gutman, G. A. & Catterall, W. A. Overview of molecular relationships in the voltage-gated ion channel superfamily. *Pharmacol. Rev.* **57**, 387–395 (2005).

142. Hamill, O. P., Marty, A., Neher, E., Sakmann, B. & Sigworth, F. J. Improved patch-clamp techniques for high-resolution current recording from cells and cell-free membrane patches. *Pflugers Arch.* **391**, 85–100 (1981).

143. Doyle, D. A. *et al.* The structure of the potassium channel: molecular basis of K+ conduction and selectivity. *Science* **280**, 69–77 (1998).

144. Julius, D. From peppers to peppermints: insights into thermosensation and pain. *Nobel Lecture* https://www.nobelprize.org/prizes/medicine/2021/julius/lecture/ (2021).

145. Patapoutian, A. How do you feel? The molecules that sense touch. *Nobel Lect.* (2021).

146. Farre, C. & Fertig, N. New strategies in ion channel screening for drug discovery: are there ways to improve its productivity? *Expert opinion on drug discovery* vol. 9 1103–1107 (2014).

147. McManus, O. B. HTS assays for developing the molecular pharmacology of ion channels. *Curr. Opin. Pharmacol.* **15**, 91–96 (2014).

148. Hanna, M. G. Genetic neurological channelopathies. *Nat. Clin. Pract. Neurol.* **2**, 252–263 (2006).

149. Verkman, A. S. & Galietta, L. J. V. Chloride channels as drug targets. *Nat. Rev. Drug Discov.* **8**, 153–171 (2009).

150. Phillips, L. & Trivedi, J. R. Skeletal Muscle Channelopathies. *Neurother. J. Am. Soc. Exp. Neurother.* **15**, 954–965 (2018).

151. Zaydman, M. A., Silva, J. R. & Cui, J. Ion Channel Associated Diseases: Overview of Molecular Mechanisms. *Chem. Rev.* **112**, 6319–6333 (2012).

152. Brown, B. M., Nguyen, H. M. & Wulff, H. Recent advances in our understanding of the structure and function of more unusual cation channels. *F1000Research* **8**, (2019).

153. Hille, B. Ionic channels in excitable membranes. Current problems and biophysical approaches. *Biophys. J.* **22**, 283–294 (1978).

154. Okada, Y. *et al.* Chapter 15 - The Puzzles of Volume-Activated Anion Channels. in (eds. Alvarez-Leefmans, F. J. & Delpire, E. B. T.-P. and P. of C. T. and C. in the N. S.) 283–306 (Academic Press, 2010). doi:https://doi.org/10.1016/B978-0-12-374373-2.00015-7.

155. Melkikh, A. V & Sutormina, M. I. Model of active transport of ions in cardiac cell. *J. Theor. Biol.* **252**, 247–254 (2008).

156. Armstrong, C. M. Interaction of tetraethylammonium ion derivatives with the potassium channels of giant axons. *J. Gen. Physiol.* **58**, 413–437 (1971).

157. Holmgren, M., Smith, P. L. & Yellen, G. Trapping of organic blockers by closing of voltage-dependent K+ channels: evidence for a trap door mechanism of activation gating. *J. Gen. Physiol.* **109**, 527–535 (1997).

158. Cuello, L. G., Jogini, V., Cortes, D. M. & Perozo, E. Structural mechanism of C-type inactivation in K(+) channels. *Nature* **466**, 203–208 (2010).

159. Uysal, S. *et al.* Mechanism of activation gating in the full-length KcsA K+ channel. *Proc. Natl. Acad. Sci. U. S. A.* **108**, 11896–11899 (2011).

160. Liu, Y., Holmgren, M., Jurman, M. E. & Yellen, G. Gated access to the pore of a voltage-dependent K+ channel. *Neuron* **19**, 175–184 (1997).

161. Perozo, E., Cortes, D. M. & Cuello, L. G. Structural rearrangements underlying K+-channel activation gating. *Science* **285**, 73–78 (1999).

162. del Camino, D. & Yellen, G. Tight steric closure at the intracellular activation gate of a voltage-gated K(+) channel. *Neuron* **32**, 649–656 (2001).

163. Jiang, Y. *et al.* The open pore conformation of potassium channels. *Nature* **417**, 523–526 (2002).

164. Rothberg, B. S., Shin, K. S., Phale, P. S. & Yellen, G. Voltage-controlled gating at the intracellular entrance to a hyperpolarization-activated cation channel. *J. Gen. Physiol.* **119**, 83–91 (2002).

165. Rothberg, B. S., Shin, K. S. & Yellen, G. Movements near the gate of a hyperpolarization-

activated cation channel. *J. Gen. Physiol.* **122**, 501–510 (2003).

166. Webster, S. M., Del Camino, D., Dekker, J. P. & Yellen, G. Intracellular gate opening in Shaker K+ channels defined by high-affinity metal bridges. *Nature* **428**, 864–868 (2004).

167. Cordero-Morales, J. F. *et al.* Molecular determinants of gating at the potassium-channel selectivity filter. *Nat. Struct. Mol. Biol.* **13**, 311–318 (2006).

168. Yang, J., Ellinor, P. T., Sather, W. A., Zhang, J. F. & Tsien, R. W. Molecular determinants of Ca2+ selectivity and ion permeation in L-type Ca2+ channels. *Nature* **366**, 158–161 (1993).

169. Zhou, Y., Morais-Cabral, J. H., Kaufman, A. & MacKinnon, R. Chemistry of ion coordination and hydration revealed by a K+ channel-Fab complex at 2.0 A resolution. *Nature* **414**, 43–48 (2001).

170. MacKinnon, R. Potassium channels and the atomic basis of selective ion conduction (Nobel Lecture). *Angewandte Chemie (International ed. in English)* vol. 43 4265–4277 (2004).

171. Payandeh, J., Scheuer, T., Zheng, N. & Catterall, W. A. The crystal structure of a voltage-gated sodium channel. *Nature* **475**, 353–358 (2011).

172. Qiu, H., Shen, R. & Guo, W. Ion solvation and structural stability in a sodium channel investigated by molecular dynamics calculations. *Biochim. Biophys. Acta* **1818**, 2529–2535 (2012).

173. Piasta, K. N., Theobald, D. L. & Miller, C. Potassium-selective block of barium permeation through single KcsA channels. *J. Gen. Physiol.* **138**, 421–436 (2011).

174. Jegla, T. J., Zmasek, C. M., Batalov, S. & Nayak, S. K. Evolution of the human ion channel set. *Comb. Chem. High Throughput Screen.* **12**, 2–23 (2009).

175. Cerana, R. & Colombo, R. Inward and Outward Rectifying K+ Channels of the Plasma Membrane have Different Physiological Roles. *J. Plant Physiol.* **142**, 685–688 (1993).

176. Vaeth, M. & Feske, S. Ion channelopathies of the immune system. *Curr. Opin. Immunol.* **52**, 39–50 (2018).

177. Garcia-Elias, A. & Benito, B. Ion Channel Disorders and Sudden Cardiac Death. *Int. J. Mol. Sci.* **19**, (2018).

178. Kerem, B. *et al.* Identification of the cystic fibrosis gene: genetic analysis. *Science* **245**, 1073–1080 (1989).

179. Riordan, J. R. *et al.* Identification of the cystic fibrosis gene: cloning and characterization of complementary DNA. *Science* **245**, 1066–1073 (1989).

180. Rommens, J. M. *et al.* Identification of the cystic fibrosis gene: chromosome walking and jumping. *Science* **245**, 1059–1065 (1989).

181. Anderson, M. P. *et al.* Demonstration that CFTR is a chloride channel by alteration of its anion selectivity. *Science* **253**, 202–205 (1991).

182. Anderson, M. P. *et al.* Nucleoside triphosphates are required to open the CFTR chloride channel. *Cell* **67**, 775–784 (1991).

183. Bear, C. E. *et al.* Purification and functional reconstitution of the cystic fibrosis transmembrane conductance regulator (CFTR). *Cell* **68**, 809–818 (1992).

184. Hwang, T.-C. & Kirk, K. L. The CFTR ion channel: gating, regulation, and anion permeation. *Cold Spring Harb. Perspect. Med.* **3**, a009498 (2013).

185. Cheng, S. H. *et al.* Defective intracellular transport and processing of CFTR is the molecular basis of most cystic fibrosis. *Cell* **63**, 827–834 (1990).

186. Lukacs, G. L. *et al.* Conformational maturation of CFTR but not its mutant counterpart (delta F508) occurs in the endoplasmic reticulum and requires ATP. *EMBO J.* **13**, 6076–6086 (1994).

187. Ward, C. L. & Kopito, R. R. Intracellular turnover of cystic fibrosis transmembrane conductance regulator. Inefficient processing and rapid degradation of wild-type and mutant proteins. *J. Biol. Chem.* **269**, 25710–25718 (1994).

188. Rich, D. P. *et al.* Expression of cystic fibrosis transmembrane conductance regulator corrects defective chloride channel regulation in cystic fibrosis airway epithelial cells. *Nature* **347**, 358–363 (1990).

189. Choi, M. *et al.* K+ channel mutations in adrenal aldosterone-producing adenomas and hereditary hypertension. *Science* **331**, 768–772 (2011).

190. Scholl, U. I. *et al.* Hypertension with or without adrenal hyperplasia due to different inherited mutations in the potassium channel KCNJ5. *Proc. Natl. Acad. Sci. U. S. A.* **109**, 2533–2538 (2012).

191. Spät, A. & Hunyady, L. Control of aldosterone secretion: a model for convergence in cellular signaling pathways. *Physiol. Rev.* **84**, 489–539 (2004).

192. Milliez, P. *et al.* Evidence for an increased rate of cardiovascular events in patients with primary aldosteronism. *J. Am. Coll. Cardiol.* **45**, 1243–1248 (2005).

193. Hübner, C. A. & Jentsch, T. J. Ion channel diseases. *Hum. Mol. Genet.* **11**, 2435–2445 (2002).

194. Cetin, H., Beeson, D., Vincent, A. & Webster, R. The Structure, Function, and Physiology of the Fetal and Adult Acetylcholine Receptor in Muscle . *Frontiers in Molecular Neuroscience* vol. 13 (2020).

195. Sine, S. M. *et al.* Mutation of the acetylcholine receptor alpha subunit causes a slow-channel myasthenic syndrome by enhancing agonist binding affinity. *Neuron* **15**, 229–239 (1995).

196. Finsterer, J. Congenital myasthenic syndromes. *Orphanet J. Rare Dis.* **14**, 57 (2019).

197. Kaneko, Y. & Szallasi, A. Transient receptor potential (TRP) channels: a clinical perspective. *Br. J. Pharmacol.* **171**, 2474–2507 (2014).

198. Kremeyer, B. *et al.* A gain-of-function mutation in TRPA1 causes familial episodic pain syndrome. *Neuron* **66**, 671–680 (2010).

199. Sun, M. *et al.* Mucolipidosis type IV is caused by mutations in a gene encoding a novel transient receptor potential channel. *Hum. Mol. Genet.* **9**, 2471–2478 (2000).

200. Slaugenhaupt, S. A. The molecular basis of mucolipidosis type IV. *Curr. Mol. Med.* **2**, 445–450 (2002).

201. Nilius, B. & Voets, T. The puzzle of TRPV4 channelopathies. *EMBO Rep.* **14**, 152–163 (2013).

202. Goretzki, B. *et al.* Crosstalk between regulatory elements in the disordered TRPV4 N-terminus modulates lipid-dependent channel activity. *bioRxiv* 2022.12.21.521430 (2022) doi:10.1101/2022.12.21.521430.

203. Goretzki, B., Tebbe, F., Mitrovic, S.-A. & Hellmich, U. A. Backbone NMR assignments of the extensive human and chicken TRPV4 N-terminal intrinsically disordered regions as important players in ion channel regulation. *Biomol. NMR Assign.* **16**, 205–212 (2022).

204. Aisenberg, W. H. *et al.* Multiubiquitination of TRPV4 reduces channel activity independent of surface localization. *J. Biol. Chem.* **298**, 101826 (2022).

205. Taga, A. *et al.* TRPV4 mutations causing mixed neuropathy and skeletal phenotypes result in severe gain of function. *Ann. Clin. Transl. Neurol.* **9**, 375–391 (2022).

206. McCray, B. A. *et al.* Neuropathy-causing TRPV4 mutations disrupt TRPV4-RhoA interactions

and impair neurite extension. *Nat. Commun.* **12**, 1444 (2021).

207. Goretzki, B. *et al.* Structural Basis of TRPV4 N Terminus Interaction with Syndapin/PACSIN1-3 and PIP(2). *Structure* **26**, 1583-1593.e5 (2018).

208. Venkatachalam, K. & Montell, C. TRP channels. *Annu. Rev. Biochem.* **76**, 387–417 (2007).

209. Nilius, B. & Owsianik, G. The transient receptor potential family of ion channels. *Genome Biol.* **12**, 218 (2011).

210. Montell, C. & Rubin, G. M. Molecular characterization of the Drosophila trp locus: a putative integral membrane protein required for phototransduction. *Neuron* **2**, 1313–1323 (1989).

211. Hardie, R. C. & Minke, B. The trp gene is essential for a light-activated Ca2+ channel in Drosophila photoreceptors. *Neuron* **8**, 643–651 (1992).

212. Cosens, D. J. & Manning, A. Abnormal electroretinogram from a Drosophila mutant. *Nature* **224**, 285–287 (1969).

213. Montell, C. Visual transduction in Drosophila. *Annu. Rev. Cell Dev. Biol.* **15**, 231–268 (1999).

214. Montell, C., Birnbaumer, L. & Flockerzi, V. The TRP channels, a remarkably functional family. *Cell* **108**, 595–598 (2002).

215. Cheng, X., Shen, D., Samie, M. & Xu, H. Mucolipins: Intracellular TRPML1-3 channels. *FEBS Lett.* **584**, 2013–2021 (2010).

216. Hellmich, U. A. & Gaudet, R. Structural biology of TRP channels. *Handb. Exp. Pharmacol.* **223**, 963–990 (2014).

217. Suo, Y. *et al.* Structural Insights into Electrophile Irritant Sensing by the Human TRPA1 Channel. *Neuron* **105**, 882-894.e5 (2020).

218. Vinayagam, D. *et al.* Electron cryo-microscopy structure of the canonical TRPC4 ion channel. *Elife* **7**, (2018).

219. Autzen, H. E. *et al.* Structure of the human TRPM4 ion channel in a lipid nanodisc. *Science* **359**, 228–232 (2018).

220. Jin, P. *et al.* Electron cryo-microscopy structure of the mechanotransduction channel NOMPC. *Nature* **547**, 118–122 (2017).

221. Huynh, K. W. *et al.* Structure of the full-length TRPV2 channel by cryo-EM. *Nat. Commun.* **7**, 11130 (2016).

222. Hirschi, M. *et al.* Cryo-electron microscopy structure of the lysosomal calcium-permeable channel TRPML3. *Nature* **550**, 411–414 (2017).

223. Shen, P. S. *et al.* The Structure of the Polycystic Kidney Disease Channel PKD2 in Lipid Nanodiscs. *Cell* **167**, 763-773.e11 (2016).

224. Himmel, N. J., Gray, T. R. & Cox, D. N. Phylogenetics Identifies Two Eumetazoan TRPM Clades and an Eighth TRP Family, TRP Soromelastatin (TRPS). *Mol. Biol. Evol.* **37**, 2034–2044 (2020).

225. Caterina, M. J. *et al.* The capsaicin receptor: a heat-activated ion channel in the pain pathway. *Nature* **389**, 816–824 (1997).

226. Runnels, L. W. TRPM6 and TRPM7: A Mul-TRP-PLIK-cation of channel functions. *Curr. Pharm. Biotechnol.* **12**, 42–53 (2011).

227. Krapivinsky, G. *et al.* Histone phosphorylation by TRPM6's cleaved kinase attenuates adjacent arginine methylation to regulate gene expression. *Proc. Natl. Acad. Sci. U. S. A.* **114**, E7092–E7100 (2017).

228. Sukumaran, P., Schaar, A., Sun, Y. & Singh, B. B. Functional role of TRP channels in modulating ER stress and Autophagy. *Cell Calcium* **60**, 123–132 (2016).

229. Kumar, P. S. *et al.* Understanding the role of Ca(2+) via transient receptor potential (TRP) channel in viral infection: Implications in developing future antiviral strategies. *Virus Res.* **323**, 198992 (2022).

230. Wang, S. *et al.* H9N2 swine influenza virus infection-induced damage is mediated by TRPM2 channels in mouse pulmonary microvascular endothelial cells. *Microb. Pathog.* **148**, 104408 (2020).

231. Abdullah, H., Heaney, L. G., Cosby, S. L. & McGarvey, L. P. A. Rhinovirus upregulates transient receptor potential channels in a human neuronal cell line: implications for respiratory virus-induced cough reflex sensitivity. *Thorax* **69**, 46 LP – 54 (2014).

232. Doñate-Macián, P. *et al.* The TRPV4 channel links calcium influx to DDX3X activity and viral infectivity. *Nat. Commun.* **9**, 2307 (2018).

233. Santoni, G. *et al.* Involvement of the TRPML Mucolipin Channels in Viral Infections and Anti-viral Innate Immune Responses . *Frontiers in Immunology* vol. 11 (2020).

234. Venkatachalam, K., Wong, C.-O. & Zhu, M. X. The role of TRPMLs in endolysosomal trafficking and function. *Cell Calcium* **58**, 48–56 (2015).

235. Xia, Z. *et al.* ML-SA1 and SN-2 inhibit endocytosed viruses through regulating TRPML channel expression and activity. *Antiviral Res.* **195**, 105193 (2021).

236. Xia, Z. *et al.* ML-SA1, a selective TRPML agonist, inhibits DENV2 and ZIKV by promoting lysosomal acidification and protease activity. *Antiviral Res.* **182**, 104922 (2020).

237. Zhou, X. *et al.* Cryo-EM structures of the human endolysosomal TRPML3 channel in three distinct states. *Nat. Struct. Mol. Biol.* **24**, 1146–1154 (2017).

238. Dong, X.-P., Wang, X. & Xu, H. TRP channels of intracellular membranes. *J. Neurochem.* **113**, 313–328 (2010).

239. Wakabayashi, K., Gustafson, A. M., Sidransky, E. & Goldin, E. Mucolipidosis type IV: an update. *Mol. Genet. Metab.* **104**, 206–213 (2011).

240. Wang, W., Zhang, X., Gao, Q. & Xu, H. TRPML1: an ion channel in the lysosome. *Handb. Exp. Pharmacol.* **222**, 631–645 (2014).

241. Sterea, A. M., Almasi, S. & El Hiani, Y. The hidden potential of lysosomal ion channels: A new era of oncogenes. *Cell Calcium* **72**, 91–103 (2018).

242. Zeevi, D. A., Frumkin, A. & Bach, G. TRPML and lysosomal function. *Biochim. Biophys. Acta* **1772**, 851–858 (2007).

243. García-Añoveros, J. & Wiwatpanit, T. TRPML2 and mucolipin evolution. *Handb. Exp. Pharmacol.* **222**, 647–658 (2014).

244. Karacsonyi, C., Miguel, A. S. & Puertollano, R. Mucolipin-2 localizes to the Arf6-associated pathway and regulates recycling of GPI-APs. *Traffic* **8**, 1404–1414 (2007).

245. Sun, L., Hua, Y., Vergarajauregui, S., Diab, H. I. & Puertollano, R. Novel Role of TRPML2 in the Regulation of the Innate Immune Response. *J. Immunol.* **195**, 4922–4932 (2015).

246. Chen, C.-C. *et al.* TRPML2 is an osmo/mechanosensitive cation channel in endolysosomal organelles. *Sci. Adv.* **6**, (2020).

247. Cuajungco, M. P. & Samie, M. A. The varitint-waddler mouse phenotypes and the TRPML3 ion channel mutation: cause and consequence. *Pflugers Arch.* **457**, 463–473 (2008).

248. Kim, H. J., Soyombo, A. A., Tjon-Kon-Sang, S., So, I. & Muallem, S. The Ca(2+) channel

TRPML3 regulates membrane trafficking and autophagy. *Traffic* **10**, 1157–1167 (2009).

249. Atiba-Davies, M. & Noben-Trauth, K. TRPML3 and hearing loss in the varitint-waddler mouse. *Biochim. Biophys. Acta* **1772**, 1028–1031 (2007).

250. Staaf, S., Oerther, S., Lucas, G., Mattsson, J. P. & Ernfors, P. Differential regulation of TRP channels in a rat model of neuropathic pain. *Pain* **144**, 187–199 (2009).

251. Grimm, C., Barthmes, M. & Wahl-Schott, C. TRPML3. *Handb. Exp. Pharmacol.* **222**, 659–674 (2014).

252. Miao, Y., Li, G., Zhang, X., Xu, H. & Abraham, S. N. A TRP Channel Senses Lysosome Neutralization by Pathogens to Trigger Their Expulsion. *Cell* **161**, 1306–1319 (2015).

253. Venkatachalam, K., Hofmann, T. & Montell, C. Lysosomal localization of TRPML3 depends on TRPML2 and the mucolipidosis-associated protein TRPML1. *J. Biol. Chem.* **281**, 17517–17527 (2006).

254. Schmiege, P., Fine, M., Blobel, G. & Li, X. Human TRPML1 channel structures in open and closed conformations. *Nature* **550**, 366–370 (2017).

255. Fine, M., Schmiege, P. & Li, X. Structural basis for PtdInsP(2)-mediated human TRPML1 regulation. *Nat. Commun.* **9**, 4192 (2018).

256. Chen, Q. *et al.* Structure of mammalian endolysosomal TRPML1 channel in nanodiscs. *Nature* **550**, 415–418 (2017).

257. Zhang, S., Li, N., Zeng, W., Gao, N. & Yang, M. Cryo-EM structures of the mammalian endo-lysosomal TRPML1 channel elucidate the combined regulation mechanism. *Protein Cell* **8**, 834–847 (2017).

258. Song, X. *et al.* Cryo-EM structure of mouse TRPML2 in lipid nanodiscs. *J. Biol. Chem.* **298**, 101487 (2022).

259. Puertollano, R. & Kiselyov, K. TRPMLs: in sickness and in health. *Am. J. Physiol. Renal Physiol.* **296**, F1245-54 (2009).

260. Dong, X. *et al.* PI(3,5)P(2) controls membrane trafficking by direct activation of mucolipin Ca(2+) release channels in the endolysosome. *Nat. Commun.* **1**, 38 (2010).

261. Zhang, X., Li, X. & Xu, H. Phosphoinositide isoforms determine compartment-specific ion channel activity. *Proc. Natl. Acad. Sci. U. S. A.* **109**, 11384–11389 (2012).

262. Vergarajauregui, S. & Puertollano, R. Two di-leucine motifs regulate trafficking of mucolipin-1 to lysosomes. *Traffic* **7**, 337–353 (2006).

263. Li, M. *et al.* Structural basis of dual Ca(2+)/pH regulation of the endolysosomal TRPML1 channel. *Nat. Struct. Mol. Biol.* **24**, 205–213 (2017).

264. Venugopal, B. *et al.* Chaperone-mediated autophagy is defective in mucolipidosis type IV. *J. Cell. Physiol.* **219**, 344–353 (2009).

265. LaPlante, J. M., Falardeau, J. L., Brown, E. M., Slaugenhaupt, S. A. & Vassilev, P. M. The cation channel mucolipin-1 is a bifunctional protein that facilitates membrane remodeling via its serine lipase domain. *Exp. Cell Res.* **317**, 691–705 (2011).

266. Kiselyov, K. *et al.* TRP-ML1 is a lysosomal monovalent cation channel that undergoes proteolytic cleavage. *J. Biol. Chem.* **280**, 43218–43223 (2005).

267. Grieben, M. *et al.* Structure of the polycystic kidney disease TRP channel Polycystin-2 (PC2). *Nat. Struct. Mol. Biol.* **24**, 114–122 (2017).

268. Wilkes, M. *et al.* Molecular insights into lipid-assisted Ca2+ regulation of the TRP channel Polycystin-2. *Nat. Struct. Mol. Biol.* **24**, 123–130 (2017).

269. Kim, H. J. *et al.* A novel mode of TRPML3 regulation by extracytosolic pH absent in the varitint-waddler phenotype. *EMBO J.* **27**, 1197–1205 (2008).

270. Spix, B., Chao, Y.-K., Abrahamian, C., Chen, C.-C. & Grimm, C. TRPML Cation Channels in Inflammation and Immunity. *Front. Immunol.* **11**, 225 (2020).

271. Marshall, J. S., Warrington, R., Watson, W. & Kim, H. L. An introduction to immunology and immunopathology. *Allergy, Asthma Clin. Immunol.* **14**, 49 (2018).

272. Dempsey, P. W., Vaidya, S. A. & Cheng, G. The art of war: Innate and adaptive immune responses. *Cell. Mol. Life Sci.* **60**, 2604–2621 (2003).

273. Schoggins, J. W. & Rice, C. M. Interferon-stimulated genes and their antiviral effector functions. *Curr. Opin. Virol.* **1**, 519–525 (2011).

274. Schoggins, J. W. Interferon-stimulated genes: roles in viral pathogenesis. *Curr. Opin. Virol.* **6**, 40–46 (2014).

275. Samie, M. *et al.* A TRP channel in the lysosome regulates large particle phagocytosis via focal exocytosis. *Dev. Cell* **26**, 511–524 (2013).

276. Bretou, M. *et al.* Lysosome signaling controls the migration of dendritic cells. *Sci. Immunol.* **2**, (2017).

277. Plesch, E. *et al.* Selective agonist of TRPML2 reveals direct role in chemokine release from innate immune cells. *Elife* **7**, (2018).

278. Chen, C.-C. *et al.* Small Molecules for Early Endosome-Specific Patch Clamping. *Cell Chem. Biol.* **24**, 907-916.e4 (2017).

279. Lanford, R. E. *et al.* Genomic response to interferon-alpha in chimpanzees: implications of rapid downregulation for hepatitis C kinetics. *Hepatology* **43**, 961–972 (2006).

280. Thompson, E. G., Schaheen, L., Dang, H. & Fares, H. Lysosomal trafficking functions of mucolipin-1 in murine macrophages. *BMC Cell Biol.* **8**, 54 (2007).

281. Roche, P. A. & Furuta, K. The ins and outs of MHC class II-mediated antigen processing and presentation. *Nat. Rev. Immunol.* **15**, 203–216 (2015).

282. Song, Y., Dayalu, R., Matthews, S. A. & Scharenberg, A. M. TRPML cation channels regulate the specialized lysosomal compartment of vertebrate B-lymphocytes. *Eur. J. Cell Biol.* **85**, 1253–1264 (2006).

283. Brown, F. D., Rozelle, A. L., Yin, H. L., Balla, T. & Donaldson, J. G. Phosphatidylinositol 4,5-bisphosphate and Arf6-regulated membrane traffic. *J. Cell Biol.* **154**, 1007–1017 (2001).

284. Naslavsky, N., Weigert, R. & Donaldson, J. G. Characterization of a nonclathrin endocytic pathway: membrane cargo and lipid requirements. *Mol. Biol. Cell* **15**, 3542–3552 (2004).

285. Radhakrishna, H. & Donaldson, J. G. ADP-ribosylation factor 6 regulates a novel plasma membrane recycling pathway. *J. Cell Biol.* **139**, 49–61 (1997).

286. Van Acker, T., Tavernier, J. & Peelman, F. The Small GTPase Arf6: An Overview of Its Mechanisms of Action and of Its Role in Host–Pathogen Interactions and Innate Immunity. *Int. J. Mol. Sci.* **20**, (2019).

287. García-Expósito, L. *et al.* HIV-1 requires Arf6-mediated membrane dynamics to efficiently enter and infect T lymphocytes. *Mol. Biol. Cell* **22**, 1148–1166 (2011).

288. Ono, A., Ablan, S. D., Lockett, S. J., Nagashima, K. & Freed, E. O. Phosphatidylinositol (4,5) bisphosphate regulates HIV-1 Gag targeting to the plasma membrane. *Proc. Natl. Acad. Sci. U. S. A.* **101**, 14889–14894 (2004).

289. Shu, Q., Lennemann, N. J., Sarkar, S. N., Sadovsky, Y. & Coyne, C. B. ADAP2 Is an Interferon

Stimulated Gene That Restricts RNA Virus Entry. *PLoS Pathog.* **11**, e1005150 (2015).

290. Murase, M. *et al.* Intravesicular Acidification Regulates Lipopolysaccharide Inflammation and Tolerance through TLR4 Trafficking. *J. Immunol.* **200**, 2798–2808 (2018).

291. Valadez, J. A. & Cuajungco, M. P. PAX5 is the transcriptional activator of mucolipin-2 (MCOLN2) gene. *Gene* **555**, 194–202 (2015).

292. Cuajungco, M. P., Silva, J., Habibi, A. & Valadez, J. A. The mucolipin-2 (TRPML2) ion channel: a tissue-specific protein crucial to normal cell function. *Pflugers Arch.* **468**, 177–192 (2016).

293. Grimm, C. *et al.* Small molecule activators of TRPML3. *Chem. Biol.* **17**, 135–148 (2010).

294. Yamaguchi, S. & Muallem, S. Opening the TRPML gates. *Chem. Biol.* **17**, 209–210 (2010).

295. Grimm, C., Jörs, S., Guo, Z., Obukhov, A. G. & Heller, S. Constitutive activity of TRPML2 and TRPML3 channels versus activation by low extracellular sodium and small molecules. *J. Biol. Chem.* **287**, 22701–22708 (2012).

296. Shen, D. *et al.* Lipid storage disorders block lysosomal trafficking by inhibiting a TRP channel and lysosomal calcium release. *Nat. Commun.* **3**, 731 (2012).

297. Pryor, P. R., Mullock, B. M., Bright, N. A., Gray, S. R. & Luzio, J. P. The role of intraorganellar Ca(2+) in late endosome-lysosome heterotypic fusion and in the reformation of lysosomes from hybrid organelles. *J. Cell Biol.* **149**, 1053–1062 (2000).

298. Medina, D. L. *et al.* Lysosomal calcium signalling regulates autophagy through calcineurin and TFEB. *Nat. Cell Biol.* **17**, 288–299 (2015).

299. Kilpatrick, B. S., Yates, E., Grimm, C., Schapira, A. H. & Patel, S. Endo-lysosomal TRP mucolipin-1 channels trigger global ER Ca2+ release and Ca2+ influx. *J. Cell Sci.* **129**, 3859–3867 (2016).

300. Somogyi, A. *et al.* The synthetic TRPML1 agonist ML-SA1 rescues Alzheimer-related alterations of the endosomal-autophagic-lysosomal system. *J. Cell Sci.* **136**, jcs259875 (2023).

301. Zhang, X. *et al.* MCOLN1 is a ROS sensor in lysosomes that regulates autophagy. *Nat. Commun.* **7**, 12109 (2016).

302. Chen, C.-C. *et al.* A small molecule restores function to TRPML1 mutant isoforms responsible for mucolipidosis type IV. *Nat. Commun.* **5**, 4681 (2014).

303. Huang, L. *et al.* Berbamine inhibits SARS-CoV-2 infection by compromising TRPMLs-mediated endolysosomal trafficking of ACE2. *Signal transduction and targeted therapy* vol. 6 168 (2021).

304. Wang, X. *et al.* TPC proteins are phosphoinositide- activated sodium-selective ion channels in endosomes and lysosomes. *Cell* **151**, 372–383 (2012).

305. Cang, C. *et al.* mTOR regulates lysosomal ATP-sensitive two-pore Na(+) channels to adapt to metabolic state. *Cell* **152**, 778–790 (2013).

306. Grimm, C. *et al.* High susceptibility to fatty liver disease in two-pore channel 2-deficient mice. *Nat. Commun.* **5**, 4699 (2014).

307. Nelson, E. A. *et al.* The phosphatidylinositol-3-phosphate 5-kinase inhibitor apilimod blocks filoviral entry and infection. *PLoS Negl. Trop. Dis.* **11**, e0005540 (2017).

308. Shan, C. *et al.* An Infectious cDNA Clone of Zika Virus to Study Viral Virulence, Mosquito Transmission, and Antiviral Inhibitors. *Cell Host Microbe* **19**, 891–900 (2016).

309. Akhras, S., Herrlein, M.-L., Elgner, F., Holzhauser, T. & Hildt, E. ZIKV Envelope Domain-Specific Antibodies: Production, Purification and Characterization. *Viruses* **11**, (2019).

310. Gasteiger, E. *et al.* ExPASy: The proteomics server for in-depth protein knowledge and

analysis. *Nucleic Acids Res.* **31**, 3784–3788 (2003).

311. Chomczynski, P. & Sacchi, N. Single-step method of RNA isolation by acid guanidinium thiocyanate-phenol-chloroform extraction. *Anal. Biochem.* **162**, 156–159 (1987).

312. Livak, K. J. & Schmittgen, T. D. Analysis of relative gene expression data using real-time quantitative PCR and the 2(-Delta Delta C(T)) Method. *Methods* **25**, 402–408 (2001).

313. Maurer, T. & Kalbitzer, H. R. Indirect Referencing of31P and19F NMR Spectra. *J. Magn. Reson. Ser. B* **113**, 177–178 (1996).

314. Himmelsbach, K. & Hildt, E. Identification of various cell culture models for the study of Zika virus. *World J. Virol.* **7**, 10–20 (2018).

315. Uhlén, M. *et al.* Proteomics. Tissue-based map of the human proteome. *Science* **347**, 1260419 (2015).

316. Schwickert, K. Design, Synthese und biologische Evaluierung neuer TRP-Ionenkanal-Aktivatoren; Synthese und Reaktivität neuer Bortezomib-Kongenere mit diversen Warheads als potenzielle Proteasom-Inhibitoren. (Johannes Gutenberg-University Mainz, 2020).

317. Yoshimori, T., Yamamoto, A., Moriyama, Y., Futai, M. & Tashiro, Y. Bafilomycin A1, a specific inhibitor of vacuolar-type H(+)-ATPase, inhibits acidification and protein degradation in lysosomes of cultured cells. *J. Biol. Chem.* **266**, 17707–17712 (1991).

318. Fedele, A. O. & Proud, C. G. Chloroquine and bafilomycin A mimic lysosomal storage disorders and impair mTORC1 signalling. *Biosci. Rep.* **40**, (2020).

319. Li, X. *et al.* Biogenesis and Function of Multivesicular Bodies in Plant Immunity. *Front. Plant Sci.* **9**, 979 (2018).

320. Martins, S. de T. & Alves, L. R. Extracellular Vesicles in Viral Infections: Two Sides of the Same Coin? *Front. Cell. Infect. Microbiol.* **10**, 593170 (2020).

321. Furuno, K., Ishikawa, T. & Kato, K. Appearance of autolysosomes in rat liver after leupeptin treatment. *J. Biochem.* **91**, 1485–1494 (1982).

322. Glaumann, H. & Ahlberg, J. Comparison of different autophagic vacuoles with regard to ultrastructure, enzymatic composition, and degradation capacity--formation of crinosomes. *Exp. Mol. Pathol.* **47**, 346–362 (1987).

323. Wu, Y. *et al.* p62/SQSTM1 accumulation due to degradation inhibition and transcriptional activation plays a critical role in silica nanoparticle-induced airway inflammation via NF-κB activation. *J. Nanobiotechnology* **18**, 77 (2020).

324. Eskelinen, E.-L. Autophagy: Supporting cellular and organismal homeostasis by self-eating. *Int. J. Biochem. Cell Biol.* **111**, 1–10 (2019).

325. Yoshii, S. R. & Mizushima, N. Monitoring and Measuring Autophagy. *International Journal of Molecular Sciences* vol. 18 (2017).

326. Bjørkøy, G. *et al.* Monitoring autophagic degradation of p62/SQSTM1. *Methods Enzymol.* **452**, 181–197 (2009).

327. Haspel, J. *et al.* Characterization of macroautophagic flux in vivo using a leupeptin-based assay. *Autophagy* **7**, 629–642 (2011).

328. Daelemans, D., Pauwels, R., De Clercq, E. & Pannecouque, C. A time-of–drug addition approach to target identification of antiviral compounds. *Nat. Protoc.* **6**, 925–933 (2011).

329. Pettke, A. *et al.* Broadly Active Antiviral Compounds Disturb Zika Virus Progeny Release Rescuing Virus-Induced Toxicity in Brain Organoids. *Viruses* **13**, (2020).

330. Churchward, M. A., Rogasevskaia, T., Höfgen, J., Bau, J. & Coorssen, J. R. Cholesterol

facilitates the native mechanism of Ca2+-triggered membrane fusion. *J. Cell Sci.* **118**, 4833–4848 (2005).

331. Steinkühler, J., Sezgin, E., Urbančič, I., Eggeling, C. & Dimova, R. Mechanical properties of plasma membrane vesicles correlate with lipid order, viscosity and cell density. *Commun. Biol.* **2**, 337 (2019).

332. Osuna-Ramos, J. F., Reyes-Ruiz, J. M. & Del Ángel, R. M. The Role of Host Cholesterol During Flavivirus Infection. *Front. Cell. Infect. Microbiol.* **8**, 388 (2018).

333. Glitscher, M. & Hildt, E. Endosomal Cholesterol in Viral Infections - A Common Denominator? *Front. Physiol.* **12**, 750544 (2021).

334. Platanias, L. C. Mechanisms of type-I- and type-II-interferon-mediated signalling. *Nat. Rev. Immunol.* **5**, 375–386 (2005).

335. Pestka, S., Langer, J. A., Zoon, K. C. & Samuel, C. E. Interferons and their actions. *Annu. Rev. Biochem.* **56**, 727–777 (1987).

336. Pestka, S., Krause, C. D. & Walter, M. R. Interferons, interferon-like cytokines, and their receptors. *Immunol. Rev.* **202**, 8–32 (2004).

337. Pestka, S. The human interferon-alpha species and hybrid proteins. *Semin. Oncol.* **24**, S9-4-S9-17 (1997).

338. ISAACS, A. & LINDENMANN, J. Virus interference. I. The interferon. *Proc. R. Soc. London. Ser. B, Biol. Sci.* **147**, 258–267 (1957).

339. Bach, E. A., Aguet, M. & Schreiber, R. D. The IFN gamma receptor: a paradigm for cytokine receptor signaling. *Annu. Rev. Immunol.* **15**, 563–591 (1997).

340. Pestka, S. *et al.* The interferon gamma (IFN-gamma) receptor: a paradigm for the multichain cytokine receptor. *Cytokine Growth Factor Rev.* **8**, 189–206 (1997).

341. Darnell, J. E. J., Kerr, I. M. & Stark, G. R. Jak-STAT pathways and transcriptional activation in response to IFNs and other extracellular signaling proteins. *Science* **264**, 1415–1421 (1994).

342. Stark, G. R., Kerr, I. M., Williams, B. R., Silverman, R. H. & Schreiber, R. D. How cells respond to interferons. *Annu. Rev. Biochem.* **67**, 227–264 (1998).

343. Darnell, J. E. J. STATs and gene regulation. *Science* **277**, 1630–1635 (1997).

344. Aaronson, D. S. & Horvath, C. M. A road map for those who don't know JAK-STAT. *Science* **296**, 1653–1655 (2002).

345. Meinke, A., Barahmand-Pour, F., Wöhrl, S., Stoiber, D. & Decker, T. Activation of different Stat5 isoforms contributes to cell-type-restricted signaling in response to interferons. *Mol. Cell. Biol.* **16**, 6937–6944 (1996).

346. Pott, J. & Stockinger, S. Type I and III Interferon in the Gut: Tight Balance between Host Protection and Immunopathology. *Front. Immunol.* **8**, (2017).

347. Kumar, A. *et al.* Zika virus inhibits type-I interferon production and downstream signaling. *EMBO Rep.* **17**, 1766–1775 (2016).

348. Grant, A. *et al.* Zika Virus Targets Human STAT2 to Inhibit Type I Interferon Signaling. *Cell Host Microbe* **19**, 882–890 (2016).

349. Bowen, J. R. *et al.* Zika Virus Antagonizes Type I Interferon Responses during Infection of Human Dendritic Cells. *PLoS Pathog.* **13**, e1006164 (2017).

350. Schoggins, J. W. Interferon-Stimulated Genes: What Do They All Do? *Annu. Rev. Virol.* **6**, 567–584 (2019).

351. Krogsaeter, E. K., Biel, M., Wahl-Schott, C. & Grimm, C. The protein interaction networks of mucolipins and two-pore channels. *Biochim. Biophys. acta. Mol. cell Res.* **1866**, 1111–1123 (2019).

352. Scotto Rosato, A. *et al.* TRPML1 links lysosomal calcium to autophagosome biogenesis through the activation of the CaMKKβ/VPS34 pathway. *Nat. Commun.* **10**, 5630 (2019).

353. Medina, D. L. & Ballabio, A. Lysosomal calcium regulates autophagy. *Autophagy* **11**, 970–971 (2015).

354. Curcio-Morelli, C. *et al.* Macroautophagy is defective in mucolipin-1-deficient mouse neurons. *Neurobiol. Dis.* **40**, 370–377 (2010).

355. Vergarajauregui, S., Connelly, P. S., Daniels, M. P. & Puertollano, R. Autophagic dysfunction in mucolipidosis type IV patients. *Hum. Mol. Genet.* **17**, 2723–2737 (2008).

356. Di Paola, S., Scotto-Rosato, A. & Medina, D. L. TRPML1: The Ca((2+))retaker of the lysosome. *Cell Calcium* **69**, 112–121 (2018).

357. Martina, J. A., Lelouvier, B. & Puertollano, R. The calcium channel mucolipin-3 is a novel regulator of trafficking along the endosomal pathway. *Traffic* **10**, 1143–1156 (2009).

358. Ma, J. *et al.* Mechanisms by Which Dendritic Cells Present Tumor Microparticle Antigens to CD8(+) T Cells. *Cancer Immunol. Res.* **6**, 1057–1068 (2018).

359. Leier, H. C. *et al.* A global lipid map defines a network essential for Zika virus replication. *Nat. Commun.* **11**, 3652 (2020).

360. Lange, Y., Ye, J., Rigney, M. & Steck, T. L. Regulation of endoplasmic reticulum cholesterol by plasma membrane cholesterol. *J. Lipid Res.* **40**, 2264–2270 (1999).

361. Liscum, L. & Munn, N. J. Intracellular cholesterol transport. *Biochim. Biophys. Acta* **1438**, 19–37 (1999).

362. Godfraind, T. & Salomone, S. Functional interaction of lacidipine with calcium channels in vascular smooth muscle. *J. Cardiovasc. Pharmacol.* **18 Suppl 1**, S1-6 (1991).

363. Spampinato, S. *et al.* Ca2+ channel blocking activity of lacidipine and amlodipine in A7r5 vascular smooth muscle cells. *Eur. J. Pharmacol.* **244**, 139–144 (1993).

364. Bezemer, B., van Cleef, K. W. R., Overheul, G. J., Miesen, P. & van Rij, R. P. The calcium channel inhibitor lacidipine inhibits Zika virus replication in neural progenitor cells. *Antiviral Res.* **202**, 105313 (2022).

365. Flocco, M. M. & Mowbray, S. L. Strange bedfellows: interactions between acidic side-chains in proteins. *J. Mol. Biol.* **254**, 96–105 (1995).

366. Eichelsdoerfer, J. L., Evans, J. A., Slaugenhaupt, S. A. & Cuajungco, M. P. Zinc dyshomeostasis is linked with the loss of mucolipidosis IV-associated TRPML1 ion channel. *J. Biol. Chem.* **285**, 34304–34308 (2010).

367. Howard, M. J. Protein NMR spectroscopy. *Curr. Biol.* **8**, R331-3 (1998).

368. Diaz-Parga, P. & de Alba, E. Chapter Fourteen - Protein interactions of the inflammasome adapter ASC by solution NMR. in *DNA Sensors and Inflammasomes* (ed. Sohn, J. B. T.-M. in E.) vol. 625 223–252 (Academic Press, 2019).

369. CAVANAGH, J., FAIRBROTHER, W. J., PALMER, A. G., RANCE, M. & SKELTON, N. J. CHAPTER 4 - MULTIDIMENSIONAL NMR SPECTROSCOPY. in (eds. CAVANAGH, J., FAIRBROTHER, W. J., PALMER, A. G., RANCE, M. & SKELTON, N. J. B. T.-P. N. M. R. S. (Second E.) 271–332 (Academic Press, 2007). doi:https://doi.org/10.1016/B978-012164491-8/50006-3.

370. ELLMAN, G. L. Tissue sulfhydryl groups. *Arch. Biochem. Biophys.* **82**, 70–77 (1959).

371. Rose-Sperling, D., Tran, M. A., Lauth, L. M., Goretzki, B. & Hellmich, U. A. 19F NMR as a versatile tool to study membrane protein structure and dynamics. *Biol. Chem.* **400**, 1277–1288 (2019).

372. Sharaf, N. G. & Gronenborn, A. M. (19)F-modified proteins and (19)F-containing ligands as tools in solution NMR studies of protein interactions. *Methods Enzymol.* **565**, 67–95 (2015).

373. Sahu, I. D. & Lorigan, G. A. Electron Paramagnetic Resonance as a Tool for Studying Membrane Proteins. *Biomolecules* **10**, (2020).

374. Stone, T. J., Buckman, T., Nordio, P. L. & McConnell, H. M. Spin-labeled biomolecules. *Proc. Natl. Acad. Sci. U. S. A.* **54**, 1010–1017 (1965).

375. Cornish, V. W. *et al.* Site-specific incorporation of biophysical probes into proteins. *Proc. Natl. Acad. Sci. U. S. A.* **91**, 2910–2914 (1994).

376. García-Rubio, I. EPR of site-directed spin-labeled proteins: A powerful tool to study structural flexibility. *Arch. Biochem. Biophys.* **684**, 108323 (2020).

377. Drescher, M. EPR in protein science : intrinsically disordered proteins. *Top. Curr. Chem.* **321**, 91–119 (2012).

378. Claxton, D. P., Kazmier, K., Mishra, S. & Mchaourab, H. S. Navigating Membrane Protein Structure, Dynamics, and Energy Landscapes Using Spin Labeling and EPR Spectroscopy. *Methods Enzymol.* **564**, 349–387 (2015).

379. Schweiger, A. & Jeschke, G. *Principles of pulse electron paramagnetic resonance*. (Oxford University Press on Demand, 2001).

380. Jeschke, G. & Polyhach, Y. Distance measurements on spin-labelled biomacromolecules by pulsed electron paramagnetic resonance. *Phys. Chem. Chem. Phys.* **9**, 1895–1910 (2007).

381. Pannier, M., Veit, S., Godt, A., Jeschke, G. & Spiess, H. W. Dead-time free measurement of dipole-dipole interactions between electron spins. *J. Magn. Reson.* **142**, 331–340 (2000).

382. Jeschke, G., Bender, A., Paulsen, H., Zimmermann, H. & Godt, A. Sensitivity enhancement in pulse EPR distance measurements. *J. Magn. Reson.* **169**, 1–12 (2004).

383. Banham, J. E., Timmel, C. R., Abbott, R. J. M., Lea, S. M. & Jeschke, G. The characterization of weak protein-protein interactions: evidence from DEER for the trimerization of a von Willebrand Factor A domain in solution. *Angew. Chem. Int. Ed. Engl.* **45**, 1058–1061 (2006).

384. Jeschke, G. Distance measurements in the nanometer range by pulse EPR. *Chemphyschem* **3**, 927–932 (2002).

385. Lev, S. *et al.* Constitutive Activity of the Human TRPML2 Channel Induces Cell Degeneration*. *J. Biol. Chem.* **285**, 2771–2782 (2010).

386. Blaby-Haas, C. E. & Merchant, S. S. Lysosome-related Organelles as Mediators of Metal Homeostasis*. *J. Biol. Chem.* **289**, 28129–28136 (2014).

387. Minckley, T. F. *et al.* Sub-nanomolar sensitive GZnP3 reveals TRPML1-mediated neuronal Zn2+ signals. *Nat. Commun.* **10**, 4806 (2019).

388. Du, W. *et al.* Lysosomal Zn2+ release triggers rapid, mitochondria-mediated, non-apoptotic cell death in metastatic melanoma. *Cell Rep.* **37**, 109848 (2021).

389. Himmelsbach, K., Bender, D. & Hildt, E. Life cycle and morphogenesis of the hepatitis E virus. *Emerg. Microbes Infect.* **7**, 196 (2018).

390. Pfalzgraf, S. Einfluss von TRPML2 auf den Lebenszyklus von HEV. (Goethe-University, Frankfurt am Main, Germany, 2021).

391. Donald, J. E., Kulp, D. W. & DeGrado, W. F. Salt bridges: geometrically specific, designable interactions. *Proteins* **79**, 898–915 (2011).

392. Samie, M. A. *et al.* The tissue-specific expression of TRPML2 (MCOLN-2) gene is influenced by the presence of TRPML1. *Pflugers Arch.* **459**, 79–91 (2009).

393. Hurtado-Lorenzo, A. *et al.* V-ATPase interacts with ARNO and Arf6 in early endosomes and regulates the protein degradative pathway. *Nat. Cell Biol.* **8**, 124–136 (2006).

394. McIntosh, M. L., Naffziger, M. R., Ashburn, B. O., Zakharov, L. N. & Carter, R. G. Highly regioselective nitrile oxide dipolar cycloadditions with ortho-nitrophenyl alkynes. *Org. Biomol. Chem.* **10**, 9204–9213 (2012).

Acknowledgements

To protect the privacy of the author, the acknowledgements are not available in the online version of this thesis.

Declaration

I hereby declare that I wrote the dissertation submitted without any unauthorized external assistance and used only sources acknowledged in the work. All textual passages which are appropriated verbatim or paraphrased from published and unpublished texts as well as all information obtained from oral sources are duly indicated and listed in accordance with bibliographical rules. In carrying out this research, I complied with the rules of standard scientific practice as formulated in the statutes of Johannes Gutenberg-University Mainz to insure standard scientific practice.

_____

Kerstin Schwickert

Mainz, _____

Curriculum vitae

To protect the privacy of the author, the CV is not available in the online version of this thesis.